

Investigating the fundamentals of drug crystal
growth using Atomic Force Microscopy.

Claire Thompson, BSc

Thesis submitted to The University of Nottingham for the degree of
Doctor of Philosophy, May 2003.

Contents

Abstract.....	7
List of abbreviations.....	9
Chapter 1. Introduction.....	11
1.1 Nucleation and crystallization processes, and their importance in the production of pharmaceutical compounds.....	11
1.1.1 Nucleation.....	11
1.1.2 Crystal growth.....	13
1.1.3 The importance of crystals to the pharmaceutical industry.....	14
1.2 The influence of crystallization conditions on the physical properties and stability of pharmaceutical drugs.....	18
1.2.1 Supersaturation: its effect on the growth and properties of drug crystals.....	19
1.2.1.1 Crystalline particles for inhalation devices.....	20
1.2.1.2 Solid drug nanoparticles.....	21
1.2.2 Recrystallizing solvent: its effect on the growth and properties of drug crystals.....	22
1.2.3 Impurities/Additives: their effect on the growth and properties of drug crystals.....	23
1.3 Unstable forms of pharmaceutical crystals.....	24
1.3.1 Polymorphism.....	24
1.3.2 Amorphous solids.....	26
1.3.3 Solvates.....	27
1.3.4 Chiral drugs.....	27
1.3.5 Solid-state transformations.....	28

1.3.6	Solvent-mediated transformations.....	29
1.4	Regulations governing the control over crystallization of pharmaceutical compounds.....	30
1.5	Techniques used to investigate nucleation and crystal growth.	31
1.5.1	Molecular simulations.	31
1.5.2	Experimental techniques used to investigate nucleation.....	32
1.5.3	Experimental techniques used to investigate crystal growth.....	33
1.5.3.1	Optical microscopy.....	35
1.5.3.2	Electron microscopy.....	37
1.5.3.3	Interferometry.....	40
1.6	Atomic Force Microscopy.....	42
1.6.1	The principles and methodology of AFM.....	43
1.6.2	Advantages of AFM over conventional techniques.	46
1.6.3	The application of AFM to the study of crystal growth.....	47
1.7	Aims of the project.....	49
	Chapter 2. An <i>in situ</i> study of the effects of supersaturation on aspirin crystal growth.....	51
2.1	Introduction.....	52
2.1.1	The effects of supersaturation on crystal growth.	52
2.1.2	The dislocation mechanism of growth.	53
2.1.3	2D nucleation.	56
2.1.4	3D nucleation.	58
2.1.5	Terrace-Ledge-Kink (TLK) model.....	61
2.1.6	Aspirin: a brief history.....	64
2.1.7	Aims of chapter.....	65

2.2	Methods and Materials	66
2.2.1	Preparation of aspirin crystals and growth media.	66
2.2.2	AFM analysis.....	67
2.3	Results and Discussion.....	72
2.3.1	Growth on the (001) face at $\sigma = 0.31$	72
2.3.2	Growth on the (001) face at $\sigma = 0.36$	78
2.4	Conclusion.....	82
Chapter 3. Using self-assembled monolayers to investigate the nucleation and growth kinetics of aspirin crystals.		85
3.1	Introduction.....	86
3.1.1	Overview of the current techniques used to promote and investigate crystallization.	86
3.1.2	Formation of self-assembled monolayers (SAMs) on surfaces.....	87
3.1.3	Aims of chapter.....	93
3.2	Methods and Materials	94
3.2.1	Preparation of self-assembled monolayers (SAMs) on epitaxial gold. ...	94
3.2.2	AFM analysis.....	96
3.2.3	SEM analysis.....	98
3.3	Results and Discussion.....	98
3.4	Conclusion.....	123
Chapter 4. The effects of additives on the morphology and growth on the (001) face of paracetamol crystals.		127
4.1	Introduction.....	128
4.1.1	The effects of impurities on crystal nucleation and growth.	128
4.1.2	Impurities in pharmaceutical compounds.....	129

4.1.3	Paracetamol and its structurally related additives.....	130	
4.1.4	Blocking activity of acetanilide and metacetamol.	136	
4.1.5	Docking activity of acetanilide and metacetamol.	137	
4.1.6	Disrupting activity of acetanilide and metacetamol.	138	
4.1.7	Aims of chapter.....	139	
4.2	Methods and Materials.....	140	
4.2.1	Preparation of paracetamol crystals grown in the presence and absence of an inhibitor.	140	
4.2.2	Preparation of solutions for growth studies.....	141	
4.2.3	AFM analysis.....	142	
4.2.4	SEM analysis.....	143	
4.3	Results and Discussion.....	143	
4.3.1	Morphology of crystals grown in the presence and absence of the additives acetanilide and metacetamol.	143	
4.3.2	Growth on the (001) face of a paracetamol crystal in solutions of pure paracetamol, and those containing acetanilide or metacetamol.	153	
4.4	Conclusion.....	160	
Chapter 5. Determination of the mechanisms of anion exchange in			
Co-ordination Polymers.....			163
5.1	Introduction.....	164	
5.1.1	The design and assembly of co-ordination polymers.....	164	
5.1.2	Ion exchange properties of co-ordination polymers and their potential uses.....	165	
5.1.3	Is the mechanism of ion exchange a solid-state or solvent-mediated process?.....	166	

5.1.4	Structures of $\{[\text{Ag}(4,4'\text{-bipy})]\text{BF}_4\}_\infty$ and $\{[\text{Ag}(4,4'\text{-bipy})]\text{NO}_3\}_\infty$	166
5.1.5	Reversible anion exchange properties of $\{[\text{Ag}(4,4'\text{-bipy})]\text{BF}_4\}_\infty$ and $\{[\text{Ag}(4,4'\text{-bipy})]\text{NO}_3\}_\infty$	172
5.1.6	Aims of chapter.....	174
5.2	Methods and Materials.....	174
5.2.1	AFM analysis.....	175
5.2.2	SEM analysis.....	175
5.3	Results and Discussion.....	176
5.3.1	AFM and SEM data for $\{[\text{Ag}(4,4'\text{-bipy})]\text{BF}_4\}_\infty$ and $\{[\text{Ag}(4,4'\text{-bipy})]\text{NO}_3\}_\infty$ crystals in air and water.	176
5.3.2	Anion exchange.	183
5.4	Conclusion.....	194
	Chapter 6. General Conclusions	198
	References	206
	Acknowledgements	236
	Publications	237

Abstract

The importance of crystals to the pharmaceutical industry is evident - over 90% of pharmaceutical products contain a drug in crystalline form. However, the crystallization phenomena of drug compounds are poorly understood. An increased understanding of these processes may allow a greater degree of control over the crystallization outcomes, such as morphology, purity, or stability. In these studies, we have applied Atomic Force Microscopy (AFM) to the *in situ* investigations of drug crystal growth.

We utilized AFM to assess the growth on the (001) face of aspirin crystals at two supersaturations, elucidating both the growth mechanisms and kinetics at each supersaturation.

We also investigated the nucleation of aspirin crystals, using microcontact printing to arrange aspirin-binding and non-binding self-assembled monolayers (SAMs) onto surfaces. This facilitated the visualization, using AFM, of the growth of aspirin crystals adhered to the surface. Additionally, secondary nucleation was observed on the growing crystals.

The effect of the additives acetanilide and metacetamol on the morphology and growth on the (001) face of paracetamol was investigated. The presence of metacetamol significantly reduced the growth rate on the face, with respect to pure paracetamol solutions. The growing steps exhibited a pinned appearance, consistent with the Cabrera and Vermilyea model. Conversely, acetanilide caused dissolution to occur.

Finally, we assessed the capabilities of AFM in following the structural transformations of crystals, which can occur in unstable pharmaceutical compounds.

We employed AFM to determine the process by which anion exchange, and the subsequent structural transformations, of the co-ordination polymers $\{[\text{Ag}(4,4'\text{-bipy})]\text{BF}_4\}_\infty$ and $\{[\text{Ag}(4,4'\text{-bipy})]\text{NO}_3\}_\infty$ occur. AFM data verified that the anion exchange process is solvent-mediated. The mechanisms underlying this process are discussed herein.

These results reiterate the capability of AFM to monitor dynamic events on crystal surfaces. Analogous studies could be applied to numerous pharmaceutical compounds, thus facilitating the optimization of their crystallization parameters. In essence, future experiments using AFM may afford greater control over crystallization, and prevent the production of unwanted or unstable pharmaceutical compounds.

List of abbreviations

1-DDT	1-Dodecane-thiol
2D	Two-Dimensional
3D	Three-Dimensional
4,4'-bipy	4,4'-Bipyridine
11-MUA	11-Mercaptoundecanoic Acid
11-MUD	11-Mercapto-1-undecanol
AFM	Atomic Force Microscopy
c	Solution concentration
c_0	Equilibrium concentration of the solution, i.e., the solubility
cGMP	Current Good Manufacturing Practice
DDA	Deposition, Diffusion, and Aggregation Model
DPI	Dry Powder Inhaler
DSC	Differential Scanning Calorimetry
ESEM	Environmental Scanning Electron Microscopy
FDA	Food and Drug Administration
HIV	Human Immunodeficiency Virus
(hkl)	Miller indices of a face
{hkl}	Set of crystal faces with Miller indices (hkl)
[hkl]	Crystallographic direction
HPLC	High Performance Liquid Chromatography
HPMC	Hydroxypropyl Methylcellulose
MDI	Metered Dose Inhaler

NDA	New Drug Application
NMR	Nuclear Magnetic Resonance
NSAID	Non-Steroidal Anti-Inflammatory Drug
p	Gradient
PA	Paracetamol/Acetanilide crystal
PAA	P-Acetoxyacetanilide
PABA	P-Acetoxybenzoic Acid
PDMS	Poly(dimethylsiloxane)
PM	Paracetamol/Metacetamol crystal
PVP	Polyvinyl Pyrrolidone
R	Normal Growth Rate
RH	Relative Humidity
SAM	Self-Assembled Monolayer
SC	Segregation Coefficient
SCF	Supercritical Fluid
SEM	Scanning Electron Microscopy
STMV	Satellite Tobacco Mosaic Virus
TEM	Transmission Electron Microscopy
TLK	Terrace-Ledge-Kink
TOF-SIMS	Time Of Flight Secondary Ion Mass Spectroscopy
USP	United State Pharmacopoeia
v	Tangential Velocity
XPS	X-ray Photoelectron Spectroscopy
XRPD	X-ray Powder Diffraction
σ	Supersaturation

Chapter

1

Introduction

1.1 Nucleation and crystallization processes, and their importance in the production of pharmaceutical compounds.

1.1.1 Nucleation.

The process of creating a new solid phase from a supersaturated mother phase is known as nucleation, and is central to all types of crystallization [1]. Crystallization begins with the aggregation of molecules, typically solute molecules in solution, leading to the formation of a nucleus. If the nucleus attains a certain critical size, it will grow into a macroscopic crystal, whereas subcritical sized nuclei redissolve.

In general, nucleation mechanisms can be divided into three main categories: homogeneous, heterogeneous, and secondary nucleation [2-7]. The thermodynamic considerations for these nucleation mechanisms are based on the works of Gibbs [8]

and Volmer [9], and are discussed extensively in a review by Rodríguez-Hornedo and Murphy [7].

Homogenous nucleation is the spontaneous nucleation of crystals, in a supersaturated solution, in the absence of any impurities or nucleation-promoting substrates. This type of nucleation rarely occurs in volumes larger than 100 μl , since “real” solutions tend to contain random impurities which may induce nucleation [10, 11].

Heterogeneous nucleation occurs when a surface or interface of different composition to that of the crystallizing solute, acts as a nucleation substrate [12, 13]. Heterogeneous nucleation can occur in the presence of impurities, or on ordered substrates, such as monolayers or micelles. The promotion of nucleation by self-assembled monolayers is detailed in Chapter 3.

The presence of impurities or nucleation-promoting surfaces can induce nucleation at supersaturations lower than those required for homogeneous nucleation. The extent of this reduction depends on the degree to which the nucleation-promoting substance mimics the structure of the crystallizing material [1]. In some instances, this process occurs by the non-oriented adsorption of solute molecules onto an existing surface until it resembles a crystal. In other cases, a specific structural relationship exists between the surface and the crystallizing solute, allowing the crystal to nucleate and grow epitaxially [1]. A number of researchers have applied the concepts of heterogeneous nucleation to the directed nucleation of specific polymorphs [14-18]. These studies provide us with the attractive possibility that “a library of organic seeds can be used to control polymorphism, or to search for unknown polymorphs” [13].

The best match between a substrate and a crystallizing solute exists when the substrate is in fact a seed crystal of the solute. Nucleation that occurs on, or is promoted by, seed crystals of the crystallizing solute is known as secondary nucleation [7]. This nucleation mechanism generally occurs at much lower supersaturations than homogeneous or heterogeneous nucleation [1].

Nucleation processes are of practical importance in production of pharmaceutical compounds, for example, in instances where crystallization is observed at times shorter than the desired product shelf-life, or where precipitation occurs upon injection. In these cases, the kinetic stability of supersaturated solutions is regulated by the nucleation mechanisms and kinetics. As previously mentioned, nucleation phenomena are equally important in the selective crystallization of a particular polymorphic form [15, 17]. It is also of great interest to understand the efficiency of crystal seeding in pharmaceutical crystallization.

1.1.2 Crystal growth.

Once the nucleation step has been overcome, nuclei grow into macroscopic crystals. The nucleation and growth processes compete for solute molecules in terms of their respective dependence on supersaturation, and their relative rates will determine the crystal size distribution [7].

Crystal growth is governed by both internal and external factors. Internal factors, such as the three-dimensional crystal structure and crystal defects, will determine the nature and strength of the intermolecular interactions between the crystal surface and the solution. On the other hand, external factors, such as the temperature, supersaturation, solvent, pH, stirring rate, and the presence of

impurities, will affect the type of interactions at the solid-liquid interface [7]. The mechanisms of growth of crystals are well characterized, and are described in detail in Chapter 2.

The dependence of nucleation and growth mechanisms of crystalline drugs upon the aforementioned crystallization parameters are ill defined [19-25]. The reproducibility of crystallization techniques requires the identification of the crystallization mechanisms and kinetics under well defined conditions [7]. In order to attain this information, in depth research must be performed on the *in situ* mechanisms of nucleation and growth of drug crystals, and the influences of crystallization parameters on these factors must be realized.

1.1.3 The importance of crystals to the pharmaceutical industry.

Crystallization from solution is a critical stage in the chemical production of pharmaceutical materials. Over 90% of all pharmaceutical products, such as tablets, aerosols, capsules, suspensions, and suppositories contain a drug in crystalline form [26]. The crystallization processes of such compounds are principally responsible for their chemical purity and physical properties, such as particle shape and size, crystal structure, and degree of crystal imperfection [27-29]. Crystalline variations or interbatch anomalies in these properties are associated with a wide range of industrial formulation problems, such as bioinequivalence (variable dissolution rate), tableting failure, and chemical and physical instability of the solid drug in its final dosage form [28, 30-32].

Table 1. 1 summarizes the most important solid-state characteristics which are affected by crystallization, and the influence these properties have on the

stability, and downstream processing of pharmaceutical compounds. Some of the problematic properties of crystalline drugs highlighted in Table 1. 1 will be discussed in more detail in the following sections.

Crystal properties	Effect on drug substance and/or drug product
Structural Crystallinity (existence of amorphous and semi-crystalline forms) Polymorphs Solvates (hydrates) Salts Crystal defects	Physical and chemical stability % relative humidity (RH) profile Solubility profile and dissolution rate All aspects of processing
Dimensional Particle size distribution Particle surface structure	Processing behaviour: bulk density, agglomeration, flow, compaction Particle permeability (i.e. particle adsorption) Bioavailability (drug absorption) Consistency and uniformity of the dosage form
Chemical Presence of impurities, residual solvent, and decomposition products Chiral forms and chiral separation	Toxicity Chemical, physical, and enantiomeric stability
Mechanical Brittle/ductile transitions, fracture stress, indentation hardness, stress/strain relaxation, Young's modulus	Milling and tableting behaviour
Electrical Electrostatic charge distribution	Agglomeration and flow properties

Table 1. 1 The most important solid-state characteristics which are affected by crystallization, and the influence these properties have on the stability and downstream processing of pharmaceutical materials. Adapted from [28].

It should be noted that, besides the crystalline drug component of pharmaceutical formulations, other crystalline components, such as excipients, may also be present in the formulation. These excipients may be bulking or binding agents, lubricants, or plasticizers. The physical properties of the crystalline excipient components are also of importance to the overall stability and efficacy of the drug formulation [28]. For example, tablets are by far the most widely used and convenient solid dosage form. In addition to the active drug component of the dosage form, a number of different solids, mostly crystalline excipients, may be included in the tablets. The overall success of any direct tableting procedure, and the resulting mechanical properties of the tablets, are strongly dependent on the quality of the crystals used in the process [28]. It is apparent that both the properties of the drug and excipient compounds are of great importance during formulation.

Two-thirds of the currently marketed tablets contain less than 100 mg of drug [33] and, hence, the mechanical properties of the excipient compounds will dominate within these formulations. Conversely, in the remaining one-third of tablet formulations, the mechanical characteristics of the drug compound will prevail [28]. However, for the purposes of this thesis, only the effects of crystallization on drug compounds shall be discussed.

1.2 The influence of crystallization conditions on the physical properties and stability of pharmaceutical drugs.

Crystallization processes in pharmaceutical science affect both the solid-state properties of the drug substances, and the drug product stability and performance. It should be emphasized that even minor changes in crystallization conditions, for example, supersaturation, temperature, cooling or evaporation rate, and impurity concentration can induce significant changes in the crystal properties, in particular, particle size, shape, purity, and defect structure [19-21, 34]. These alterations in crystallization parameters can, in turn, induce significant variations in the thermodynamic and mechanical properties [28]. These effects have been recognized as the major batch-to-batch variation problems, leading to inconsistency in the final drug formulation properties.

Variations in crystallization conditions may also confer instability upon the product, leading to disordered and amorphous states, polymorphism, chiral separation, or the occurrence of solid-state reactions [35].

In order to apply the concepts of crystal engineering to pharmaceutical substances, the reproducibility of the solid-state properties and stability must, first of all, be attained. It is apparent that, in order to achieve full control over the characteristics of drug compounds, we must gain a greater insight into their crystallization procedures, and design more advanced crystallization methods. The complexity and variety of crystallization problems warrant investigations of the more fundamental aspects of crystal growth.

In the following section, a description is given of some of the crystallization parameters which affect the properties of drug crystals. It should be noted that the list of parameters discussed is not intended to be exhaustive.

1.2.1 Supersaturation: its effect on the growth and properties of drug crystals.

The supersaturation of a solution may be created by various methods that regulate the solute concentration. These include solvent removal by evaporation or freezing, addition of salts with ions that participate in precipitation, and the dissolution of metastable solid phases. Supersaturation can also be created by methods that regulate the solute solubility, such as temperature change, pH change, and addition of a solvent that lowers the solubility of the solute [7].

Supersaturation can have a profound affect on crystal growth, resulting in morphological changes in the crystallizing compound over a range of supersaturations [24, 27, 29, 36-38]. It is also known to affect many of the physical properties of crystals including, the solvent content, melting point, enthalpy and entropy of fusion, and the dissolution rate [21].

In general, the number of crystals produced increases with the supersaturation, whilst the size of crystals decreases [39]. This is due to the fact that the number of molecules necessary to achieve an effective nucleating cluster is inversely proportional to the level of supersaturation. Therefore, as the supersaturation is increased, the probability of nucleation increases. The much larger number of nuclei produced per unit of time is detrimental to growth, so that smaller crystals are obtained [40]. On the contrary, large crystals are most often produced by using low supersaturations [39].

All of the above properties are very important in pharmaceutical systems, with particular emphasis on the dissolution rate, size, and morphology of crystals. The bioavailability of a drug crystal is, evidently, dependent upon its dissolution rate. Hence, the supersaturation of a growth medium must be controlled in order that the bioavailability of a drug is maintained. In addition, the size and morphology (habit) of drug crystals have downstream effects on their processing.

Processing factors such as separation, flow, compaction, dissolution, and packing all depend to a considerable extent on the crystal shape and size distribution [37]. Variations in crystal habit also present serious problems in pharmaceutical manufacturing, influencing the uniformity of tablet weight [37], and causing difficulty in tableting [31]. These problems may be overcome by grinding or milling the materials to provide more acceptable and reproducible properties. However, these treatments may promote changes in crystal structure [41] and crystal perfection [35].

Two specific examples of drug formulations which require crystals of a defined size and morphology are described below.

1.2.1.1 Crystalline particles for inhalation devices.

Dry powder inhalers (DPI) and metered dose inhalers (MDI) are types of delivery systems for inhalation drugs. These contain crystalline particles in the form of a drug/excipient mixture or a particle suspension respectively. Currently, these devices have a relatively low efficiency of delivering drugs to the alveoli region, mainly because of problems with the particle size distribution and particle morphology [28]. Only particles with a diameter below 5 μm are able to reach the deep lung alveoli region, which contain the majority of the blood vessels. Submicron particles are

likely to be exhaled and, therefore, a narrow particle size distribution of between 1 μm and 5 μm is required for efficient drug delivery [28]. In addition, the crystal morphology dictates its effective aerodynamic diameter, and defines the mechanism by which the particle clouds are intercepted by the airways [42].

Novel crystallization methods which can afford the production of crystals with a narrow size distribution are, therefore, required [28].

1.2.1.2 Solid drug nanoparticles.

Polymer-drug nanoparticle systems have attracted much attention over the past decade as they can be designed for the targeted delivery of drugs to specific organs or tissues [43]. The particle size and crystalline structure of nanoparticles define, most importantly, the dissolution rate of these drugs. Nanoparticles are crystallized at high supersaturation or, alternatively, are formed under harsh conditions of mechanical processing [28]. At high supersaturation, the crystallization of nanoparticles occurs at a very fast nucleation rate. Coupled with intensive mixing, this can lead to problems related to the agglomeration of particles [28]. Harsh mechanical processing can result in the formation of crystal defects, less stable crystalline forms, or partially amorphous material, all of which lead to an increase in solubility and dissolution rate. Thus, the development of alternative crystallization methods is necessary.

It is clear that a better understanding of the underlying crystallization processes, such as the effect of supersaturation on the process, could lead to the optimization and control of drug crystal size and morphology.

1.2.2 Recrystallizing solvent: its effect on the growth and properties of drug crystals.

The manufacture of pharmaceuticals often involves crystallization from organic solvents or mixtures of solvents. The solvent composition influences the nucleation rate, as well as the relative growth rate of each crystal face, and, thus, affects the shape of the product crystals and the size distribution of the crystallized mass [44-46]. For example, changing the solvent polarity during crystallization of nitrofurantoin and ibuprofen [47, 48] provided crystals with an elongated morphology, and enhanced compression behaviour. The solvent composition may also influence the aggregation properties, as well as the solvent incorporation of the crystals [49].

Although the role played by the solvent at the molecular level is still unclear, two theories have been proposed regarding the influence of the solvent on nucleation and growth [50]. One theory postulates that favourable interactions between solute and solvent molecules on specific faces lead to a reduction in the solid-liquid interface energy. Hence, the activation energy for nucleation on the crystal is reduced and the crystal becomes rougher, leading to enhanced crystal growth.

Alternatively, it has been proposed that, for solvent molecules that can be strongly bound to the crystallizing compound, the solute-solvent dissociation can determine the nucleation and growth rates [46]. To determine which of these theories is accurate, *in situ* studies must be carried out on the nucleation and growth of drug crystals in a wide range of solvents.

1.2.3 Impurities/Additives: their effect on the growth and properties of drug crystals.

The effects of impurities or additives on pharmaceutical crystals are described, in depth, in Chapter 4. In summary, impurities can have a substantial effect on the kinetics of nucleation and growth, and, hence, the resulting morphology [23, 29, 34, 39, 49-60] and polymorphic form [14, 16, 18, 61]. These molecules induce their effects by interacting with the crystal faces during growth. Some impurities can completely suppress growth, some enhance growth, whilst others act selectively or to varying degrees on each crystal face, consequently modifying the crystal morphology [4].

Additives are frequently used in pharmaceutical technology to modify the habit of crystals. It has also been found that additives, such as polymers or surfactants, prevent undesirable polymorphic changes in pharmaceutical preparations [62]. The modes by which additives induce habit alterations and stabilize polymorphs lie in their mechanisms of interaction at the crystal surface during growth. It is clear, therefore, that more information on the incorporation of additives into crystals at the molecular level is required.

Fundamental to understanding the influence of these factors on the physical properties of the product crystal, is defining their role in both the structural and mechanistic aspects of the growth process. Hence, their role in the macro- and micromorphological development of the crystal must be determined [37].

The macromorphology of a crystal depends on the relative growth rates of the different crystal faces. Those which grow rapidly have little or no effect on the

crystal shape, whilst the slow growing faces have the most influence [37]. The growth of a particular face is defined by the crystal structure, the density of active growth sites, and by the crystallization conditions.

The micromorphology of crystal surfaces, that is their structure on the nanometre to micrometre scale, is the governing factor in the process of crystal growth. One means of developing a quantitative understanding of growth under a variety of conditions, is to study the microtopography of the crystal surfaces. This would provide direct evidence for the mechanisms governing the growth of each crystal face which, in turn, can be related to the macromorphological behaviour of the crystal [37]. The techniques which allow the acquisition of such microtopographical information shall be discussed later in the chapter.

1.3 Unstable forms of pharmaceutical crystals.

In the subsequent sections, the potentially unstable forms of pharmaceutical crystals, and the transformations they undergo to enhance their stability, are highlighted. An excellent, comprehensive review of the properties of potentially unstable pharmaceutical compounds, and the effects these have on drug formulation, is given by Shekunov and York [28].

1.3.1 Polymorphism.

Polymorphism occurs when a molecule can pack in more than one stable orientation, giving two or more different crystal structures. Thus, polymorphs have divergent physical properties. Most important of these characteristics are the differing

solubilities and dissolution rates, as they can significantly alter important pharmacokinetic factors, such as rates of absorption, drug availability, and the resulting physiological concentrations [62].

Polymorphism is notably common for certain groups of drugs, for example, barbiturates, sulphonamides, and steroids. In fact, it is rare when a medicinally active substance exhibits only one crystalline structure [30, 62-66].

Polymorphs may grow under the same set of environmental conditions, or may be dependent upon specific crystallization parameters, such as the crystallizing solvent. For example, two polymorphs of the drug sulphathiazole (II and III) can be crystallized from water, two other polymorphs (I and IV) are obtained from acetone, and only one (I) can be recrystallized from n-propanol [67]. The proposed mechanism for this polymorphic selectivity involves the selective adsorption of solvent molecules onto the crystal faces, followed by the inhibition of nucleation and growth of particular polymorphic forms [28]. Factors, such as temperature and supersaturation, can also influence the polymorphic selection [28].

In some cases, solid-state transformations of one polymorph to another may take place [68, 69]. The time periods of these reactions range from seconds to years [28]. This occurrence is particularly worrying for drug compounds. One such example occurred in 1998, when a shortage in the supply of capsules of Norvir, an HIV protease inhibitor, was caused by the sudden formation of a crystalline structure different from the one harvested for months [70]. These transformations must be suppressed in order to maintain the integrity of the drug product during its shelf-life. If a mixture of polymorphs occurs in a pharmaceutical formulation, quantitative control over crystallization is necessary in order to ensure a fixed proportion of each form.

The “disappearing” or “elusive” polymorphs described by Dunitz and Bernstein [71], provide further evidence for the consequences of poor process control in the crystallization of polymorphic systems. It is, therefore, imperative to achieve a greater understanding of the kinetic mechanisms of polymorphism, and an enhanced degree of control over the crystallization techniques of drug substances.

It should also be noted that processing techniques, such as milling, drying, and compression, can also introduce polymorphic modifications and transformations [28]. Thus, further investigation of the effects of processing on crystal structure is also required.

1.3.2 Amorphous solids.

Partially crystalline and amorphous drugs are more soluble than their crystalline counterparts and can, therefore, be used to promote therapeutic activity. The classic example of such an application is the formulation of insulin consisting of various proportions of amorphous, crystalline, and complexed forms of insulin to achieve short, intermediate, and long acting therapeutic effects [28].

However, formulations containing amorphous forms are less stable than purely crystalline forms, and are at a significant risk to crystallize at a later stage during their product shelf-life [72]. These materials are often reactive and unstable to mechanical and thermal stresses [73]. These instabilities are the major factors impeding the more widespread use of amorphous solids. Thus, one of the basic questions of pharmaceutical formulation is to define what conditions make the solid form unstable [28]. An understanding of the crystallization kinetics of amorphous solids would provide a considerable advantage in the formulation of such drugs [28].

1.3.3 Solvates.

The presence of solvent molecules in a crystal lattice provides another opportunity for the modification of the crystal structure, which affects the thermodynamic activity, and the corresponding physicochemical characteristics [28]. Hence, such compounds are often referred to as pseudopolymorphs. The incorporation of solvent into the crystal structure can modify a variety of crystal properties, such as flowability, compaction, chemical stability, bioavailability, and dissolution rate [30, 31, 74].

Dosage forms such as creams, gels, and suspensions are formulated with water, which may, therefore, facilitate the formation of different hydrates. Hydrates may be stable within a wide range of relative humidity (RH), or may transform into higher or lower solvates, or anhydrous desolvated forms. Consequently, partially solvated forms with different degrees of crystallinity and, thus, stability can be obtained [28].

1.3.4 Chiral drugs.

More than half of all marketed drugs are chiral and exist in at least two enantiomeric forms [75]. The most important pharmaceutical problems associated with chiral drugs are related to the purity of their crystalline form. The undesirable enantiomers, if present in the crystallization medium, can become incorporated into the crystal lattice. The similarity of their molecular structure ensures that these enantiomeric impurities are very difficult to remove completely. A chiral impurity which is incorporated into the crystal will give rise to a variation in the solid-state properties

of the crystalline substance [28]. Uncontrollable impurity content may cause the unpredictable and erratic performance of the drug, leading to interbatch variations.

In most cases, crystallization yields either a mixture of enantiomorphous crystals (a racemic conglomerate), or a racemic crystalline material (a racemic compound) [28]. As a result, drug substances are often administered as a mixture of enantiomeric forms [76]. In addition, a metastable racemic compound or conglomerate in the dosage form will be inclined to convert into a more stable form, thus causing significant formulation problems [28].

The mechanisms and kinetics of enantiomeric drug crystallization and metastable enantiomeric conversion have not been sufficiently studied. Hence, the resolution of chiral drugs currently relies on methods of trial and error [28]. It is, therefore, necessary to provide a means of promoting the nucleation and growth of specific enantiomers, and to increase the stability of metastable enantiomers.

1.3.5 Solid-state transformations.

During the shelf-life of a drug compound, it may undergo a solid-state transformation to a more stable form. The transformations may be photochemically-induced, thermally-induced, or a result of solid-gas reactions [35]. These transformations can involve restructuring of the compound into another polymorphic form, or may result from internal chemical reorganization, such as dimerization, polymerization, cyclization, or decomposition [35].

It has been proposed that solid-state reactions are initiated at nucleation sites, such as defects in the crystal surface [35]. Clearly, more investigations must be conducted to enable greater stability of these crystalline compounds.

1.3.6 Solvent-mediated transformations.

Similarly, drug compounds may undergo solvent-mediated transformations to attain a more stable form. Knowledge of the stability of a crystal in a solvent is crucial in many of the stages of pharmaceutical development because pharmaceutical solids are designed to be dissolved in, and to come into contact with, solvents from the early stages of their development (during crystallization) and during processing (wet granulation, spray drying, and freeze drying) [7]. Given that the sudden disappearance or appearance of a crystalline modification can threaten the development process, the characterization of the kinetics and mechanisms of solvent-mediated transformations is of practical importance [7].

All of the aforementioned examples illustrate the instability of pharmaceutical compounds under certain conditions, the transformations they undergo to enhance their stability, and the consequences of such transformations on drug formulations. Transformations of crystalline structures may have a dramatic effect on the properties of the drug substance, in particular the toxicity, dissolution rate, and bioavailability. It is, therefore, imperative to not only increase the stability of pharmaceutical compounds, but to increase the understanding of the crystallization processes and the parameters which confer stability upon these compounds and produce the desired characteristics, such as size, shape, or polymorphic form. In order to accomplish these objectives, we must investigate the fundamental mechanisms of nucleation and growth of drug compounds, and the effects that crystallization parameters have on these mechanisms.

The resolution of many of the crystallization problems encountered during the production of drug crystals lie in the development of more advanced crystallization processes. Crystallization techniques using supercritical fluids (SCF) have been suggested as a novel method of production of pharmaceutical compounds [28]. The flexible conditions used during SCF crystallization have been shown to provide control over particle size, morphology, and water content [28]. Nonetheless, the methods of crystallization currently used during the production of pharmaceutical compounds require in-depth investigation. This fact has become apparent to regulatory bodies, whose guidelines on the control of crystallization are outlined in the following section.

1.4 Regulations governing the control over crystallization of pharmaceutical compounds.

The critical role of crystallization mechanisms and kinetics in determining the appearance of crystallization modifications has been recognized by many regulatory bodies, including the United States Food and Drug Administration (FDA). Their guidelines for the manufacture of drug substances state that [77]:

“Appropriate manufacturing and control procedures (including in-process testing when needed) should be established for the production of the desired solid-state form(s). It should be emphasized that the manufacturing process (or storage condition) is responsible for producing particular polymorphs or solvates; the control methods merely determine the outcome”.

The potential impact of modifications in crystal properties during the late stages of drug development, in terms of both cost and product delay, has led to the proposal of specific guidelines on the control of physicochemical properties. The guidelines are in the form of a New Drug Application (NDA), which must be submitted to a government regulatory body when a new drug product has completed its series of clinical trials [28]. These guidelines have been developed as a result of collaboration between regulators, industry, and academia [72, 78, 79]. The above regulations, in conjunction with internationally accepted rules governing current good manufacturing practices (cGMP) [80], make the crystallization process one of the most widely recognized issues in pharmaceutical development [28].

1.5 Techniques used to investigate nucleation and crystal growth.

1.5.1 Molecular simulations.

Recently, a structural approach has been taken to investigate crystal growth, due to the availability of commercial software for the prediction of crystal structures from molecular structures (*ab initio* predictions) [7]. Desiraju [81, 82] and Gavezzotti [66, 83-86], amongst others [45, 87-89], have demonstrated the methods used for the prediction of crystal structure, polymorphism, and molecular aggregation processes. They have also illustrated how molecular dynamics calculations can simulate the effects of solvents on molecular aggregation.

These studies, although very useful, must be complemented by *in situ* experimental studies to ascertain fully the processes occurring during nucleation and growth.

1.5.2 Experimental techniques used to investigate nucleation.

Nucleation phenomena are often described in terms of macroscopic properties, due to the scarcity of experimental techniques that allow for monitoring events at the molecular level. The current approach to detecting nucleation events is to measure, continuously, an appropriate property of the system as nucleation proceeds. A number of properties can be measured, including:

- i) *Temperature.* Since nucleation reduces the free energy of a system, heat is frequently evolved. This may be detected either by the direct measurement of temperature change, or by differential scanning calorimetry (DSC). DSC measures the heat flow into and out of a sample as its temperature is raised and lowered in tandem with a reference sample. The corresponding exo- and endotherms relate to the crystallization and melting of the sample [1].
- ii) *Volume.* Solid phases have different densities from their mother phases, and, hence, dilatometry is used to measure the volume of the crystallizing system with time [1].
- iii) *Optical transmittance.* Nucleation produces a dispersion of fine crystals. Consequently, the optical properties of a solution change at the point of nucleation. This allows the use of laser light scattering or Raman spectroscopy for the detection of nucleation [1].
- iv) *Concentration measurement.* Nucleation of the solute results in a decrease in the solution concentration. This can be monitored by following the change in a concentration-dependent physical property, such as conductivity, density, or refractive index [1]. Alternatively,

the concentration itself can be monitored, using techniques such as spectrophotometry chromatography [7].

1.5.3 Experimental techniques used to investigate crystal growth.

The experimental techniques which are commonly used to study crystallization, and the information they provide on crystallization mechanisms and kinetics are given in Table 1. 2 [7].

Until recent years, knowledge of crystal surface dynamics and morphology has been based principally on data acquired using optical microscopy [62, 90-92], electron microscopy [93-95] and *in situ* optical interferometry [27, 96, 97] and supported by the theories of Burton, Cabrera and Frank [98], Bennema [99-101], Gilmer *et al.* [102], and Chernov [103]. These techniques are described in the following sections.

Technique	Information that the technique provides about crystal growth
Optical Microscopy	<ul style="list-style-type: none"> - Study crystallization processes <i>in situ</i> - Monitor transformations in suspensions - Characterize additive or solvent interactions with specific crystal faces - Identify nucleation mechanisms - Measure crystal growth rates
Electron Microscopy	<ul style="list-style-type: none"> - Characterize additive or solvent interactions with specific crystal faces - Identify nucleation and growth mechanisms - Measure crystal growth rates
Interferometry	<ul style="list-style-type: none"> - Examine surface topography - Identify nucleation and growth mechanisms - Measure crystal growth rates
Atomic Force Microscopy	<ul style="list-style-type: none"> - Examine surface topography - Study crystallization processes <i>in situ</i> at high resolution, and in real-time - Characterize additive or solvent interactions with crystal faces - Identify nucleation and growth mechanisms - Measure crystal growth rates

Table 1. 2 The experimental techniques which are commonly used to study crystallization, and the information they provide on crystallization mechanisms and kinetics. Adapted from [7].

1.5.3.1 Optical microscopy.

A detailed account of the mechanical description of optical microscopes has been reported by Needham [104]. Optical microscopy, in its simplest form, employs a series of lenses to focus a beam of visible light, after it has interacted with a sample. This provides an image of the sample which is usually observed through an eyepiece. However, due to the relatively long wavelength of visible light, the resolution of an optical microscope is limited (working beyond 600X is difficult when observing microcrystalline materials) [105]. A diagram illustrating the basic components of an optical microscope is shown in Figure 1. 1.

The application of optical microscopy with the use of a flow cell system has facilitated the acquisition of growth rates of individual crystal faces of many crystal systems [106-108], including sulphathiazole [62, 90], methylprednisolone [90], and phenytoin [91, 92].

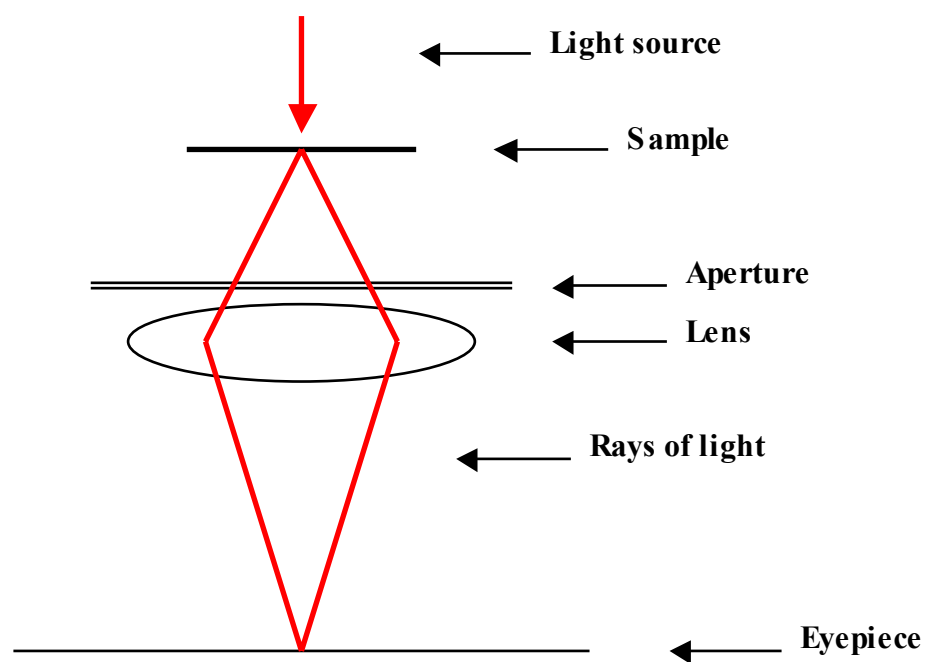


Figure 1. 1 A schematic illustration of a conventional optical microscope [105].

1.5.3.2 Electron microscopy.

The short wavelength attainable for a beam of high energy electrons allows the resolution of an electron microscope to be several hundred-fold higher than that of a light microscope. A wide variety of electron microscopes exist, each of which, as the name suggests, employ a source of electrons to provide information about a sample. A full technical description of these techniques are given in references [109, 110].

A diagrammatic representation of one of these techniques, scanning electron microscopy (SEM), is given in Figure 1. 2. In SEM, electrons from a source (usually a hot tungsten filament) are accelerated using an electric field to give the required wavelength. After acceleration, the electrons are initially focused by a lens to give a very small spot, typically 2 - 50 nm in diameter. The focused spot is then raster scanned across the sample. The detected signal is displayed on an oscilloscope in unison with the movement of the focused spot.

The spatial resolution of SEM is limited by the diameter of the focused beam, which is related to the voltage used to generate the electron beams. Higher voltage operation results in a smaller spot and better resolution, but this can also lead to an increase in heat generation and radiation damage. Both of these factors can cause sample damage. In addition to these limitations, non-conducting samples may need to be gold coated prior to analysis [111].

It should be noted that the majority of electron microscopy techniques require the analysis of a sample to be carried out in a vacuum. This, therefore, precludes these techniques for the *in situ* study of wet samples, such as crystals in their growth media.

However, the more recent development of environmental SEM (ESEM) has enabled the application of these techniques to biological and wet samples [112, 113].

This technique allows the investigation of samples in their natural state, under environmental conditions. Magnifications of up to 50,000X, with a resolution of 10 nm, are possible in such environments. ESEM operates without coating the sample, and is non-destructive. It is thought that ESEM may facilitate the examination of swelling, dissolution, and growth of pharmaceutical compounds.

Electron microscopy techniques have been utilized to determine the growth mechanisms of crystals, such as calcite [114] and lysozyme [93], and have also been applied to characterize the aggregation properties of nanoparticulate drugs [115], and the stability of crystalline drugs [116, 117].

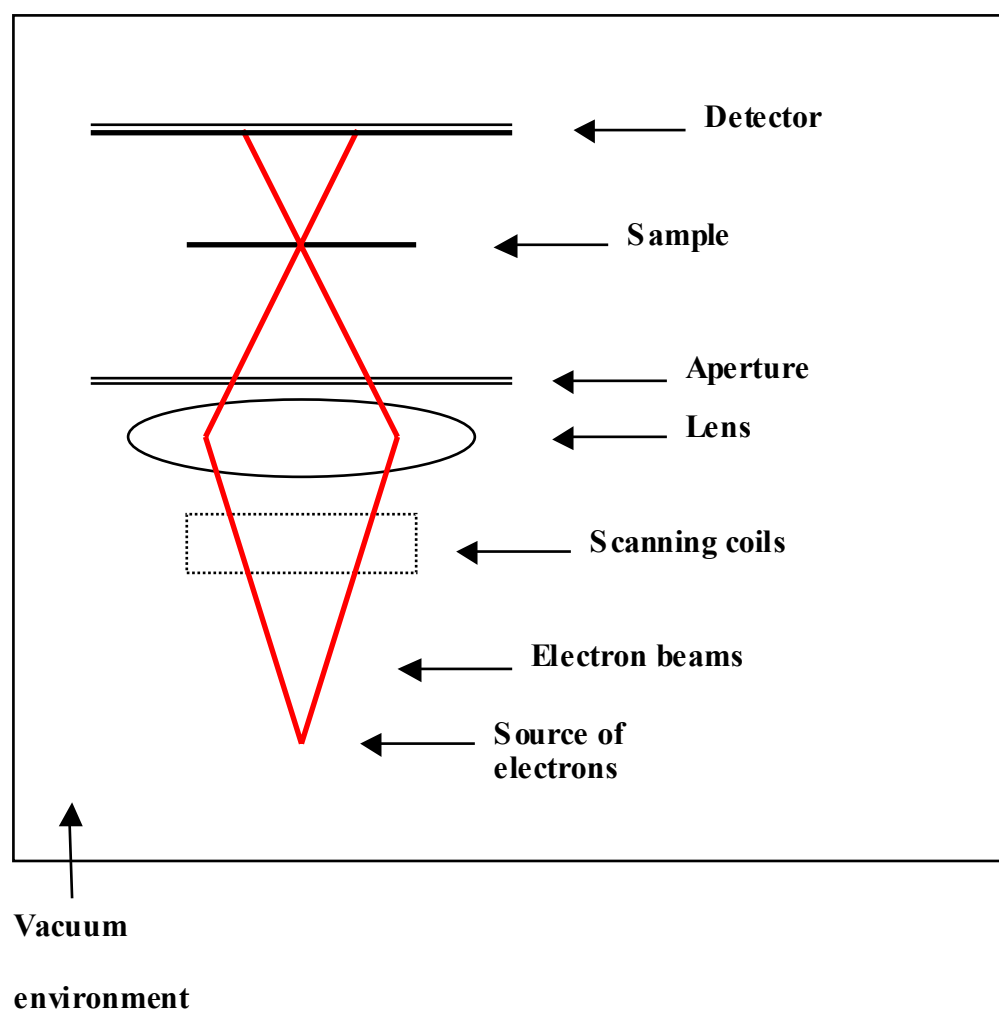


Figure 1. 2 Schematic illustration of a scanning electron microscope [105].

1.5.3.3 Interferometry.

In interferometers, an illuminating coherent light beam is split into two beams, one of which is reflected by a mirror, and the other is reflected by the sample. The reflected beams recombine in a detector and interfere with each other. The basic set-up of an interferometer is shown in Figure 1. 3. The resulting interferometric patterns provide topographic information on a growing crystal surface [97].

This technique allows the acquisition of growth data by exploiting the light interference phenomena which take place on a flat or curved mirror-like surface. If a flat, dislocation-free face is observed, the interference patterns will be parallel, straight fringes. In contrast, a growth hillock developing on such an atomically flat face will produce concentric interference fringes. Each of these fringes passes through points located at the same height from a reference single plane, and plays the role of a contour line on a topographic map. This allows the gradient of the surface, p , to be measured.

During growth, the concentric fringes increase in size, spreading outwards from the hillock centre. The tangential velocity, v , of the growing hillock is the frequency at which the fringes are passing through a given point on the pattern. Movement of the fringes gives additional information about the normal growth rate, R , which can be calculated using the equation:

$$v = R/p \qquad \text{Equation 1.1}$$

Such microtopographic observations can reveal the growth mechanisms and kinetics of crystal faces under a variety of growth conditions. Interferometric studies have been performed on paracetamol crystals to probe the growth kinetics, crystal defects, solvent-crystal interactions, and the influence of additives [27, 37, 96].

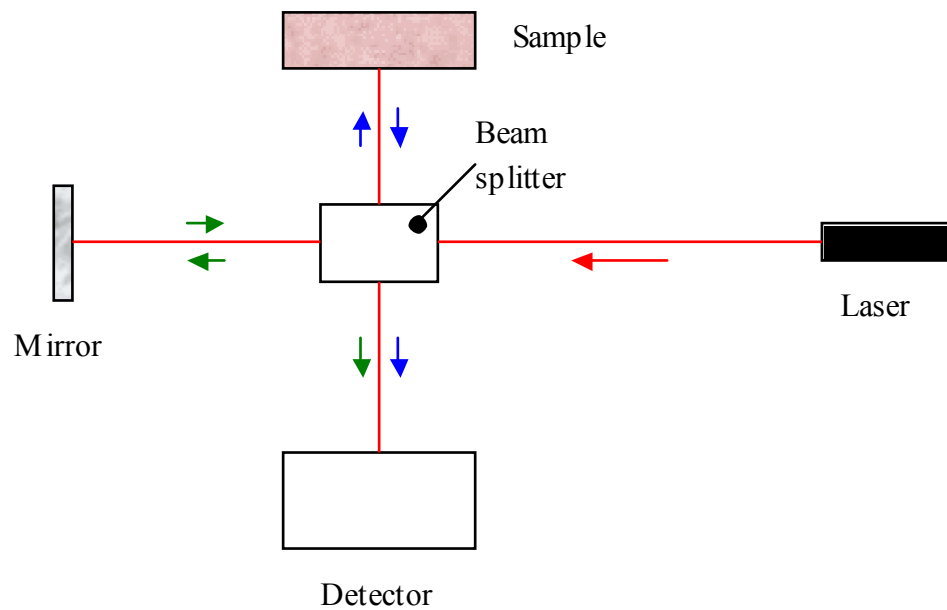


Figure 1. 3 A diagram illustrating the basic set-up of an interferometer. A beam of laser light is sent to a beam splitter, where it is split into two separate beams. One of the beams is focused on a mirror (green arrows), and the other is focused on the sample (blue arrows). The direction of the beams are indicated by the coloured arrows. The reflected beams from both the mirror and the sample are transmitted to the detector, where they recombine and interfere with each other. These interference patterns reveal information about the sample surface. Adapted from [97].

The above techniques evidently have drawbacks. Both optical and electron microscopies have limited resolution, and electron microscopy techniques, with the exception of ESEM, must be performed in a vacuum. Interferometry also possesses limited x and y resolution and, although it allows the analysis of crystal growth in solution, it does not enable the direct observation of the growing features on crystal surfaces.

Over the past decade, a powerful technique, known as Atomic Force Microscopy or AFM, has come to the fore in the study of crystals and their growth, and has considerably advanced our appreciation of their detailed physical properties. In contrast to the above techniques, AFM allows the direct observation of crystal surfaces in solution, at near molecular resolution. A description of the principles of this technique, and its now almost ubiquitous use in the study of crystal growth, are presented below.

1.6 Atomic Force Microscopy.

Since its inception, atomic force microscopy (AFM) has established itself as a leading technique in the nanoscale investigation of mechanisms and rates of crystal growth. It was first reported, in 1986, to image material surfaces with high resolution in aqueous solutions, thus enabling the study of a wide range of solid-liquid interfaces [118].

1.6.1 The principles and methodology of AFM.

The theory behind AFM and its methodology are well documented [119-126] and, hence, shall be only briefly described here. Most modern instruments can be operated in both contact and tapping mode. Contact mode has been used throughout the experiments described in this thesis, and hence will be focused upon in this section.

In contact mode, an AFM probe, typically made of silicon nitride, is impressed on the surface of interest and then raster scanned over the surface. The AFM probe is a sharp stylus, analogous to a minute record player needle, which has a tip of radius approximately 5 - 40 nm. Probes which incorporate carbon nanotubes as their tips, and thus are much sharper than conventional tips, are currently under development [127]. The probe is mounted at the end of a short, flexible cantilever, typically 100 – 250 μm in length, and having a low spring constant ($< 1 \text{ Nm}^{-1}$) to minimize the force between the sample during imaging [127].

Scanning is performed by translating the probe over the sample along a continuous sequence of raster lines. As the probe tip passes over the surface, it interacts, through aggregate atomic forces, with the structural features on the surface. These interactions cause the probe to be deflected. These extremely small deflections are amplified by the deflections of a laser beam, which is reflected from the upper side of the cantilever. These deflections are subsequently detected by a position-sensitive split photodiode. Photoelectric circuitry converts the laser beam deflections into height information [118]. The resulting data, recorded as a topological image, can then be presented in a number of visual forms [127]. A diagram depicting the experimental set-up of AFM is shown in Figure 1. 4.

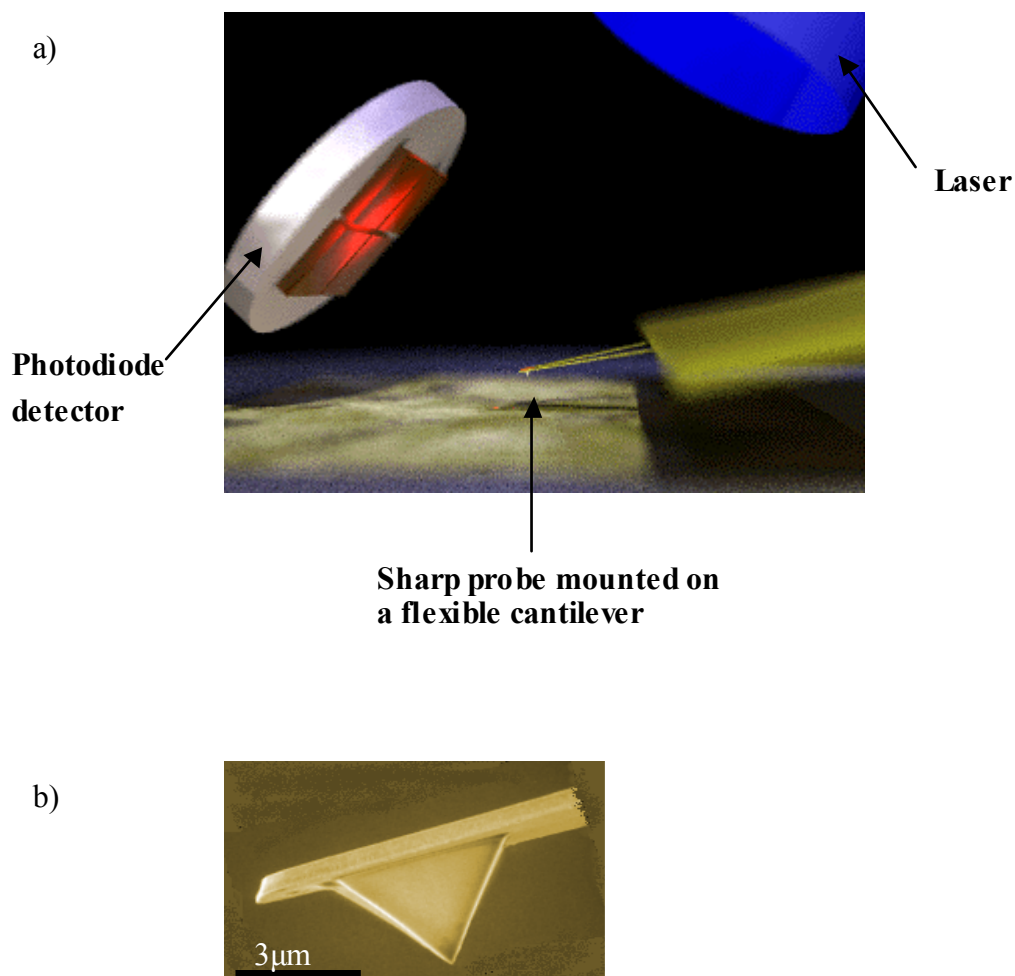


Figure 1. 4 Diagram a) depicts the experimental set-up of AFM. A sharp probe attached to a flexible cantilever is scanned across a sample surface. Any deflections of the cantilever, induced by the structural features of the sample, are amplified by the laser beam which is reflected from the upper side of the cantilever. The reflected laser beams are detected by a photodiode, and converted by the circuitry of instrument into a topographical image of the sample surface. b) shows an SEM image of an AFM probe [128].

AFM can be operated in both “height” and “deflection” modes. In the former, a feedback mechanism raises and lowers the tip, and maintains the cantilever deflection at a nearly constant level. The system monitors the piezo “height” and produces a corresponding image. In “deflection” mode, the piezo remains stationary and the actual cantilever deflection data are recorded [127].

When the AFM is operated in “height mode”, quantitatively accurate information on the surface morphology is obtained. The “deflection” mode of operation can be particularly useful for imaging surface features which vary widely in height over the field of observation [127]. Indeed, some of the images depicted in the forthcoming chapters are shown as deflection images, as their features can vary from a few nanometres to hundreds of nanometres in height.

In contact mode, AFM probes can exert a significant amount of pressure on the surface of a sample. The quality of an image depends on the degree of force exerted by the tip on the surface. The greater the force between the tip and the surface, the more sensitive the probe is to variations in height [127]. Conversely, too large a force can perturb or damage a sample surface. Although this may not be a severe limitation for robust materials such as crystals, it must be a major consideration when imaging relatively soft biological materials.

The development of tapping mode has overcome some of the problems which arise through unfavourable probe-surface interactions. During tapping mode, the probe is in intermittent contact with the sample surface, that is, it oscillates up and down as it is scanned over the surface, essentially “tapping” its way across the surface. The vertical position of the probe is continually adjusted by the feedback mechanism in order to maintain its amplitude. Tapping mode, thus, minimizes the contact between the probe and the sample surface, and greatly reduces lateral forces.

This technique has allowed the visualization of materials which would otherwise be too fragile to tolerate contact mode imaging [129-133].

1.6.2 Advantages of AFM over conventional techniques.

AFM can yield images of crystal surfaces having exceptional clarity and detail. Scan fields range in size from less than 20 nm to around 150 μm , with a lateral resolution of around 1 nm, and a vertical resolution of 0.1 nm. Thus, it provides precise visual detail over a size range that exceeds most other techniques [127]. Its application extends over the range lying between individual macromolecules, which are accessible by X-ray crystallography, macromolecular assemblies amenable to electron microscopy, and living cells, which can just be seen using optical microscopy [120, 123].

As AFM has the capacity to image in a liquid environment, samples do not undergo dehydration, as is generally the case with electron microscopy [127], and capillary forces between the tip and sample are eliminated. In addition, no fixing or staining is required, and the image contrast depends only on the relative height of the features in the image.

The benefits of AFM lie not only in its imaging capability, but also in the non-perturbing nature of the probe on interaction with the sample surface [127]. As the sample is virtually unaware of the presence of the probe, process such as dissolution and growth appear to be minimally affected [134]. Thus, a sequence of consecutive images allows the visualization of steps dissolving or growing on a crystal surface, and kinetic information to be obtained.

1.6.3 The application of AFM to the study of crystal growth.

AFM was first introduced to the field of crystal growth by Durbin and Carlson in 1992 [135], who observed the growth of steps on the surface of lysozyme crystals in mother liquor. Its subsequent application has substantially changed the way we view protein, virus, and simple molecular crystals [127]. A vast number of researchers have taken advantage of AFM to investigate the mechanisms of crystal growth. Crystalline materials whose growth has been probed using AFM range from inorganic systems, such as calcite [136, 137], potassium sulphate [138, 139], and potassium hydrogen phthalate [140], to complex macromolecules, such as insulin [130], lysozyme [38, 135, 141, 142], canavalin [143-145], catalase [141, 144], hydroxyapatite [146-148], and amylase [149].

An excellent review of the applications of AFM to the visualization of crystal growth is given by McPherson *et al.* [127].

AFM allows crystals to be observed over long periods (hours to days). Hence, it is possible to obtain precise quantitative measures of the kinetic parameters of growth to supplement the topographical data obtained through imaging [127].

In addition to exposing the crystallization process to direct visualization, AFM has provided an insight into many of the complex phenomena on which crystallization relies. It has increased the emphasis on the importance of impurities and their consequences [150], provided new information on defect structures [150], and revealed some of the mechanisms which regulate crystal growth [151]. In the case of protein crystals, these are all factors which affect their ultimate resolution and diffraction quality [36, 127, 130]. Similarly, these factors may affect the purity, morphology, and stability of drug crystals.

Although the growth of drug crystals, such as sulphathiazole [62, 90], methylprednisolone [90], ibuprofen [45] and paracetamol [24, 27, 37, 96, 97] have been investigated previously using traditional imaging techniques, such as interferometry and optical microscopy, this has not been achieved through the use of the AFM.

As previously mentioned, the optimization of drug crystallization would be aided significantly by the direct, real-time visualization of nucleation and growth, particularly with regard to observing critical nucleation events, identifying polymorphs, and examining the role of factors such as the recrystallizing solvent, supersaturation, and impurities on growth. These needs have prompted us to study the nucleation and growth of drug crystals using *in situ* AFM.

We also wish to further assess the capabilities of AFM to follow dynamic events on crystal surfaces, in particular, structural transformations. For this we have used crystalline compounds known as co-ordination polymers, which undergo anion exchange when in a solution of non-host anions. This anion exchange process is accompanied by a significant structural transformation within the crystal. Significant controversy currently surrounds the mechanism by which this anion exchange process, and its consequent structural transformation, occurs. One theory suggests that the process is solvent-mediated, whereas another hypothesizes that a solid-state transformation takes place. To date, there have been no detailed microscopic investigations of the anion exchange reactions of co-ordination polymers. We are optimistic that AFM will provide an insight into the true mechanism occurring during this process, and that these studies may pave the way for future investigations on drug crystal transformations.

1.7 Aims of the project.

The importance of crystallization processes to the pharmaceutical industry is, evidently, profound. However, despite the significant role that crystallization plays in the manufacture of drug compounds, process control, and determination of solid phase outcome, crystallization phenomena are often neglected and are, hence, poorly understood. In this project we, therefore, apply AFM to the investigation of nucleation and growth mechanisms of drug crystals.

In Chapter 2, AFM is employed to probe the growth on the (001) face of aspirin crystals at two levels of supersaturation, to assess whether the mode of growth changes with increasing supersaturation, or the kinetics of growth simply increase with supersaturation. Aspirin has been chosen for these initial studies as it has previously been imaged using AFM (its dissolution and molecular structure have been probed using AFM).

In Chapter 3, we investigate the nucleation and early stages of crystal growth by nucleating aspirin crystals on various self-assembled monolayer (SAM) surfaces. Recent findings have demonstrated the superiority of SAMs over other surfaces, such as Langmuir monolayers and functionalized polymer interfaces, in promoting nucleation and growth of oriented crystals in predetermined areas. Microcontact printing is used to pattern aspirin-binding and non-binding SAMs onto gold surfaces. The resulting templates are used to study the nucleation and fundamental growth mechanisms of aspirin crystals. AFM and SEM are utilized throughout to visualize and quantify these processes.

The studies detailed in Chapter 4 focus on the effects of impurity molecules on the morphology and growth of paracetamol crystals. We investigate the

morphology and kinetics of growth on the (001) face of paracetamol crystals in the presence and absence of two of its known structurally related additives, namely acetanilide and metacetamol. The influence of acetanilide and metacetamol on the morphology and growth of entire paracetamol crystals has previously been studied. However, there have been no investigations into the effects of these additives on the growth of individual faces of paracetamol crystals. In this chapter, we utilize both AFM and SEM to characterize the morphology of pure paracetamol crystals and those crystallized in the presence of an additive. In addition, we employ AFM to envisage and quantify the effects of these additives on growth on the crystal surface.

Finally, we employ AFM to probe the anion exchange mechanisms of two crystalline co-ordination polymers, namely $\{[\text{Ag}(4,4'\text{-bipy})]\text{BF}_4\}_\infty$ and $\{[\text{Ag}(4,4'\text{-bipy})]\text{NO}_3\}_\infty$, in Chapter 5. As previously mentioned, there is, currently, significant controversy surrounding the mechanism by which this anion exchange process, and its consequent structural transformation, occurs. The acquisition of *in situ* AFM data may reveal the true mechanism occurring during this process.

Chapter

2

An in situ study of the effects of supersaturation on aspirin crystal growth.

AFM has been extensively used in the investigation of growth of a plethora of crystalline compounds. However, to date, it has not been used to probe the growth dynamics of any pharmaceutical drug crystal. In this chapter, we use AFM to assess the mechanisms and kinetics of growth on the (001) face of aspirin crystals at two levels of supersaturation. Supersaturation is known to have profound effects on both the morphology and, at the molecular level, the growth mechanisms of crystals. We envisage that these experiments will pave the way for future studies on the other parameters which affect drug crystal growth, such as temperature, pH, and impurity concentration. Such studies would provide essential, fundamental information, to the pharmaceutical industry on the growth of drug compounds, and would facilitate the optimization of drug crystallization.

2.1 Introduction

2.1.1 The effects of supersaturation on crystal growth.

Significant uncertainty still remains over many fundamental aspects of crystallization, including the evolution and activity of growth modes as a function of supersaturation, the effect of defects on nucleation and step motion and, perhaps most importantly, the pathway by which ions or molecules leave the solution and become units within the crystal lattice [143]. Increased understanding of these events would potentially lead to a greater degree of control over the rate of crystallization, resulting crystal size, habit, and polymorphic form.

As highlighted in Chapter 1, supersaturation (σ) can have a profound affect on crystal growth, resulting in morphological changes in the crystallizing compound over a range of supersaturations [24, 27, 29, 36-38]. Supersaturation induces these effects by altering the modes of growth on the faces of crystals, as a function of the σ of the growth medium [143, 145, 152].

There are three main mechanisms by which growth can occur on a crystal surface, each of which may be favoured within a particular σ range. These are:

- i) The Dislocation mechanism,
- ii) Two-dimensional (2D) nucleation, and
- iii) Three-dimensional (3D) nucleation.

The σ ranges over which each of these modes of growth are prevalent are specific to individual compounds, however, in general, the dislocation mechanism is favoured at low σ , with 2D and 3D nucleation favoured at moderate and high σ respectively [152, 153]. Low σ is defined as the concentration of the solute just above its

solubility in the solvent; i.e. slightly above equilibrium. High σ is defined as the concentration slightly below that which allows the formation of visible microcrystals in the growth medium. The three modes of growth are described and illustrated in the following sections.

2.1.2 The dislocation mechanism of growth.

A dislocation on the crystal surface results from stresses which occur during crystal growth. These induce sections of the crystal to become misaligned with respect to their neighbouring areas [1, 98]. The origin of a dislocation and the growth pattern which emerges from it are illustrated in Figure 2. 1. The arrows shown on Figure 2. 1a) represent the displacement of the two sections of the crystal. As a result, a ledge is formed onto which molecules can absorb and continue growth. However, as the ledge is of non-uniform height, growth occurs in a spiral pattern around the dislocation, and the growth mechanism is often referred to as screw dislocation [98, 103]. The features which arise from growth around such a dislocation are growth hillocks, illustrated in Figure 2. 1b) and c). A screw dislocation hillock is shown from above and from the side, with the corresponding layers indicated by dashed red lines. Dislocations may be simple or complex in nature, that is, they may consist of only one misaligned section, or may be composed of a series of dislocation sites within the same area. When two or more dislocations emerge onto a crystal face in close proximity, the resulting spirals may co-operate to produce a step source with an activity greater than that of a single dislocation spiral [98]. For such co-operation to take place, the separation of the spiral centres must be less than half of the step spacing of an isolated spiral. In these instances, dislocations grow around each other,

leading to a more complex structure than that depicted in Figure 2. 1b) and c). More widely separated spirals exhibit an activity that is no greater than that of an isolated spiral [140]. The presence of simple or complex dislocations ensures the permanent existence of steps on the surface during growth [98]. As the steps grow away from their dislocation source, they progressively lose the curved appearance they possessed when they originated from the dislocation, becoming straighter and forming step trains [143].

This dislocation mechanism is favoured at low σ because the dislocations provide an inherent source for growth, and render it unnecessary to produce further growth sources, such as required for 2D and 3D nucleation, which are energetically more expensive.

Growth via the dislocation mechanism has been observed, using AFM, at low σ on crystals of amylase [149], canavalin [143, 145, 154, 155], thaumatin [141], lysozyme [38, 141], xylanase [141], and tRNA [152].

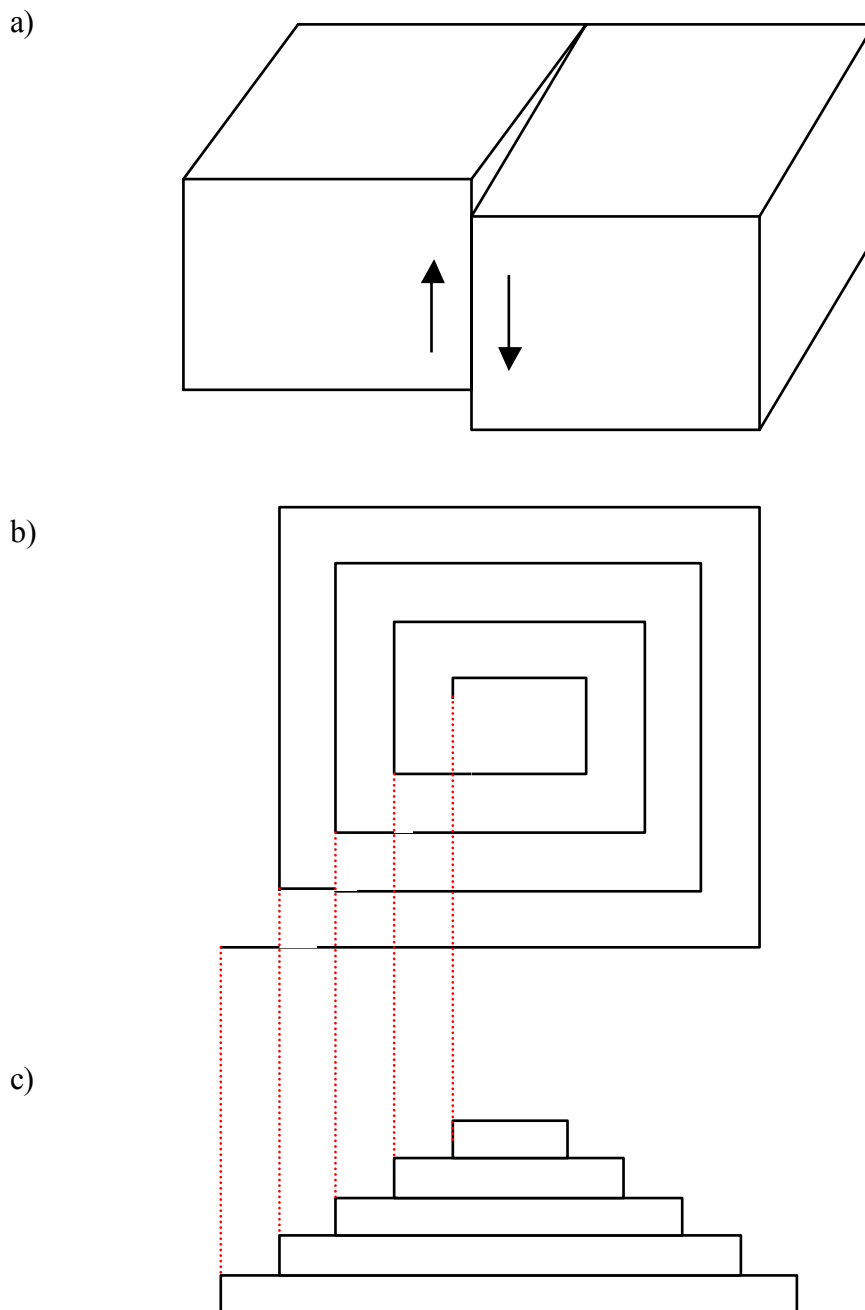


Figure 2. 1 Diagram demonstrating the origin and growth of a dislocation. a) illustrates the displacement of the two sections of the crystal, indicated by the arrows. The resulting dislocation facilitates the attachment of molecules to the surface, and promotes a spiral growth pattern around the dislocation. The features which arise from such growth are hillocks, illustrated in b) and c). A dislocation hillock is shown from above (b) and from the side (c), with the corresponding layers indicated by dashed red lines.

2.1.3 2D nucleation.

2D nucleation occurs when an island of molecules adsorb onto the crystal face, thus providing the basis for a new crystalline layer. Attachment of further molecules to the newly formed step edges of the nucleus allows the new layer to spread across the entire crystal face [103]. It is clear that the formation of 2D nuclei on the surface of a crystal would require more energy than the simple attachment of molecules to existing growth sites, such as dislocations [103]. 2D nuclei can form at moderate σ because the greater concentration of solute in the growth medium induces a larger degree of solute-solute collisions and, therefore, solute-solute interactions. The formation of a two-dimensional layer of solute molecules is, thus, more feasible at moderate than at low σ . Hence, 2D nucleation typically occurs at higher σ values than dislocation facilitated growth, or on surfaces which lack dislocations.

The first successful observation of dislocation-free growth from aqueous solution by Kuznetsov *et al.* [156] paved the way for studies on growth by 2D nucleation. These studies lead to the proposal of the model of multiple 2D nucleation [103]. This model suggests that 2D nuclei appear independently at various points on a crystal faces and, upon reaching each other, they merge to complete the next lattice layer on this face [103]. This process has been observed using AFM [135]. A diagram illustrating the formation and growth of 2D nuclei is shown in Figure 2. 2.

Growth via 2D nucleation at moderate σ has been observed, using AFM, on crystals of amylase [149], canavalin [143], thaumatin [141], lysozyme [38, 141], catalase [141], xylanase [141], and tRNA [152].

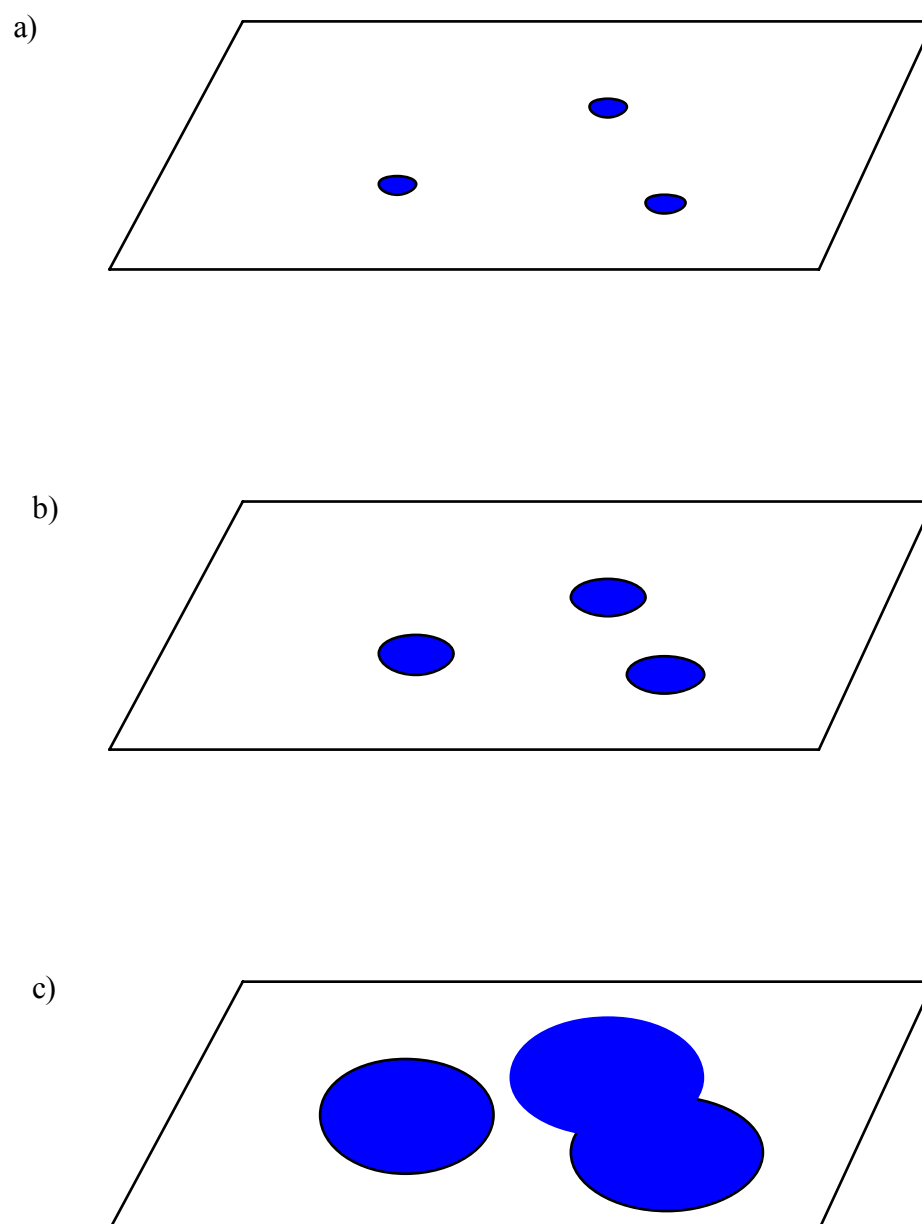


Figure 2. 2 Diagram illustrating the formation and growth of two-dimensional (2D) nuclei on a crystal face. In a) the 2D nuclei deposit onto the surface. Growth of these nuclei occurs via attachment of molecules to their edges, allowing them to spread across the face (b) and coalesce when they meet (c).

2.1.4 3D nucleation.

3D nucleation is an unusual growth phenomenon, and one that appears to be unique to macromolecular protein and virus crystals [127]. At high σ , three-dimensional aggregates, composed of hundreds to thousands of molecules, form in the growth medium. These aggregates exhibit short-range order, maintained by non-specific hydrophobic interactions and random arrangements of hydrogen bonds [127, 144]. Upon sedimentation on the crystal surface, these aggregates develop in one of two ways. They either restructure immediately to form crystalline, multilayer stacks, known as 3D nuclei, or form faceted microcrystals on the surface of the crystal.

The formation of 3D aggregates is analogous with that of 2D nuclei. As the concentration of solute molecules in the growth medium increases, the number of solute-solute collisions and interactions increases further. Therefore, at high σ values 3D solute structures can form in solution and adsorb to crystal surfaces, providing potential 3D nuclei or microcrystals.

Kuznetsov *et al.* [144] proposed that the degree of conformity between the underlying crystal surface and the depositing aggregate, is likely to be the determining factor in whether the aggregate develops as a 3D nucleus, or a microcrystal. In the former case, the conformations are virtually exact, so that bonds between the substrate crystal and the aggregate interface align in a periodic manner. The aggregate then becomes an ordered extension of the substrate crystal. In the case of microcrystal formation, the underlying crystal promotes the formation of a crystalline state in the aggregate, but there remains physical or mechanical discontinuity, or misalignment between the two. Hence, they do not grow as a single entity, but as two individuals.

3D nuclei restructure on crystal surfaces, forming plateaus with step bunches. 3D nuclei grow epitaxially on the crystal, without introducing defects, and their step trains merge with those of the growing crystal, and other 3D nuclei [127, 141, 145]. Growth in the normal direction occurs due to the deposition of 2D nuclei on the terraces of the 3D nuclei [141].

The deposition and growth of 3D nuclei on a surface are illustrated in Figure 2. 3a). Growth via 3D nucleation at high σ has been observed, using AFM, on crystals of canavalin [143, 145, 157], tRNA [152], lysozyme [157], lipase [157], satellite tobacco mosaic virus (STMV) [151, 157-159] and thaumatin [157, 160].

The lack of continuity between the underlying crystal and the microcrystal results in it becoming incorporated into the growing crystal. The incorporation of microcrystals that have become embedded into the growing crystal surface, has been observed to generate defects such as complex dislocation sources, areas with misaligned lattices, and stacking faults [145]. All of these defects degrade the quality of the crystal, but provide sources for addition of further solute molecules, and growth on the surface. The deposition and incorporation of microcrystals are depicted in Figure 2. 3b). The incorporation of microcrystals into catalase [141, 161], lysozyme [38], and STMV crystals [159], at high σ , has been visualized using AFM.

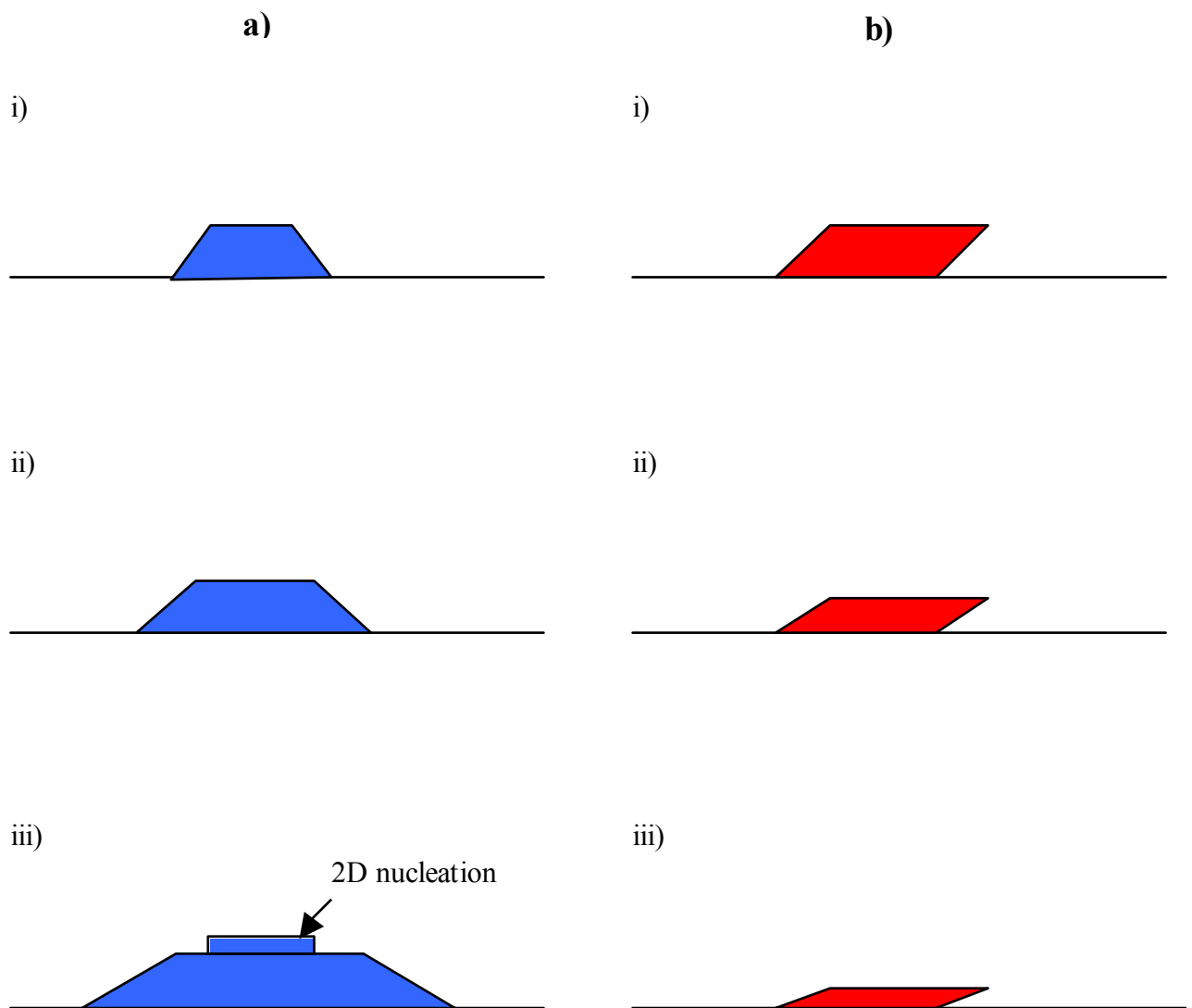


Figure 2. 3 Diagrammatic illustration of the deposition of 3D aggregates on the surface of a crystal, their development into 3D nuclei (a) or microcrystals (b). In a) i) the aggregate restructures immediately to form a crystalline, multilayer stack, known as a 3D nucleus. The layers of steps within the 3D nucleus grow tangentially (ii), and growth in the normal direction occurs due to the deposition of 2D nuclei on the terraces of the 3D nucleus (iii). In b) i) the aggregate is misoriented with respect to the underlying crystal, and hence forms a microcrystal. Its lack of congruence with the crystal renders it unable to grow on the surface, and it progressively becomes incorporated into the growing crystal, as shown in ii) and iii).

In general, an individual crystal does not grow exclusively by a single mechanism. It may employ different mechanisms on different crystal faces, and these may vary at different σ values [127]. Although the mechanisms of growth described in the preceding sections are typical at their respective σ , some compounds do not alter their growth mode with increasing σ . For example, the growth on the (001) face of $K_2Cr_2O_7$ crystals occurs solely via the dislocation mechanism at all the σ values investigated [162]. Similarly, the growth of the (001) face of catalase crystals proceeds exclusively by 2D nucleation at all σ ranges [141], as does growth on the (110) face of lysozyme crystals [142].

Conversely, some crystals grow via more than one mechanism at a particular σ . This is the case for cadmium mercury thiocyanate crystals, upon which growth proceeds via the dislocation mechanism and 2D nucleation simultaneously [163].

2.1.5 Terrace-Ledge-Kink (TLK) model.

All of the growth sources described above provide growth steps in either a continuous (dislocation mechanism) or discontinuous (2D and 3D nucleation) manner, and then proceed tangentially over the face of the crystal by addition of molecules to their step edges [127]. The attachment of molecules to each of these growth sources is hypothesized to occur via the Terrace-Ledge-Kink (TLK) model [98]. Although step edges may appear to be smooth, on an atomic scale they are blurred by thermal fluctuations, giving rise to kinks. The TLK model, which is illustrated in Figure 2. 4, proposes that a solute molecule (α) adsorbs to the terrace regions of the crystal surface and migrates across the surface (β) to the ledge of a step (γ). Here it can occupy a vacant kink site (δ) which exists in the ledge. The

subsequent adsorption, migration, and attachment of further solute molecules to crystal surfaces in this manner, facilitates the growth of steps across the terraces, and consequently the growth of the crystal faces.

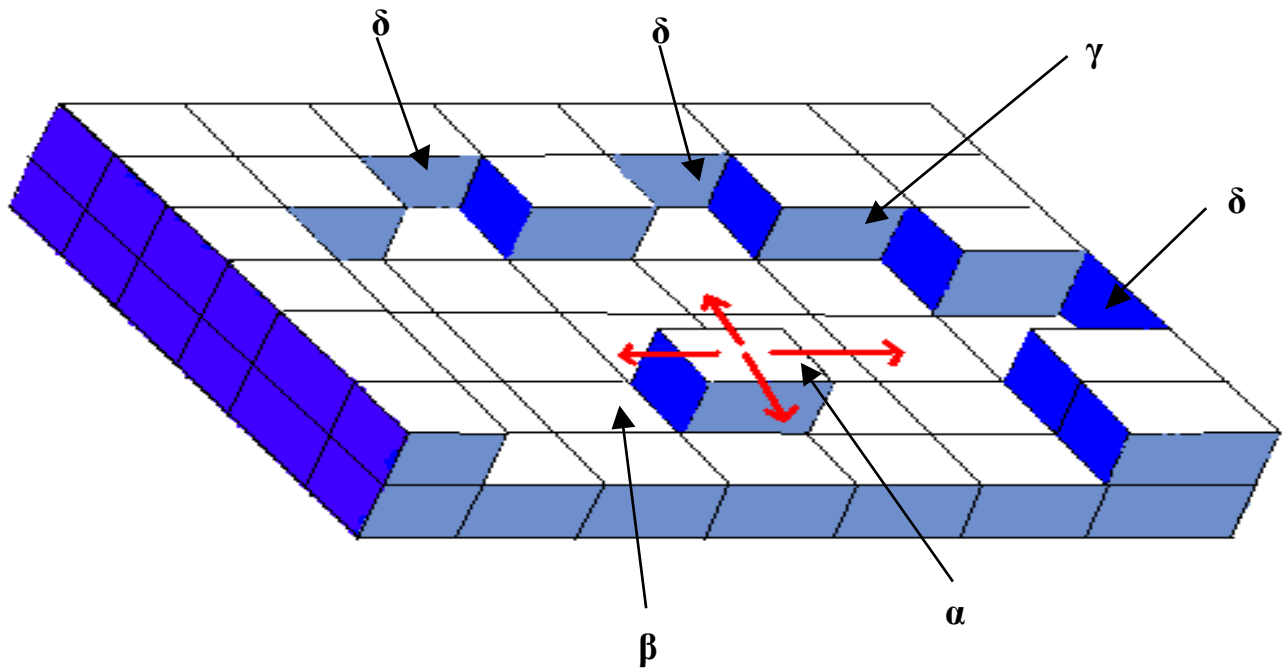


Figure 2. 4 A schematic diagram of the Terrace-Ledge-Kink (TLK) model of crystal growth. In this model, a solute molecule adsorbs to the crystal terrace (adatom, α) and migrates across the terrace (β) to the ledge of a step (γ). Here it can occupy a vacant kink site (δ). The further addition of such adatoms to kink sites results in the progression of a step across a terrace.

As mentioned in Chapter 1, the growth of drug crystals such as sulphathiazole [62, 90], methylprednisolone [90], ibuprofen [45] and paracetamol [24, 27, 37, 96, 97] have been investigated previously using traditional imaging techniques, for example, *in situ* interferometry and optical microscopy. The observation of drug crystal growth has not, to date, been achieved through the use of AFM. This technique has, however, been utilized to probe aspirin crystals in order to obtain molecular resolution images of their surfaces [164, 165], to identify specific faces [166], and to investigate the relative dissolution behaviour of its (100) and (001) faces [134].

AFM has proved its capabilities in following the growth of many crystalline compounds [38, 130, 135-149] and has, in addition, revealed how their growth mechanisms and growth kinetics change as a function of σ [38, 143, 152]. In this chapter, we propose to use AFM to study the effects of σ on the growth of the (001) face of aspirin crystals.

2.1.6 Aspirin: a brief history.

Aspirin, the trade name for the compound acetylsalicylic acid, has roots which can be traced back to the fifth century B.C., when the Greek physician Hippocrates used a bitter powder obtained from the bark of willow trees to treat pain and fever [167]. The pain-relieving constituent of the willow bark was salicin, the parent of the salicylate drug family of which aspirin is the best known. The predecessor of aspirin was sodium salicylate, which was developed in 1875 and used as a general pain reliever. However, it had one serious side effect in that it induced severe stomach irritation. This made sodium salicylate intolerable to many patients, including the father of Bayer chemist Felix Hoffmann. In 1897, Hoffmann endeavoured to develop

a drug which would ease his father's arthritis without causing such stomach discomfort. His search led him to synthesize acetylsalicylic acid, a compound which shares the therapeutic properties of sodium salicylate, but causes less irritation [168]. Acetylsalicylic acid was first synthesized by Bayer in 1897, and was given the name Aspirin in 1899 [169]. Needless to say, it quickly became the preferential pain reliever of physicians.

Aspirin is a non-steroidal anti-inflammatory drug (NSAID) which is commonly used to alleviate headaches, muscle pain, arthritis, and fever. It is estimated that around 80 billion aspirin tablets are consumed in America every year [169]. In 1971, Vane [170] discovered the mechanisms underlying the therapeutic effects of aspirin. Vane found that aspirin interferes with the biosynthesis of prostaglandins, and in 1982, he was awarded the Nobel Prize in medicine in recognition of his work. The elucidation of the mode of action of aspirin paved the way for its use in the prevention of heart attacks and strokes.

Aspirin was chosen for the current study because it is easily and reproducibly crystallized, its crystal structure is well characterized [44, 171-176], and it has previously been imaged using AFM [134, 164-166].

2.1.7 Aims of chapter.

The modes of growth of drug crystals have, as yet, only been studied using the traditional imaging techniques of optical microscopy and interferometry. AFM has been widely applied to investigations into the effects of supersaturation on the growth of protein and virus crystals, as the growth of these substances is slower than that of molecular crystals, and, hence, is easier to observe. In this chapter we will use

AFM to probe the mechanisms of growth on the (001) face of aspirin crystals at two levels of σ . From these data, we will assess whether the growth mode changes with increasing supersaturation, as seen with tRNA [152] and canavalin [143, 145] crystals, or whether it remains the same, but the kinetics of growth increase, as observed with $K_2Cr_2O_7$ [162], catalase [141], and lysozyme crystals [142].

2.2 Methods and Materials

2.2.1 Preparation of aspirin crystals and growth media.

Aspirin crystals were prepared using the method described by Tawashi [177]. U.S.P. grade aspirin (Sigma Aldrich, Dorset, U.K.) was dissolved to saturation in 100ml of 95 % ethanol (Sigma Aldrich, Dorset, U.K.). This solution was maintained at 37°C with a stirring rate of 238 rpm until all of the solute had dissolved. It was then slowly cooled over a period of hours to room temperature. Typically after 24 hours crystallization was complete and crystals were filtered, washed with cold ethanol, air-dried and stored in a desiccator. Crystals were immobilized on AFM sample stubs, and then onto a suitable liquid cell using Temp fix (A gar, Stansted, U.K.).

Growth solutions were prepared by dissolving 0.054g and 0.057g of U.S.P. grade aspirin (Sigma Aldrich, Dorset, U.K.) in 10 ml HPLC grade water, which had been filtered once. These solutions were heated to approximately 40°C, with a stirring rate of 238 rpm, until all of the solute had dissolved. They were then allowed to cool to room temperature, before being placed in the AFM liquid cell with an aspirin crystal sample. Approximately 2.5 ml of supersaturated aspirin solution was

placed in the liquid cell as a growth medium in each experiment. The σ values of the solutions used as growth media were calculated using the following equation [7, 24, 27, 29, 132, 142]:

$$\sigma = \ln (c/c_0) \quad \text{Equation 2.1}$$

where c_0 is the concentration of aspirin in a saturated solution, i.e. the solubility of aspirin at a given temperature, and c is the concentration of aspirin dissolved in the growth medium. All experiments were carried out at 23.5°C: the solubility of aspirin in water (c_0) at this temperature is 0.022 mol. kg⁻¹ [178]. The σ values of the two growth media used were calculated as 0.31 and 0.36, respectively. These solutions were chosen as the growth media as they were in the range of σ values where growth occurred on the surface. Solutions with $\sigma \leq 0.15$ were observed, with AFM, to induce dissolution on the surface of the crystals. Conversely, solutions of $\sigma \geq 0.48$ allowed the formation of visible microcrystals in the growth medium. Thus, at this σ , the nucleation of new crystals was more favourable than growth on the existing crystal. Similar observations have been made during studies on paracetamol crystal growth [37].

2.2.2 AFM analysis.

Contact mode imaging was employed throughout, using a ThermoMicroscopes Explorer AFM (Veeco, Bicester, Oxon, U.K.). V-shaped silicon nitride cantilevers (200 μ m length) with integrated pyramidal tips (Nanoprobes, Veeco, Santa Barbara, CA) and spring constant ranging from $k = 0.01 - 0.064$ Nm⁻¹ were used. When scanning, care was taken to continually adjust the set point voltage to the lowest value for which tip-crystal contact could be maintained, in order to minimize the

force applied to the crystal surface. The utilization of minimal force has allowed the crystal surfaces of various compounds to be imaged during growth without degradation of their growing steps [135, 143, 145].

The speed of acquisition of the images was determined by the rate of change of the features on the crystal surface. The employed scan rate was typically 10 Hz. Both topography and deflection images were acquired in all experiments. The topography images are a result of the deflections of the laser beam, and thus the cantilever, upon interaction with the underlying sample surface. These deflections are converted, by the photoelectric circuitry of the instrument, into height data. Deflection images emphasize areas of rapid topography changes, such as steps, but do not give any information about relative heights of features on the surface.

A video clip of growth in a $\sigma = 0.36$ solution, composed of over one hundred AFM topography images, was compiled using Take One software (Rainer Döele, Tuttlingen, Germany) and is available on the attached disk.

The possibility of instrumental drift during or between scans was considered. An AFM calibration grid (Veeco, Bicester, Oxon, U.K.) was imaged sequentially, in HPLC grade water, at the same scan rates as those used in each experimental set up. The grid was composed of SiO₂ raised features on a silicon surface. The grid was affixed to an AFM sample stub, and then onto a suitable liquid cell using Tempfix (Agar, Stansted, U.K.). A typical image of the AFM calibration grid is shown in Figure 2. 5. The dimensions of the repeating components within the calibration grid are 2.4 μm x 1.5 μm . We utilized the software available on the AFM, which allowed each image to be subtracted from the previous image in the sequence, to assess whether any drifting had occurred during scanning. Our measurements on the subtracted images indicated that negligible drift occurred in both x and y directions.

The steps observed in the image sequences seldom grew in the x or y directions and, therefore, trigonometry had to be used in order to calculate the actual distance moved by the step in the time period between images. Figure 2. 6 is a schematic illustration of the method used to calculate the growth rate of a step. If we consider the growth of a step, within a certain time period, as the movement from point A_0 to the point A_1 , then the actual distance moved by the step is a nm. By measuring the horizontal distance moved by the step, x , a can be calculated using the equation:

$$a = x / \cos\theta \quad \text{Equation 2.2}$$

As the time of acquisition of each image was known, the rate of growth of steps could be calculated in nm/s.

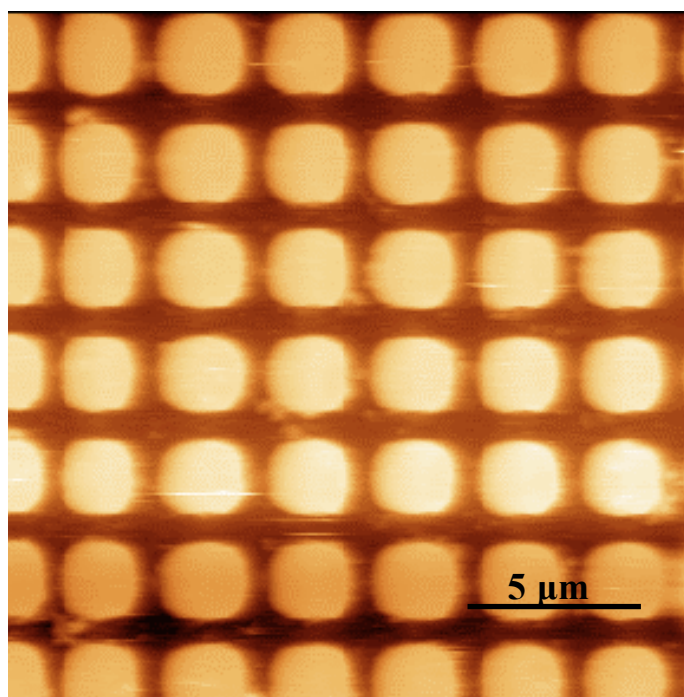
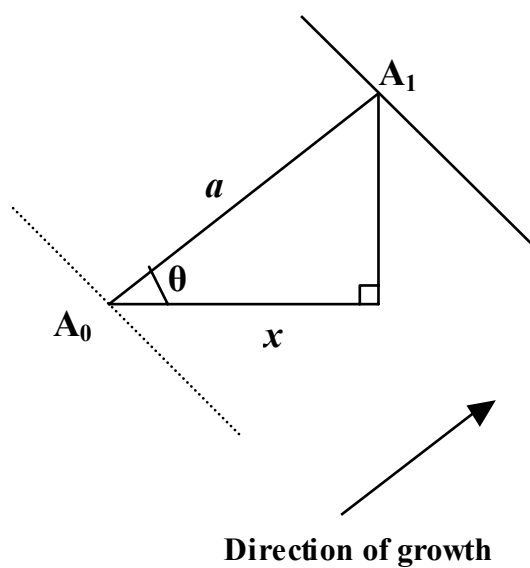


Figure 2. 5 A typical 20 μm x 20 μm AFM topography image of the calibration grid used to assess the extent of instrumental drift occurring during imaging.



Distance grown by step = a

$$\cos\theta = x / a$$

therefore, $a = x / \cos\theta$

Figure 2.6 A schematic illustration of the method used to calculate the growth rate of steps. The point A_0 on the dashed line is the initial position of the growing step, and A_1 on the solid line is the final position of the growing step over a certain time period. The actual distance moved by the step is a nm. Both x and θ can be measured directly and, hence, a can be deduced from the equation above.

2.3 Results and Discussion

2.3.1 Growth on the (001) face at $\sigma = 0.31$.

A diagrammatic representation of a single aspirin crystal which has been recrystallized from a saturated ethanolic solution is displayed in Figure 2. 7. The Miller indices are depicted on each face, the most prominent of these is the (001) face upon which all experiments are carried out. Typical images of this face exposed to a solution with $\sigma = 0.31$ are shown in Figure 2. 8. The actual number of experiments from which this data is calculated is six. This sequence of images displays the movement of steps, varying from 1 nm in height, which corresponds to the unit cell height of aspirin of 1.14 nm [172], to macrosteps which are 85 nm in height. The development of macrosteps occurs as the growing steps merge. As the distance from the growth centre increases, the height and mutual separation of the macrosteps is known to increase [162]. On $K_2Cr_2O_7$ crystals, steps which had originated at dislocations were observed to exceed hundreds of nanometres in height [162].

The speed of acquisition of the images is determined by the rate of change of the features on the crystal surface. In this instance, the raster image time is approximately 87 secs. The time of acquisition of each image is indicated in the figure legend. The growth of one particular step across the surface is indicated by a black arrow on each image in Figure 2. 8. Growth occurs predominantly in the [100] direction, with negligible growth occurring in the [010] direction. The observed steps have growth rates ranging from 4.6 nm/s – 10.8 nm/s, with an average of 7.2 nm/s, and show no correlation between step height and growth rate. This lack of

congruency between step height and growth rate has also been observed on hydroxyapatite crystals [146]. The mode of growth of steps at this level of σ follows that of the dislocation mechanism. Although the dislocation centre is not visible, the steps are rounded in appearance, indicating that they have spiralled around a dislocation source.

It is important to note that aspirin can undergo ester hydrolysis to salicylic acid and acetic acid [134, 179] as shown in Figure 2. 9, and that these impurities may potentially influence the growth mechanisms or kinetics of the aspirin crystal. The molecular structure of the growing face is illustrated in Figure 3. 15 and indicates that the ester group of the aspirin molecule is exposed at the (001) surface. The expression of the ester groups at the surface provides a potentially reactive site for hydrolysis by the growth medium. The lack of correlation between the height and velocity of the growing steps may indicate that acid catalysed hydrolysis is occurring. However, the pH of the growth solutions used here is approximately 2. Figure 2. 10 illustrates the dependence of the rate of aspirin hydrolysis on pH, at 17°C [180]. From Figure 2. 10, it is evident that the rate constant (k) for the hydrolysis of aspirin at this pH is merely 0.05 day^{-1} [180]. Although our experiments are carried out at 25°C, we assume that a similarly low rate of hydrolysis occurs. In addition, growth solutions are freshly prepared immediately prior to each experiment, and crystal samples are exposed to the growth media for a matter of hours, thus reducing the potential for hydrolysis to take place. It is therefore unlikely that the trace amounts of the products of hydrolysis, salicylic acid and acetic acid, would have a significant effect on the growth mechanisms and kinetics observed in these experiments.

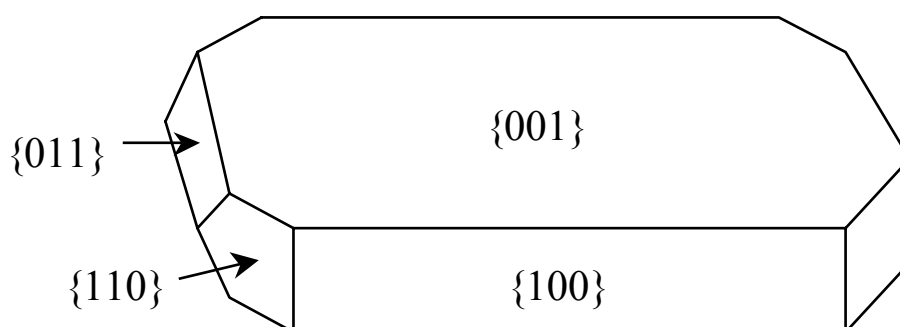


Figure 2. 7 A diagrammatic representation of an aspirin crystal recrystallized from a saturated ethanolic solution. The respective Miller indices are depicted on each face
Adapted from [44].

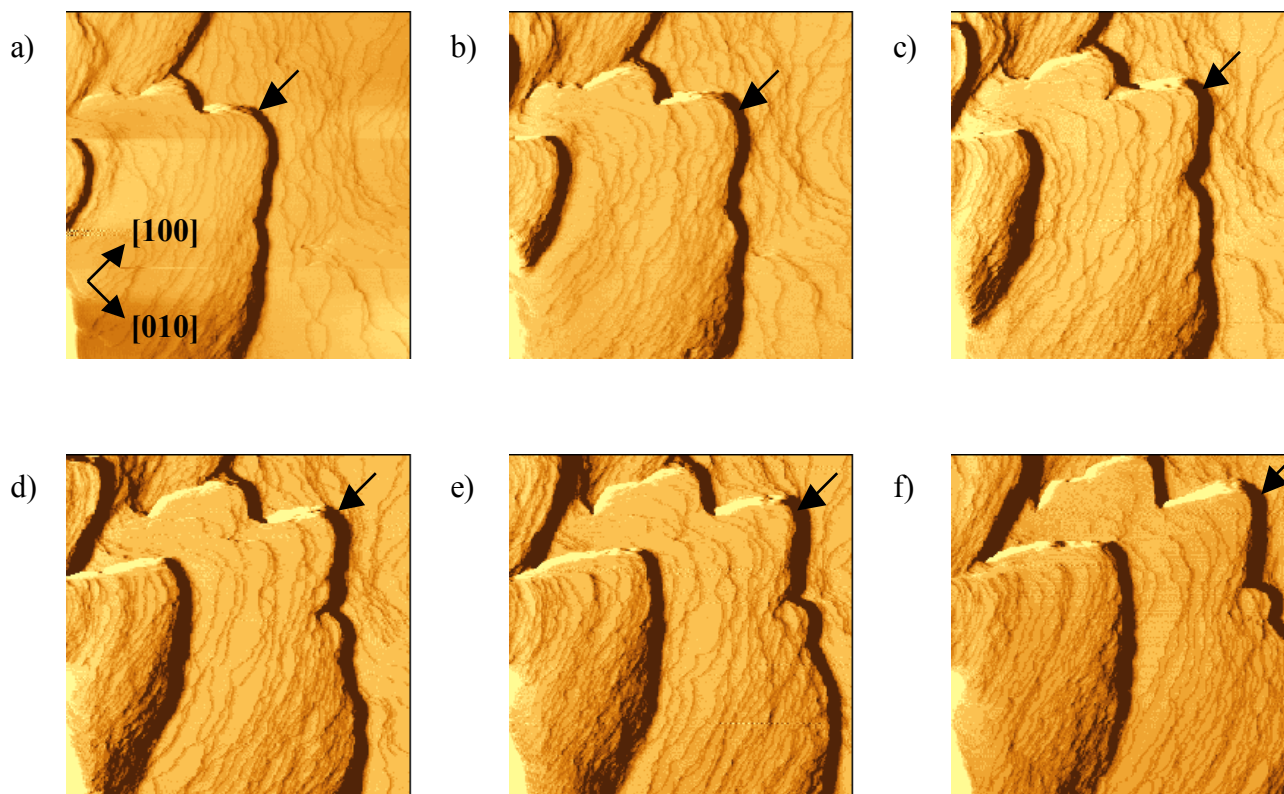


Figure 2. 8 A sequence of 10 μm x 10 μm AFM images of the (001) face of an aspirin crystal during incubation in a solution of supersaturation 0.31. In image a) time $t = 0$ secs, b) $t = 102$ secs, c) $t = 188$ secs, d) $t = 275$ secs, e) $t = 361$ secs, and f) $t = 448$ secs. All images are deflection images.

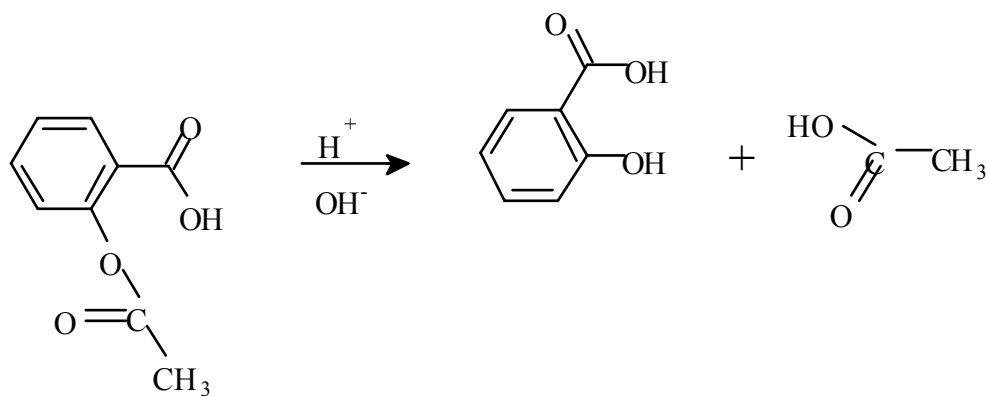


Figure 2.9 A schematic illustration of the ester hydrolysis of aspirin.

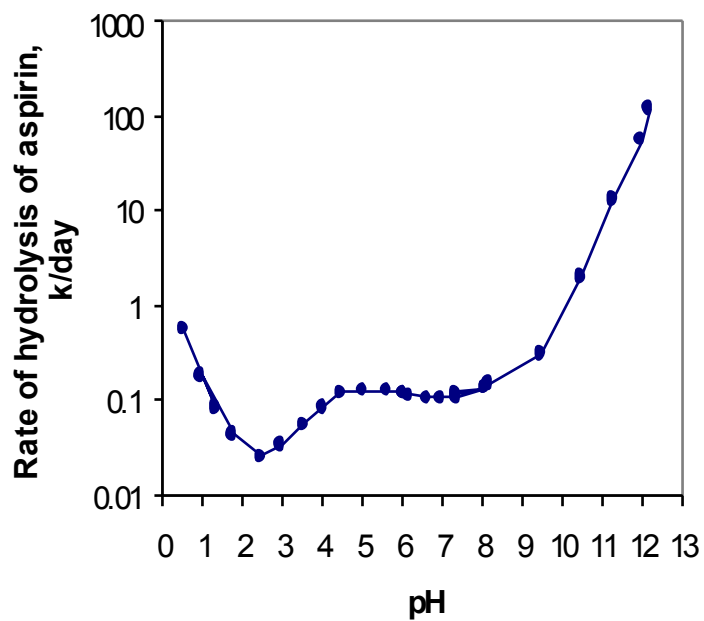


Figure 2. 10 A graph illustrating the dependence of the rate ($k \text{ day}^{-1}$) of aspirin hydrolysis on pH, at 17°C . Adapted from [180].

Growth via other phenomena, such as 2-dimensional or 3-dimensional nucleation, was not observed. However, growth via these methods has been observed only at much higher σ on canavalin [145], catalase [161], and thaumatin [160] crystals, and therefore the presence of such growth modes for aspirin at higher levels of σ cannot be dismissed.

2.3.2 Growth on the (001) face at $\sigma = 0.36$.

Figure 2. 11 shows a series of images of the (001) face exposed to a solution with $\sigma = 0.36$. Growth on the crystal surface occurs implicitly via the dislocation mechanism. Again no 2D or 3D nuclei are evident, and the dislocation source is not visible in any of the images. The morphology of the steps is different to those observed in Figure 2. 8, which appear rounded. The growing steps visible in Figure 2. 11 are straighter, which may infer that they are a greater distance from the source of the dislocation, and may thus have formed step trains [143]. The fact that 2D nuclei were not observed indicates that the $\sigma = 0.36$ solution does not provide enough driving force to create 2D islands. This infers that the steps on the surface must emanate from dislocation sources and, thus, the dislocations supply all of the new steps on the crystal face.

From the sequence of images in Figure 2. 11, it is apparent that the steps grow in both [100] and [010] directions. The growth of two steps, one in the [100] and one in the [010] direction, are indicated by a black and a white arrow on the images. A video clip, composed of sequential AFM topography images of growth in this medium, is available on the attached disk in the file asp_crys.avi. It should be

noted that there is no evidence of 2D or 3D nuclei in any of the images which comprise the video.

The steps growing in the [100] direction vary in height from 1 nm to 315 nm, and grow at rates ranging from 17.4 nm/s to 34.5 nm/s, showing no correlation between step height and growth rate. The average growth rate of these steps is 25.7 nm/s. The steps which advance in the [010] direction ranging height from 1 nm to 365 nm, and their growth rates range from 6.0 nm/s to 17.0 nm/s. Again, there is no correlation between step height and growth rate, and the average growth rate of the steps is 10.7 nm/s.

From these data, it is clear that, as σ increases, there is a concurrent increase in both the heights and growth rates of steps growing in the [100] direction. Such observations have been noted using AFM, as a function of σ , for other crystals including lysozyme [38, 142], thaumatin [181], $K_2Cr_2O_7$ [162], hydroxyapatite [148], canavalin [143], and apoferritin [132], and are consistent with theoretical implications [103].

The proposed reason for the observation of larger macrosteps at higher σ is as follows. As steps grow, fluctuations in the local temperature or σ can alter their growth rate. This leads to the non-uniform growth of steps. As a result, faster-growing steps merge with slower-growing steps, thus increasing the height of the cumulative step. This process is commonly referred to as step bunching. As the step height increases, the diffusion fields which surround the individual steps within the bunch overlap [103, 143, 182-187]. A greater degree of step bunching leads to a more complete overlap of the diffusion fields and, thus, lowers the σ in the direct vicinity of the step bunch. This, in turn, decreases the growth rate of the complete macrostep [103]. It has been established that the growth rate of steps increases with σ

[38, 142, 143, 148, 153, 162, 181] and, hence, more steps bunch per unit time at higher σ than at lower σ . As a result, larger macrosteps are formed at higher σ .

The average growth rate of steps in the [100] direction at $\sigma = 0.31$ and $\sigma = 0.36$ is calculated as 7.2 nm/s and 25.7 nm/s respectively. Therefore, at $\sigma = 0.36$, the growth rate of the steps is a factor of 3.6 times higher than at $\sigma = 0.31$, irrespective of the larger macrosteps observed at $\sigma = 0.36$.

In addition, this increase in σ from 0.31 to 0.36 promotes the growth of monomolecular and macrosteps in the [010] direction. However, the growth rates of steps in each direction are not comparable, that is, they are anisotropic. Step anisotropy has previously been observed on crystals of thaumatin, catalase, lysozyme, xylanase [141], and potassium hydrogen phthalate [140], and was shown to depend on σ [141]. Under identical σ conditions, the growth rates of steps on thaumatin and catalase crystals were shown to vary up to five fold [141]. It is probable that the step anisotropy arises due to the difference in molecular structure of the steps advancing in different crystallographic directions [93, 135, 141].

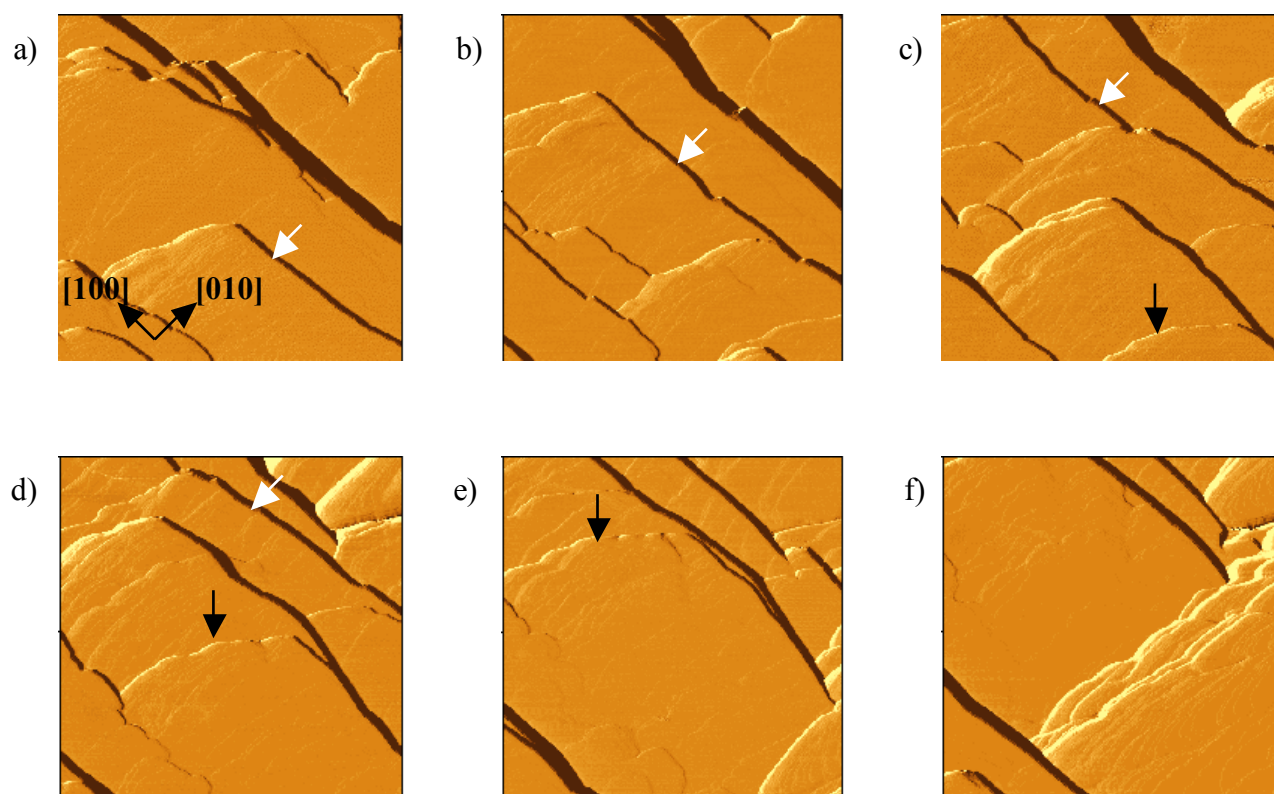


Figure 2.11 A sequence of $20\ \mu\text{m} \times 20\ \mu\text{m}$ AFM images of the (001) face of an aspirin crystal during incubation in a solution of supersaturation 0.36. In image a) time $t = 0$ secs, b) $t = 288$ secs, c) $t = 576$ secs, d) $t = 864$ secs, e) $t = 1152$ secs, and f) $t = 1440$ secs. All images are deflection images.

These data may suggest that growth on the (001) face of aspirin crystals occurs solely via the dislocation mechanism at all values of σ . Similar observations have been made using AFM on the (001) face of $K_2Cr_2O_7$ crystals [162]. However, as dissolution was observed at $\sigma \leq 0.15$, and at $\sigma \geq 0.48$ microcrystals were visible in the growth medium, the range of σ values over which growth on the surface occurs is relatively narrow. The two σ values investigated in this chapter are, according to this range, moderate to high. As the dislocation mechanism is the most energetically favourable at low σ , due to the fact that they provide an intrinsic source of growth steps, we assume that at σ values lower than those studied here, growth would again progress via the dislocation mechanism.

It is therefore necessary to conduct similar experiments on the crystal face at higher σ to assess whether 2D or 3D nucleation become the prevalent growth mechanism at any level of σ .

It would also be beneficial to carry out experiments on the other faces of aspirin crystals. The (001) face is the largest of the crystal faces and, hence, it has the slowest growth rate. Therefore, at the σ values used here, alternative growth mechanisms could be taking place [127], allowing the remaining faces to advance faster.

2.4 Conclusion

We have used AFM to directly visualize, *in situ*, the mechanisms of growth which occurred on the (001) face of aspirin crystals at two levels of σ . AFM also allowed the acquisition of kinetic information at each σ . Although AFM has previously been used to probe the molecular structure of aspirin crystals, neither the growth dynamics

of aspirin nor that of any other pharmaceutical drug crystal have been investigated using this technique.

Surface features were monitored in solutions with $\sigma = 0.31$ and $\sigma = 0.36$. At both σ values, the mechanism of growth observed was consistent with that of the dislocation mechanism. Other growth modes, such as 2-dimensional or 3-dimensional nucleation, were not observed. However, it is thought that 3D nucleation is unique to macromolecular protein and virus crystals [127]. At $\sigma = 0.31$, the step heights ranged from 1 nm to 85 nm. The rate of growth of steps ranged from 4.6 nm/s to 10.8 nm/s, and showed no correlation between step height and growth rate. All steps were observed to grow in the [100] direction.

At $\sigma = 0.36$, the steps growing in the [100] direction varied in height from 1 nm to 315 nm, and grew at rates ranging from 17.4 nm/s to 34.5 nm/s. Again there was no relation between step height and growth rate. The average growth rate of steps in the [100] direction at $\sigma = 0.31$ and $\sigma = 0.36$ was calculated as 7.2 nm/s and 25.7 nm/s respectively. Therefore, at $\sigma = 0.36$, the growth rate of the steps was a factor of 3.6 times higher than at $\sigma = 0.31$, irrespective of the larger macrosteps observed at $\sigma = 0.36$.

At $\sigma = 0.36$, growth was also initiated in the [010] direction, with steps ranging in height from 1 nm to 365 nm. In this direction the growth rates ranged from 6.0 nm/s to 17.0 nm/s, with no relation between step height and growth rate. However, the growth rates of steps in the [100] and [010] direction are not comparable, that is, they are anisotropic. It is probable that the step anisotropy arises due to the difference in molecular structure of the steps advancing in different crystallographic directions [93, 135, 141].

These data may suggest that growth on the (001) face of aspirin crystals occurs solely via the dislocation mechanism at all values of σ . However, as dissolution was observed at $\sigma \leq 0.15$, and at $\sigma \geq 0.48$ microcrystals were visible in the growth medium, the range of σ values over which growth on the surface occurs is narrow. Hence, the two σ values investigated in this chapter were moderate to high. As the dislocation mechanism is the most energetically favourable at low σ , we assume that at σ values lower than those studied here, growth would again progress via the dislocation mechanism. It is therefore necessary to conduct similar experiments on the (001) crystal face at higher σ to assess whether 2D or 3D nucleation occur at any level of σ .

The (001) face is the most prominent, and therefore the slowest growing, face of the crystal. It would, hence, be of great interest to carry out such experiments on the remaining faces of the crystal, as the faster growing faces may employ other modes of growth at these levels of σ .

These results reiterate the capability of AFM to monitor dynamic events at the nanoscale, such as *in situ* growth on crystal faces, and can be used to deduce the mechanisms and rates as a function of σ . Similar experiments could be conducted on crystalline drugs varying not only the σ , but also other parameters which affect crystal growth, such as temperature, pH, or impurity concentration of the growth medium.

This study emphasizes the fact AFM can provide essential fundamental information on the growth of drug compounds to the pharmaceutical industry. Such knowledge may facilitate the optimization of crystallization parameters of these compounds.

Chapter

3

Using self-assembled monolayers to investigate the nucleation and growth kinetics of aspirin crystals.

In recent years self-assembled monolayers (SAMs) have proved their ability to promote and control the growth of crystals at interfaces. In this chapter, an assessment is made of the capability of SAMs to promote the growth of aspirin crystals. Microcontact printing of SAMs allowed face-selective nucleation, patterning of crystal growth into predetermined areas, and facilitated the observation of secondary nucleation. This technique enabled the fabrication of a large number of nucleation sites in controlled microenvironments. Hence, these experiments should allow the study of fundamental aspects of crystallization and may pave the way for future investigations into the parameters governing drug crystal growth, including the factors controlling polymorphism.

3.1 Introduction

3.1.1 Overview of the current techniques used to promote and investigate crystallization.

The significance of crystallization processes in the manufacture of drug compounds, during process control, and in the overall determination of the solid-phase outcome is unquestionable. However, crystallization phenomena are often neglected by the pharmaceutical industry until a problem, such as an undesired polymorph, emerges [7]. The overwhelming need to provide information on the crystallization process of drug molecules has been discussed extensively in Chapter 1. In particular, detailed knowledge of nucleation and fundamental growth mechanisms is essential in order to understand, predict, and potentially control crystallization.

The successful control of nucleation and crystal growth is possible, assuming that all the required information on these processes is available. Research in this area has seen the exploration of a range of strategies which seek to control the nucleation and growth of crystals based on molecular recognition at interfaces [188]. These techniques promote heterogeneous nucleation, where nucleation and crystallization are initiated on a surface or interface of different composition to that of the crystallizing substance. The substrates used for these investigations vary from crystal surfaces to synthetically engineered templates. Organic crystal surfaces have been shown to control the nucleation and growth of small organic crystals and polymer crystals [12, 13], and to direct the nucleation of particular polymorphs [15, 17].

In some of nature's biomaterials, such as bone, macromolecules are used to control the nucleation and growth of crystalline phases and thus manipulate the

structure and physical properties of the resulting crystal [189-192]. Consequently, over the past twenty years a biomimetic approach to crystal engineering has been developed, employing synthetic substrates which exhibit specific functional groups at their surface. Substrates such as Langmuir monolayers [193, 194], surface-adsorbed biological macromolecules [195-199], functionalized polymer surfaces [190, 200-203], and organic thin films [204] have successfully promoted oriented growth of inorganic and organic crystals. One advantage of using these substrates is that their functionality and packing can be readily modified, allowing the affect of these factors on growth to be investigated. However, these surfaces are, in general, neither homogeneous nor well defined, and as a result the nucleation and growth processes cannot be easily controlled [205].

Currently, a group of compounds which are capable of forming self-assembled monolayers (SAMs) are emerging as potential substrates for not only orienting, but also controlling and patterning nucleation and crystal growth. A plethora of SAMs exist with a diverse variety of functional groups. In addition, they possess long-range order and have been extensively characterized. All of these properties make SAMs ideal surfaces upon which to investigate the processes and parameters involved in crystal growth, and are discussed below.

3.1.2 Formation of self-assembled monolayers (SAMs) on surfaces.

SAMs are produced when alkanethiols, $\text{HS}(\text{CH}_2)_n\text{X}$, chemisorb from solution or vapour, onto surfaces of gold, silver or copper, giving complete, highly compact coverage of the surface. As gold is the substrate we have chosen to use for our studies, we shall concentrate only on SAMs on gold surfaces. Alkanethiols attach to

the surface via their thiol head-group. The nature of the gold-sulphur bond is still the subject of considerable debate, however current opinion is that the species present at the surface is a gold(I) thiolate. The mechanism of this reaction is not yet fully understood, but is believed to occur via Equation 3.1 [206]:



Once formed, SAM-covered gold surfaces are stable in air or liquid, but SAMs will desorb when irradiated with ultraviolet light in an oxygen atmosphere, when exposed to ozone, or when heated above 70°C [206].

Substrates used to initiate SAM formation are usually gold-coated mica, glass, or silicon. A layer of gold as thin as 12 nm is sufficient for the formation of continuous, well-structured SAMs [206]. The thermal evaporation of gold on these substrates produces films of gold with (111) crystallographic orientation and gold molecules arranged in a hexagonal relationship [207]. On binding to the gold, sulphur atoms are believed to be localized in three-fold hollow sites of the Au (111) surface [208]. Alkyl chains of SAMs reside at an angle of 30° to the normal of the gold surface in order to minimize the free volume and maximize van der Waals interactions between the chains [206]. As a result, SAMs of alkanethiolates on gold pack at densities that approach those of a crystalline solid [206, 209-211]. A diagrammatic representation of a SAM on gold is shown in Figure 3. 1.

The ability to present a variety of functional groups, X, including structurally complex groups, at the terminal position of the alkanethiol makes it possible to control the surface chemistry at the molecular level, and thus to control the interfacial properties of these surfaces.

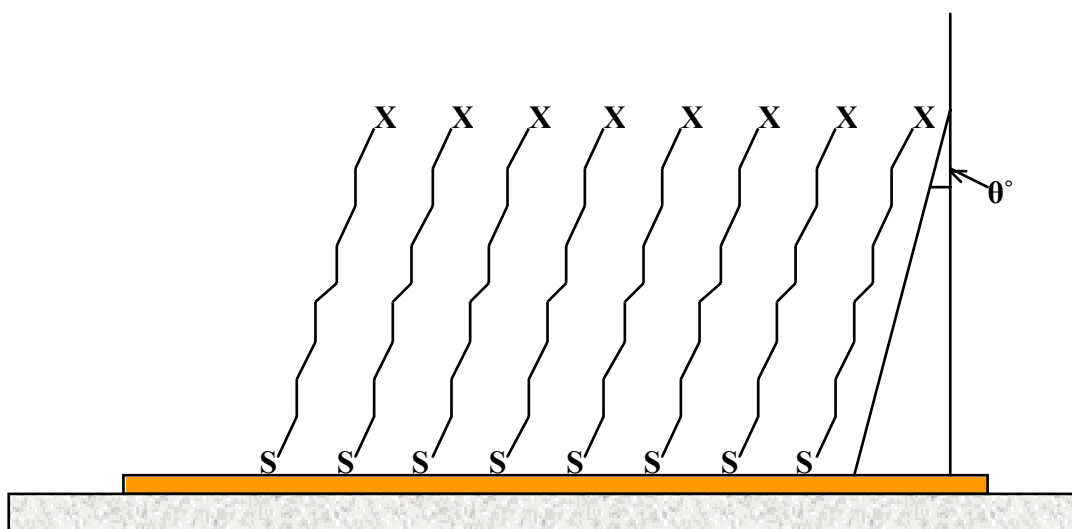


Figure 3. 1 Diagrammatic representation of alkanethiols arranged into a self-assembled monolayer (SAM) on gold-coated mica. Alkanethiols attach to the gold surface via their thiol head-groups and their alkyl chains protrude from the surface at an angle θ° to the normal, where θ° is approximately 30° . Thus, their variable terminating-groups, X, are exposed to the surrounding environment and govern the chemical nature of the SAM.

The additional use of soft lithographic techniques [212, 213] make it possible to pattern SAMs with different functionalities onto surfaces. The key to soft lithography is the use of an elastomeric polymer, with a pattern in bas-relief on its surface, as a means of transferring alkanethiols to a surface in desired formations. These “stamps” or “moulds” are fabricated by casting and curing poly(dimethylsiloxane), PDMS, against a master silicon substrate. Soft lithographic techniques allow the patterning of surfaces with features ranging from 200 nm [214] to 50 μm in diameter [206] and provide a method in which the spacing, ordering, and orientation of terminal groups can be accurately and reproducibly determined [188].

Microcontact printing is one such technique, and is illustrated in Figure 3. 2. The procedure involves wetting the PDMS stamps with an ethanolic solution of alkanethiol, allowing excess solvent to evaporate, and placing the stamp on the gold substrate. As PDMS is an elastomer, it contacts the substrate conformally resulting in a pattern of SAMs complementary to the features of the stamp. Exposure of the remaining bare gold substrate to a second alkanethiol permits the formation of a surface presenting patterned regions of two distinct terminal groups. The flexibility of PDMS has also enabled patterning of curved surfaces [206, 215].

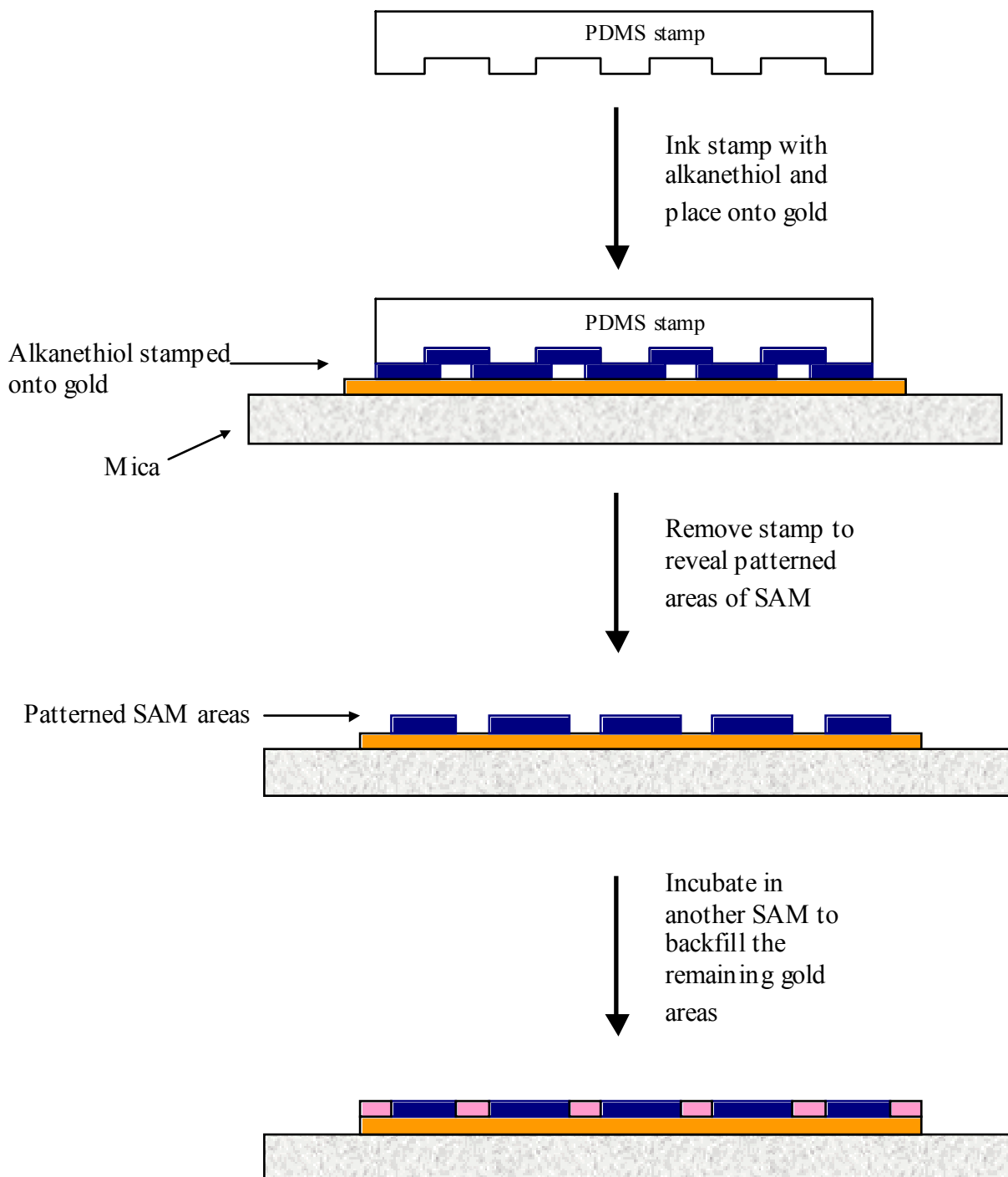


Figure 3. 2 Diagram illustrating the patterning of SAMs onto a gold-coated mica surface using microcontact printing. A PDMS stamp is inked with alkanethiol solution and placed onto the gold surface. A SAM is formed on the gold in the areas which have contacted the stamp. Incubation of the substrate in a second alkanethiol solution allows the bare areas to be filled, generating a SAM-covered surface that presents different chemical functionalities in different areas. Adapted from [213].

The two-dimensional distribution of functional groups has previously been exploited to control and pattern the adsorption of many biological macromolecules to surfaces. These include lipids [216], DNA [216-219], proteins [220-223], and entire cells [220, 224-226]. A comprehensive review of the use of SAMs in patterning and investigating protein binding, cell attachment, growth and apoptosis is given in references [206, 212, 213]. The proficiency of SAMs to arrange proteins or cells on a surface without diminishing their activity or specificity has led to their use in commercial products such as DNA arrays [227] and biosensors [228, 229]. Further applications lie in biocatalytic electrodes, catalysts, high throughput screening [206], and in microelectronics [230].

This technique has also enabled the direction of nucleation and growth of crystals and liquid crystals. SAMs have been used to promote heterogeneous nucleation and growth of glycine crystals [231], iron hydroxide crystals [232], malonic acid crystals [233], to orient the crystallization of calcite [188, 205, 234], and to direct the growth of particular polymorphs of calcium carbonate [235].

The structure and size of defects within liquid crystals were also controlled by this method [216]. Hence this procedure also has the capability to produce highly oriented crystal samples which may be used for structural analysis via X-ray diffraction.

Both Kang *et al.* [231] and Aizenberg *et al.* [188, 205, 234] have shown that, by varying the chemical nature of the SAM, the nucleating face of glycine and calcite crystals respectively could be altered. Consequently the morphology of the resulting crystals was dictated by the SAM surface to which it adhered. The selective nucleation of calcite from six crystallographic faces was observed using these methods, whereas the use of Langmuir monolayers and adsorbed biological

macromolecules as substrates resulted in growth from only one or two faces [198, 199, 236-238], indicating the superiority of SAMs. Although nucleation mechanisms and kinetics were not studied in any of these investigations, micropatterning of SAMs was shown to control the density and pattern of nucleation events, and the sizes of the growing crystals [188, 234].

These studies have demonstrated that varying the geometry, chemistry, and pattern of SAM functional groups provides a means of regulating the orientation of crystal growth, allows the formation of high resolution patterns of oriented crystals [205], and also provides a template upon which nucleation processes can be investigated.

These factors, combined with the ease of preparation of SAMs, make them an ideal surface for investigating the nucleation and growth mechanisms of drug crystals.

3.1.3 Aims of chapter.

SAMs have already proven to be a model system for investigating the interactions of proteins and cells with surfaces. Recent findings have demonstrated their superiority over surfaces such as Langmuir monolayers and functionalized polymer interfaces in promoting nucleation and growth of oriented crystals in predetermined areas. Here we assess the abilities of three SAMs to bind aspirin molecules, and allow aspirin crystals to grow on their surface. Microcontact printing will be employed to pattern aspirin-binding and non-binding SAMs onto gold. The resulting templates will be used to study the nucleation and fundamental growth mechanisms of aspirin crystals. AFM and SEM will be used to visualize and quantify these processes throughout.

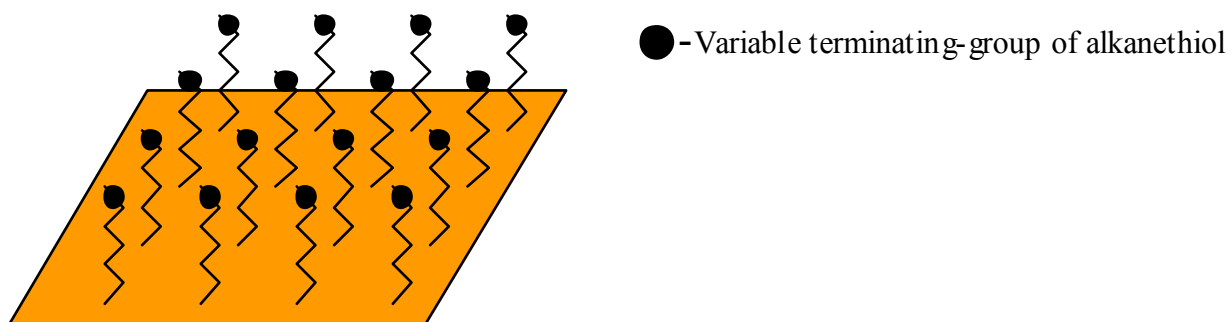
3.2 Methods and Materials

3.2.1 Preparation of self-assembled monolayers (SAMs) on epitaxial gold.

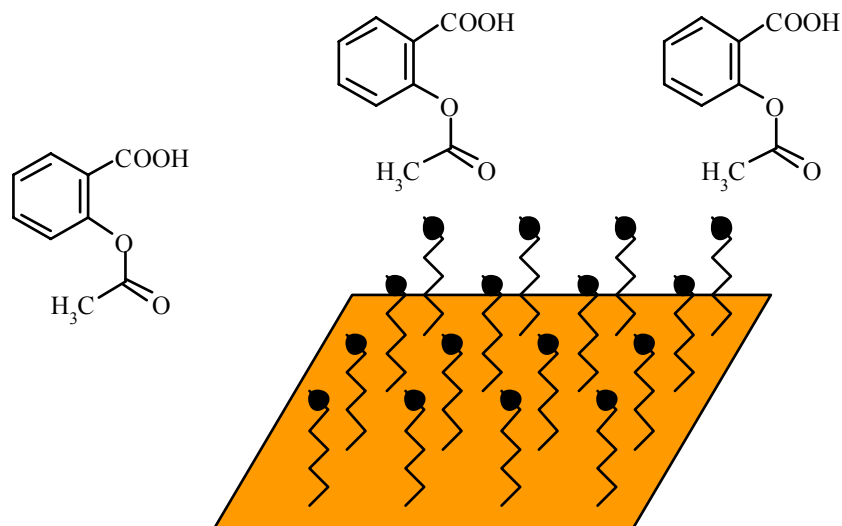
The epitaxial gold on mica substrates, prepared using the method described by DeRose *et al.* [207], was cleaned using a hydrogen flame before incubation in SAM solution at room temperature. SAMs utilized were 11-mercapto-1-undecanol (11-MUD) (Aldrich Chem. Co. Milw. WI, USA), 11-mercaptopundecanoic acid (11-MUA) (Aldrich Chem Co. Milw. WI, USA), and 1-dodecane-thiol (1-DDT) (Sigma Aldrich, Dorset, U.K.). The 11-MUD, 11-MUA, and 1-DDT SAMs have OH, COOH, and CH₃ as their terminating-groups respectively. 11-MUD and 11-MUA SAM solutions were prepared by dissolving 6mg of the compound in 10ml of ethanol (Sigma Aldrich, Dorset, U.K.). 1-DDT SAM solution was prepared by mixing 60 μ l of the compound in 10ml ethanol. The final concentrations of the SAM solutions were approximately 2.7mM.

After cleaning, the gold was incubated in a SAM solution for 24hrs. Controls were prepared by incubating the gold in HPLC grade water after cleaning. After incubation the gold pieces were removed, dried in a stream of nitrogen, and incubated in 0.015M aspirin solution where HPLC grade water is the solvent. Aspirin (Sigma Aldrich, Dorset, U.K.) used was U.S.P. grade. Figure 3. 3 shows a schematic representation of the incubation of SAM-covered gold in aspirin solution. The SAM-covered gold substrates were imaged periodically, using AFM, in 1ml aspirin solution to assess whether nucleation and growth were occurring on any of the surfaces.

Stage 1



Stage 2



Stage 3

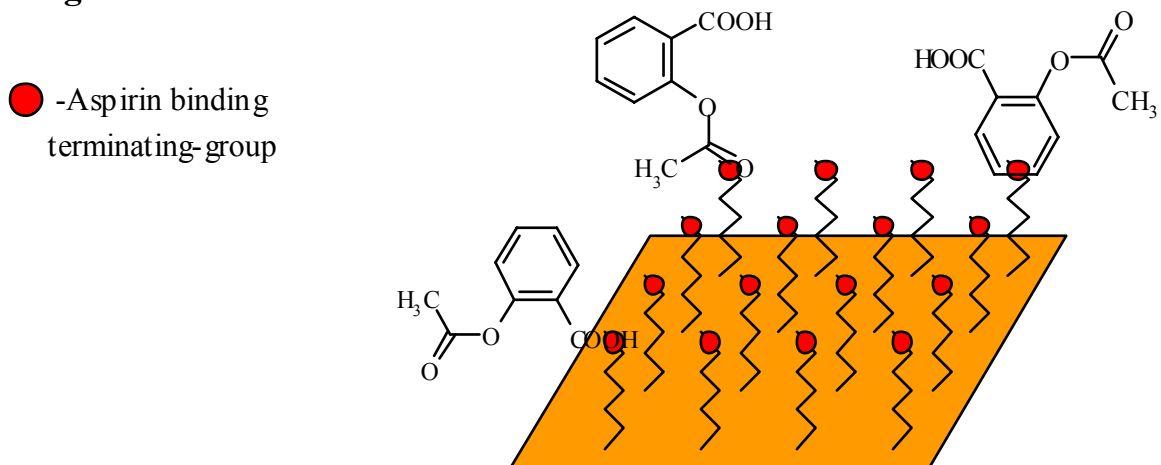


Figure 3. 3 Schematic of the incubation of SAM-covered gold in aspirin solution. Stage 1: SAM on gold with terminating-group exposed. Stage 2: incubation of the substrate in aspirin solution. Stage 3: possible conformation of aspirin molecules bound to the SAM.

A PDMS stamp, to be used for microcontact printing, was cast from a silicon microchip. The pre-polymer of PDMS, Silgard 184, was obtained from Dow Corning (ISL, W. Midlands, U.K.). The stamp was prepared by pouring the pre-polymer of PDMS (Silgard 184), in a 10:1 (W/W) ratio of base:curing agent, onto the silicon microchip. The PDMS was cured at 35°C for 24 hours and removed from the microchip master, washed in ethanol, deionized water, and hexane before drying under a stream of nitrogen. This stamp was stored under a stream of argon prior to use. The resulting PDMS stamp was imaged using SEM to show its surface features.

This PDMS stamp was incubated in a solution of 11-MUA or 1-DDT SAM to form an inked stamp which, when applied to a gold substrate, would transfer the SAM only to the areas in contact with the gold. The “inking” solutions were prepared by dissolving 12mg 11-MUA or 120 μ l 1-DDT in 5ml ethanol, resulting in solutions with a concentration of approximately 10.8mM. The stamp was incubated in the inking solution for 15 minutes. After incubation, the inked PDMS stamp was removed from the SAM solution, dried in a stream of nitrogen and carefully placed onto the gold substrate. Contact between the stamp and gold was maintained for 30 seconds, the stamp was then peeled away from the surface. It has been shown that using ethanolic solutions of SAMs with concentration greater than 10mM for printing generates SAMs which are structurally comparable to high-quality SAMs formed from a solution [239, 240]. Prior to each stamping experiment, the PDMS stamp was washed in 5ml ethanol, then hexane, and ethanol again to remove any residual SAM or impurities. In between each wash it was dried with lens tissue.

The resulting 11-MUA and 1-DDT patterned gold substrates were incubated in 1-DDT and 11-MUA solutions respectively, to backfill the unstamped areas of the gold. The “backfill” solutions were prepared by dissolving 6mg of 11-MUA or 60 μ l

1-DDT in 10ml ethanol. After incubation in the backfill solutions for 24 hours, the patterned gold substrates were dried in a stream of nitrogen. The two resulting types of gold substrates consist of:

- i) areas of 11-MUA SAM in patterns which are mirror images of the PDMS stamp features, surrounded by 1-DDT SAM, and
- ii) patterned areas of 1-DDT SAM surrounded by 11-MUA SAM.

Both types of patterned gold substrate were incubated in 0.015M aspirin solution to assess which areas would promote nucleation and growth of aspirin crystals. After incubation in aspirin solution for several days, the substrates were imaged using AFM and SEM. The 11-MUA stamped/1-DDT backfilled substrate was monitored more closely and imaged periodically in aspirin solution to assess growth of crystals on this template.

3.2.2 AFM analysis.

Contact mode imaging was employed throughout, using a ThermoMicroscopes Explorer AFM (Veeco, Bicester, Oxon, U.K.). V-shaped silicon nitride cantilevers (200 μ m length) with integrated pyramidal tips (Nanoprobes, Veeco, Santa Barbara, CA) were used. Both topography and deflection images were acquired in all experiments. Deflection images emphasize areas of rapid topography changes, such as steps, but do not give any information about the relative heights of features on the surface.

3.2.3 SEM analysis.

All samples were initially gold coated for four minutes using a Balzers SCD 030 Sputter Coater (Balzers Union Limited, Liechtenstein), operated at 0.1mbar with a sputtering current of 30mA. A Philips 505 SEM (Philips Electron Optics, Eindhoven, Netherlands) was used to image all samples under a range of magnification settings at a voltage of 23KeV, with a spot size of 50nm.

3.3 Results and Discussion

The images in Figure 3. 4 show the surface of bare gold after incubation in 0.015M aspirin solution for 3 days, 9 days, and 8 weeks. There are large features present on this surface after 3 days and 9 days, indicated by arrows on images a) and b), which may be clusters of aspirin crystals. However, after 8 weeks of incubation in aspirin solution, there are no crystalline features visible on the surface. Therefore the features present after 3 and 9 days must be due to debris on the surface. The debris may be clumps of gold which not have annealed properly to the mica, or may be deposits of impurities present in the aspirin solution. The globular features apparent in image c) are due to annealing of gold into spherical grains rather than in a layer, as shown in images a) and b). Therefore the clean gold surface, without any SAM attached, does not promote nucleation of aspirin crystals. Figure 3. 5 displays images of 1-DDT SAM covered gold after 3 days, 9 days, and 8 weeks of incubation in aspirin solution. Throughout this time period, the gold retains its characteristic appearance of pits and islands, without the formation of any crystals on the surface. Note that the monolayers are approximately 2 nm in height [206, 226, 230] and

hence are not visible at this resolution using AFM. Even after 8 weeks there is no discernible crystallization on this surface.

Figure 3. 6 shows the features on the surface of the 11-MUA SAM covered gold during incubation. After only 2 days the appearance of crystals on the surface is evident. These continue to develop and grow until, after 8 weeks, crystals with distinct faces reside on the SAM covered surface. One of these can be observed in the upper left-hand side of image c), indicated by an arrow.

The images shown in Figure 3. 7 depict the 11-MUD SAM covered gold surface during incubation. Again the surface features remain consistent with that of bare gold throughout the incubation period, and hence crystallization does not occur on this surface. The globular features observed in images b) and c) are again due to the annealing of gold in spherical grains. The presence of such features does not impede the formation of SAMs on the surface [219], and therefore will not influence the nucleation of crystals.

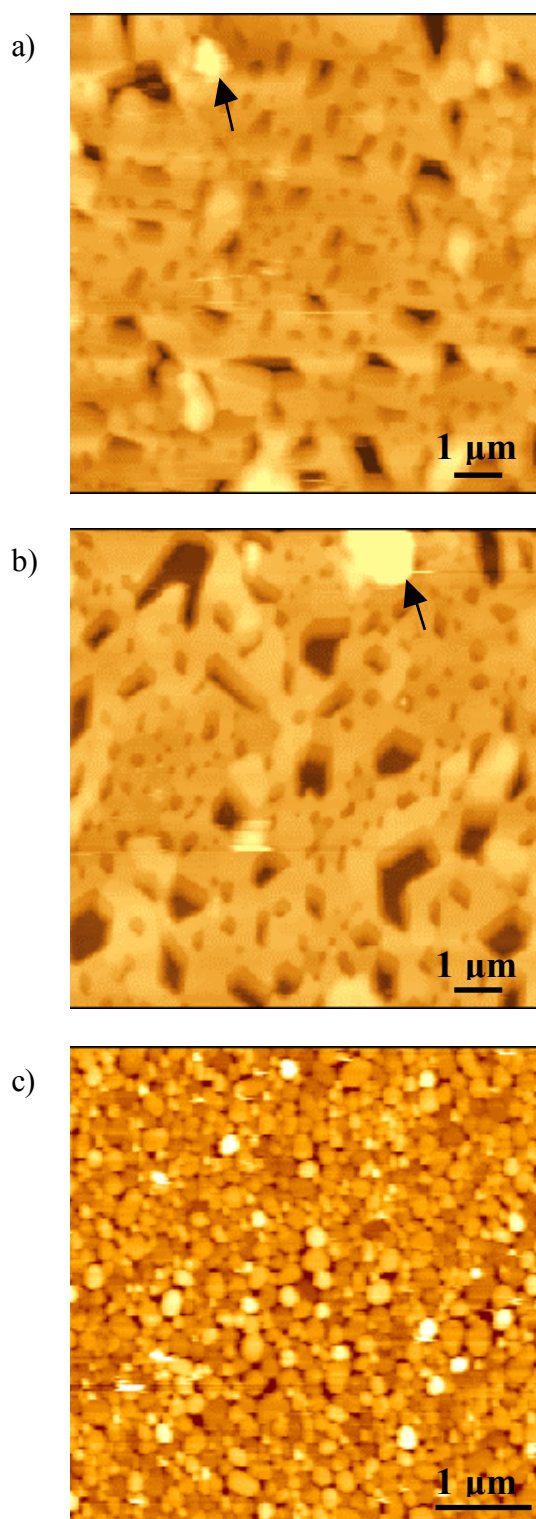


Figure 3. 4 AFM topography images of the control, bare gold, after incubation in 0.015M aspirin solution for a) 3 days, b) 9 days, and c) 8 weeks. Both a) and b) are 10 μm x 10 μm images whereas c) is a 5 μm x 5 μm image. The arrows indicate clumps of gold, or impurities from the aspirin solution which have deposited on the surface.

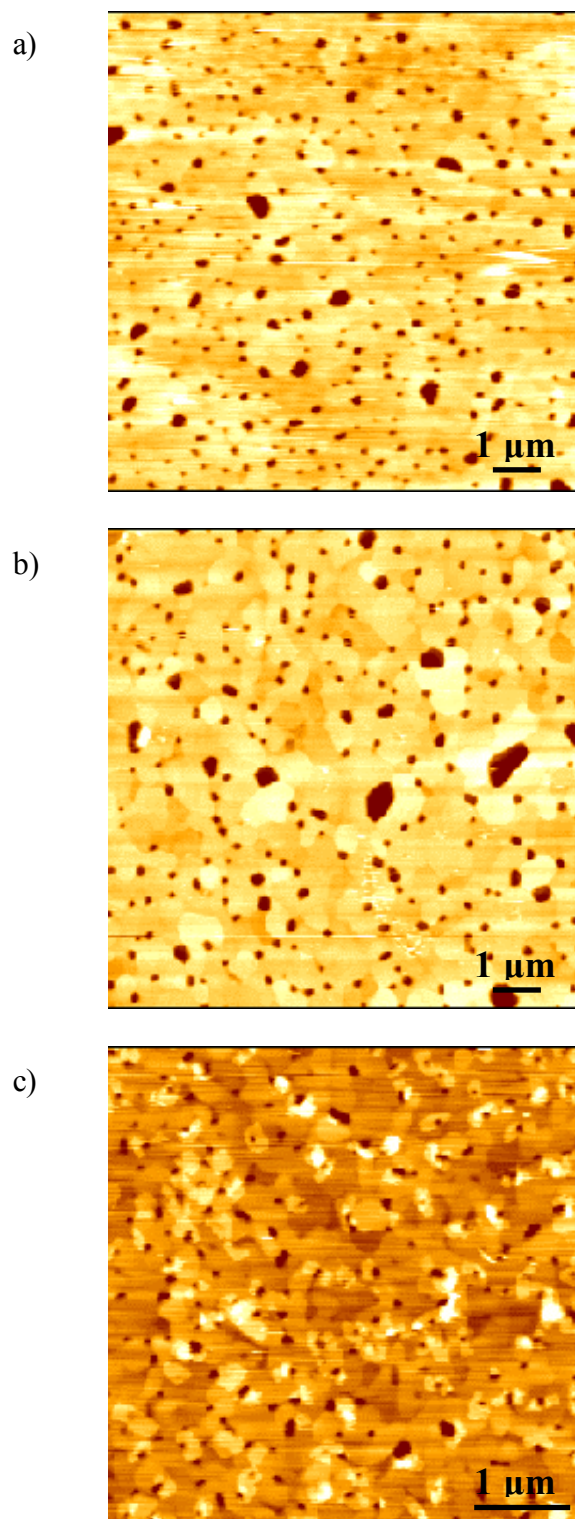


Figure 3. 5 AFM topography images of 1-DDT SAM-covered gold after incubation in 0.015M aspirin solution for a) 3 days, b) 9 days, and c) 8 weeks. Both a) and b) are 10 μm x 10 μm images whereas c) is a 5 μm x 5 μm image.

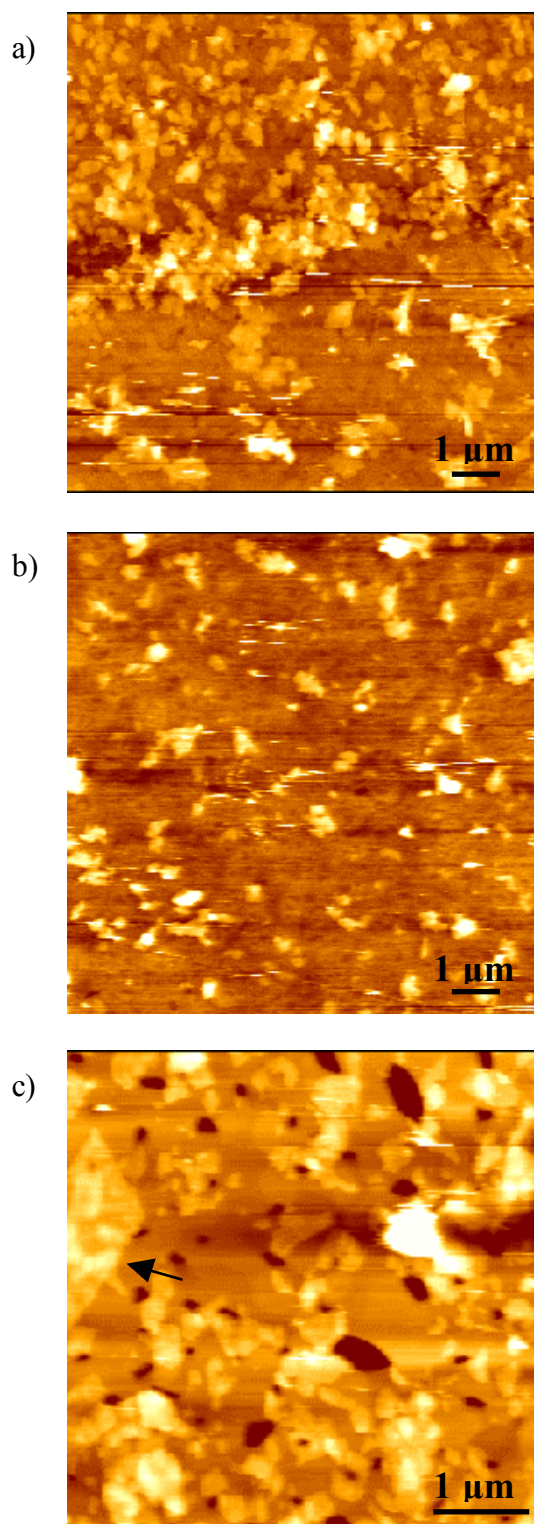


Figure 3. 6 AFM topography images of 11-MUA SAM-covered gold after incubation in 0.015M aspirin solution for a) 2 days, b) 7 days, and c) 8 weeks. Both a) and b) are 10 μm x 10 μm images whereas c) is a 5 μm x 5 μm image. The arrow indicates a crystal with distinct faces which has grown on the SAM-covered surface.

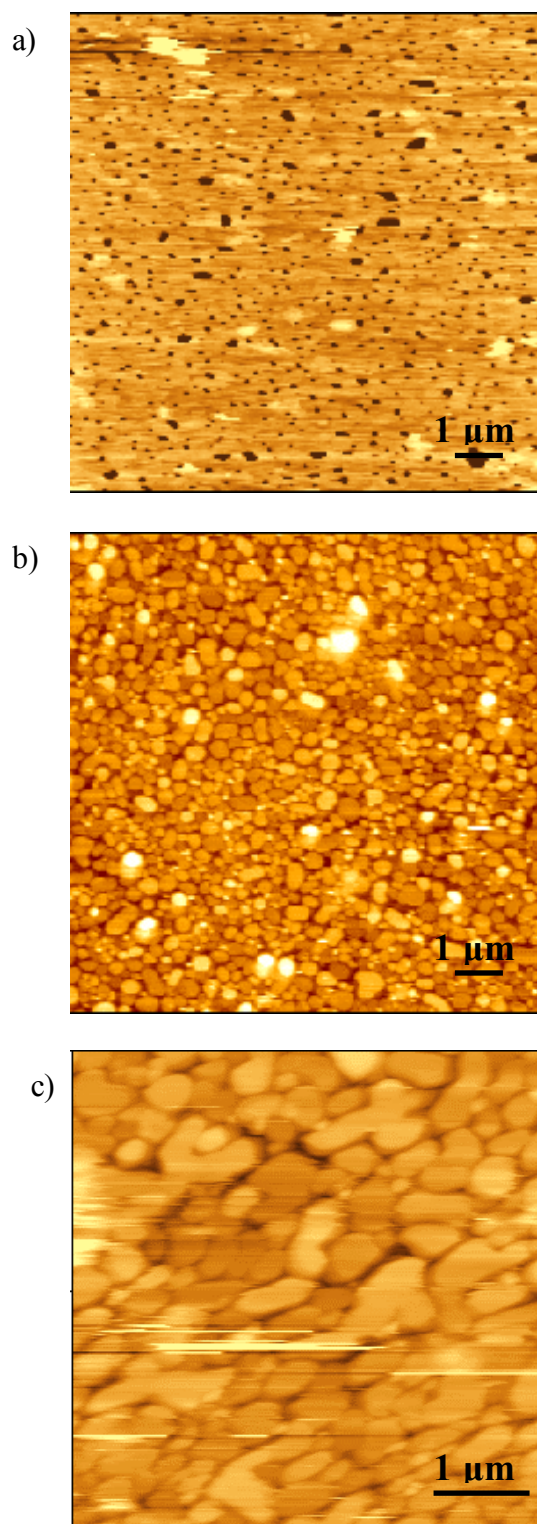


Figure 3. 7 AFM topography images of 11-MUD SAM-covered gold after incubation in 0.015M aspirin solution for a) 1 day, b) 9 days, and c) 8 weeks. Both a) and b) are 10 μm x 10 μm images whereas c) is a 5 μm x 5 μm image.

From these data we can conclude that of the four substrates investigated, only the 11-MUA SAM-covered gold surface promotes aspirin nucleation and subsequent crystal growth. This is clearly due to molecular recognition between the aspirin molecules and the chemical functionality of the surface. In the crystal structure of aspirin the molecules dimerize, and are linked together via a pair of hydrogen bonds between their carboxyl groups [172]. Figure 3. 8 illustrates the orientation of aspirin molecules in a hydrogen-bonded dimer. A similar type of bonding could occur between aspirin molecules and the carboxyl-terminated MUA SAMs, allowing aspirin molecules to attach to the surface. Given that the pKa values for aspirin and 11-MUA are 3.5 [241, 242] and 6.5 [243] respectively, and the measured pH of the aspirin solution is 2, both SAM and aspirin molecule would be protonated. This would therefore increase the strength of the bonding between these components, and hence the stability of the resulting complex. If bonding does occur in this manner, we can assume that aspirin molecules attach to the SAM individually, and not as a dimer. Successive aspirin molecules must then attach to the initial aspirin molecule and/or the juxtaposed SAM molecules.

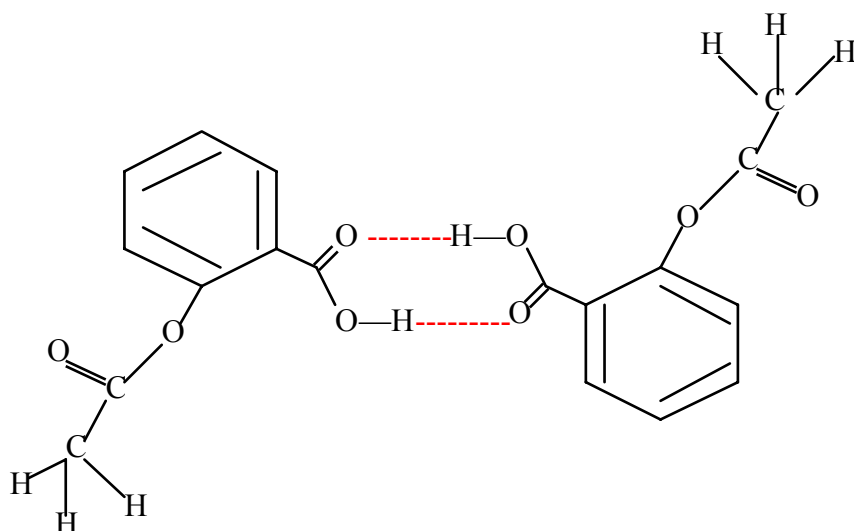


Figure 3. 8 Structure of a hydrogen-bonded aspirin dimer in the crystalline state.

Hydrogen bonds are represented by dashed red lines. Adapted from [172].

Molecules bind progressively to form a stable nucleus and continue to grow to form microscopically visible crystals. The process by which these crystals grow on the surface is described by the Deposition, Diffusion, and Aggregation (DDA) model [244-247], and is illustrated in Figure 3. 9. This model proposes that atoms or molecules (adatoms) deposit onto the surface (Figure 3. 9 a) and diffuse across it until they reside in a site immediately next to another adatom (b) or cluster (c). When two adatoms occupy neighbouring sites, they and the clusters to which they belong bind irreversibly. These clusters can continue to diffuse across the surface (illustrated in d) and e)), but their rate of diffusion is inversely proportional to their size.

As previously mentioned, SAMs on gold pack with densities approaching those of crystalline solids [206, 209-211], and thus this process could be considered epitaxial growth.

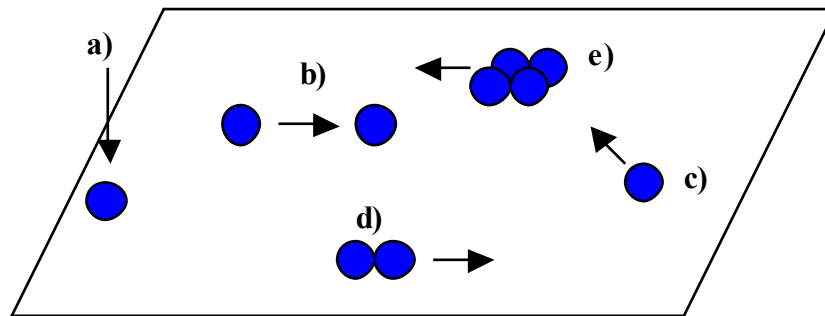


Figure 3. 9 Diagrammatic illustration of the Deposition, Diffusion, and Aggregation (DDA) model for growth on surfaces. In a) an adatom adsorbs (deposits) onto the surface. It then diffuses across the surface until it meets another adatom, b), or cluster, c). When two adatoms occupy neighbouring sites, they and the clusters to which they belong bind irreversibly. These clusters can continue to diffuse across the surface, shown in d) and e). Adapted from [244].

In order to investigate nucleation and the initial stages of aspirin crystal growth, we require a substrate upon which aspirin crystals will nucleate in predetermined areas. In order to create such templates for nucleation and growth, we patterned 11-MUA and 1-DDT SAMs on gold using microcontact printing with a PDMS stamp cast from a microchip. SEM images of areas of the PDMS stamp are shown in Figure 3. 10 and Figure 3. 11. The stamp consists of two main areas, one with linear features composed of raised and lowered domains, and one with almost square raised features. The dimensions of both sets of features are illustrated in Figure 3. 11 b) and d). The almost square features are $14.1\ \mu\text{m} \times 12.7\ \mu\text{m}$, and are separated by $7.3\ \mu\text{m}$ channels horizontally and $4.1\ \mu\text{m}$ vertically. The raised components of the linear features are $13.6\ \mu\text{m} \times 5.5\ \mu\text{m}$, and are separated by $7.3\ \mu\text{m}$ channels horizontally and $8.2\ \mu\text{m}$ vertically.

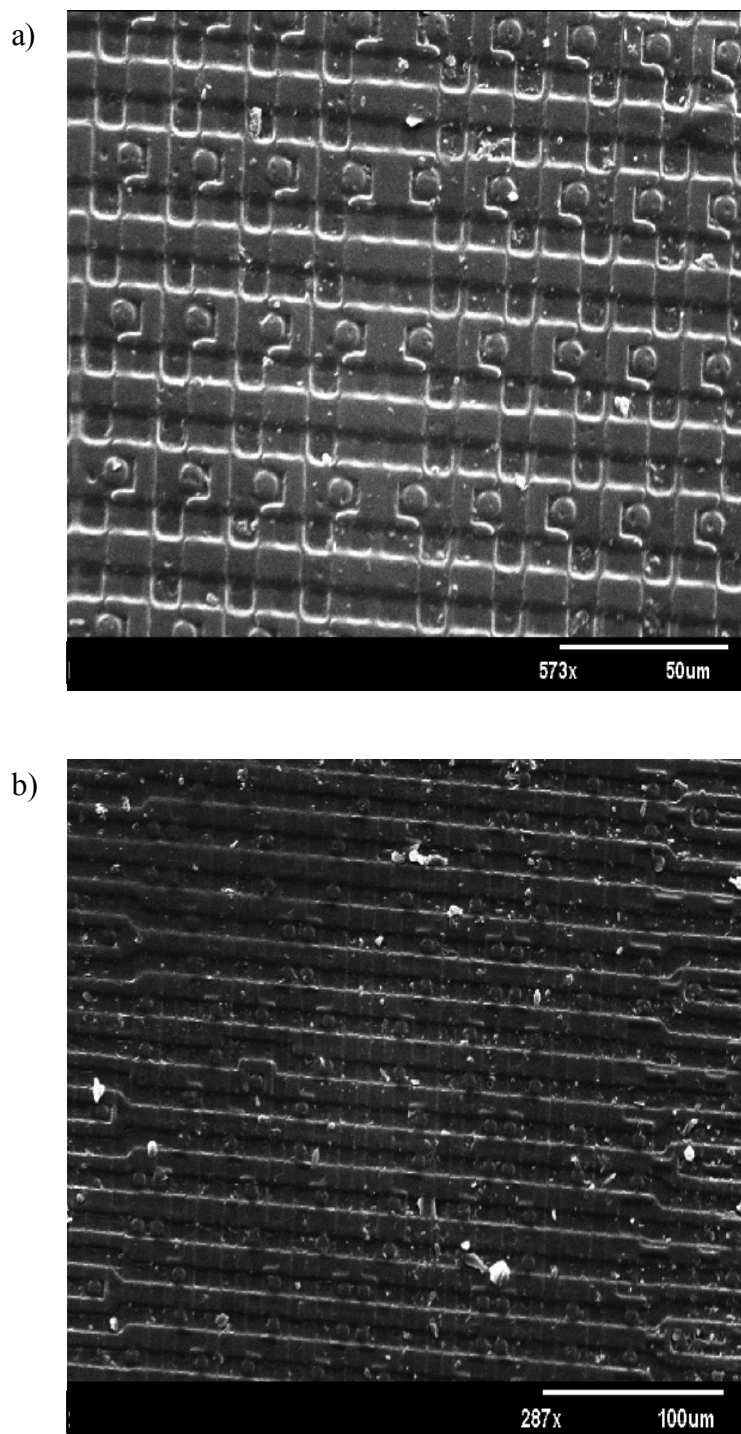


Figure 3. 10 SEM images of the surface features of the PDMS stamp used to pattern gold templates. Image a) shows the repeating almost square features consisting of a “C” shaped element and a dot. This image is taken at magnification x 573. Image b) illustrates the linear features on the surface which have both raised and lowered components. This image is taken at magnification x 287.

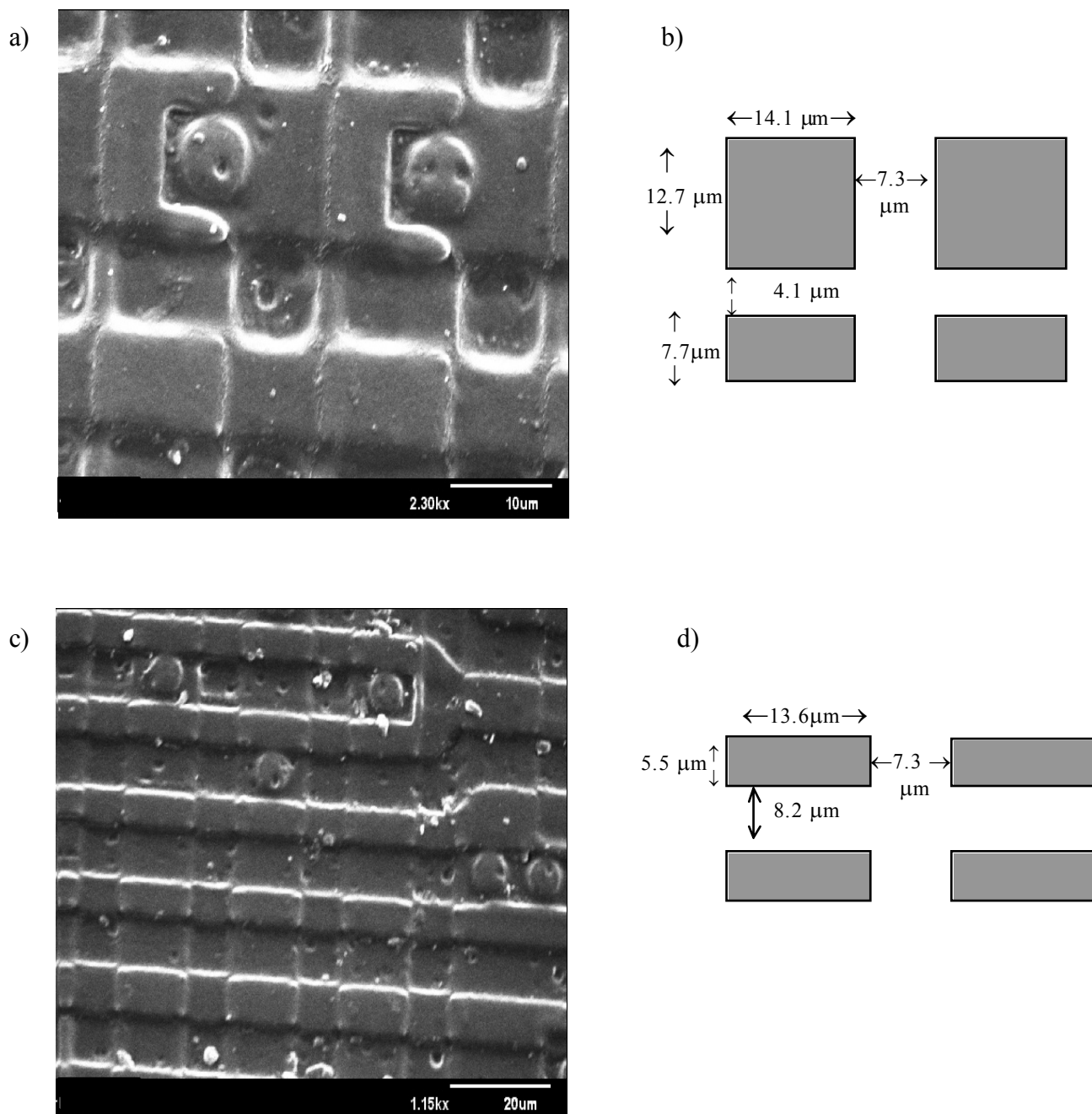


Figure 3. 11 Higher magnification SEM images of the surface features of the PDMS stamp used to pattern gold templates. Image a) shows the almost square features at magnification $\times 2300$. b) shows the dimensions of the raised features of this area of the stamp, and the width of the channels between them. Image c) shows the linear features of the stamp at magnification $\times 1150$. d) shows the dimensions of the raised and lowered features in this area of the stamp.

The templates were prepared by stamping 1-DDT onto the gold surface, and incubating in 11-MUA solution to fill the unstamped regions of the gold (template A), or by stamping 11-MUA onto the surface and incubating in 1-DDT solution (template B). The templates were incubated in 0.015M aspirin solution and AFM images of the resulting surfaces are shown in Figure 3. 12 and Figure 3. 13. As can be seen in Figure 3. 12, crystallization is apparent all over template A. It may appear from these images that 1-DDT SAM does in fact promote aspirin crystal nucleation, in direct contrast to our earlier findings (Figure 3. 5). However the images of the template B, shown in Figure 3. 13, display tabular crystals, approximately 300 nm in height, in patterned formations across the surface. These images indicate that crystallization occurs only in areas of the 11-MUA SAM, and suggest that the features apparent in Figure 3. 12 are due to the fact that, when 1-DDT was stamped onto the gold surface, a complete monolayer was not formed in all the stamped areas. Therefore when the template was incubated in 11-MUA solution, this SAM filled not only the channels around the stamped areas, but also the gaps within the stamped areas. This shows that discrete areas of 11-MUA SAM are sufficient to promote aspirin crystal nucleation.

SEM images, Figure 3. 14, corroborate these findings, showing that after four weeks of incubation the crystals on the template surface still remain almost rectangular in shape, and reside in discrete areas.

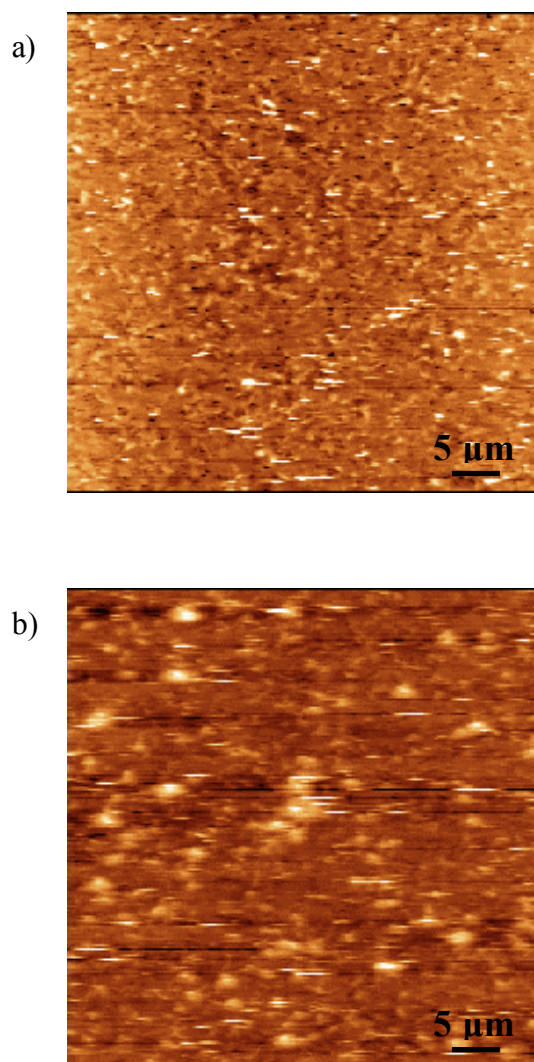


Figure 3. 12 AFM topography images of template A after incubation in 0.015M aspirin solution for a) 1 day, and b) 6 days. Both a) and b) are 50 μm x 50 μm images.

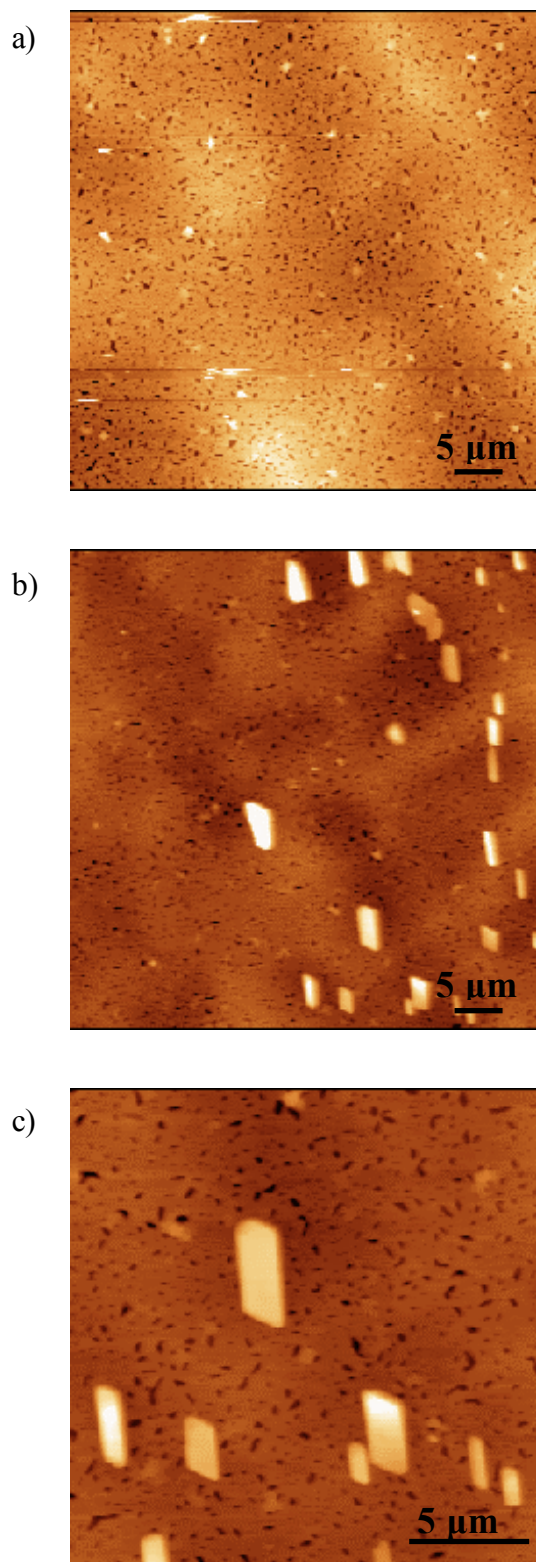


Figure 3. 13 AFM topography images of template B after incubation in 0.015M aspirin solution for a) 1 day, and b) 6 days. Image c) is a higher resolution image of the bottom right area of image b). Both a) and b) are 50 μm x 50 μm images, whereas c) is a 20 μm x 20 μm image.

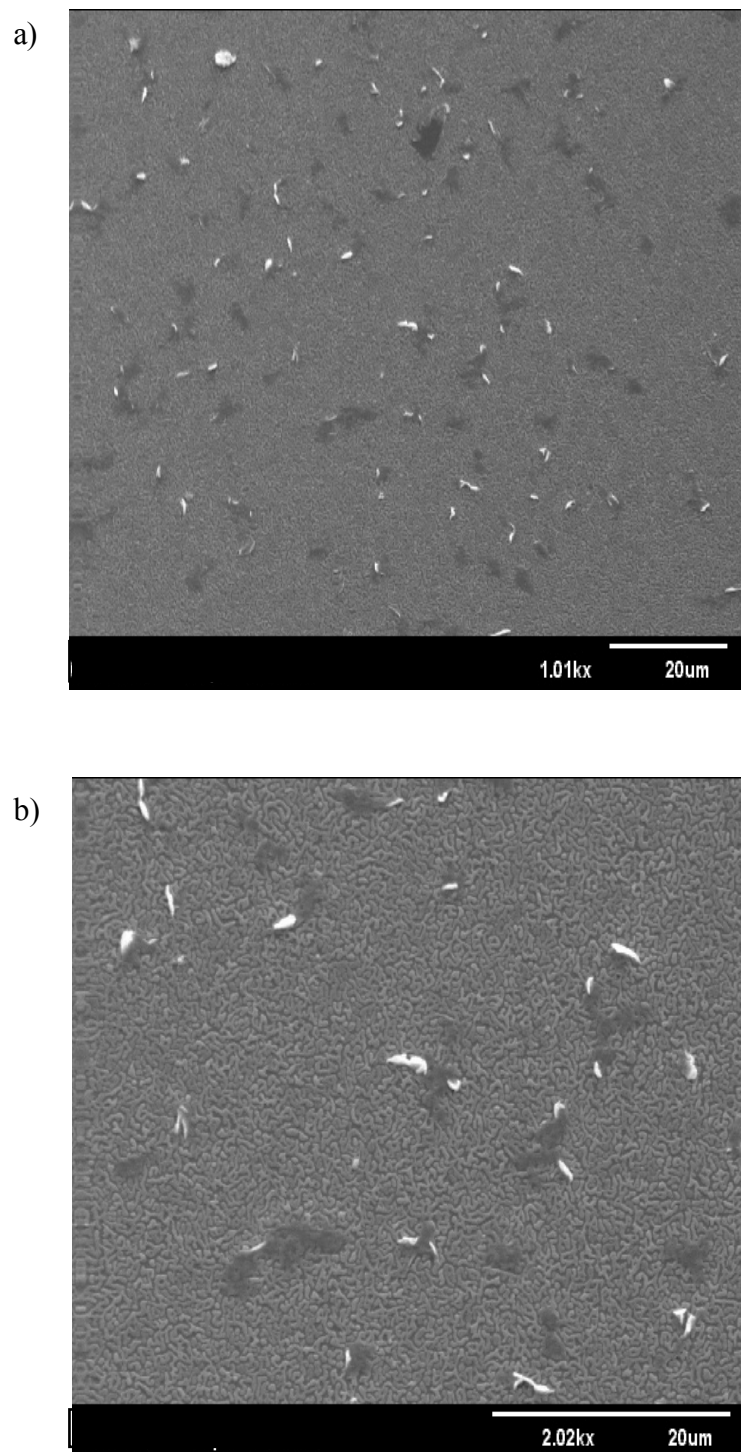


Figure 3. 14 SEM images of template B after incubation in 0.015M aspirin solution for 4 weeks. Image a) shows the template surface at magnification x 1010, and image b) at magnification x 2020.

From the AFM images of template B shown in Figure 3. 13, it is clear that patterning the surface in this manner promotes the growth of highly oriented tabular crystals. In Figure 3. 13 c) the dimensions of the crystallizing areas are approximately $4.6\ \mu\text{m} \times 1.9\ \mu\text{m}$, and the distance between these areas is approximately $2.5\ \mu\text{m}$. We do not know which of the two characteristic areas of the PDMS stamp will have contacted this area of template B. However, the dimensions of the crystals and channels do not mirror the dimensions of either area of the stamp. It is apparent that more than one crystal nucleates within each stamped area, unlike the studies reported by Aizenberg *et al.* [188, 234] where only one calcite crystal nucleated in each nucleating region of the patterned SAM surface, which varied in size from $15\ \mu\text{m}$ to $50\ \mu\text{m}$. These researchers stated that the number of crystals which nucleate within each nucleating region depends linearly upon its area. Therefore, the parameters of the stamp used for our experiments need to be optimized in order to create patterns which promote nucleation of only one aspirin crystal per nucleating site, and thus mimic more precisely the surface features of the stamp.

Nevertheless, template B, where the gold surface is stamped with 11-MUA and backfilled with 1-DDT, promotes the growth of highly oriented tabular crystals. This template, therefore, allows nucleation to occur at specific sites. The periodic pattern of crystals on the surface reflects the influence of mass transport [234]. Again the growth of crystals on the surface follows the DDA model (Figure 3. 9). However, we suspect that the flux of aspirin molecules to the specific nucleation sites increases as the crystals begin to grow. Mass transport of aspirin molecules to the growing crystals depletes the concentration of aspirin in the vicinity, thus locally undersaturating the solution. This sets up local diffusion gradients and elevates the transport of aspirin molecules to the nucleating sites. A positive feedback process is

induced which perpetuates the growth of crystals at nucleation sites, and produces non-nucleating zones surrounding the growing crystals where the aspirin concentration is depleted [234]. The channels or distances between the crystals on the surface represent the non-nucleating zones.

The fact that the orientation of crystals grown on template B (Figure 3. 13) is uniform implies that the interfacial structure of the SAM is governing the orientation of the incipient crystals. As suggested earlier in the chapter, aspirin molecules may attach to the MUA SAM via hydrogen bonding between carboxyl groups of aspirin and SAM molecules. Figure 3. 15 shows the crystal structure of aspirin projected along the *b*-axis, and displays the functional groups present on the (001) and (100) faces. From this diagram it is evident that carboxyl groups project from the (100) face. Hence we assume that this face attaches to the SAM surface via hydrogen bonding during these experiments. The crystal habit of aspirin obtained during these experiments is shown in Figure 3. 16. The Miller indices are shown on each of the crystal faces.

Techniques such as chemical force microscopy [166, 248-251] or X-ray diffraction could be used in the future to identify which surface groups protrude from the crystal faces, and hence which face is binding to the SAM surface. Chemical force microscopy is a modification of conventional AFM. In this technique, probe tips are functionalized with SAMs to enhance the chemical sensitivity of the AFM. During raster scanning it is possible to detect interactions between the functionalized tip and the sample surface, thus allowing chemical inhomogeneities of the surface to be identified.

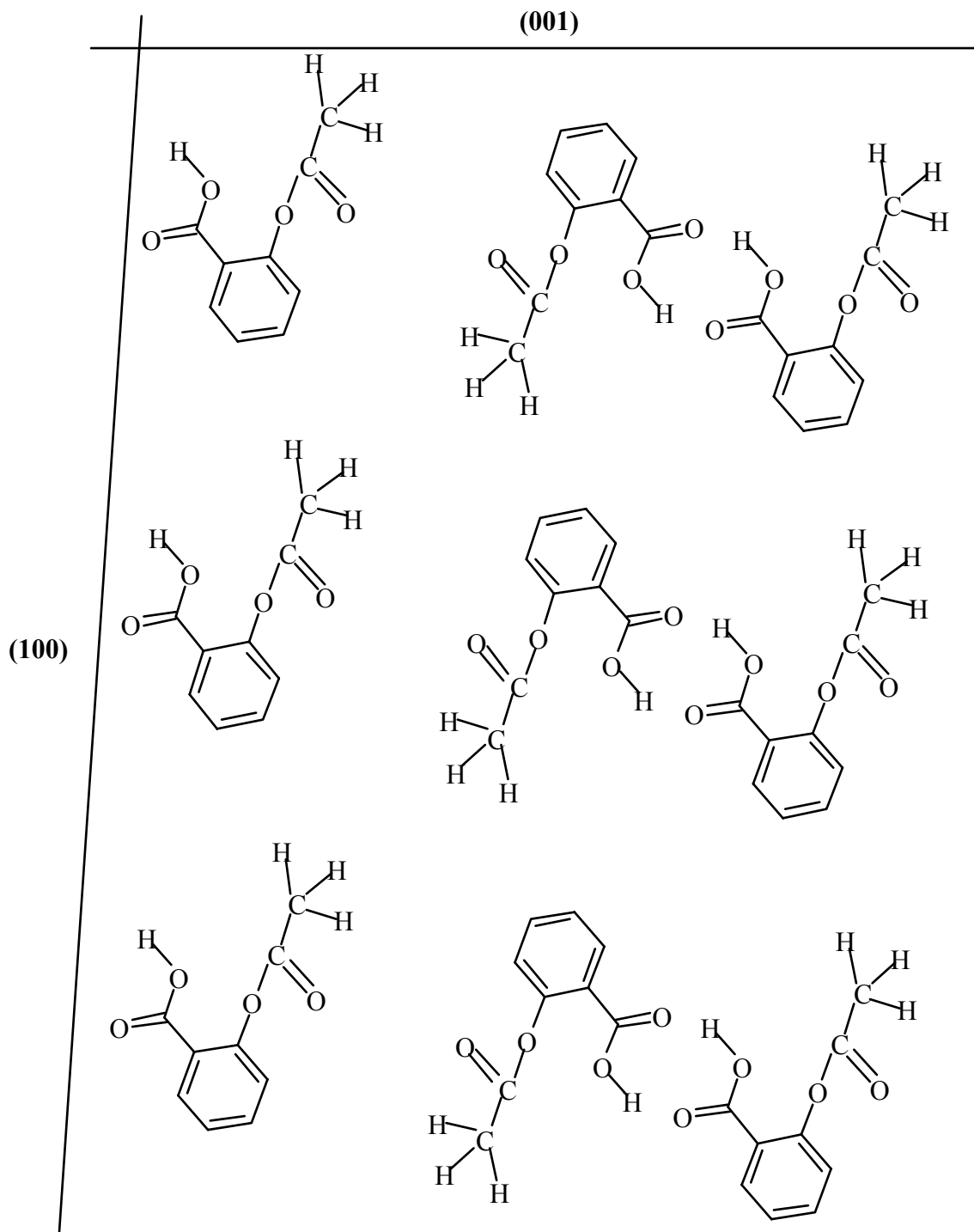


Figure 3. 15 Aspirin crystal structure viewed along the b -axis projection. The horizontal and almost vertical lines indicate the position of the (001) and (100) faces respectively. Adapted from [165].

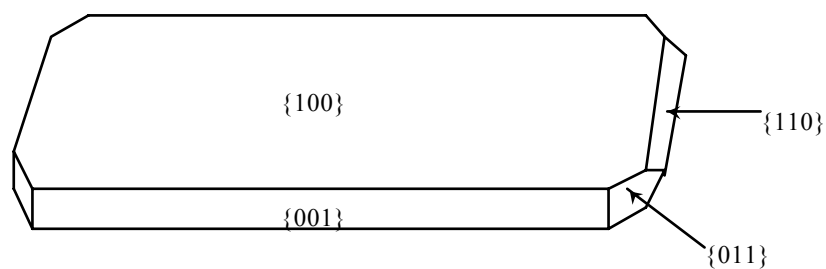


Figure 3. 16 A diagrammatic illustration of the habit of aspirin crystals grown on template B, which consisted of 11-MUA SAM stamped regions surrounded by 1-DDT backfilled areas. The crystals attached to the 11-MUA SAM by hydrogen bonding through the terminating carboxyl groups of the SAM and the carboxyl groups projecting from the (100) faces. The respective Miller indices are shown on each of the faces.

These experiments were repeated using template B, periodically imaging the surface in an attempt to observe nucleation occurring on the surface. Figure 3. 17 shows the results of these experiments. Image a) is taken 7 days after addition of aspirin solution and displays the characteristic aspirin crystal on the template surface. Image b) shows the same area after 74 minutes, and an island of aspirin is clearly visible on the crystal surface. Throughout the sequence this structure continues to grow across the face of the crystal, in both [100] and [001] directions. In images a) to c) growth in the [001] direction is predominant, with an average growth rate of 29.2 nm/min, compared with 8.0 nm/min in the [100] direction. However, the island grows uniformly in the [100] direction during this period. After this time, growth in the [001] direction ceases, but growth in both positive and negative [100] directions rapidly increases. The growth is no longer uniform, and the rates of growth of the different regions of the island range from 23.5 nm/min to 37.6 nm/min. The type of nucleation observed here is known as secondary nucleation, due to the fact that it occurs on a crystal of the same composition as the crystallizing solute [7]. The heights of the crystal and growing nucleus are 474 nm and 151 nm respectively.

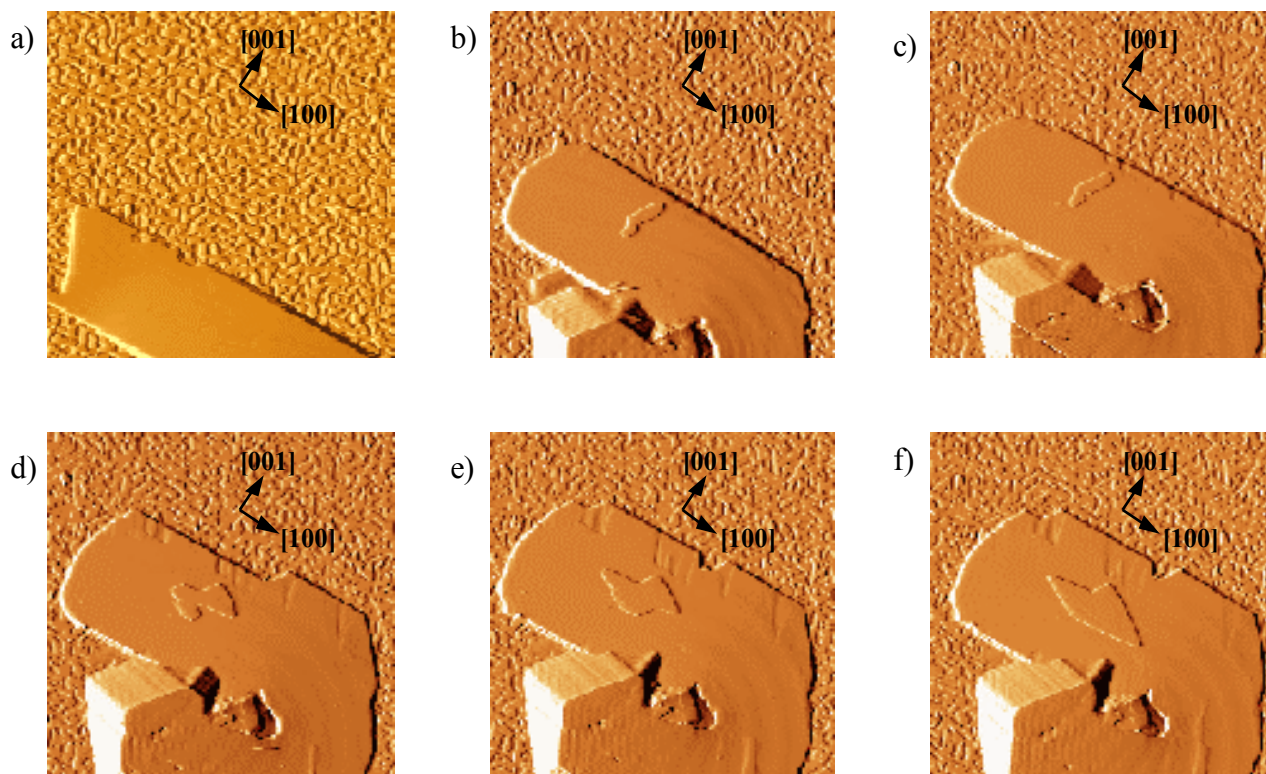


Figure 3. 17 AFM images of a single aspirin crystal growing and facilitating secondary nucleation on the surface of template B. This sequence of images is taken after incubation in 0.015M aspirin solution for 7 days. In image a) time $t = 0$, b) $t = 74$ mins, c) $t = 139$ mins, d) $t = 186$ mins, e) $t = 212$ mins, and f) $t = 257$ mins. The imaged area was moved slightly between a) and b) to centralize the crystal apparent on the surface. All are $23 \mu\text{m} \times 23 \mu\text{m}$ deflection images.

These findings show that during secondary nucleation, growth in the [001] direction is initially dominant. The progressive decrease in growth rate in the [001] direction is concurrent with an increase in the growth rate in the [100] direction. Applying these growth mechanisms to the early stages of growth of the original crystal on the SAM surface, may aid in the explanation of the observed tabular crystal habit.

These images also illustrate the growth of the original crystal, bound to the SAM surface. Growth is negligible in the [100] direction throughout this period. However growth in the [001] direction is observed in images c) to f), and the growth rate is calculated as 18.1 nm/min.

This technique, therefore, enables us to direct and pattern crystallization of aspirin, as previously illustrated with glycine [231] and calcite [188, 205, 234] crystals. However, we have also utilized this technique to monitor growth rates of these patterned crystals, as well as observe secondary nucleation upon them. The specific habit attained by all of the crystals patterned on to these templates is also indicative of the potential uses of this technique in pharmaceutical crystal growth. Of the problems encountered throughout the crystallization of pharmaceutical components, highlighted in Chapter 1, the occurrence of polymorphic and chiral drugs are prominent, as they present both economic and health issues. Polymorphic forms of a drug can have very diverse physical properties, which can result in diverging solubility and bioavailability of the drug products. The kinetic mechanisms underlying polymorphism are largely unknown and crystallization often results in the formation of more than one polymorph.

More than half of all marketed drugs are chiral and exist in at least two symmetrical enantiomer forms [75]. Currently crystallization is the most efficient method of separation of enantiomers, but in most cases this results in either crystals

of both enantiomers, or crystals containing proportions of each enantiomer. Difficulties in separation make the development of a single enantiomeric drug compound economically impractical. Consequently drugs are often administered as a mixture of enantiomers, even if the two enantiomers exhibit different pharmacological activity profiles [28]. The most well-known and tragic example of such a drug is thalidomide. During the 1960's thalidomide was administered to pregnant women to relieve morning sickness. The R-enantiomer of the drug has a sedative effect whereas the S-enantiomer is highly teratogenic, causing deformities in unborn children.

The ability to control and dictate crystallization of a particular polymorph or enantiomer of a drug is an aspiration of those involved in drug design and delivery. Here we illustrate a technique which enables crystallization of a particular habit of aspirin. In principle these experiments could be adapted and exploited to direct nucleation of particular polymorphs or enantiomers of drugs, or indeed to search for unknown polymorphs, and may thus provide critical information to the pharmaceutical industry.

In order to fully scrutinize the mechanisms taking place during nucleation and the fundamental stages of aspirin crystal growth, the preparation of templates with smaller nucleation areas is imperative. In addition, more precise determination of the location of these areas is necessary. The preparation of PDMS stamps is relatively easy and inexpensive, so the creation of stamps with smaller features would be a simple task. As mentioned earlier in the chapter, microcontact printing allows the production of features as small as 200 nm, and can therefore be utilized to produce smaller nucleating areas. Chemical force microscopy has previously been used to

differentiate the locations of SAMs on a patterned surface and thus could be used in a similar manner here [248-251].

Although the lattice of SAMs bearing different functional groups are similar, the structure, chemical nature, and co-ordination number of their terminal groups vary [205]. Thus the application of a wider range of SAMs, including those with terminal groups akin to the aspirin molecule, may enable directed growth or selective attachment of aspirin crystal faces on the SAM surface. These experiments could also be employed to control resulting crystal habit, size, and overall morphology of this and other drug crystals.

This technique enables the fabrication of a large number of nucleation sites in controlled microenvironments on the same surface. It should hence allow us to study the influence of crystallization parameters such as supersaturation, solvent, pH and temperature, on crystal growth and polymorphism.

3.4 Conclusion

The control, design, and promotion of crystal growth are greatly desired objectives of crystal engineers and the pharmaceutical industry alike. In order to achieve this goal more information is required on all aspects of the crystal growth procedure. In the previous chapter we investigated the growth on the face of an aspirin crystal at two supersaturations. Here we have focused on the nucleation and promotion of aspirin crystal growth. Methods previously used to promote crystal growth employed synthetic surfaces, such as Langmuir monolayers and functionalized polymer surfaces. The drawbacks of these surfaces lie in their lack of homogeneity, and as a result, the control of crystal growth on such surfaces is problematic. In recent years

SAMS have come to the fore as surfaces upon which crystallization can not only be promoted, but can also be directed and patterned in predetermined locations.

In this chapter we have assessed the aspirin binding capabilities of three SAMs chemisorbed on gold. Of the three SAMs investigated, only the carboxyl-terminated 11-MUA SAM allowed aspirin crystals to nucleate on its surface. We assume that aspirin molecules bind to the SAM via hydrogen bonding between the two carboxyl groups, in a manner similar to that of aspirin molecules dimerizing in the crystal structure.

Further investigation is required to precisely determine the mechanism of crystal formation on the SAM surface. However, nanostructure growth on surfaces is postulated to occur via the Deposition, Diffusion, and Aggregation (DDA) model. This model suggests that atoms or molecules (adatoms) deposit onto the surface and diffuse across it until they reside in a site next to another adatom or cluster. Here they bind irreversibly and the resulting cluster of molecules can continue to diffuse across the surface. SAMS have similar densities to crystalline solids, and hence this process could be considered epitaxial growth.

Microcontact printing facilitated the patterning of gold substrates with 11-MUA and 1-DDT SAMs, and has allowed us to create templates comprising aspirin-binding and non-binding regions. Incubation of these templates in aspirin solution resulted in the patterned formation of tabular unidirectional aspirin crystals. However, the dimensions of the crystals and channels did not mirror the dimensions of the stamp features and more than one crystal nucleated within each stamped area. Therefore the parameters of the stamp used for our experiments need to be optimized in order to create patterns which promote nucleation of only one aspirin crystal per nucleating site.

Nevertheless, the observation that this template promoted the growth of highly oriented crystals implies that it allowed nucleation to occur at specific sites. The periodic pattern of crystals formed on the surface reflects the influence of mass transport. Again the growth of crystals on the surface followed the DDA model. However, we suspect that the flux of aspirin molecules to the specific nucleation sites increased as the crystals began to grow. Mass transport of aspirin molecules to the growing crystals therefore depleted the concentration of aspirin in the vicinity, thus locally undersaturating the solution. This set up local diffusion gradients and elevated the transport of aspirin molecules to the nucleating sites. A positive feedback process was thus induced, which perpetuated the growth of crystals at nucleation sites, and produced non-nucleating zones surrounding the growing crystals where the aspirin concentration was depleted [234]. The channels or distances between the crystals on the surface represented the non-nucleating zones.

The face of the crystal which bound to the SAM was (100), and the resulting crystals formed on the SAM had a tabular habit bounded by the faces {001}, {011}, and {110}. Techniques such as chemical force microscopy, time of flight secondary ion mass spectroscopy (TOF-SIMS), and imaging X-ray photoelectron spectroscopy (XPS), would further prove the location of the 11-MUA and 1-DDT SAMs within the templates, and would also identify the surface groups on the protruding crystal faces. These techniques could, thus, verify our findings.

These templates have also permitted us to observe the secondary nucleation and growth of a cluster of aspirin molecules on the surface of another aspirin crystal. The observation that growth of the nucleus in the [001] direction was initially dominant but was then curtailed, whilst growth in the [100] direction increased, may

aid in the explanation of the tabular habit of the crystals grown on the underlying SAM.

This technique, in conjunction with AFM, also allowed visualization of the growth of a crystal bound to the SAM surface. Only growth in the [001] direction was observed, with the growth rate calculated as 18.1 nm/min.

In order to further investigate the mechanisms of nucleation of these crystals, the preparation of templates with smaller nucleation areas is imperative. In addition, the location of aspirin-binding regions must be more precisely known. These criteria can be met by microcontact printing and chemical force microscopy respectively.

In addition, the application of a wider range of SAMs, including those with terminal groups akin to the aspirin molecule, may be used. These may prove to direct the growth or attachment of specific aspirin crystal faces on the SAM surface. These experiments could also be employed to control the resulting crystal habit, size, and overall morphology of this and other drug crystals. They may also provide a surface upon which nucleation and growth can be monitored under differing crystallization parameters. Thus the effect of such factors as supersaturation, pH, solvent, and temperature can all be quantified.

The methods described here can be adapted to investigate the nucleation and fundamental stages of growth of drug crystals to provide much needed information to the pharmaceutical industry. Such knowledge may assist in predicting the outcomes of crystallization, controlling polymorphism, directing nucleation of polymorphs or enantiomers, or searching for unknown polymorphs. These techniques may thus aid in preventing the formation of unwanted morphologies of drugs.

Chapter

4

The effects of additives on the morphology and growth on the (001) face of paracetamol crystals.

It is well known that the presence of impurities can dramatically affect the nucleation, morphology, and chemical properties of crystals. Although literature is replete with examples of impurity or additive-induced modifications of crystals, few have probed the interaction of these compounds with distinct growing faces. In this chapter we utilize AFM and SEM to investigate the influence of two structurally related additives of paracetamol on its crystal morphology. We also probe, *in situ*, the effects of these additives on the morphology and growth rate of steps on the (001) face of the crystal. This, in conjunction with further studies, may establish the specific mechanisms of inhibition of these additives on each face of paracetamol, and provide a means of overcoming the poor compaction behaviour of paracetamol.

4.1 Introduction

4.1.1 The effects of impurities on crystal nucleation and growth.

Chapter 1 highlighted the need to develop crystallization studies which investigate how factors such as solvent, supersaturation, temperature, and impurities influence the bulk and surface properties of crystalline materials. Such information may enable a greater degree of control over crystallization, and may facilitate the manufacture of crystals with a particular processing behaviour. In this chapter, we focus upon the effects of impurities.

It has long been recognized that the presence of trace amounts of impurities can have substantial effects on the kinetics of crystal nucleation, growth morphology and dissolution [49, 50, 56, 58]. Mullin [4] stated that the suppression of nucleation may result from changes in the equilibrium solubility or the solution structure, or by physical or chemical adsorption of the impurity on homogeneous or heterogeneous nuclei. During growth, impurities can adsorb onto the crystal surfaces, changing the relative surface free energies of the faces and blocking the active growth sites. Some impurities can suppress growth entirely, some may enhance growth, whilst others may produce a selective effect, acting to varying degrees on each crystallographic surface, and consequently modifying the crystal habit [4].

The classic model of Cabrera and Vermilyea [252] proposes that impurities can adsorb onto terraces or steps of growing crystals, and become almost immobile. Impurities which have adsorbed onto a terrace cannot be passed by a straight growing step, because impurities act as local pinning points. Therefore, these impurities serve as a “fence” to growing steps. Consequently, growing steps must

bend in order to squeeze through the impurity “fence” and, as a result, the velocity of the steps is reduced compared to that of straight steps growing in the absence of impurities.

4.1.2 Impurities in pharmaceutical compounds.

Impurities may be additives that are introduced for specific purposes, such as habit modification or to control crystal size, or may be impurities that result from the synthesis or degradation of the desired end product. If the solubility of an impurity or additive is close to that of the product, its removal during the purification process may be difficult. Impurities or additives have the potential to modify the solubility of the primary solute and thus affect the crystallization process. One specific application of additives in the crystallization process is in transdermal delivery. Additives, such as the polymers polyvinyl pyrrolidone (PVP) [25, 62] and hydroxypropyl methylcellulose (HPMC) [25, 253-256], are used as nucleation inhibitors to allow the supersaturation of a drug to be enhanced without inducing crystallization. Hence, the concentration of the drug is increased, as is the subsequent permeation of the drug through the skin [25, 253-257].

Structurally related compounds are common impurities in pharmaceutical components. These compounds become incorporated with varying efficiencies, and can, hence, influence the nucleation and subsequent crystal growth rate of the solute. As the distinct faces of crystals are influenced to different degrees, due to their contrasting molecular structure, morphological changes are often observed, sometimes at concentrations as low as several parts per million [96]. The presence of structurally related compounds has been shown to distinctly alter the habit of

pharmaceutical excipients, such as adipic acid [34, 51, 53, 54, 57] and α -lactose monohydrate [39].

It has been suggested that growth of drug crystals in the presence of low concentrations of additives can provide a means of controlling water content, crystal energy and order, dissolution rate, and possibly bioavailability [19].

Literature is replete with references to the additive-induced effects on crystalline drug compounds [34, 39, 51, 53, 54, 57, 258-260]. Of these studies, only a limited number are sufficiently quantitative to provide adequate insight into the specific mechanisms involved. For pharmaceutical technology, understanding of these mechanisms may help to control the quality and purity of raw crystalline substances and, consequently, to improve the manufacture and performance of the final dosage forms [96].

4.1.3 Paracetamol and its structurally related additives.

Paracetamol, also known as *p*-hydroxyacetanilide or acetaminophen, was first launched as a drug in 1956 and has now grown to be the most widely accepted antipyretic and analgesic in the world, used by over 30 million people in the U. K. every year [261].

Two crystalline polymorphs of paracetamol have been reported, although evidence has been published which suggests that a third polymorph could exist [262]. The crystal structures of the two known forms of paracetamol are monoclinic [263-270] and orthorhombic [262, 267, 270-273]. The monoclinic form is the

thermodynamically stable polymorph at room temperature and, hence, is the commercially used form of paracetamol.

A particular problem with the monoclinic form of paracetamol is that it displays poor compaction behaviour, that is, it resists compression into tablets [274-276]. It has been suggested that a modification of the structure or defect density of paracetamol crystals may produce more readily compressible structures [274]. Currently, there is considerable interest in modifying the properties of paracetamol using different crystallization techniques or additives in order to improve the compaction behaviour of the crystals [272, 274-280].

There are six known structurally related additives of paracetamol which have been observed to inhibit the nucleation and growth rates of paracetamol crystals to varying degrees [19-23, 29, 37, 59, 96, 281]. These are acetanilide, p-acetoxyacetanilide (PAA), orthocetamol, methylparaben, p-acetoxybenzoic acid (PABA), and metacetamol. The molecular structures of paracetamol and its structurally related additives are illustrated in Figure 4. 1.

Of these additives, the effects of PAA, (a suggested prodrug of paracetamol) [282, 283], on paracetamol crystallization have been the most extensively studied [19-23, 29, 59, 96, 281]. The effects of PAA on the morphology [23, 29, 59], nucleation [22, 23, 59], dissolution, *in situ* growth [96], melting point, enthalpy and entropy of fusion, uptake of water [19], and defect content [59] of paracetamol have all been investigated. On the contrary, the influence of the remaining additives on only the morphology [23] and nucleation [22, 23] of paracetamol crystals has been reported.

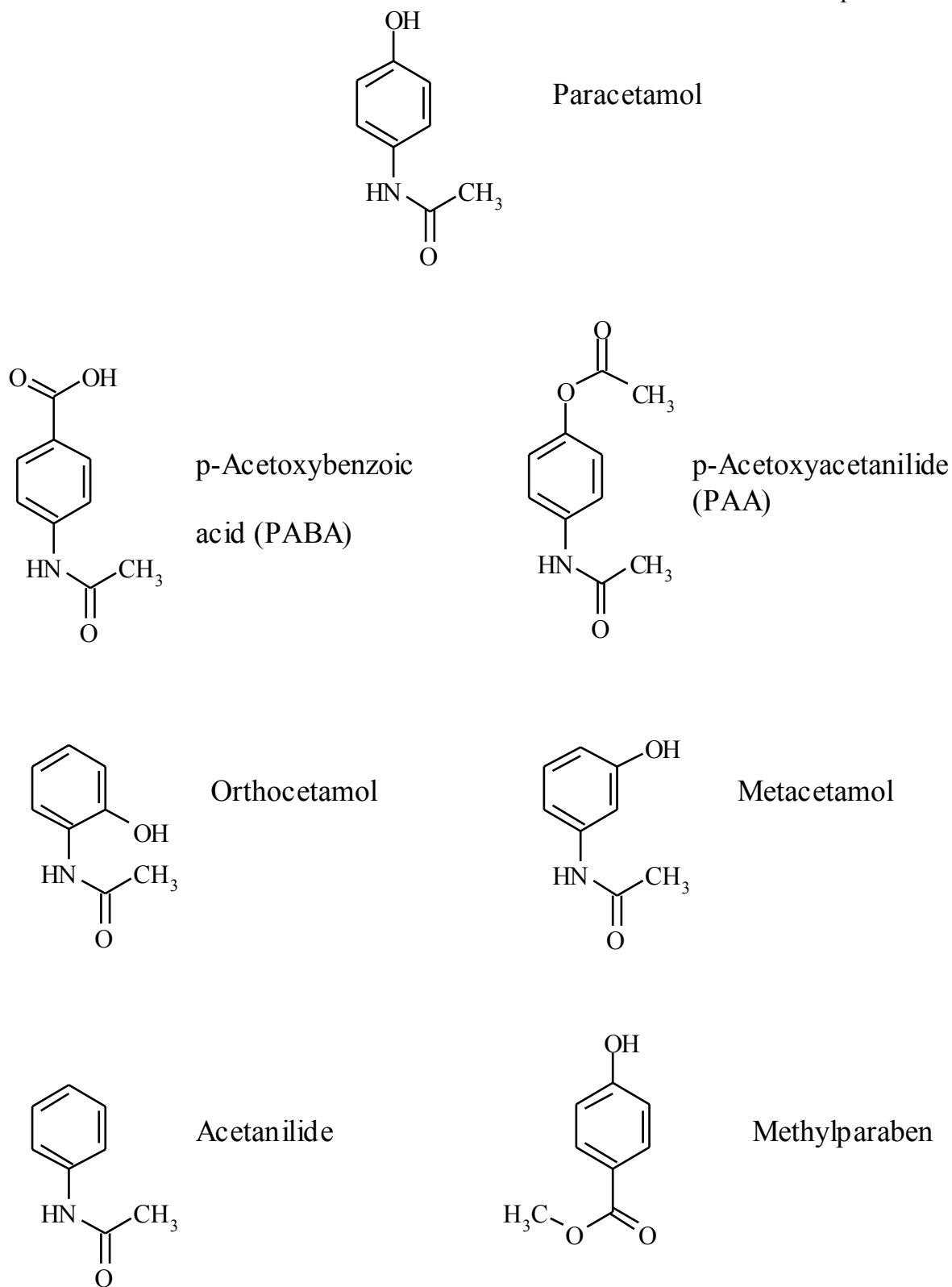


Figure 4. 1 The molecular structures of paracetamol and the structurally related additives which are known to inhibit its growth.

A primary feature of the paracetamol crystal structure is hydrogen bonding. This bonding leads to the formation of hydrogen bonded chains of molecules, packed in a herring bone conformation within the crystal structure. The molecular structure of a paracetamol crystal on the (001) face is shown in Figure 4. 2. The molecules form corrugated hydrogen bonded sheets which stack in the [010] direction. The consecutive stacks are bound by van der Waals interactions [281]. Any disruption to this bonding motif will lead to a change in the corresponding crystal growth rate and hence lead to a modification of the crystal habit [23]. There are two hydrogen bonding donors within the paracetamol molecule, N-H and O-H, and one hydrogen bond acceptor, C=O. The degree of hydrogen bonding which occurs within the paracetamol crystal has been quantified as $8.31 \text{ kcal mol}^{-1}$ [23]. This corresponds to approximately 30% of the total lattice energy. Thus, any additive which disrupts the hydrogen bonding network within the crystal has the potential to significantly alter its morphology.

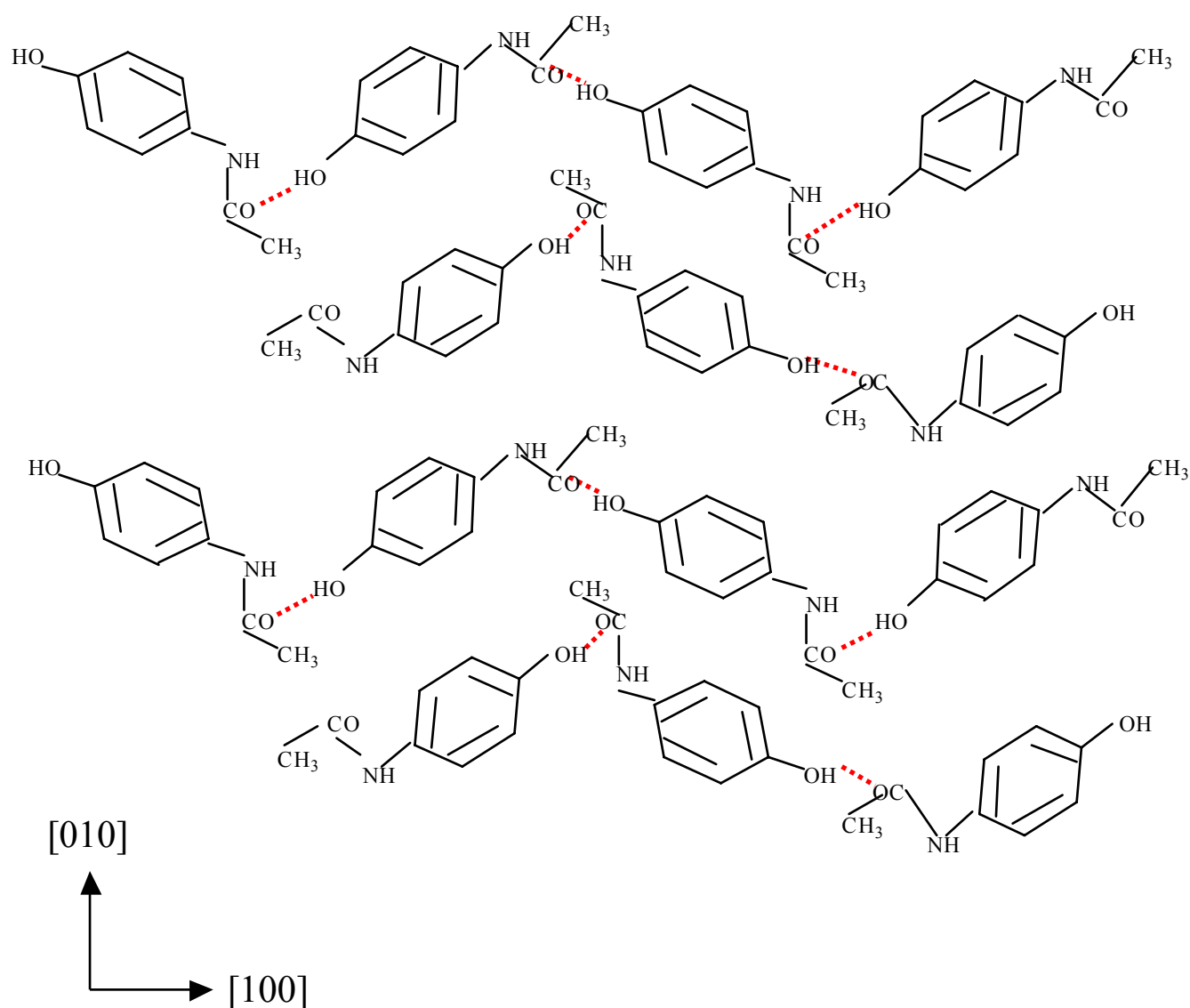


Figure 4. 2 Diagrammatic representation of the molecular packing of paracetamol on the (001) face of the crystal. Both [010] and [100] directions are shown. The molecules adopt a “herring bone” arrangement, where the molecules within each layer are held together by hydrogen bonds, indicated by dashed red lines. Adapted from [281].

It has been proposed that structurally related additives may influence the nucleation and crystal growth of paracetamol in three principal ways [23]. Additives may:

- i) Block adsorption of solute molecules and therefore induce morphological changes.
- ii) Dock onto the surface and become incorporated into the crystal lattice. An effective measure of the docking ability of additives is given by the segregation coefficient (SC). The SC is defined as the ratio of the mole fraction of additive in the crystals, to that in the crystallizing solution. Thus, additives that are incorporated as readily as paracetamol itself have an SC value of 1, whereas those not incorporated at all have an SC value of 0.
- iii) Disrupt the emerging nucleus and thus inhibit the nucleation process.

Each of these interactions depends upon the molecular similarity of the additive to paracetamol, both energetically and sterically. Although these interactions are interrelated, it is convenient to consider each separately [23]. The blocking, docking, and disrupting behaviours of the six additives which inhibit paracetamol growth have been extensively studied by Hendriksen *et al.* [23]. However, these studies have been conducted on entire crystals. We, therefore, wish to supplement this information by performing AFM studies on the *in situ* growth on the (001) face of paracetamol crystals, in the presence and absence of additive molecules. For these initial studies, two of the lesser studied additives have been selected, namely acetanilide and metacetamol. The blocking, docking, and disrupting activities of these two additives are described in the following sections.

4.1.4 Blocking activity of acetanilide and metacetamol.

“Blocking” is the ability of an adsorbed additive molecule to hinder the subsequent adsorption of further layers of host molecules. As the additive molecules block different faces of the crystal to differing degrees, the growth rates of some faces will be dramatically altered, whilst others will remain unchanged. Consequently, the morphology of the resulting paracetamol crystals may be altered.

Acetanilide caused appreciable morphological changes, despite its relatively low level of uptake into paracetamol crystals, as indicated by the SC value of 0.11. It was therefore considered a potent blocking molecule [23].

Metacetamol also caused a high degree of morphological change, inducing a large shift in the aspect ratio. The aspect ratio is defined as the ratio of distances between the centre of the crystal and the furthest and nearest faces [89]. However, its uptake level was much higher than that of acetanilide, at SC = 0.25, and was thus considered to be a less effective blocker [23]. The reasons proposed for the observed morphological effects of these additives are discussed below.

In order to successfully block the adsorption of a host molecule in a subsequent crystalline layer, a blocking molecule must present a conformation sterically and energetically different from that of paracetamol. If we consider a face or faces in which paracetamol molecules are oriented with their acetamido groups positioned inwards (away from the crystal-solution interface), we can discuss the potential blocking effects of these additives.

Acetanilide has no group in the *p*-position (Figure 4. 1), so no steric hindrance is present. However, it does not possess a proton donor to contribute to the

existing hydrogen bonding network, and hence it strongly blocks further addition of paracetamol molecules [23].

Similarly, metacetamol presents no great steric hindrance. It possesses an OH group in the *m*-position, allowing the hydrogen bonding network to be largely preserved, although distorted. As a result, metacetamol appears to be a less effective blocker than acetanilide [23].

4.1.5 Docking activity of acetanilide and metacetamol.

“Docking” is the ability of a molecule in solution to be adsorbed onto the growing crystal surface in an orientation which will allow its inclusion into the crystal lattice. A molecule which successfully docks onto a crystal face may not block the arrival of further paracetamol molecules. If it does block effectively, the level of incorporation of this molecule into the crystal lattice will be less than that of a poor blocker. The level of incorporation of an additive is a reasonable measure of its docking ability, provided that its blocking ability is taken into consideration [23].

Using these criteria, metacetamol was judged to be a strongly docking molecule, due to its high level of incorporation ($SC = 0.25$) and only moderate blocking activity. Metacetamol contains an acetamido group identical to that of paracetamol, which may aid in its successful docking.

Acetanilide too contains an acetamido group identical to paracetamol. Its SC value was 0.11 and, as already mentioned, it is thought to be an excellent blocker of the growth of subsequent layers of paracetamol. It is therefore presumed that its moderate level of incorporation may be due to good docking on the crystal surface, coupled with the effective blocking of further crystal growth [23]. On the basis of

molecular similarity, acetanilide and metacetamol were regarded as equally efficient dockers.

4.1.6 Disrupting activity of acetanilide and metacetamol.

“Disruption” is the ability of an incorporated additive molecule to reduce the stability of an emerging nucleus. Thus, the nucleation size critical for growth increases, inhibiting the nucleation process. The incorporated molecule generates this effect by a combination of steric and energetic disruptions of the hydrogen bonding network.

Experimentally, acetanilide and metacetamol were found to be only moderately disruptive [23]. The authors of these studies did not comment upon the disruptive activities of acetanilide and metacetamol. However, we propose that the disruptive ability of acetanilide is greater than that of metacetamol for the following reasons. The acetanilide molecule has no proton donor which can contribute to the hydrogen bonding network, and displayed this degree of disruption at a relatively low level of incorporation ($SC = 0.11$). Conversely, the *m*-OH group of metacetamol acts as a proton donor, allowing the formation of a preserved but distorted network of hydrogen bonds, and creates only a small steric disruption.

As described in the preceding sections, acetanilide is an effective blocker of the adsorption of paracetamol molecules during crystallization, is a strong docker, and is also moderately disruptive. Metacetamol is a less competent blocker than acetanilide, but its docking and disrupting abilities are equal to those of acetanilide.

As the growth studies performed in this chapter will be carried out on the faces of complete crystals, the disruptive effects of the additives cannot be

quantified. In addition, the AFM is unable to monitor the incorporation of additive molecules into the growing crystals and, hence, the docking activities of the additives cannot be further investigated through these experiments.

However, this method should enable the blocking activities of the additives to be both visualized and quantified. We envisage that growth in the presence of molecules which efficiently block adsorption of paracetamol onto the (001) face of the crystal should result in a change in morphology of growing steps, and should reduce the growth rate of steps, with respect to those grown in the absence of any additive. If these predictions prove to be accurate, similar experiments can be conducted to establish the blocking activity of each of the six additives on this and the other faces of paracetamol crystals. These data could be applied to the modification of paracetamol crystals, in order to optimize their compaction behaviour. Furthermore, AFM can be added to the series of techniques used to reveal the degree of inhibition induced by additives on specific faces of crystals.

4.1.7 Aims of chapter.

The influence of acetanilide and metacetamol on the morphology and growth of entire paracetamol crystals has previously been studied. However, there have been no investigations into the effects of these additives on the growth of individual faces of paracetamol crystals. In this chapter, we utilize both AFM and SEM to characterize the morphology of pure paracetamol crystals and those crystallized in the presence of an additive. In addition, we employ AFM to visualize and quantify the effects of these additives on growth on the most prominent, (001), face of paracetamol crystals.

4.2 Methods and Materials

4.2.1 Preparation of paracetamol crystals grown in the presence and absence of an inhibitor.

All crystals were prepared using a modified version of the cooling method described by Hendriksen *et al.* [23]. Pure paracetamol crystals were prepared by dissolving 2.674g of paracetamol (99%, Sigma Aldrich, Dorset, U.K.) in 200ml of HPLC grade water, which had been filtered once. This solution was heated to approximately 40°C, with a stirring rate of 238 rpm, until all of the solute had dissolved. It was then transferred to a refrigerator and maintained at 5°C. The solubility of paracetamol at 5°C is 8.21g/l [284]. The supersaturation (σ) of the crystallization media was calculated using Equation 2.1 from Chapter 2:

$$\sigma = \ln (c/c_0) \quad \text{Equation 2.1}$$

where c and c_0 are the actual and saturated solution concentrations respectively. The σ value of the crystallization media was calculated as 0.49. The crystals formed in solution over a period of four to five days, after which they were filtered, air-dried, and stored in a desiccator. Crystals containing additives were prepared in the same manner as described above, with an additive concentration equivalent to 4 mol%, with respect to paracetamol. This additive level was chosen as it has been previously used to investigate the effect of these compounds on the crystallization of paracetamol [23]. Thus, 0.096g of acetanilide (97%, Sigma Aldrich, Dorset, U.K.) or 0.107g of metacetamol (97%, Sigma Aldrich, Dorset, U.K.) were added to the solution prior to heating. Again, crystals formed over a period of four to five days, and were subsequently filtered, air-dried, and stored in a desiccator. The morphology

and surface features of these crystals were examined using SEM and AFM. Crystals were immobilized on AFM sample stubs using Temp fix (A gar, Stansted, U. K.) prior to examination.

4.2.2 Preparation of solutions for growth studies.

Growth solutions, without any additive present, were prepared by dissolving 0.192g of paracetamol (99%, Sigma Aldrich, Dorset, U.K.) in 10 ml HPLC grade water, which had been filtered once. These solutions were heated to approximately 40°C, with a stirring rate of 238 rpm, until all of the solute had dissolved. They were then allowed to cool to room temperature, before being placed in the AFM liquid cell with a paracetamol crystal sample. Growth solutions containing an additive were prepared in the same manner as described for pure paracetamol solutions. Solutions containing additive were prepared with a concentration equivalent to 4 mol%, with respect to paracetamol. In the case of the acetanilide-containing solution, 0.007g of acetanilide were added to the solution prior to heating, whereas 0.008g of metacetamol were added to its respective solution. All growth solutions were prepared immediately prior to each experiment. The σ value of paracetamol in each solution was expressed using Equation 2.1.

The saturated concentration or solubility of paracetamol (mol %) was calculated using the following equation [24, 27, 29, 285]:

$$\ln c_0 = 12200/T + 49.69 \ln T - 330.4 \quad \text{Equation 4.1}$$

where T is the absolute temperature in Kelvin. The temperature in all experiments was approximately 25°C (298K). Using Equation 4.1, the solubility of paracetamol at

this temperature was calculated as $0.095 \text{ mol dm}^{-3}$, which correlates well with measured values [284-286].

Hence, using Equation 2.1, the supersaturation of paracetamol, σ , in the solutions used for the growth experiments was calculated as 0.29. It should be noted that structurally related compounds are known to increase the solubility of paracetamol [19, 22, 287]. However, the degree to which acetanilide and metacetamol affect the solubility of paracetamol is yet to be determined, and hence the solubility of paracetamol in the growth solutions is taken to be that of a pure solution.

Prior to each experiment, paracetamol crystals were immobilized on AFM sample stubs, and then onto a suitable liquid cell using Temp fix (Agar, Stansted, U.K.). In each growth experiment, approximately 2.5 ml of the respective solution was placed in the liquid cell. Each sample was imaged continuously using AFM, after addition of the growth medium, to assess the growth rate in each solution, and to establish the extent of inhibition induced by acetanilide and metacetamol.

4.2.3 AFM analysis.

Contact mode imaging was employed throughout, using a ThermoMicroscopes Explorer AFM (Veeco, Bicester, Oxon, U.K.). V-shaped silicon nitride cantilevers (200 μm length) with integrated pyramidal tips (Nanoprobes, Veeco, Santa Barbara, CA) were used. Both topography and deflection images were acquired in all experiments.

4.2.4 SEM analysis.

All samples were initially gold coated for two minutes using a Balzers SCD 030 Sputter Coater (Balzers Union Limited, Liechtenstein), operated at 0.1mbar with a sputtering current of 30mA. A Philips 505 SEM (Philips Electron Optics, Eindhoven, Netherlands) was used to image all samples under a range of magnification settings at a voltage of 23KeV, with a spot size of 50 nm.

4.3 Results and Discussion

4.3.1 Morphology of crystals grown in the presence and absence of the additives acetanilide and metacetamol.

The SEM images of paracetamol crystals, Figure 4. 3, illustrate the habit of the pure paracetamol crystals. The tabular morphology attained by these crystals is consistent with that of paracetamol crystals grown at σ values greater than 0.15 [24, 29, 37, 59, 281], here $\sigma = 0.49$. A schematic diagram of the morphology of paracetamol crystals grown at $\sigma > 0.15$ is given in Figure 4. 4.

Figure 4. 5 shows AFM images of the surface of a paracetamol crystal. These images show steps ranging in height from 1 nm to 21 nm. The small, single molecular steps, which were previously found to be 10 Å in height [37], are curved in appearance, whereas the larger, multi-molecular steps have straight edges.

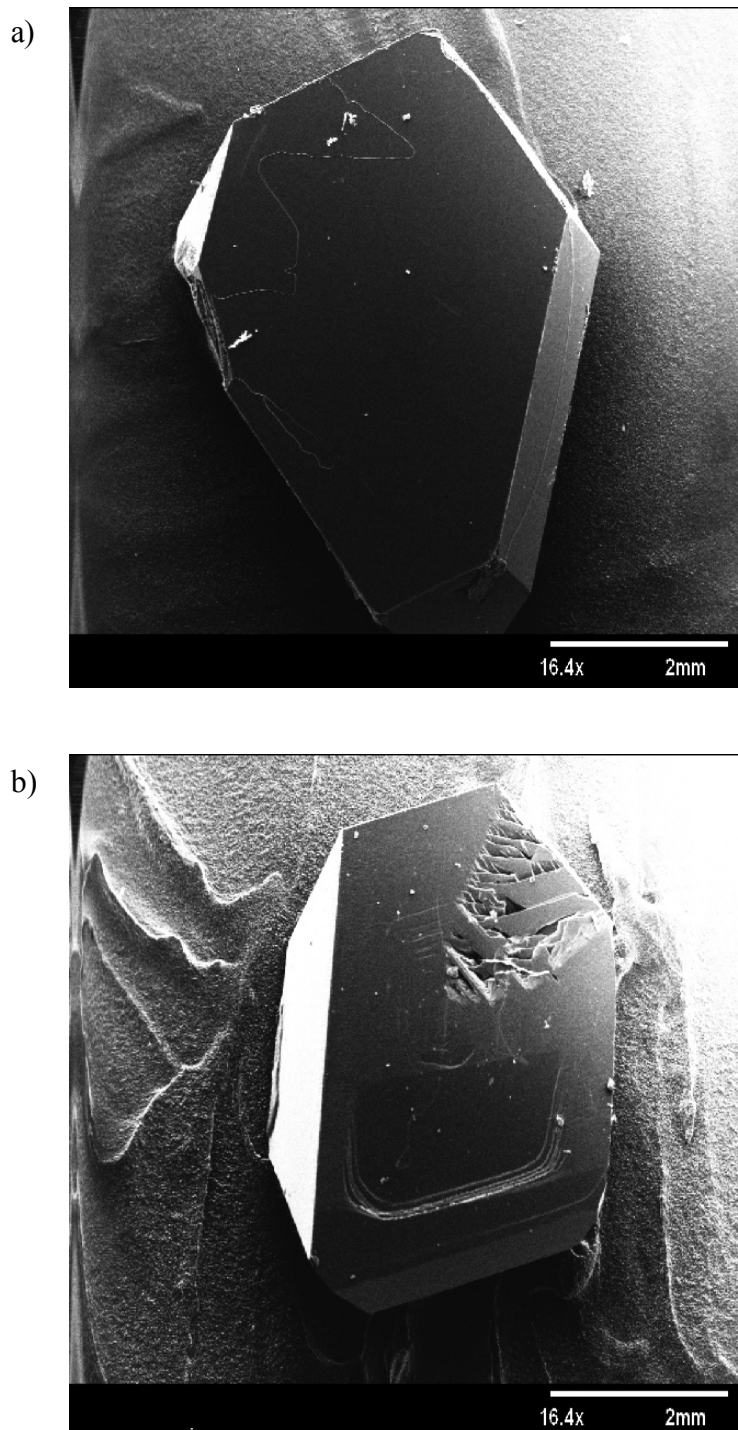


Figure 4. 3 SEM images of paracetamol crystals showing their tabular habit. Both images are at magnification x 16.4.

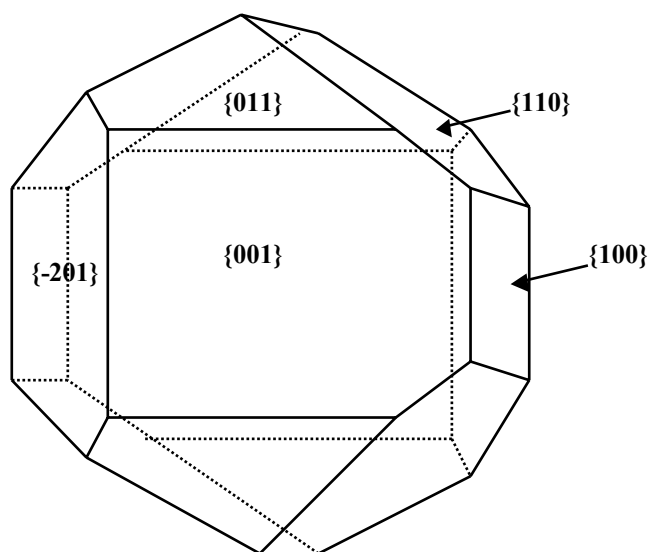


Figure 4.4 Diagrammatic representation of the morphology of paracetamol crystals grown at supersaturation values greater than 0.15. Adapted from [24].

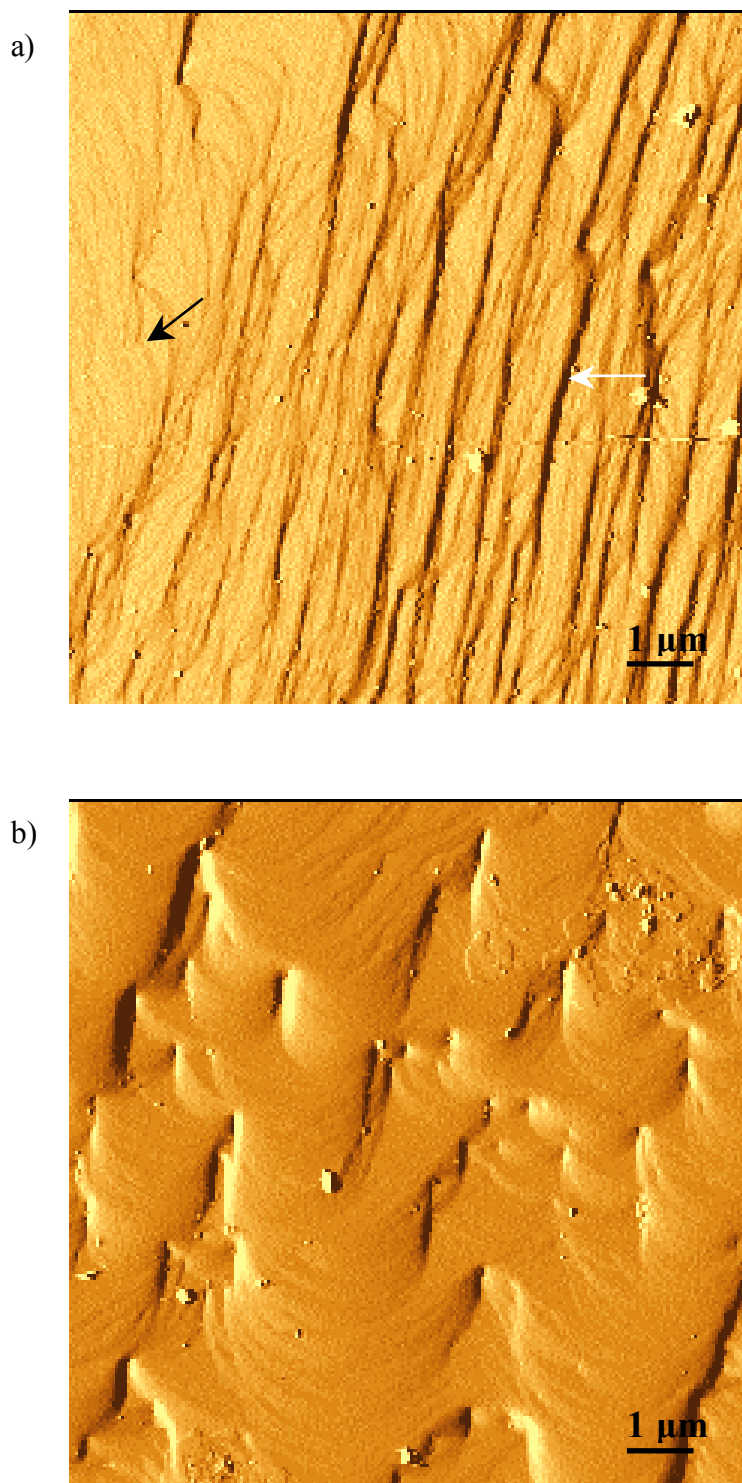


Figure 4. 5 10 μm x 10 μm AFM images of the surface of a paracetamol crystal acquired in air. Image a) illustrates the appearance of both small, curved steps (black arrow) and larger, straight-edged steps (white arrow) on the surface of the crystal. Image b) highlights the small steps visible on the surface. Both a) and b) are deflection images.

Figure 4. 6 shows SEM images of paracetamol crystals grown in the presence of 4 mol% acetanilide. Hereafter, these crystals shall be referred to as PA crystals. It is evident from these images that the habit of the PA crystals is comparable with that of paracetamol crystals, however, the PA crystals are smaller than paracetamol crystals. The AFM images shown in Figure 4. 7 reveal the surface features of the PA crystals. These images portray steps which appear to have thin, branched terraces, rather than having curved or straight edges, as seen for pure paracetamol crystals (Figure 4. 5). The steps, which are approximately 20 nm in height, may adopt this branched appearance due to the “pinning” of steps by the acetanilide molecules. Pinning occurs when additives adsorb onto step or terrace regions of the growing crystal and impede the progression of growing steps. These steps must bend in order to squeeze through the impurity “fence”, and hence acquire a convoluted appearance. A large number of holes, indicative of defects, are also present in the surface.

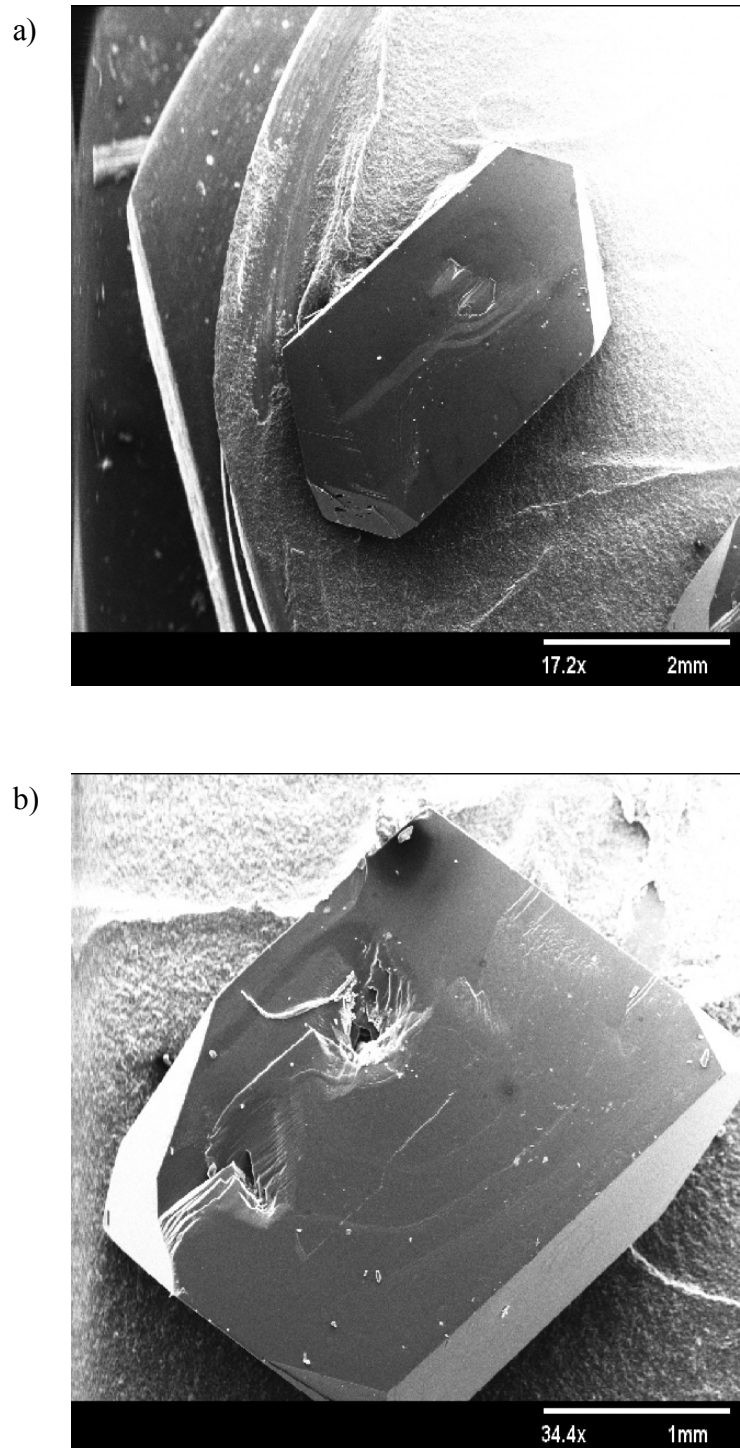


Figure 4. 6 SEM images of paracetamol crystals grown in the presence of 4 mol% acetanilide. Image a) is at magnification x 17.2, and b) is at magnification x 34.4.

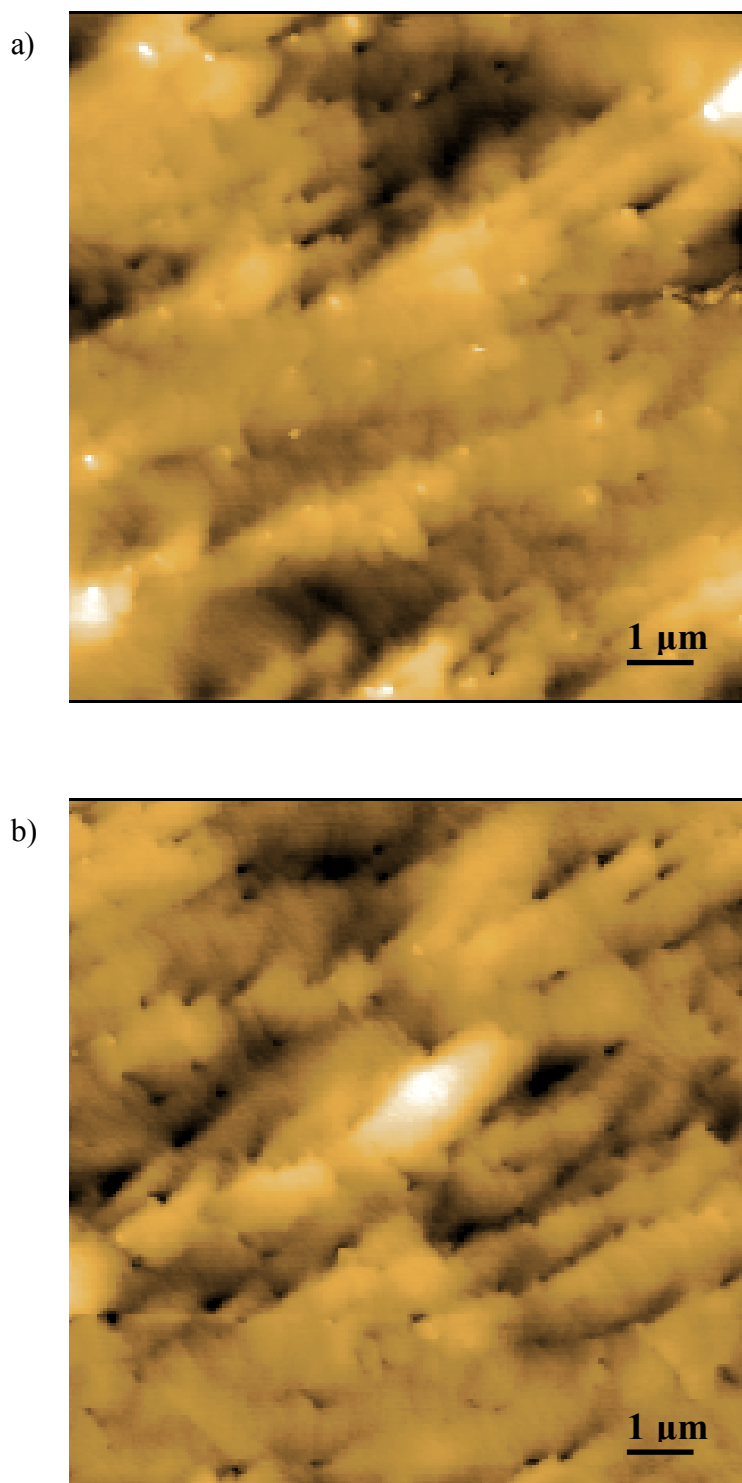


Figure 4. 7 10 μm x 10 μm AFM topographical images of the surface of a paracetamol crystal grown in the presence of 4 mol% acetanilide.

SEM images of paracetamol crystals grown in the presence of 4 mol% metacetamol are shown in Figure 4. 8. Hereafter, these crystals shall be referred to as PM crystals. Clearly, PM crystals attain a columnar habit, distinctly different from the tabular morphology observed with both paracetamol and PA crystals. From these data it is evident that the aspect ratio of the paracetamol crystal is more significantly affected by the addition of metacetamol to the crystallization medium than by acetanilide. These data are consistent with previous findings which calculated aspect ratios of paracetamol crystals grown in the absence of any additive as 1.2, whereas those grown in the presence of 4 mol% of metacetamol or acetanilide had aspect ratios of 7.33 and 2.84 respectively [23].

Figure 4. 9 shows AFM images of the surface of a PM crystal. Image a) depicts steps of approximately 15 nm in height interspersed with holes in the surface. A defect is also evident in the centre of the image. Figure 4. 9b) illustrates the cavities formed in the surface as a result of the crystallization in the presence of 4 mol% of metacetamol. The cavities are up to 65 nm in depth. It is clear from these images that metacetamol considerably increases the defect density of the (001) face of paracetamol crystals. These data suggest that the crystal lattice is significantly disrupted by metacetamol molecules during growth.

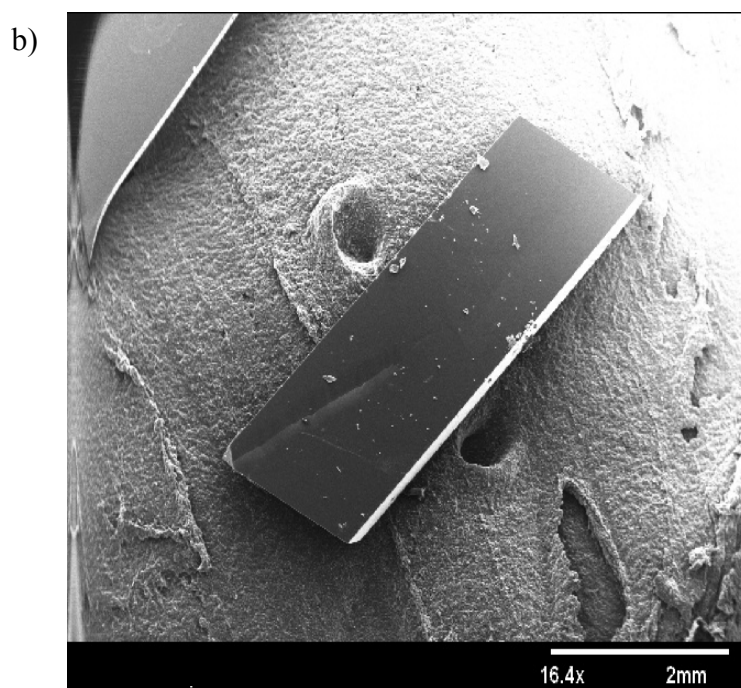
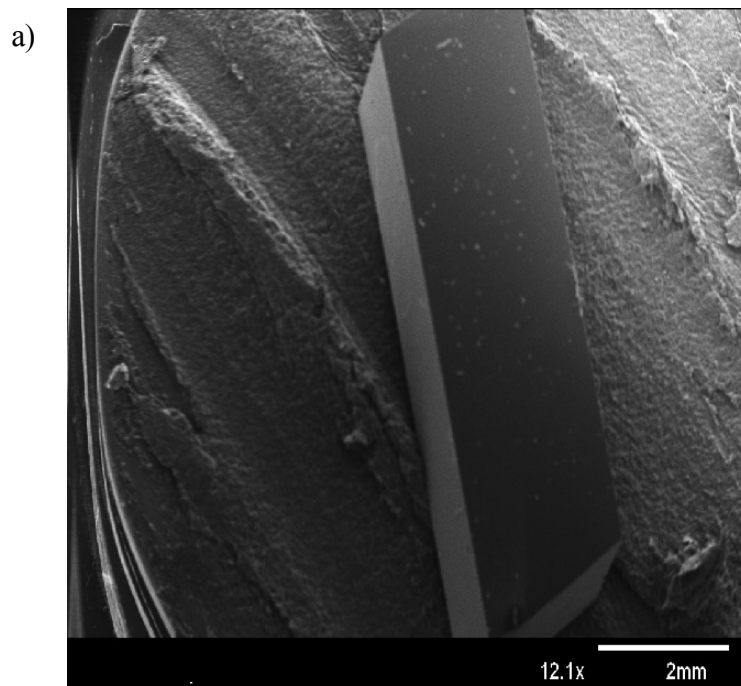


Figure 4. 8 SEM images of paracetamol crystals grown in the presence of 4 mol% metacetamol. Image a) is at magnification x 12.1, and b) is at magnification x 16.4.

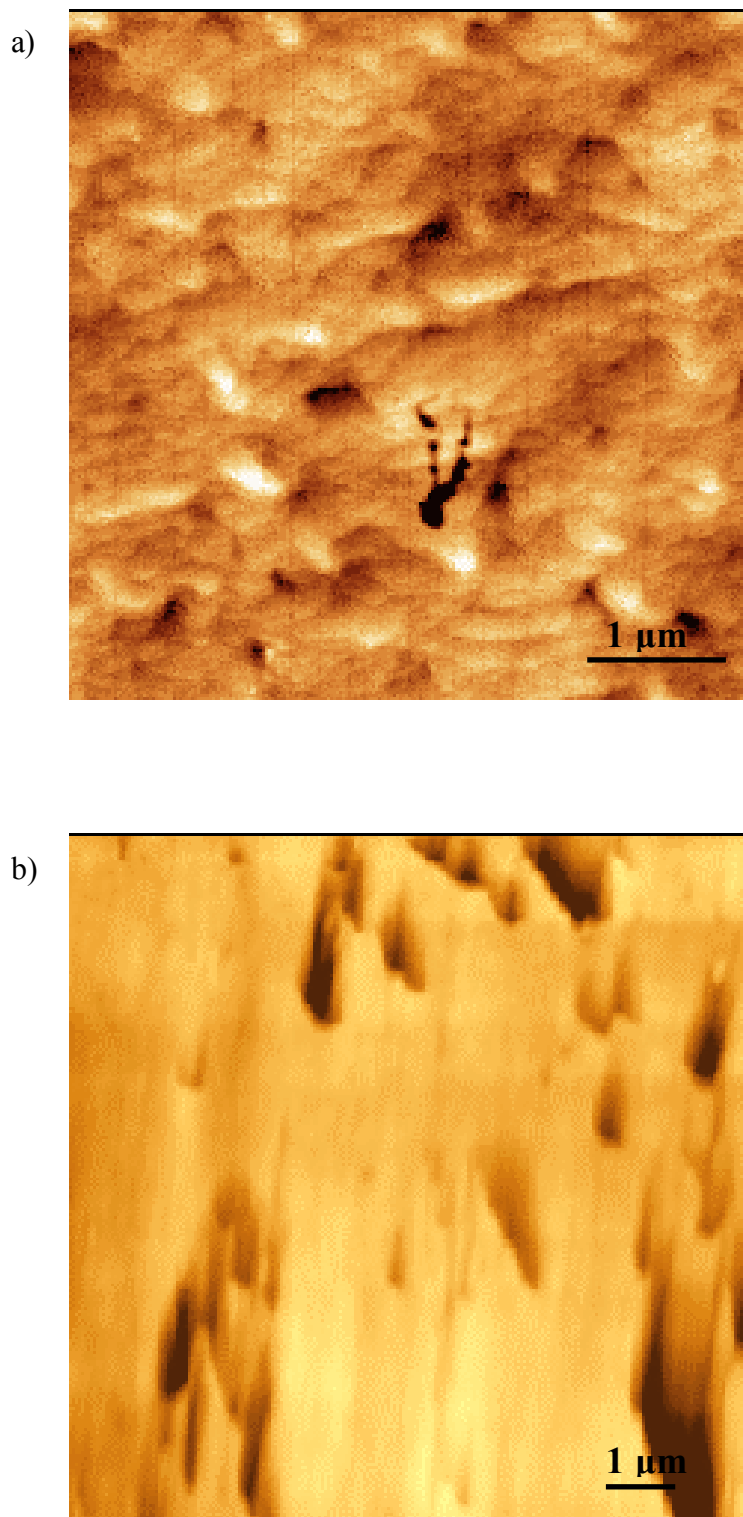


Figure 4. 9 AFM topographical images of the surface of a paracetamol crystal grown in the presence of 4 mol% metacetamol. a) is a 5 μm x 5 μm image, b) is a 10 μm x 10 μm image.

4.3.2 Growth on the (001) face of a paracetamol crystal in solutions of pure paracetamol, and those containing acetanilide or metacetamol.

The sequence of images in Figure 4. 10 illustrate the growth of steps on the (001) face of a paracetamol crystal during incubation in a pure solution, where $\sigma = 0.29$. The steps range from 95 nm to 588 nm in height, and hence are macrosteps. The steps are curved in appearance, indicating that they are growing via the dislocation mechanism. This mechanism of growth is described in Chapter 2, and illustrated Figure 2. 1. In summary, a dislocation occurs as a result of stresses on the crystal during growth. These stresses induce sections of the crystal to become misaligned with respect to their neighbouring areas [1, 98]. As a result, a ledge is formed onto which molecules can absorb and continue growth. However, as the ledge is of non-uniform height, growth occurs in a spiral pattern around the dislocation, and the growth mechanism is often referred to as screw dislocation [98, 103]. The features which arise from growth around such a dislocation are growth hillocks.

These data are consistent with previous studies which have shown that all of the major faces of paracetamol ($\{110\}$, $\{001\}$, and $\{-201\}$) grow via a dislocation mechanism [27]. The rate of growth of the observed steps ranges from 26.4 nm/s to 76.2 nm/s, and decreases with increasing step height. The steps are observed to grow in the $[-100]$ direction.

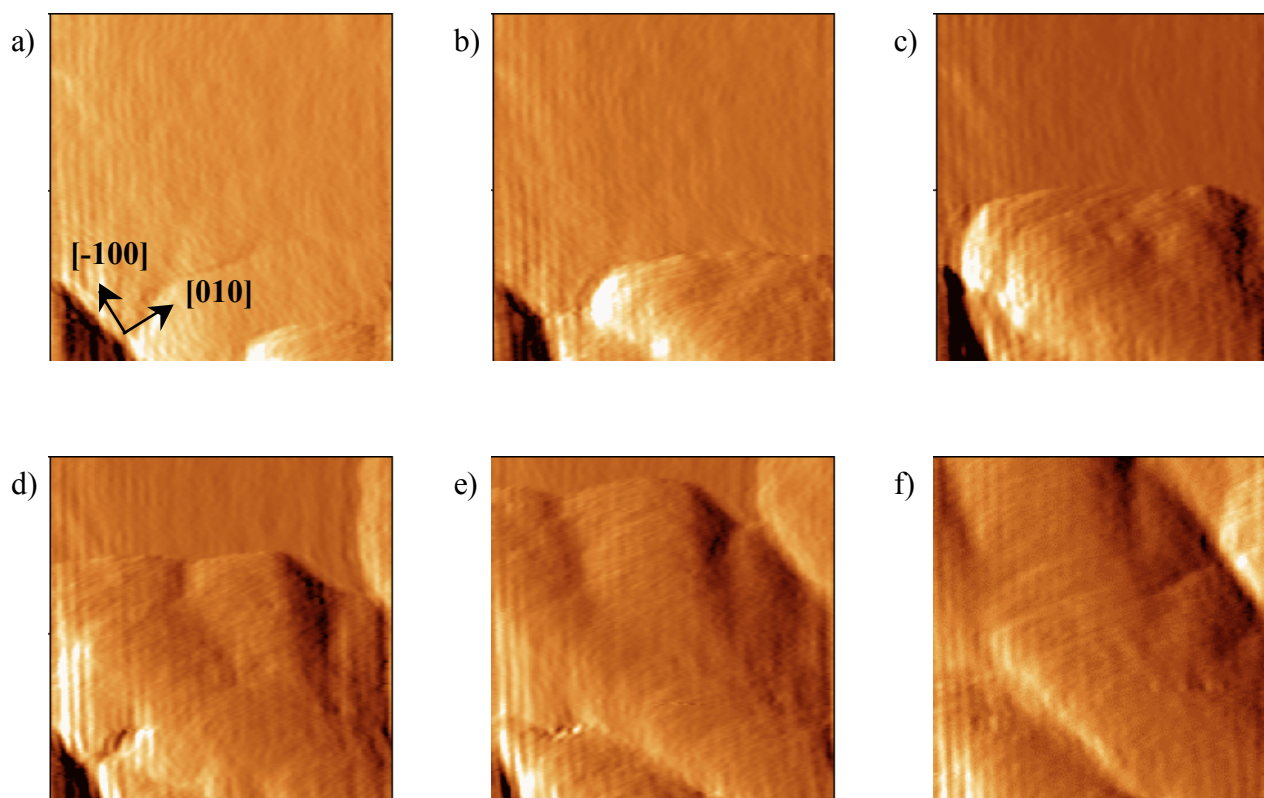


Figure 4. 10 A sequence of $10\ \mu\text{m} \times 10\ \mu\text{m}$ AFM images of the (001) face of a paracetamol crystal during incubation in paracetamol solution of supersaturation 0.29. In image a) time $t = 0$ secs, b) $t = 60$ secs, c) $t = 118$ secs, d) $t = 176$ secs, e) $t = 234$ secs, and f) $t = 292$ secs. All images are deflection images.

The images shown in Figure 4. 11 display the (001) face of a paracetamol crystal during incubation in paracetamol/4 mol% acetanilide solution. The supersaturation of the solution is 0.29, with respect to paracetamol. From these images it is clear that dissolution is occurring on the face. Prior to incubation in paracetamol/4 mol% acetanilide solution, the surface of the crystal exhibited features comparable to those shown in Figure 4. 5. However, after 11½ minutes of incubation, holes emerged in the surface. One such hole is highlighted by an arrow in Figure 4. 11a), and its dissolution is followed by an arrow in subsequent images. These holes may originate from defects in the crystal surface. The steps, which range from 13 nm to 45 nm in height, are observed to dissolve at rates between 1.3 nm/s and 2.7 nm/s, in the [100] direction. The dissolution rate of the steps decreases with increasing step height. The holes or clefts in the surface are also observed to deepen over time, indicating that dissolution is taking place towards the crystal core as well as laterally.

As previously mentioned, the presence of additive molecules increases the solubility of paracetamol, which may induce the dissolution demonstrated here. However, we cannot assume that dissolution is ubiquitous over the crystal, as the remaining faces may be influenced to different degrees by the additive molecules. Further studies must be undertaken to evaluate the affect of such levels of acetanilide on the other faces of paracetamol crystals. These studies should allow a more precise determination of the extent to which acetanilide inhibits paracetamol crystal growth.

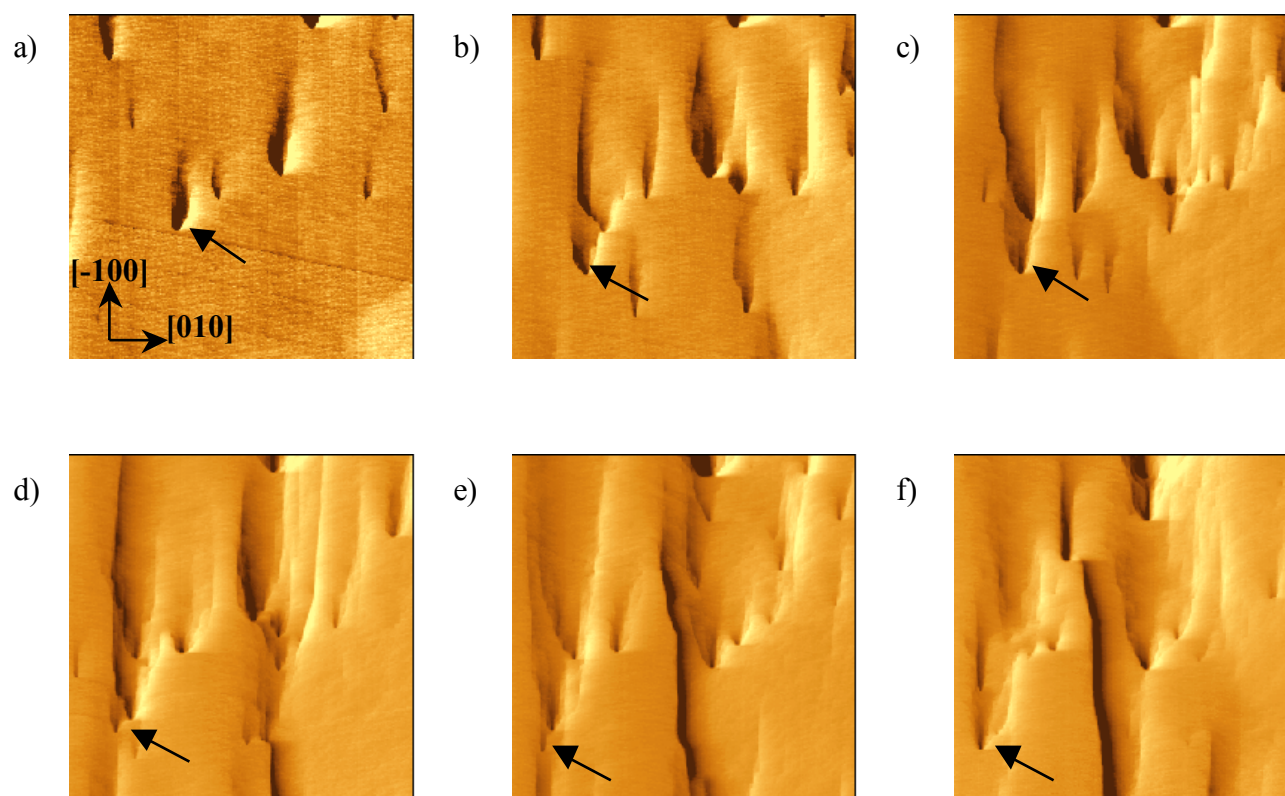


Figure 4. 11 A sequence of $10\ \mu\text{m} \times 10\ \mu\text{m}$ AFM images of the (001) face of a paracetamol crystal during incubation in paracetamol/4 mol% acetanilide solution. The supersaturation of the solution is 0.29, with respect to paracetamol. In image a) time $t = 0$ secs, b) $t = 146$ secs, c) $t = 290$ secs, d) $t = 436$ secs, e) $t = 582$ secs, and f) $t = 728$ secs. All images are deflection images.

Figure 4. 12 shows a sequence of AFM images of the (001) face of a paracetamol crystal during incubation in paracetamol/4 mol% metacetamol solution. The supersaturation of the solution is again 0.29, with respect to paracetamol. A black and a white arrow follow the movement of two steps on the surface. From these images, it is clear that steps are growing in the [-100] direction. The steps range from 4 nm to 21 nm in height, and their calculated growth rates range from 19.0 nm/s to 37.8 nm/s, with no relation between step height and growth rate.

From the AFM images alone, it is evident that the progression of steps is hindered by metacetamol molecules. Those images showing growth during incubation in pure paracetamol solution, Figure 4. 10, illustrate that in such an environment, the face grows via the dislocation mechanisms of macrosteps. However, the images shown in Figure 4. 12 portray significantly smaller steps which are pointed in appearance, implying that “pinning” may be taking place. As previously stated, pinning occurs when additives adsorb onto step or terrace regions of the growing crystal, and thus, the steps must bend in order to squeeze through the impurity “fence”. Here, the steps acquire a pointed appearance. These characteristic pointed, and thus pinned, steps have been observed using AFM in other crystal-additive systems [138, 139, 288, 289].

The presence of metacetamol molecules not only alters the morphology of the growing steps, it also reduces their growth rates from an average of 49.5 nm/s to 27.1 nm/s in the [-100] direction. These data are also consistent with previous AFM studies on additive effects on growth interfaces, which show a considerable retardation in step velocity in the presence of additive molecules [138, 139, 288, 289]. It is evident, therefore, that metacetamol induces considerable inhibition of growth on the (001) face of paracetamol at this level (4 mol%).

Figure 4. 2 illustrates the molecular structure of paracetamol on the (001) face of the crystal. From this diagram, it is clear that the groups protruding from the surface in the direction of growth, $[-100]$, are OH and NHCOCH_3 . Both of these groups allow the perpetuation of the hydrogen bonding network within the crystal, via attachment of molecules to the OH and CO groups. The only difference between paracetamol and metacetamol is the *p*- and *m*-position of their OH group, respectively. Hence, metacetamol could readily attach to the protruding OH and CO groups of the crystal surface via its CO group, which is equivalent to that of paracetamol, and its OH group, which resides juxtaposed to that of paracetamol. The former case would allow the hydrogen bonding network to be fully preserved, whereas the latter would cause it to be slightly distorted. It appears that metacetamol molecules could attach to the (001) face of paracetamol crystals and induce the degree of inhibition detected here.

Again, we cannot assume that the same degree of inhibition would be observed on the other faces of the crystal, and hence further studies are required to assess the metacetamol-induced inhibition on the remaining faces. These studies may reveal the mechanisms by which metacetamol modifies the habit of paracetamol from tabular to columnar (Figure 4. 3 and Figure 4. 8 respectively).

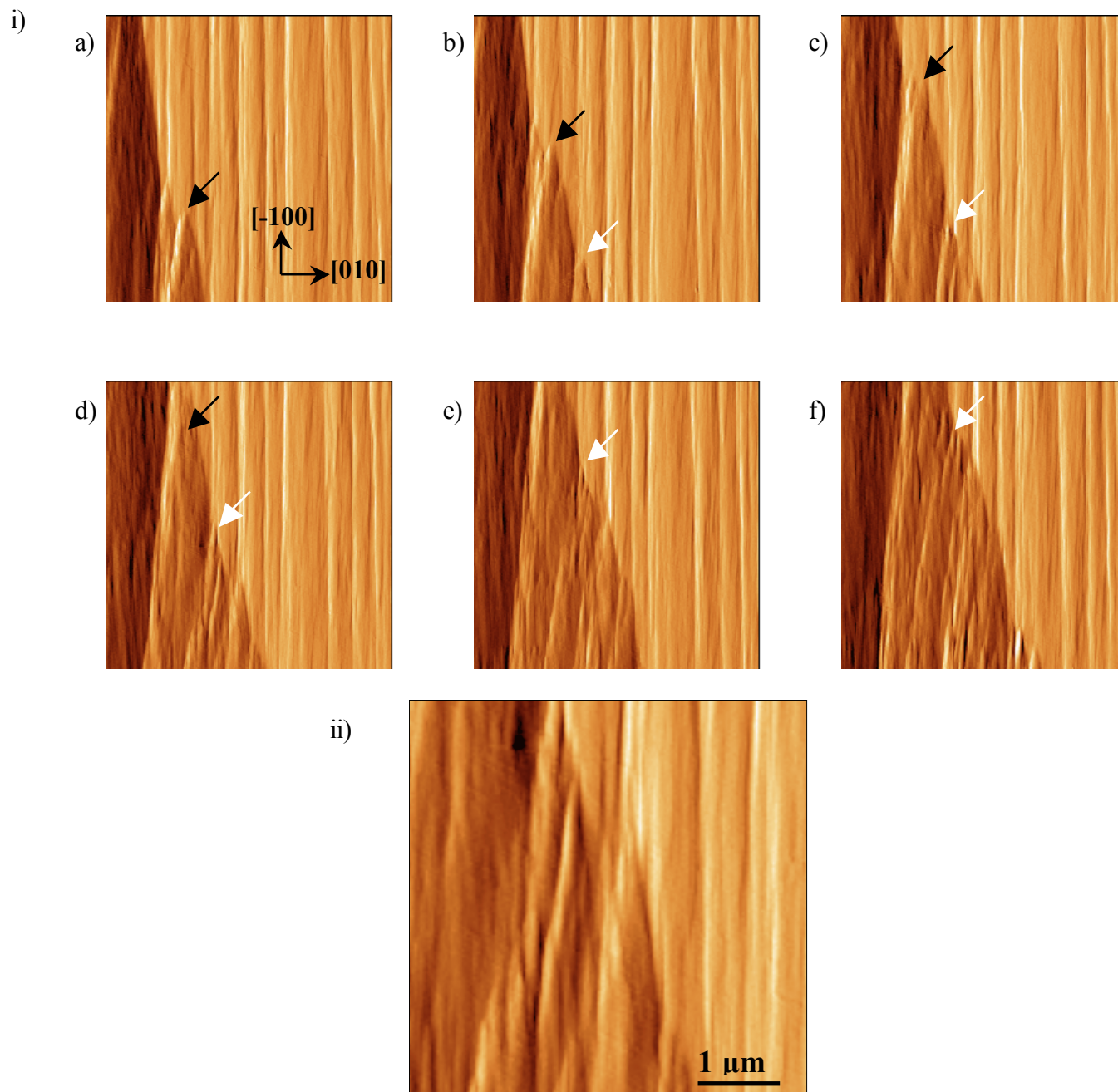


Figure 4. 12 i) A sequence of 10 μ m x 10 μ m AFM images of the (001) face of a paracetamol crystal during incubation in paracetamol/4 mol% metacetamol solution. The supersaturation of the solution is 0.29, with respect to paracetamol. In image a) time $t = 0$ secs, b) $t = 90$ secs, c) $t = 182$ secs, d) $t = 272$ secs, e) $t = 364$ secs, and f) $t = 454$ secs. ii) is a 4.8 μ m x 4.8 μ m image showing a portion of image i) d) at higher magnification, to highlight the pointed steps. All images are deflection images.

4.4 Conclusion

The use of AFM and SEM has permitted the investigation of the effects of the additives, acetanilide and metacetamol, on the morphology and the growth on the (001) face of paracetamol crystals. SEM images showed the characteristic tabular habit of pure paracetamol crystals was only moderately altered by the presence of acetanilide, but the crystals adopted a columnar habit when grown in the presence of metacetamol.

On a microscopic level, AFM revealed that the surface features of pure paracetamol crystals were steps ranging from 1 nm to 21 nm in height. On the contrary, crystals grown with acetanilide possessed thin, branched steps of approximately 20 nm in height. We suspect that the branched appearance of the steps is due to the adsorption of acetanilide molecules onto terraces or steps during growth, causing pinning and bending of the growing steps. Crystals grown in the presence of metacetamol also displayed different surface features to those of pure paracetamol. The presence of metacetamol during growth resulted in steps of approximately 15 nm in height interspersed with holes, and also induced the formation of defects in the crystal surface. These data suggest that the crystal lattice, and hence the hydrogen bonding network, were considerably disrupted by metacetamol during growth.

Growth on the (001) face of paracetamol crystals in the presence and absence of acetanilide or metacetamol was monitored via AFM. In the absence of any additive, growth was observed to occur by a dislocation mechanism. Growing steps ranged from 95 nm to 588 nm in height. The rate of growth of the steps ranged from 26.4 nm/s to 76.2 nm/s, and decreased with increasing step height. All steps were observed to grow in the [-100] direction.

In the presence of acetanilide, holes emerged in the surface after 11½ minutes of incubation. These holes may have originated from defects in the crystal surface. Steps, ranging from 13 nm to 45 nm in height, emanated from these holes and dissolved at rates between 1.3 nm/s and 2.7 nm/s, in the [100] direction. The dissolution rate of the steps decreased with increasing step height. The holes or clefts in the surface were also observed to deepen over time, indicating that dissolution was occurring into the crystal core as well as laterally.

The presence of additives is known to increase the solubility of paracetamol, which may have induced such dissolution. However, we cannot assume that dissolution was ubiquitous over the crystal, as each of the faces may have been influenced to different degrees by the additive molecules, and some may have grown under these conditions. Nonetheless, the presence of acetanilide in the growth medium caused dissolution in the [100] direction, whereas a pure paracetamol solution of the same σ facilitated growth of macrosteps in the [-100] direction.

The presence of metacetamol resulted in the growth of steps, of 4 nm to 21 nm in height, at rates of 19.0 nm/s to 37.8 nm/s in the [-100] direction. The steps were pointed in appearance and significantly smaller than those observed in the absence of metacetamol, suggesting that the additive molecules pinned the steps. The average growth rates in the absence and presence of metacetamol were 49.5 nm/s and 27.1 nm/s respectively. Hence, metacetamol dramatically altered not only the morphology, but also the rate of the growing steps. AFM enabled the observation of the effects of metacetamol on the growing interface on a micrometre scale. However, we could not establish, at this resolution, whether additive adsorption occurred at step edges or on terraces, as both generate the formation of pointed, pinned steps

[138, 139]. Nonetheless, pinning of steps and reduction in growth rates were observed, in accordance with the Cabrera and Vermilyea model.

The functional groups which protrude from the (001) face, in the [-100] direction, are NHCOCH_3 and OH. These groups may enable attachment of metacetamol molecules via their CO group, which is equivalent to that of paracetamol, or their OH group, which is located juxtaposed to that of paracetamol. In either case, the hydrogen bonding network of the crystal would be largely preserved. Hence, metacetamol may bind with relative ease to this face and induce the degree of inhibition observed.

We suggest that further similar experiments should be carried out using each of the structurally related additives, not only on the (001) face, but on all other faces of the crystal. These investigations would help to achieve a ranking order of the inhibitory effects of the additives on each of the crystal faces. Particular attention should be paid to the inhibitory activities on the {110} faces. These are considered to be morphologically the most influential, because their growth rates and mechanisms change with increasing σ , altering the habit of the crystal from columnar to tabular [24, 29, 37, 59].

Once the degree of inhibition of these additives has been established for each face of paracetamol, they could, individually or as a mixture, be employed to control the habit of paracetamol crystals, their chemical properties, and perhaps their problematic compaction behaviour.

Chapter

5

Determination of the mechanisms of anion exchange in Co-ordination Polymers.

Co-ordination polymers are currently attracting extensive interest due to the vast scope of potential applications for their supramolecular structures. Many applications rely on the ion exchange capabilities of these compounds. Considerable debate surrounds the mechanism by which ion exchange occurs in co-ordination polymers. Here we investigate the process by which the anion exchange and subsequent structural transformations of the crystalline co-ordination polymers $\{[\text{Ag}(4,4'\text{-bipy})]\text{BF}_4\}_\infty$ and $\{[\text{Ag}(4,4'\text{-bipy})]\text{NO}_3\}_\infty$ occur. The experiments described in the following chapter have been the subject of a publication in *Crystal Engineering Communications* [290], and a further manuscript has been submitted to the *Journal of Microscopy* [291].

5.1 Introduction

5.1.1 The design and assembly of co-ordination polymers.

Polymeric compounds generated via the interaction between metal cations and organic ligands have led to the emergence of a wide variety of fascinating one-, two-, and three-dimensional structures. Commonly referred to as co-ordination polymers, this class of compounds has been termed “living polymers” due to their ability to grow and shorten, rearrange their interaction patterns, exchange components, undergo annealing, healing and adaptation processes [292].

These materials self-assemble from their elementary components of organic molecules and transition metal ion salts (see, for example, references [293-298]). The metal-anion complexes within the salt dissociate, allowing the metal ions to form a polymeric framework with the organic molecules, and the anions to become incorporated into the pores of the framework as molecular or ionic guests depending on the framework charge [293]. Thus, the intrinsic structure of the framework is held together by co-ordination bonds, and is dictated by the bonding geometry of the metal linker, the functionality and denticity of the organic ligand [299, 300], and nature of the anions [293, 299, 301, 302]. Extended anionic, cationic, and neutral frameworks can be produced, depending on the constituent building blocks of the co-ordination polymers. The design of co-ordination polymers takes into account factors such as the co-ordination nature of the metal ion, the structural characteristics of the polydentate organic ligand, the metal-ligand ratio, and the possible anion influence. A subtle alteration in any of these factors can lead to new extended network structures. Consequently, a great variety of supramolecular architectures have been

ingeniously constructed [294, 295, 297, 298, 303-305]. Theoretically, there are a vast number of porous frameworks of varying size, structure, dimension and pore size, and hence function which may be produced by exploiting the binding characteristics of both the metal ions and the organic molecules which constitute co-ordination polymers. Indeed the production of tailor-made compounds with desired structure, pore size, or function may soon be an attainable goal as the level of research dedicated to these compounds continues to increase.

5.1.2 Ion exchange properties of co-ordination polymers and their potential uses.

An exciting, yet little explored area of these supramolecular compounds, is the ability of these rigid porous frameworks to exchange the ions within their pores with ions from solution, without destruction of their framework [293, 301, 305-312]. This phenomenon induces the interconversion of a framework containing host ions, to a framework containing solution ions. Ion exchange frequently involves a structural transformation occurring in the crystalline state [298, 301, 302, 304, 306]. For example, anionic species within polycationic hosts may be involved in interactions with metal centres or organic ligands, and in some cases can play an important role in supporting the overall framework of the polymer [300, 313]. Removal of such anions would induce the collapse of the polymer framework. However, anions often interact only weakly with the framework, and hence their removal or exchange does not disrupt the integrity of the framework. This observation has recently led researchers to use co-ordination polymers as ion exchange materials [293, 298, 301-304, 314-316]. It has been shown that anions freely located in the co-ordination polymer framework can be completely replaced when the solid co-ordination

polymer is treated with an aqueous solution containing other anionic species [293, 298, 301-304, 307, 316]. Spectroscopic methods of analysis and X-ray powder diffraction (XRPD) show that the exchange is fast (occurs within a few hours), complete and often reversible in various types of co-ordination polymers [290, 293, 298, 301-304, 307, 308, 312, 314-317].

It has been postulated that cationic frameworks capable of anion exchange may be utilised in the removal and recovery of inorganic and organic anions such as, MoO_4^{2-} , CN^- , HS^- , and $\text{C}_6\text{H}_5\text{O}^-$ from industrial wastewater [293]. Neutral frameworks may also prove to be extremely useful in the removal and recovery of aromatic compounds and halogenated hydrocarbons from industrial processes [293].

The ion exchange capabilities of these compounds have led to an extensive list of potential uses for co-ordination polymers. These include reversible solvent inclusion [305, 318-323], molecular sieving [298, 318-321], catalysts for specific reactions [309, 312, 318, 324-327], drug and chemical delivery [298], molecular recognition, chemical sensor technologies [302, 304], in optoelectronic [328, 329], magnetic [330], microporous [313, 331], and biomimetic materials [298].

5.1.3 Is the mechanism of ion exchange a solid-state or solvent-mediated process?

The mechanisms by which this ion exchange process occurs are currently the subject of considerable debate. There are two main hypotheses regarding the ion exchange mechanisms of these compounds. One hypothesis suggests that the exchange is a solid-state process [293, 317], namely that, when in a solution of anions, the host anions migrate out of the crystalline solid through the channels between layers. Concurrently, the anions from solution move into the crystalline complex [293, 298,

301]. It has been postulated that the facility with which the ion exchange occurs, coupled with the fact that the crystal morphology is retained throughout the exchange process, is evidence that the anions diffuse into the framework without any dissolution/recrystallization of the material or destruction of the host network [293]. However, as already mentioned, many anion exchange processes require a dramatic structural reorganization from the initial phase to the resulting phase [298, 301, 302, 304, 306], which is not consistent with a solid-state mechanism.

The alternative hypothesis suggests that the process occurs via a solvent-mediated recrystallization process [332], involving the dissolution of one crystalline phase and subsequent precipitation of another. Such processes have been illustrated in inorganic crystals [333-336], and followed using AFM [333, 335, 336]. Previous reports on anion exchange show that, although crystals retain their shape and size, they lose their crystallinity rapidly during the exchange process [293, 301, 314, 315]. This would indicate the occurrence of significant restructuring within the crystal and would, hence, support this hypothesis. However, the apparent insolubility of coordination polymers in water [304, 314] would tend to contradict this theory. In order to assess which of the proposed hypotheses is correct, we have used AFM to investigate, *in situ*, the processes by which anion exchange occurs in the coordination polymers $\{[\text{Ag}(4,4'\text{-bipy})]\text{BF}_4\}_\infty$ and $\{[\text{Ag}(4,4'\text{-bipy})]\text{NO}_3\}_\infty$.

5.1.4 Structures of $\{[\text{Ag}(4,4'\text{-bipy})]\text{BF}_4\}_\infty$ and $\{[\text{Ag}(4,4'\text{-bipy})]\text{NO}_3\}_\infty$.

Ag^{I} [293, 295, 298, 299, 301, 302, 304, 310, 314] and 4,4'-bipyridine (4,4'-bipy) [293, 299, 305, 314, 316, 337, 338] are common building blocks of co-ordination polymers. The structure of the 4,4'-bipyridine ligand is shown in Figure 5. 1. The co-

ordination sphere of Ag^{I} is very flexible and can adopt co-ordination numbers from two to six, and varying geometries from linear to tetrahedral, trigonal, pyramidal and octahedral [339].

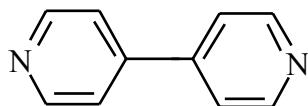


Figure 5. 1 Structure of the 4,4'-bipyridine ligand.

Similarly, (4,4'-bipy) is known to yield diamond-like, hexagonal, square grid, and ladder structures [293]. The crystal structures of both $\{[\text{Ag}(4,4'\text{-bipy})]\text{NO}_3\}_\infty$ (Figure 5. 2) [299, 314, 315] and the two isomers of $\{[\text{Ag}(4,4'\text{-bipy})]\text{BF}_4\}_\infty$ (Figure 5. 3 and Figure 5. 4) [299, 340] have been elucidated, and reveal the presence of linear polymeric chains in all three structures.

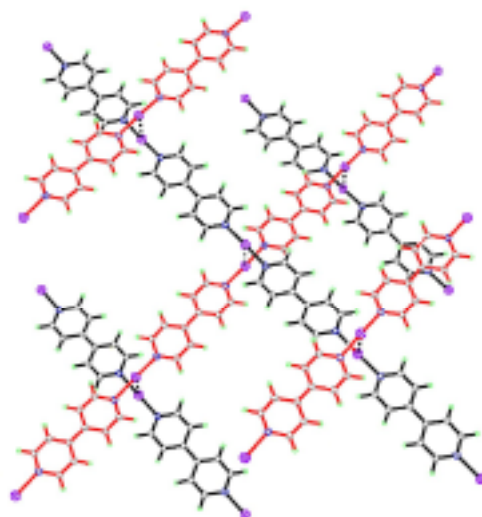


Figure 5. 2 Illustration of the packing of polymeric chains within the crystal structure of $\{[\text{Ag}(4,4'\text{-bipy})]\text{NO}_3\}_\infty$, where two consecutive layers of chains are depicted in black and red. The filled purple circles represent the silver ions within the chains [341].

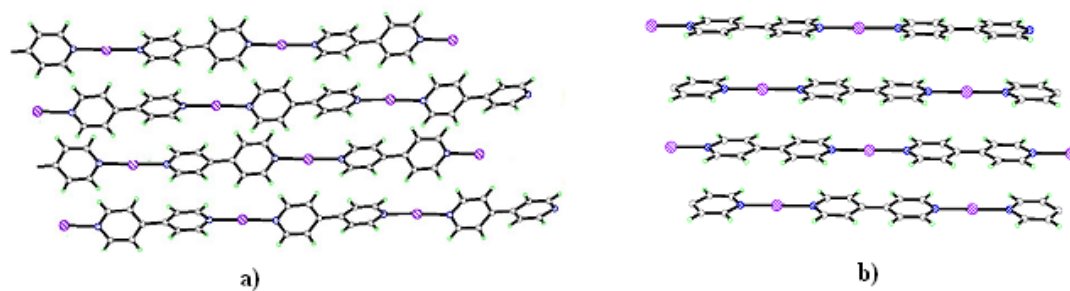


Figure 5. 3 Illustrations of the alignment of single stacks of polymeric chains within isomer B (a) and isomer A (b) of $\{[\text{Ag}(4,4'\text{-bipy})]\text{BF}_4\}_\infty$. The silver ions are shown as filled purple circles [341].

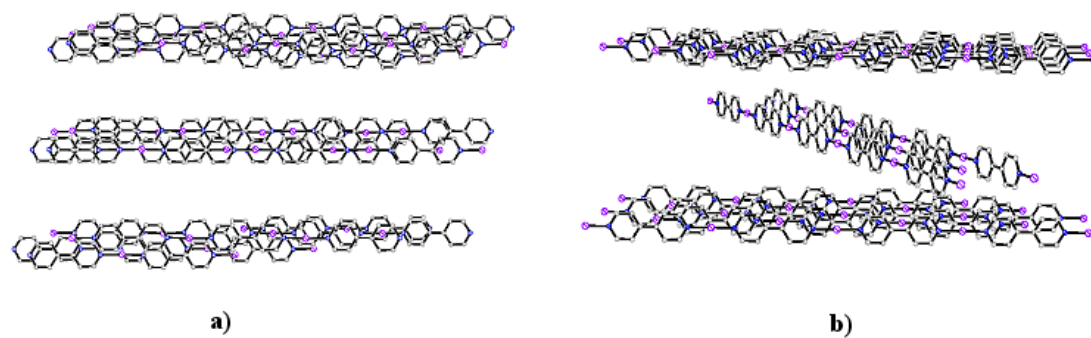


Figure 5. 4 Arrangement of the stacks of polymeric chains in the crystal structures of isomer B (a) and isomer A (b) of $\{[Ag(4,4'-bipy)]BF_4\}_\infty$. Again the silver ions are shown as filled purple circles [341].

Despite the very similar structure of the single polymeric chains, the spatial arrangement of these chains within each polymer and, hence, the overall three-dimensional structures of the polymers are considerably different. In $\{[\text{Ag}(4,4'\text{-bipy})]\text{NO}_3\}_\infty$ and isomer A of $\{[\text{Ag}(4,4'\text{-bipy})]\text{BF}_4\}_\infty$, the chains are orthogonal, that is, they are stacked in a criss-cross pattern (Figure 5. 2 and Figure 5. 4b). In isomer B of $\{[\text{Ag}(4,4'\text{-bipy})]\text{BF}_4\}_\infty$ the chains stack in parallel layers (Figure 5. 4a), whereas in the isomer A the neighbouring stacks are inclined at 74.2° angle (Figure 5. 4b) [340]. In $\{[\text{Ag}(4,4'\text{-bipy})]\text{NO}_3\}_\infty$ the Ag-(4,4'-bipy) chains are cross-linked through Ag-Ag bonds (2.977 Å) to form a three-dimensional porous framework with large rectangular channels of dimension 23 x 6 Å [293]. The T-shaped co-ordination of silver leaves an open co-ordination site pointing towards the centre of the channels, where the nitrate guests form very weak interactions with silver (Ag-O bond length is 2.78 Å) [293, 314]. NO_3^- anions reside in the pores of the hatched $\{[\text{Ag}(4,4'\text{-bipy})]\text{NO}_3\}_\infty$ complex. $\{[\text{Ag}(4,4'\text{-bipy})]\text{BF}_4\}_\infty$ chains are bound together by only aromatic interchain interactions [315]. BF_4^- anions are located in the space between stacks in both forms of the complex $\{[\text{Ag}(4,4'\text{-bipy})]\text{BF}_4\}_\infty$. Anions in crystalline complexes of $\{[\text{Ag}(4,4'\text{-bipy})]\text{X}\}_\infty$ are effectively non-co-ordinating and, therefore, available for exchange.

5.1.5 Reversible anion exchange properties of $\{[\text{Ag}(4,4'\text{-bipy})]\text{BF}_4\}_\infty$ and $\{[\text{Ag}(4,4'\text{-bipy})]\text{NO}_3\}_\infty$.

Evaluation of the ion exchange properties of $\{[\text{Ag}(4,4'\text{-bipy})]\text{NO}_3\}_\infty$ has revealed that the NO_3^- ions residing in the channels of the complex can be reversibly

exchanged with PF_6^- , BF_4^- , SO_4^{2-} , and MoO_4^{2-} without destruction of the framework [293, 314]. Experiments using single crystals of $\{[\text{Ag}(4,4'\text{-bipy})]\text{BF}_4\}_\infty$ and $\{[\text{Ag}(4,4'\text{-bipy})]\text{NO}_3\}_\infty$ immersed in aqueous solutions of anions have shown that the crystals do not change size or shape upon exchange, but quickly lose optical transparency and the single crystal integrity [290, 293, 314]. This may indicate that significant restructuring has occurred. In each instance, ion exchange occurs simply and reversibly via incubation of the crystalline polymer in an aqueous solution of anions. These findings have been confirmed by infrared spectroscopy [290, 293, 314], elemental microanalysis [293, 314], XRPD [290, 293, 314], optical microscopy [293, 314], transmission electron microscopy (TEM) [290], and ^1H nuclear magnetic resonance (NMR) [290]. These techniques collectively illustrate that the ion exchange process results in a pure crystalline phase of the new co-ordination polymer. The apparent loss of crystallinity observed during the ion exchange process may imply that the mechanism follows that of the solvent-mediated hypothesis.

The assumption that co-ordination polymer compounds are insoluble [304, 314], appears to be untrue for $\{[\text{Ag}(4,4'\text{-bipy})]\text{NO}_3\}_\infty$ and $\{[\text{Ag}(4,4'\text{-bipy})]\text{BF}_4\}_\infty$. Recent studies using electroconductance measurements, atomic absorption spectrophotometry, and AFM (illustrated later in this chapter) show polymers $\{[\text{Ag}(4,4'\text{-bipy})]\text{NO}_3\}_\infty$ and $\{[\text{Ag}(4,4'\text{-bipy})]\text{BF}_4\}_\infty$ have water solubility values of 0.84 mmol/L and 0.82 mmol/L respectively [290]. The albeit low solubility values of these two polymers may prove to be enough to facilitate the proposed solvent-mediated mechanism.

5.1.6 Aims of chapter.

There have been no previous detailed microscopic investigations of the crystal phase transformations during ion exchange reactions of these types of systems. In order to address the discrepancies in the current ion exchange theories, and assess which of the proposed hypotheses is correct, here we use AFM to investigate, *in situ*, the processes by which anion exchange and the subsequent structural transformations occur in the co-ordination polymers $\{[\text{Ag}(4,4'\text{-bipy})]\text{NO}_3\}_\infty$ and $\{[\text{Ag}(4,4'\text{-bipy})]\text{BF}_4\}_\infty$.

5.2 Methods and Materials

All reagents (Aldrich) were used as received. The co-ordination polymers were prepared by the literature methods [299, 314, 342]. Crystals were immobilized on AFM sample stubs, and then to a suitable liquid cell using Tempfix (Agar, Stansted, U. K.). $\{[\text{Ag}(4,4'\text{-bipy})]\text{BF}_4\}_\infty$ crystals were imaged in HPLC grade water to investigate their apparent insolubility. The anion exchange process was investigated by imaging $\{[\text{Ag}(4,4'\text{-bipy})]\text{BF}_4\}_\infty$ crystals in 3M NaNO_3 solution, and imaging $\{[\text{Ag}(4,4'\text{-bipy})]\text{NO}_3\}_\infty$ crystals in 1M NaBF_4 solution. It was found that solutions of NaBF_4 of concentration greater than 1M induced the formation of salt crystals throughout the AFM liquid cell, on the scanner, and tip, thus preventing imaging. In all experiments HPLC grade water was used as a solvent. In each case, approximately 2.5 ml of the respective solution was placed in the liquid cell.

5.2.1 AFM analysis.

Contact mode imaging was employed throughout, using a ThermoMicroscopes Explorer AFM (Veeco, Bicester, Oxon, U.K.). V-shaped silicon nitride cantilevers (200 μ m length) with integrated pyramidal tips (Nanoprobes, Veeco, Santa Barbara, CA) were used. Both topography and deflection images were acquired in all experiments. Deflection images emphasize areas of rapid topography changes, such as steps, but do not give any information about relative heights of features on the surface.

5.2.2 SEM analysis.

$\{[\text{Ag}(4,4'\text{-bipy})]\text{NO}_3\}_\infty$ and $\{[\text{Ag}(4,4'\text{-bipy})]\text{BF}_4\}_\infty$ crystals were also imaged using SEM. After incubation in 3M NaNO_3 and 1M NaBF_4 solution for 24 hours respectively, $\{[\text{Ag}(4,4'\text{-bipy})]\text{BF}_4\}_\infty$ and $\{[\text{Ag}(4,4'\text{-bipy})]\text{NO}_3\}_\infty$ were imaged using SEM. All samples were initially gold coated for four minutes using a Balzers SCD 030 Sputter Coater (Balzers Union Limited, Liechtenstein), operated at 0.1mbar with a sputtering current of 30mA. A Philips 505 SEM (Philips Electron Optics, Eindhoven, Netherlands) was used to image all samples under a range of magnification settings at a voltage of 23KeV, with a spot size of 50 nm.

5.3 Results and Discussion

5.3.1 AFM and SEM data for $\{[\text{Ag}(4,4'\text{-bipy})]\text{BF}_4\}_\infty$ and $\{[\text{Ag}(4,4'\text{-bipy})]\text{NO}_3\}_\infty$ crystals in air and water.

The topographical features of $\{[\text{Ag}(4,4'\text{-bipy})]\text{BF}_4\}_\infty$ crystal revealed by AFM are shown in Figure 5. 5. These AFM images reveal long, narrow, finger-like processes on the surface, which may reflect the underlying parallel chains of isomer B within the crystal structure. The average height of these features is 87 nm. SEM images, Figure 5. 6, confirm the presence of finger-like features on the surface of these crystals, but also display regions which appear disordered or amorphous in nature. These regions may correspond to the ends of vertical finger-like features, or may indeed correspond to areas of isomer A within the crystal.

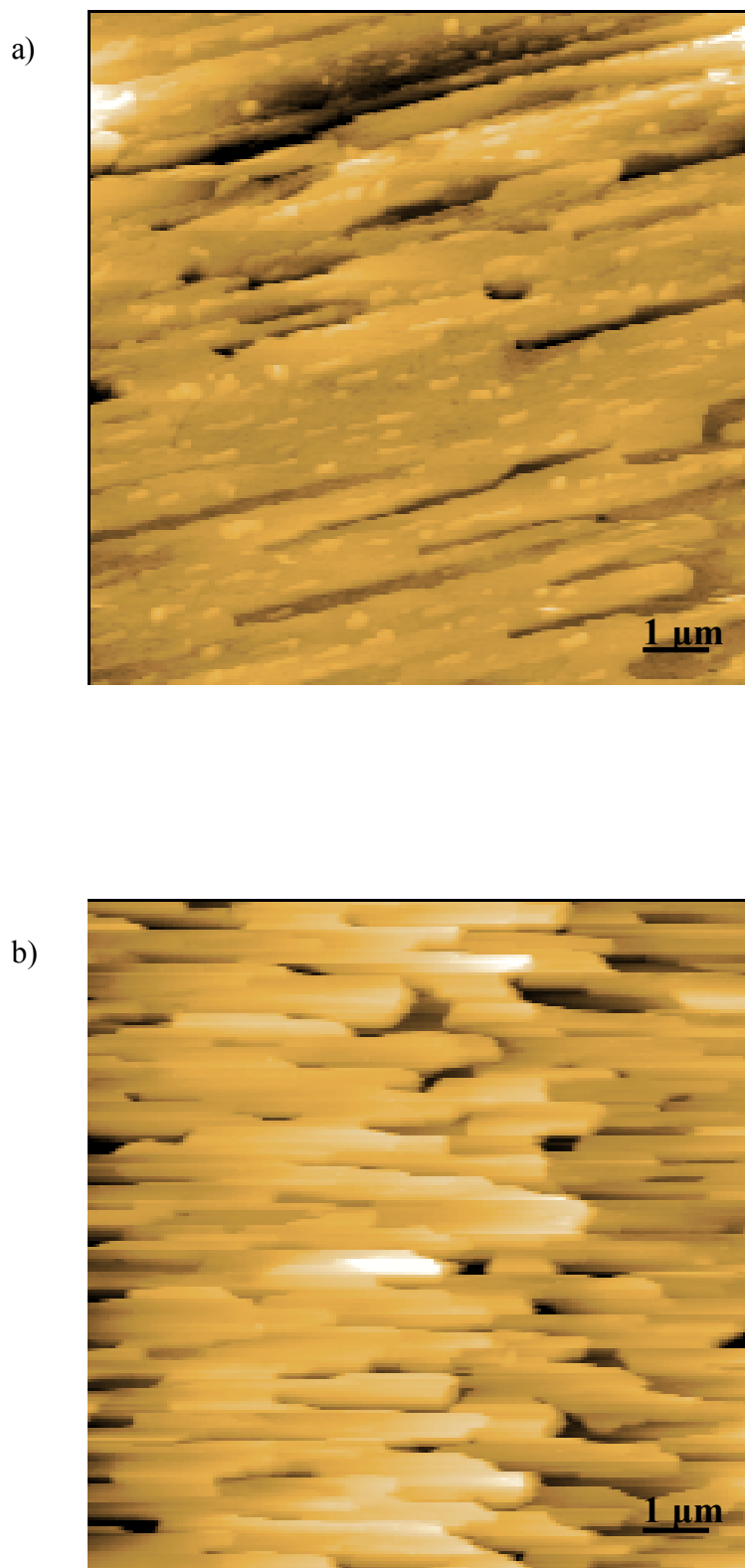


Figure 5. 5 10 μm x 10 μm AFM topographical images of the surface of a $\{[\text{Ag}(4,4'\text{-bipy})]\text{BF}_4\}_\infty$ crystal, acquired in air.

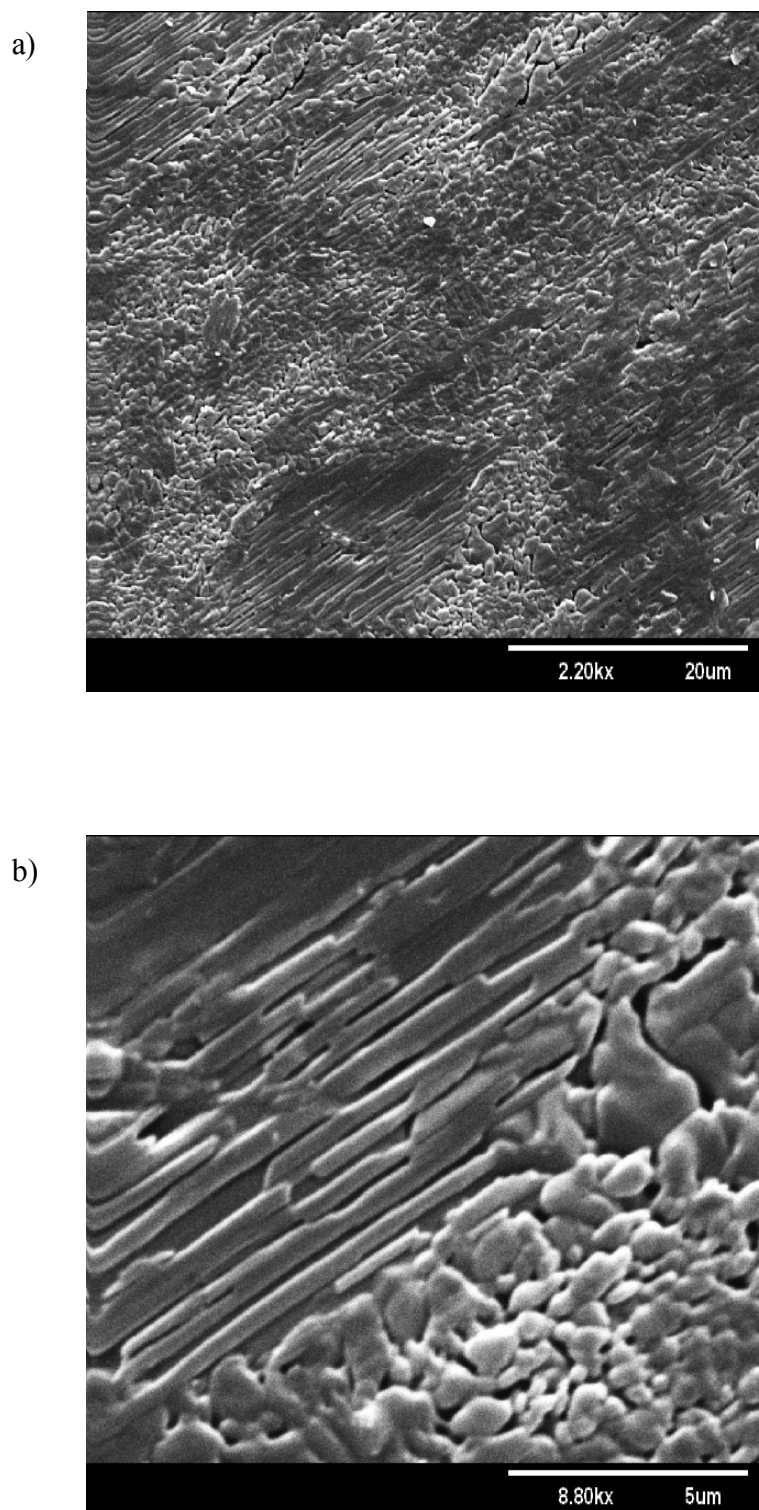


Figure 5. 6 SEM images of the surface of a $\{[Ag(4,4'\text{-bipy})]BF_4\}_\infty$ crystal. Image a) is at magnification $\times 2200$, and b) is the lower central area of image a) at magnification $\times 8800$.

AFM images of $\{[\text{Ag}(4,4'\text{-bipy})]\text{NO}_3\}_\infty$ crystal in Figure 5. 7 illustrate much larger features than those present on $\{[\text{Ag}(4,4'\text{-bipy})]\text{BF}_4\}_\infty$ crystals, with an average height of 1835 nm. The features are almost triangular in shape which, again, may reflect the underlying hatched pattern of the chains within the crystal. We do note that some of the triangular features apparent in these images may be artefacts induced by the AFM tip imaging itself when scanning large surface features. However SEM data, Figure 5. 8, confirm the presence of much larger, triangular topographical features on the surface of $\{[\text{Ag}(4,4'\text{-bipy})]\text{NO}_3\}_\infty$ crystals.

The sequence of images in Figure 5. 9 show the surface of a $\{[\text{Ag}(4,4'\text{-bipy})]\text{BF}_4\}_\infty$ crystal during incubation in water. It is evident that immediately after exposure the surface features of the crystal have changed as a result of dissolution. The progressive dissolution of steps is apparent throughout the sequence of images, and hence dispels the widely accepted presumption that these co-ordination polymers are insoluble [304, 314]. Dissolution of one step is indicated on each image by an arrow.

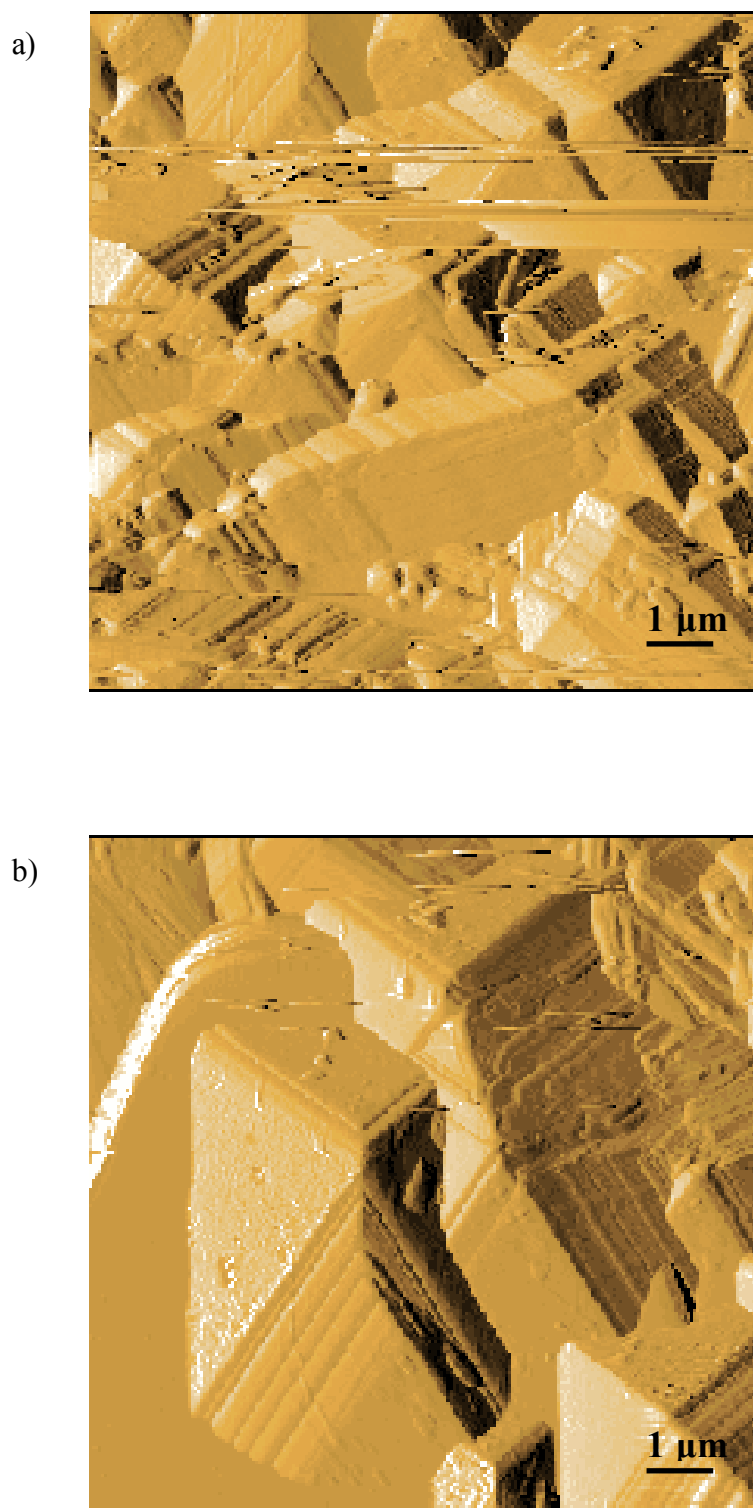


Figure 5. 7 10 μm x 10 μm AFM images of the surface of a $\{[\text{Ag}(4,4'\text{-bipy})]\text{NO}_3\}_\infty$ crystal, acquired in air. Both a) and b) are topography images which have been left-shaded to allow the features to be more easily visualized.

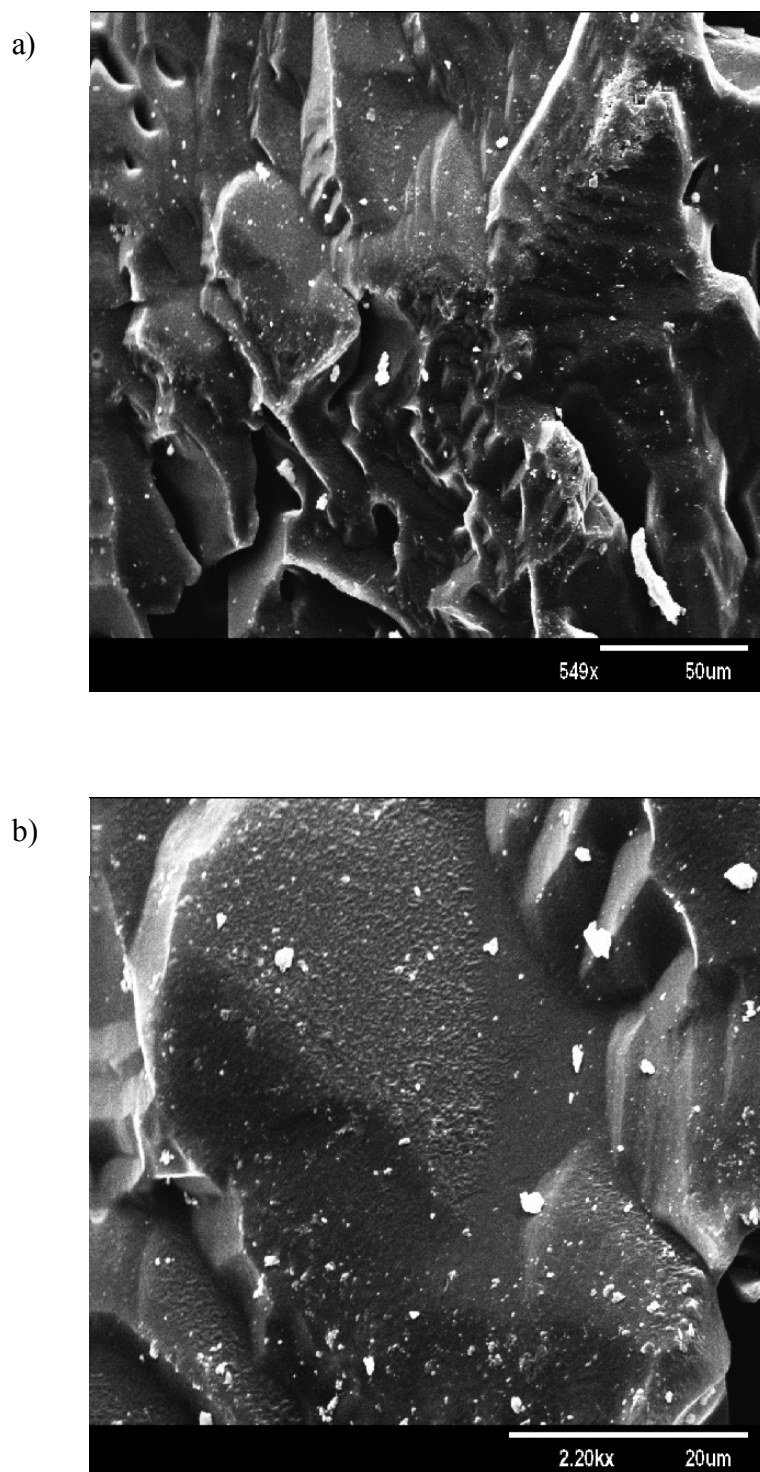


Figure 5. 8 SEM images of the surface of a $\{[\text{Ag}(4,4'\text{-bipy})]\text{NO}_3\}_\infty$ crystal. Image a) is at magnification x 549, and b) is at magnification x 2200.

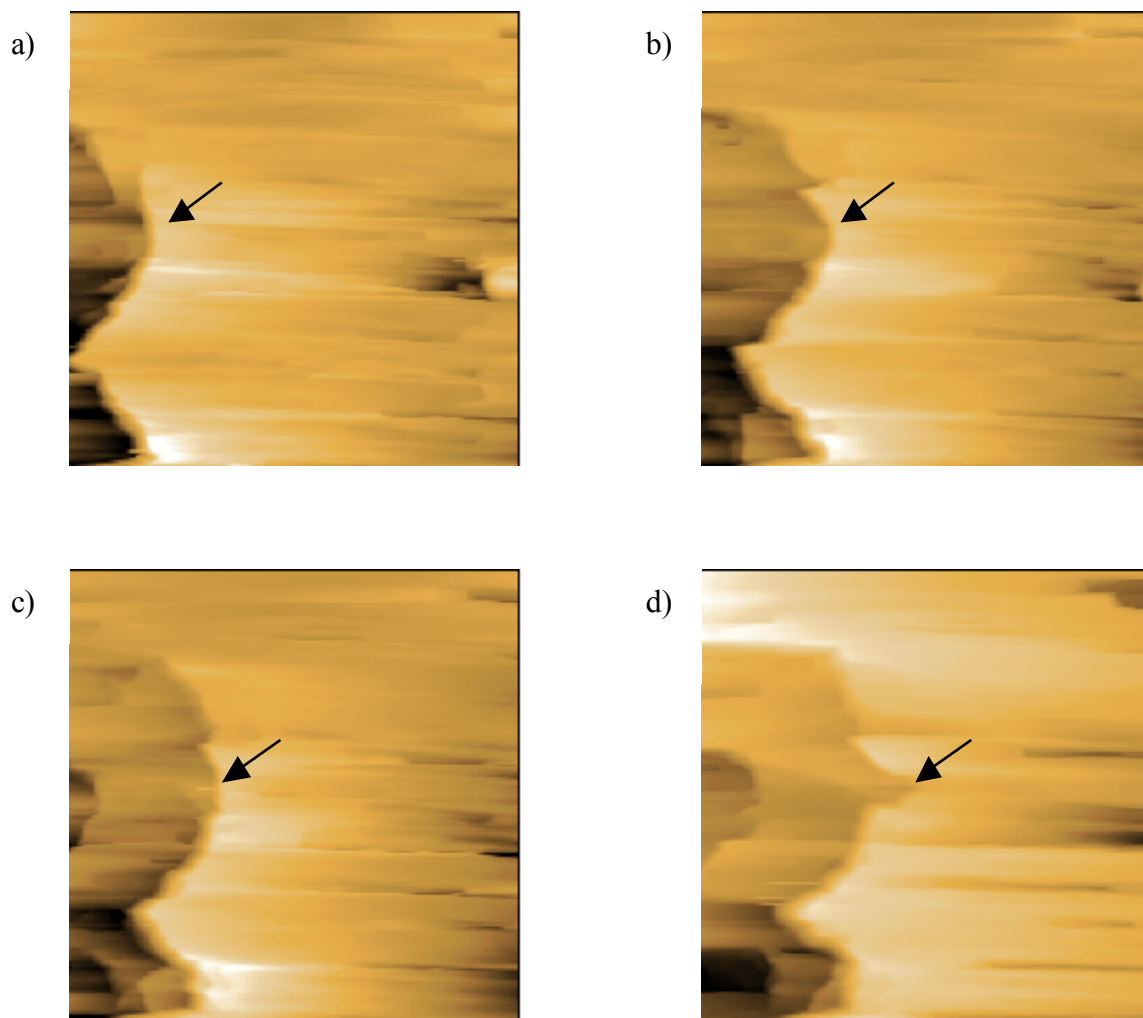


Figure 5. 9 $10\ \mu\text{m} \times 10\ \mu\text{m}$ AFM topographical images of the surface of a $\{[\text{Ag}(4,4'\text{-bipy})]\text{BF}_4\}_\infty$ crystal during incubation in water. Image a) shows the surface at time $t = 0$, immediately after addition of water, b) after 5 min 34 s, c) after 9 min 19 s, and d) after 13 min 13 s. Dissolution one particular step is followed on each image with an arrow.

5.3.2 Anion exchange.

The images shown in Figure 5. 10 depict the surface changes of a $\{[\text{Ag}(4,4'\text{-bipy})]\text{BF}_4\}_\infty$ crystal during incubation in 3M NaNO_3 solution. Immediately after addition of NaNO_3 solution, the surface topography has changed in a manner indicating that dissolution is occurring. After only 30 minutes, new features begin to emerge on the surface. The features appear triangular in shape, analogous with those found in AFM and SEM images of $\{[\text{Ag}(4,4'\text{-bipy})]\text{NO}_3\}_\infty$ crystals. Within one hour of the addition of NaNO_3 solution the triangular features dominate this area of the surface, and the surface is comparable to that of the $\{[\text{Ag}(4,4'\text{-bipy})]\text{NO}_3\}_\infty$ crystal in air, Figure 5. 10 e). These images clearly show that the anion exchange process which the $\{[\text{Ag}(4,4'\text{-bipy})]\text{BF}_4\}_\infty$ crystal undergoes in the presence of NaNO_3 solution, occurs via the initial dissolution of $\{[\text{Ag}(4,4'\text{-bipy})]\text{BF}_4\}_\infty$, followed by subsequent recrystallization of $\{[\text{Ag}(4,4'\text{-bipy})]\text{NO}_3\}_\infty$ onto the crystal surface. AFM data show that the reaction was complete within 12 hours, which correlates well with previous findings [290, 293, 314]. Prior to the addition of NaNO_3 solution the average height of the surface features is 158 nm, but immediately after addition of NaNO_3 solution this increases to 308 nm, to 437 nm after 30 minutes, and to 518 nm after 3 hours. The progressive enlargement of surface features may, in part, be due to the recrystallization of $\{[\text{Ag}(4,4'\text{-bipy})]\text{NO}_3\}_\infty$ on the surface, but may also be as a result of dissolution. The latter would allow clefs in the crystal to become deeper, and thus provide the solution with access to the successive crystalline layers. These observations are typical for solvent-mediated transformations [141, 333, 335].

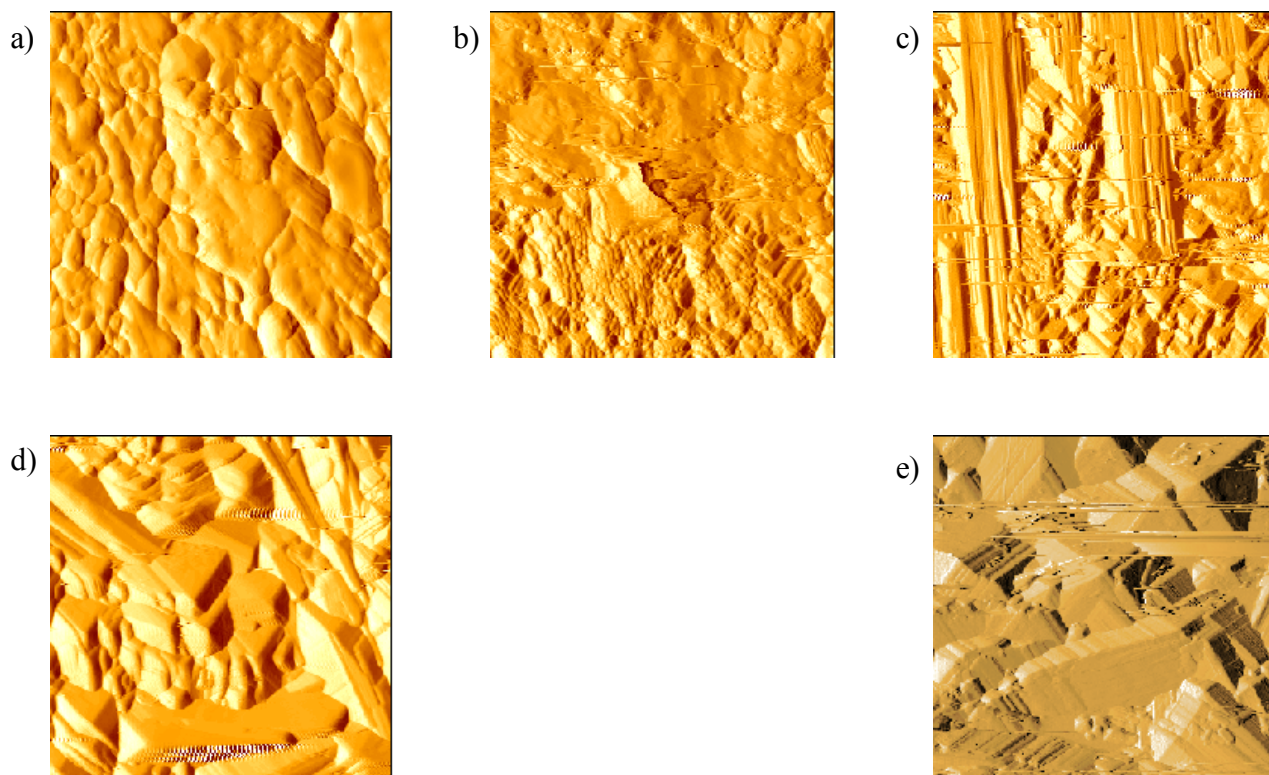


Figure 5.10 10 μm x 10 μm AFM images of the surface of a $\{[\text{Ag}(4,4'\text{-bipy})]\text{BF}_4\}_\infty$ crystal before and during incubation in 3M NaNO_3 solution. Image a) shows the surface of the crystal in air prior to the addition of NaNO_3 solution, b) at time $t = 0$, immediately after addition of NaNO_3 solution, c) $t = 30$ min, and d) $t = 60$ min. Image e) is a comparative 10 μm x 10 μm AFM image of the surface of a $\{[\text{Ag}(4,4'\text{-bipy})]\text{NO}_3\}_\infty$ crystal in air. All are topography images which have been left-shaded to allow the features to be more easily visualized.

This process allows dissolution and recrystallization to occur deeper into the crystal core, resulting in a self-perpetuating (autocatalytic) transformation from $\{[\text{Ag}(4,4'\text{-bipy})]\text{BF}_4\}_\infty$ to $\{[\text{Ag}(4,4'\text{-bipy})]\text{NO}_3\}_\infty$. These findings aid the explanation of TEM and XRPD data [290] which show that upon anion exchange of $\{[\text{Ag}(4,4'\text{-bipy})]\text{BF}_4\}_\infty$ to $\{[\text{Ag}(4,4'\text{-bipy})]\text{NO}_3\}_\infty$ or $\{[\text{Ag}(4,4'\text{-bipy})]\text{NO}_3\}_\infty$ to $\{[\text{Ag}(4,4'\text{-bipy})]\text{BF}_4\}_\infty$, crystals X retained their shape but became a mass of microcrystals of pure crystal Y.

The conditions required and the mechanisms operating during autocatalysis have been extensively studied [343, 344]. A typical autocatalytic process involves a new phase growing on the surface of a parent phase which acts as a sink because it lies within the diffusion distance. This may indeed be the mechanism of dissolution-recrystallization observed during the ion exchange process of these co-ordination polymers.

The solvent-mediated transformations of organic crystalline solids are well documented [345-347], and are essentially rearrangements of hydrogen bonds, dipole-dipole, van der Waals and/or other non-covalent interactions. We suggest that the structural reorganization observed in these co-ordination polymers is initiated by the depolymerization (dissolution) of the initial polymer from the crystal surface. Once in the solution, anion exchange occurs, and a new polymeric phase is formed. This new phase precipitates on the surface of the initial crystal. This process proceeds via autocatalysis, facilitated by emerging clefts and fundamental defects in the crystal. This results in a self-perpetuating cascade of dissolution and recrystallization throughout the crystal.

SEM images of $\{[\text{Ag}(4,4'\text{-bipy})]\text{BF}_4\}_\infty$ crystals after incubation in NaNO_3 solution for 24 hours, Figure 5. 11, also support previous TEM data. Here it is

evident that the crystal retains its shape, but loses its integrity as it becomes a mass of microcrystals of $\{[\text{Ag}(4,4'\text{-bipy})]\text{NO}_3\}_\infty$. In addition, these SEM images show that only certain areas of the crystals have converted to microcrystalline $\{[\text{Ag}(4,4'\text{-bipy})]\text{NO}_3\}_\infty$, while other regions retain the characteristic finger-like features observed on the surface of $\{[\text{Ag}(4,4'\text{-bipy})]\text{BF}_4\}_\infty$ crystals (Figure 5. 6). From these images it appears that the crystal may have been removed from 3M NaNO_3 solution before the growth of the new phase had spread across the entire crystal. This would, however, contradict previous findings in which the process has been shown to be complete within 12 hours [290, 293, 314]. One plausible explanation for this is that during anion exchange, recrystallization occurs on the crystal, followed by growth of the phase across the surface in a manner analogous to that of two-dimensional nucleation [141, 145].

Alternatively, the geographical location of the differing phases may be due to the different isomers of $\{[\text{Ag}(4,4'\text{-bipy})]\text{BF}_4\}_\infty$ crystal. The proportion of each isomer in these crystals is unknown, and hence the location of each isomer within the crystal structure is unknown. However it is easy to rationalize that one of the isomers may dissolve faster than the other, or allow recrystallization to occur with greater ease or more compatibility. For example, isomer A has a hatched structure, comparable to that of $\{[\text{Ag}(4,4'\text{-bipy})]\text{NO}_3\}_\infty$ and hence may allow the dissolution/recrystallization process to occur with greater ease because it does not need to undergo such a pronounced structural change. In addition, the structure of isomer A may facilitate the recrystallization of $\{[\text{Ag}(4,4'\text{-bipy})]\text{NO}_3\}_\infty$, by allowing an almost epitaxial growth of the new phase to occur, similar to that observed by Booth *et al.* [335]. Organic crystals are commonly used for such a purpose, and act

as nucleation promoters and crystallizing aids in the manufacturing of polymers whose properties require a specific degree of crystallinity [13].

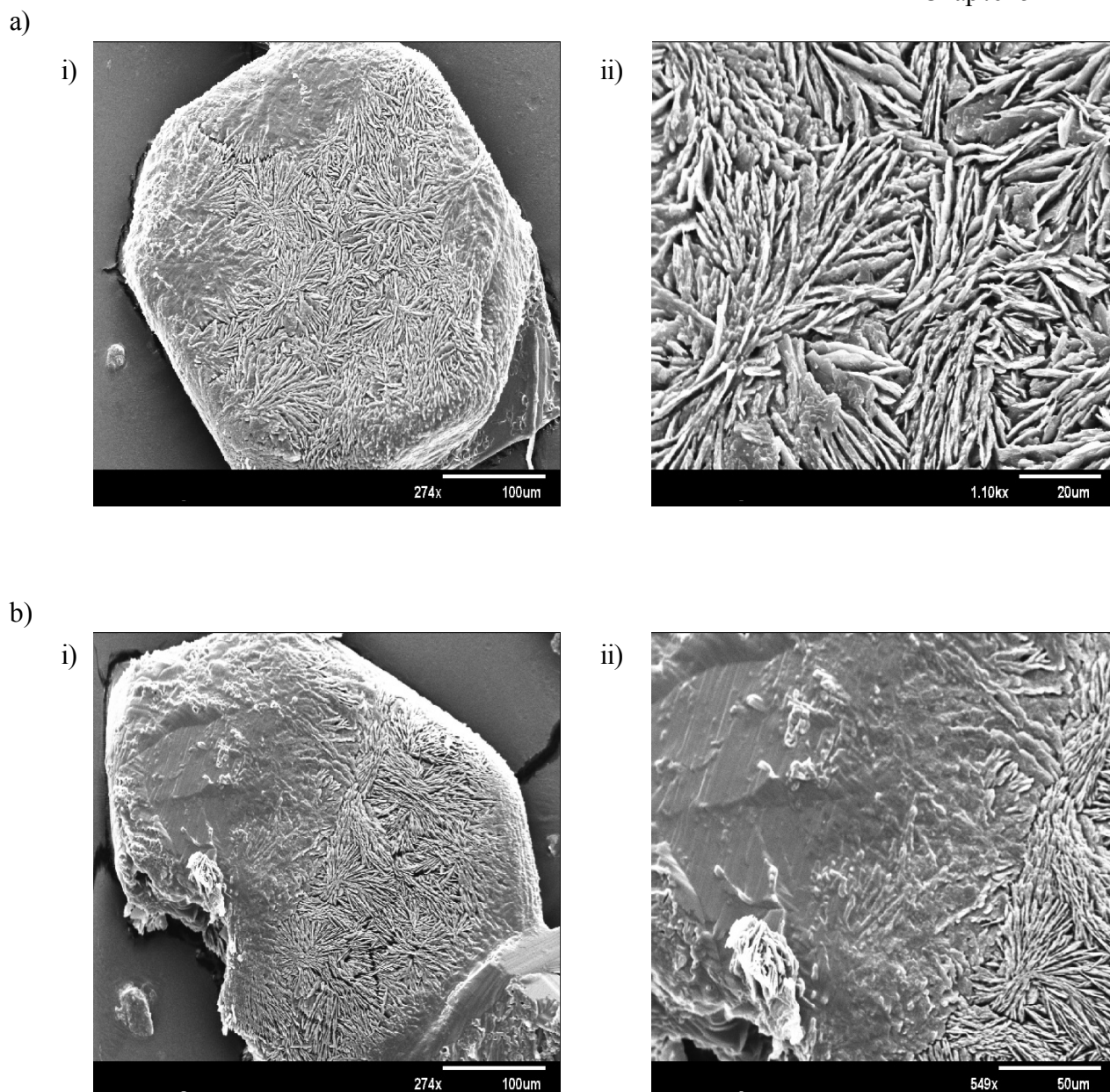


Figure 5. 11 SEM images of $\{[\text{Ag}(4,4'\text{-bipy})]\text{BF}_4\}_\infty$ crystals after incubation in 3M NaNO_3 solution for 24 hours. Image a) i) shows a crystal, at magnification x 274, which has retained its shape but almost entirely become a mass of microcrystals. These microcrystals are shown at magnification x 1100 in image a) ii). Image b) i) also shows a crystal at magnification x 274. Only approximately half of this crystal has converted to microcrystals, whereas the other half retains the original $\{[\text{Ag}(4,4'\text{-bipy})]\text{BF}_4\}_\infty$ surface structure. The boundary between the two halves is shown in image b) ii) at magnification x 549.

Further investigations are necessary to fully assess the proportion of each isomer in $\{[\text{Ag}(4,4'\text{-bipy})]\text{BF}_4\}_\infty$ crystals, and their effect on this ion exchange process.

The AFM image sequence shown in Figure 5. 12 follows the surface changes on a $\{[\text{Ag}(4,4'\text{-bipy})]\text{NO}_3\}_\infty$ crystal during incubation in 1M NaBF_4 solution. This is the reverse process of that visualized in Figure 5. 10. At time $t = 0$ the height of the apex of the triangular feature is 1194 nm. After 1 hour, the height of the feature decreases to 847 nm and a cleft is emerging at its point, indicating dissolution is taking place. At $t = 1\frac{1}{2}$ hours the height of the feature is 894 nm and depth of the cleft is 275 nm, suggesting that dissolution is occurring on and around the feature. Dissolution continues and after 2 hours the height of the feature is 1141 nm and the cleft, which has almost divided the feature into two distinct areas, has a depth of 730 nm. Recrystallization is observed after $2\frac{1}{2}$ hours during this process, which is later than in the $\{[\text{Ag}(4,4'\text{-bipy})]\text{BF}_4\}_\infty$ to $\{[\text{Ag}(4,4'\text{-bipy})]\text{NO}_3\}_\infty$ process. This is probably due to the relative solubilities of the two polymers, as discussed later in the chapter. The new phase continues to recrystallize and grow across the surface and the entire process is again complete within 12 hours.

These images clearly illustrate the dissolution and recrystallization processes which constitute the anion exchange mechanisms, and the emergence of clefts which perpetuate the autocatalytic process.

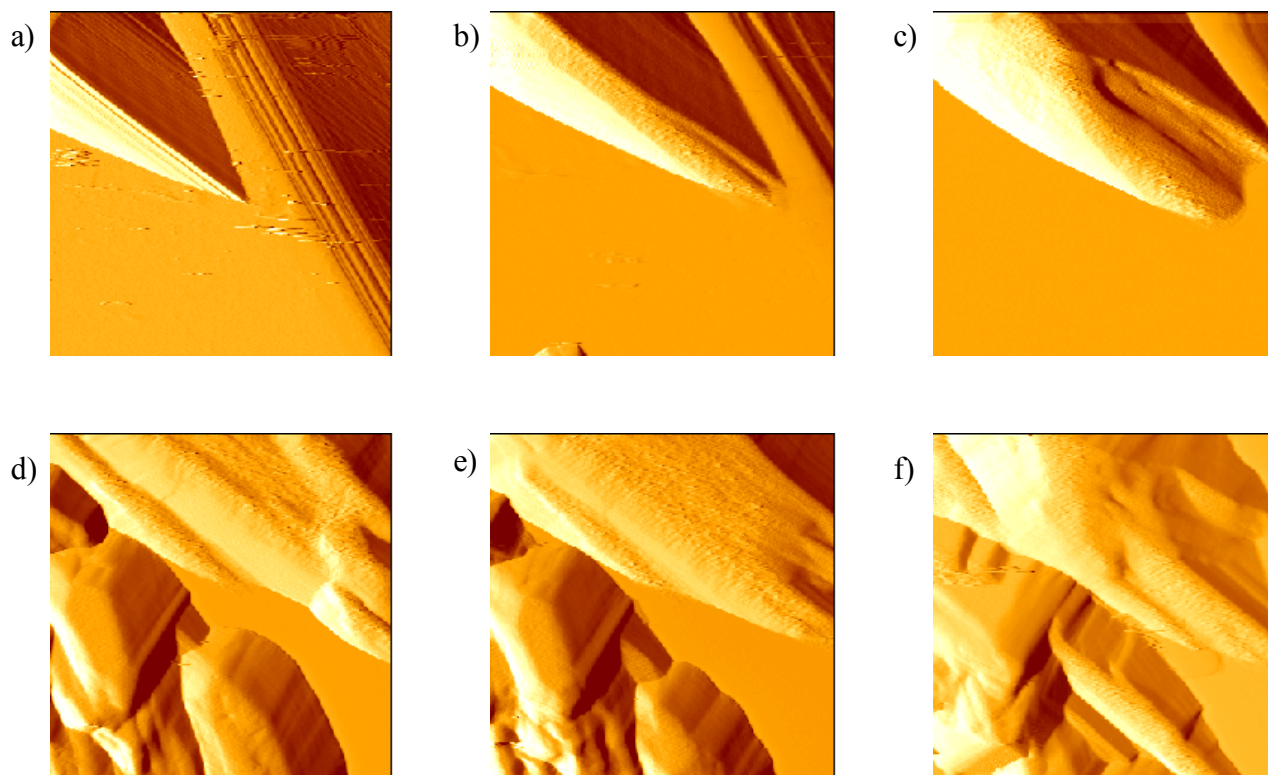


Figure 5. 12 Images a) to f) are 10 μm x 10 μm AFM images of the surface of a $\{[\text{Ag}(4,4'\text{-bipy})]\text{NO}_3\}_\infty$ crystal during incubation in 1M NaBF_4 solution. In image a) time $t = 0$, b) $t = 1$ hr, c) $t = 2$ hrs, d) $t = 2\frac{1}{2}$ hrs, e) $t = 3$ hrs, and f) $t = 4\frac{1}{2}$ hrs. All are topography images which have been left-shaded to allow the features to be more easily visualized.

SEM images, Figure 5. 13, of $\{[\text{Ag}(4,4'\text{-bipy})]\text{NO}_3\}_\infty$ crystal after incubation in 1M NaBF_4 for 24 hours demonstrate the presence of microcrystals which remained within the boundary of the initial $\{[\text{Ag}(4,4'\text{-bipy})]\text{NO}_3\}_\infty$ crystal. These findings reiterate those of previous TEM and XRPD data [290]. Unlike the $\{[\text{Ag}(4,4'\text{-bipy})]\text{BF}_4\}_\infty$ crystals, after incubation in NaNO_3 solution (Figure 5. 11) these crystals had completely converted from $\{[\text{Ag}(4,4'\text{-bipy})]\text{NO}_3\}_\infty$ to $\{[\text{Ag}(4,4'\text{-bipy})]\text{BF}_4\}_\infty$ microcrystals.

The kinetics of solvent-mediated processes are dependent upon the dissolution and growth rates of the corresponding phases [332]. However, the driving force for the process is invariably the difference in solubility of a metastable initial phase (more soluble) and a stable new phase (less soluble) [332]. These principles are applicable to the anion exchange process of these co-ordination polymers.

The solubility values for $\{[\text{Ag}(4,4'\text{-bipy})]\text{BF}_4\}_\infty$ and $\{[\text{Ag}(4,4'\text{-bipy})]\text{NO}_3\}_\infty$ in 3M NaNO_3 are 0.06 mmol L^{-1} and 0.02 mmol L^{-1} respectively [290]. Hence solid $\{[\text{Ag}(4,4'\text{-bipy})]\text{BF}_4\}_\infty$ is the metastable phase in 3M NaNO_3 , and will therefore dissolve. As it dissolves the solution becomes progressively more saturated with Ag^+ ions and bipyridyl molecules. When the saturation reaches a critical value, the monomeric components reassemble to form the more stable $\{[\text{Ag}(4,4'\text{-bipy})]\text{NO}_3\}_\infty$ phase, which then recrystallizes on the surface of the crystal. This process undersaturates the solution and induces further dissolution of $\{[\text{Ag}(4,4'\text{-bipy})]\text{BF}_4\}_\infty$. During the solvent-mediated transformations of the sparingly soluble solids, the solution is always saturated with respect to the metastable phase and supersaturated in respect of the stable phase [332].

The solubility values for these polymers in 1M NaBF_4 are unknown. However, the values are known for 3M NaBF_4 , they are 0.13 mmol L^{-1} and 0.57

mmol L⁻¹ for {[Ag(4,4'-bipy)]BF₄}_∞ and {[Ag(4,4'-bipy)]NO₃}_∞ respectively [290]. Clearly the solubility of the polymers would be greater in 1M NaBF₄, but from these values it is evident that, in NaBF₄ solution, {[Ag(4,4'-bipy)]NO₃}_∞ is the metastable phase whereas {[Ag(4,4'-bipy)]BF₄}_∞ is the stable phase. Therefore a similar scenario to that described above can be envisaged for the transformation of {[Ag(4,4'-bipy)]NO₃}_∞ to {[Ag(4,4'-bipy)]BF₄}_∞ in NaBF₄ solution.

In general it can be assumed that, when {[Ag(4,4'-bipy)]X}_∞ is immersed in a solution containing an excess of anion Y, it can be regarded as a metastable phase and, therefore, undergoes a transformation into the new stable phase {[Ag(4,4'-bipy)]Y}_∞.

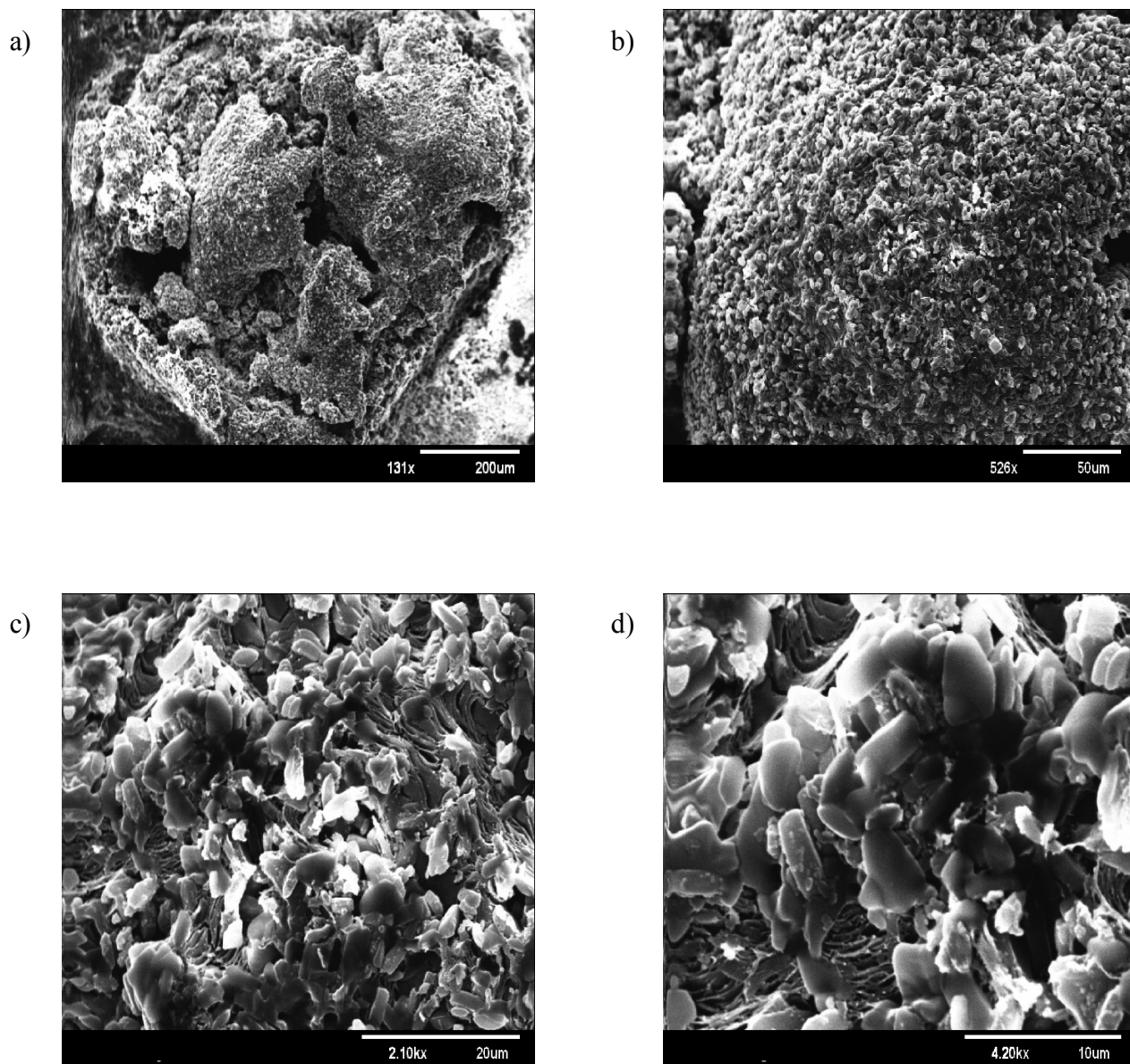
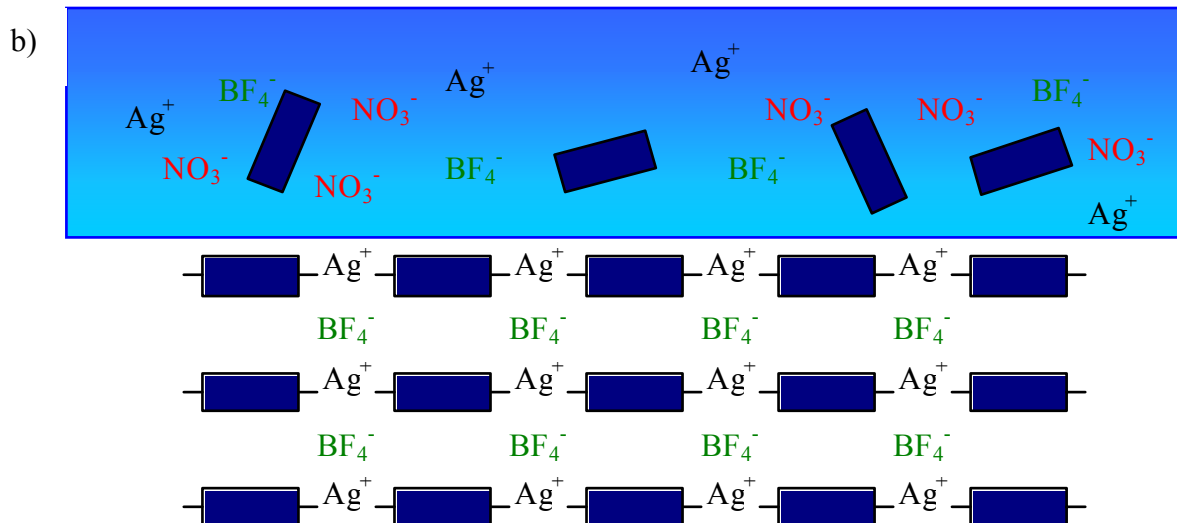
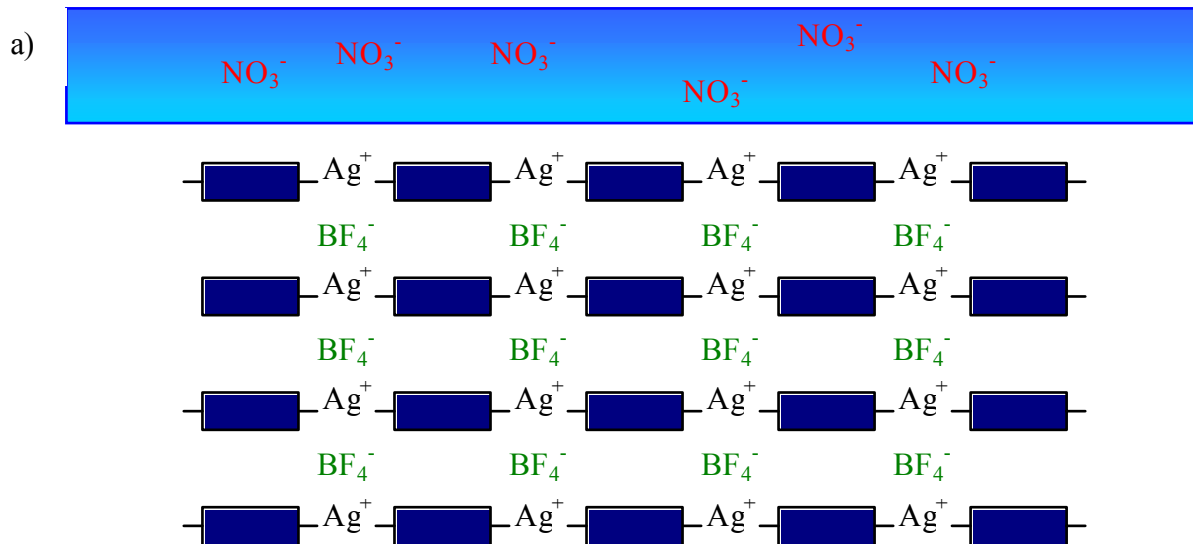


Figure 5. 13 SEM images of a $\{[Ag(4,4'-bipy)]NO_3\}_\infty$ crystal after incubation in 1M $NaBF_4$ solution for 24 hours. The magnification used in each image is a) x 131, b) x 526, c) x 2100, and d) x 4200.

5.4 Conclusion

AFM has proven to be an essential tool in elucidating the true mechanism by which the reversible anion exchange process of the co-ordination polymers $\{[\text{Ag}(4,4'\text{-bipy})]\text{BF}_4\}_\infty$ and $\{[\text{Ag}(4,4'\text{-bipy})]\text{NO}_3\}_\infty$ occurs. AFM data has confirmed the solubility of these co-ordination polymers and verified that the anion exchange process is indeed solvent-mediated, involving the dissolution of one crystalline phase and subsequent recrystallization of another, as illustrated in Figure 5. 14. As the crystal dissolves, clefts form within the crystal allowing the solution to access layers beneath the crystal surface. We suggest that the structural reorganization observed in these co-ordination polymers is initiated by the depolymerization (dissolution) of the initial polymer from the crystal surface. Once in the solution phase, anion exchange occurs, and a new polymeric phase is formed. This new phase precipitates on the surface of the initial crystal. This process proceeds via autocatalysis, facilitated by emerging clefts and fundamental defects in the crystal. This results in a self-perpetuating cascade of dissolution and recrystallization throughout the crystal. This data supports previous findings which speculated that the solvent-mediated process was the true one [290].



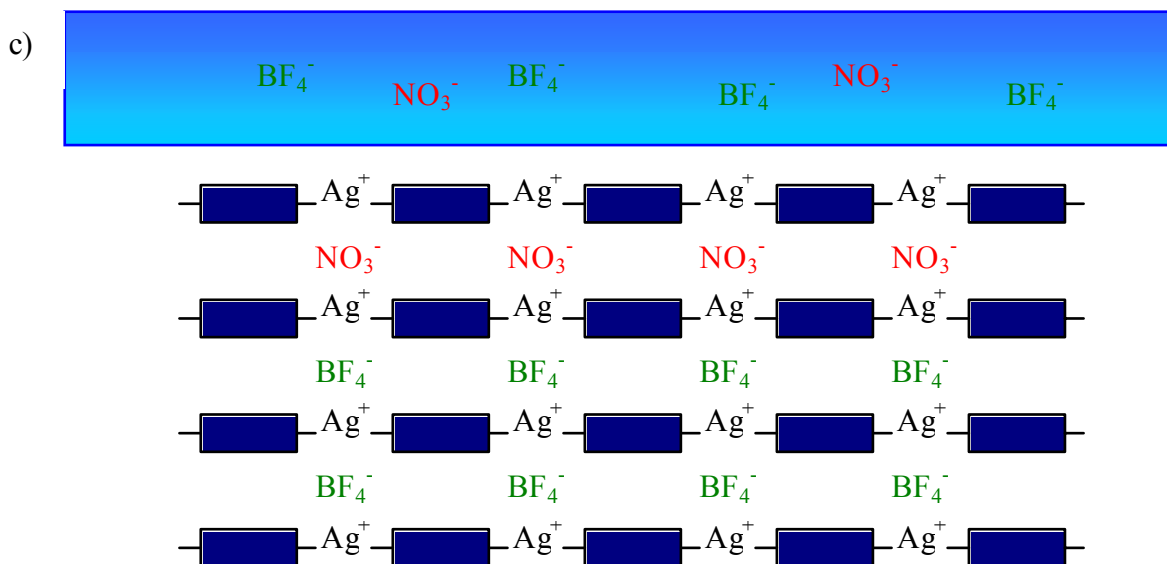


Figure 5. 14 Schematic diagram illustrating the mechanism by which ion exchange, and consequent structural conversion occurs in the co-ordination polymers $\{[\text{Ag}(4,4'\text{-bipy})]\text{BF}_4\}_\infty$ and $\{[\text{Ag}(4,4'\text{-bipy})]\text{NO}_3\}_\infty$. In a) $\{[\text{Ag}(4,4'\text{-bipy})]\text{BF}_4\}_\infty$ is in a solution of nitrate ions, b) shows the dissolution of the top layer of the $\{[\text{Ag}(4,4'\text{-bipy})]\text{BF}_4\}_\infty$ crystal in the nitrate solution. This is followed by the recrystallization of the polymeric layer, with weakly bound nitrate ions, onto the initial crystal, as displayed in c).

SEM data support and consolidate the AFM data, showing the appearance of microcrystals which retain the shape of the initial crystal, after each co-ordination polymer crystal had been incubated in their respective solution of ions. In addition, these SEM data also highlight the possible effect of the two isomers of $\{[\text{Ag}(4,4'\text{-bipy})]\text{BF}_4\}_\infty$ on the anion exchange process. Further studies are imperative in order to assess the impact of these isomers on the potential applications of $\{[\text{Ag}(4,4'\text{-bipy})]\text{BF}_4\}_\infty$.

These findings reiterate the ability of such interconversion processes to produce pure crystalline states of other compounds, which may be difficult to produce by other means [297]. These characteristics may prove to be very desirable to crystal engineers, whose ultimate aim is the rational design and control of crystal structures as well as the fine-tuning of their structure by modifying the constituent components [317, 348-350].

Chapter

6

General Conclusions

AFM has been extensively used to investigate the growth of a plethora of crystalline compounds. However, to date, it has not been used to probe the growth dynamics of any pharmaceutical drug crystal. In Chapter 1, the parameters which affect drug crystal growth, and their subsequent effects on processing, were comprehensively discussed. One of the parameters highlighted was supersaturation. Supersaturation (σ) is known to have profound effects on both the morphology and, at the molecular level, the growth mechanisms of crystals. In Chapter 2, we utilized AFM to assess the mechanisms and kinetics of growth on the (001) face of aspirin crystals at two levels of supersaturation. We used AFM to directly visualize, *in situ*, the mechanisms of growth which occurred on the (001) face of aspirin crystals at $\sigma = 0.31$ and $\sigma = 0.36$. AFM also allowed the acquisition of kinetic information at each σ .

At both σ values, the mechanism of growth observed was consistent with that of the dislocation mechanism. Other growth modes, such as 2-dimensional or 3-dimensional nucleation, were not observed. However, it is thought that 3D nucleation

is unique to macromolecular protein and virus crystals. At $\sigma = 0.31$, the step heights ranged from 1 nm to 85 nm. The rate of growth of steps ranged from 4.6 nm/s to 10.8 nm/s, and showed no correlation between step height and growth rate. All steps were observed to grow in the [100] direction.

At $\sigma = 0.36$, the steps growing in the [100] direction varied in height from 1 nm to 315 nm, and grew at rates ranging from 17.4 nm/s to 34.5 nm/s. Again there was no relation between step height and growth rate. The average growth rate of steps in the [100] direction at $\sigma = 0.31$ and $\sigma = 0.36$ was calculated as 7.2 nm/s and 25.7 nm/s respectively. Therefore, at $\sigma = 0.36$, the growth rate of the steps was a factor of 3.6 times higher than at $\sigma = 0.31$, irrespective of the larger macrosteps observed at $\sigma = 0.36$.

At $\sigma = 0.36$, growth was also initiated in the [010] direction, with steps ranging in height from 1 nm to 365 nm. In this direction, the growth rates ranged from 6.0 nm/s to 17.0 nm/s, with no relation between step height and growth rate. Thus, the growth rates of steps in the [100] and [010] directions were anisotropic. It is probable that the step anisotropy arises due to the difference in molecular structure of the steps advancing in different crystallographic directions.

These data may suggest that growth on the (001) face of aspirin crystals occurs solely via the dislocation mechanism at all values of σ . However, as dissolution was observed at $\sigma \leq 0.15$, and at $\sigma \geq 0.48$ microcrystals were visible in the growth medium, the range of σ values over which growth on the surface occurs is narrow. Hence, the two σ values investigated in this chapter were moderate to high. As the dislocation mechanism is the most energetically favourable at low σ , we assume that at σ values lower than those studied here, growth would again progress via the dislocation mechanism. It is therefore necessary to conduct similar

experiments on the (001) crystal face at higher σ to assess whether 2D or 3D nucleation occur at any level of σ .

The (001) face is the most prominent, and therefore the slowest growing, face of the crystal. It would, hence, be of great interest to carry out such experiments on the remaining faces of the crystal, as the faster growing faces may employ other modes of growth at these levels of σ .

The control, design, and promotion of crystal growth are greatly desired objectives of crystal engineers and the pharmaceutical industry alike. In order to achieve this goal more information is required on all aspects of the crystal growth procedure. In Chapter 3, we focused on the nucleation and promotion of aspirin crystal growth. In recent years, SAMs have come to the fore as surfaces upon which crystallization can not only be promoted, but can also be directed and patterned in predetermined locations.

We assessed the aspirin binding capabilities of three SAMs chemisorbed on gold. Of the three SAMs investigated, only the carboxyl-terminated 11-MUA SAM allowed aspirin crystals to nucleate on its surface. We assume that aspirin molecules bind to the SAM via hydrogen bonding between the two carboxyl groups, in a manner similar to that of aspirin molecules dimerizing in the crystal structure. Further investigation is required to precisely determine the mechanism of crystal formation on the SAM surface. However, nanostructure growth on surfaces is postulated to occur via the Deposition, Diffusion, and Aggregation (DDA) model.

Microcontact printing facilitated the patterning of gold substrates with 11-MUA and 1-DDT SAMs, and allowed us to create templates comprising aspirin-binding and non-binding regions. Incubation of these templates in aspirin solution

resulted in the patterned formation of tabular unidirectional aspirin crystals. The face of the crystal which bound to the SAM was (100), and the resulting crystals formed on the SAM had a tabular habit bounded by the faces {001}, {011}, and {110}. However, the dimensions of the crystals and channels did not mirror the dimensions of the stamp features, and more than one crystal nucleated within each stamped area. Therefore the parameters of the stamp used for our experiments need to be optimized in order to create patterns which promote nucleation of only one aspirin crystal per nucleating site.

Nevertheless, the observation that this template promoted the growth of highly oriented crystals implies that it allowed nucleation to occur at specific sites. Again the growth of crystals on the surface followed the DDA model.

This method, in conjunction with AFM, allowed visualization of the growth of a crystal bound to the SAM surface. Only growth in the [001] direction was observed, with the growth rate calculated as 18.1 nm/min. These templates also permitted the observation of the secondary nucleation and growth of a cluster of aspirin molecules on the surface of another aspirin crystal. Initially, growth in the [001] direction was predominant, with an average growth rate of 29.2 nm/min, compared with 8.0 nm/min in the [100] direction. After approximately 140 minutes, growth in the [001] direction ceased, but growth in the [100] direction rapidly increased, with rates ranging from 23.5 nm/min to 37.6 nm/min.

The observation that growth in the [001] direction was initially dominant but was then curtailed, whilst growth in the [100] direction increased may aid in the explanation of the tabular habit of the crystals grown on the underlying SAM.

These experiments could be employed to control the resulting crystal morphology and size of this and other drug crystals. SAMs may also provide a

surface upon which nucleation and growth can be monitored under differing crystallization parameters. Such knowledge may assist in predicting the outcomes of crystallization, controlling polymorphism, directing nucleation of polymorphs or enantiomers, and searching for unknown polymorphs.

It is well known that the presence of impurities can dramatically affect the nucleation, morphology, and chemical properties of crystals. Although literature is replete with examples of impurity or additive-induced modifications of crystals, few have probed the interaction of these compounds with distinct growing faces. In Chapter 4, we utilized AFM and SEM to investigate the influence of two structurally related additives of paracetamol, namely acetanilide and metacetamol, on its crystal morphology. We also probed, *in situ*, the effects of these additives on the morphology and growth rate of steps on the (001) face of the crystal.

SEM images showed the characteristic tabular habit of pure paracetamol crystals was only moderately altered by the presence of acetanilide, but the crystals adopted a columnar habit when grown in the presence of metacetamol.

On a microscopic level, AFM revealed that the surface features of pure paracetamol crystals were steps ranging from 1 nm to 21 nm in height. On the contrary, crystals grown with acetanilide possessed thin, branched terraces of approximately 20 nm in height. We suspect that the branched appearance of the steps is due to the adsorption of acetanilide molecules onto terraces or steps during growth, causing pinning and bending of the growing steps.

The presence of metacetamol during growth resulted in steps of approximately 15 nm in height interspersed with holes, and also induced the formation of defects in the crystal surface. These data suggest that the crystal lattice,

and hence the hydrogen bonding network, were considerably disrupted by metacetamol during growth.

Growth on the (001) face of paracetamol crystals in the presence and absence of acetanilide or metacetamol was monitored via AFM. In the absence of any additive, growth was observed to occur by a dislocation mechanism. Growing steps ranged from 95 nm to 588 nm in height. The rate of growth of the steps ranged from 26.4 nm/s to 76.2 nm/s, and decreased with increasing step height. All steps were observed to grow in the [-100] direction.

In the presence of acetanilide, holes, which may have originated from defects, emerged in the surface during incubation. Steps, ranging from 13 nm to 45 nm in height, emanated from these holes and dissolved at rates between 1.3 nm/s and 2.7 nm/s, in the [100] direction. The dissolution rate of the steps decreased with increasing step height. The holes or clefts in the surface were also observed to deepen over time, indicating that dissolution was occurring into the crystal core as well as laterally. The presence of additives is known to increase the solubility of paracetamol, which may have induced such dissolution.

The presence of metacetamol in the growth medium resulted in the growth of steps, of 4 nm to 21 nm in height, at rates of 19.0 nm/s to 37.8 nm/s in the [-100] direction. The steps were pointed in appearance and significantly smaller than those observed in the absence of metacetamol, suggesting that the additive molecules pinned the steps. The average growth rates in the absence and presence of metacetamol were 49.5 nm/s and 27.1 nm/s respectively. Hence, metacetamol dramatically altered not only the morphology, but also the rate of the growing steps.

AFM enabled the observation of the effects of metacetamol on the growing interface on a micrometre scale. However, we could not establish, at this resolution,

whether additive adsorption occurred at step edges or on terraces, as both generate the formation of pointed, pinned steps. Nonetheless, the observed pinning of steps and reduction in growth rates are in accordance with the Cabrera and Vermilyea model.

The functional groups which protrude from the (001) face, in the [-100] direction, are NHCOCH_3 and OH. These groups may facilitate the attachment of metacetamol molecules via their CO group, which is equivalent to that of paracetamol, or their OH group, which is located juxtaposed to that of paracetamol. In either case, the hydrogen bonding network of the crystal would be largely preserved. Hence, metacetamol may bind with relative ease to this face and induce the degree of inhibition observed.

We suggest that further similar experiments should be carried out using each of the six known structurally related additives of paracetamol, not only on its (001) face, but on all other faces of the crystal. Particular attention should be paid to the inhibitory activities on the {110} faces. These are considered to be morphologically the most influential, because their growth rates and mechanisms change with increasing σ , altering the habit of the crystal from columnar to tabular.

Once the degree of inhibition of these additives has been established for each face of paracetamol, they could be employed to control the chemical properties of crystalline paracetamol and, perhaps, its problematic compaction behaviour.

Finally, we wished to assess the capabilities of AFM in following the structural transformations of crystals. Thus, in Chapter 5, we used AFM to determine the process by which the anion exchange, and the subsequent structural transformations, of the crystalline co-ordination polymers $\{[\text{Ag}(4,4'\text{-bipy})]\text{BF}_4\}_\infty$ and $\{[\text{Ag}(4,4'\text{-$

bipy)]NO₃]_∞ occur. Many of the applications of co-ordination polymers rely on the ion exchange capabilities of these compounds. Currently, there has been considerable debate over whether the anion exchange process is solid-state or solvent-mediated.

AFM data confirmed the solubility of the aforementioned co-ordination polymers and verified that the anion exchange process is indeed solvent-mediated, involving the dissolution of one crystalline phase and subsequent recrystallization of another. As the crystal dissolves, clefs form within the crystal allowing the solution to access layers beneath the crystal surface. We suggest that the structural reorganization observed in these co-ordination polymers is initiated by the dissolution of the initial polymer from the crystal surface. Once in the solution phase, anion exchange occurs, and a new polymeric phase is formed. This new phase precipitates on the surface of the initial crystal. This process proceeds via autocatalysis, facilitated by emerging clefs and fundamental defects in the crystal. This results in a self-perpetuating cascade of dissolution and recrystallization throughout the crystal.

The results presented here reiterate the capability of AFM to monitor dynamic events, such as *in situ* growth, dissolution, and structural transformation on crystal faces, at the nanoscale. It has also proven its capacity to deduce the mechanisms and rates of growth of drug crystals, as a function of crystallization parameters. These studies emphasize the fact that AFM can provide essential fundamental information on the growth of drug compounds to the pharmaceutical industry. Such knowledge may facilitate the optimization of crystallization parameters of these compounds, and may assist in preventing the production of unwanted or unstable pharmaceutical compounds.

References

- 1 Davey, R. and Garside, J. (2000) From molecules to crystallizers, Oxford University Press, New York
- 2 Zettlemoyer, A. C. (1969) Nucleation, Marcel Dekker, New York
- 3 Söhnel, O. and Garside, J. (1992) Precipitation: Basic principles and industrial applications, Butterworth-Heinemann, Oxford
- 4 Mullin, J. W. (1993) Industrial crystallization, Butterworth-Heinemann, London
- 5 Myerson, A. S. (1993) Handbook of industrial crystallization, Butterworth-Heinemann, Oxford
- 6 Gunton, J. D. (1999) Homogeneous nucleation. *J. Stat. Phys.* **95**, 903-923
- 7 Rodríguez-Hornedo, N. and Murphy, D. (1999) Significance of controlling crystallization mechanisms and kinetics in pharmaceutical systems. *J. Pharm. Sci.* **88**, 651-660
- 8 Gibbs, J. W. (1948) Collected works, Vol. I, Thermodynamics, Yale University Press, New Haven
- 9 Volmer, M. (1939) Kinetic Der Phasenbildung, Steinkopff, Leipzig
- 10 Perepezko, J. H. (1994) Nucleation reactions in undercooled liquids. *Mater. Sci. Eng. A.* **178**, 105-111
- 11 Perepezko, J. H. (1997) Kinetic processes in undercooled melts. *Mater. Sci. Eng. A.* **226**, 374-382
- 12 Carter, P. W. and Ward, M. D. (1993) Topographically directed nucleation of organic crystals on molecular single-crystal substrates. *J. Am. Chem. Soc.* **115**, 11521-11535
- 13 Ward, M. D. (1997) Organic crystal surfaces: structure, properties and reactivity. *Curr. Opin. Colloid Interface Sci.* **2**, 51-64
- 14 Weissbuch, I., Zbaida, D., Addadi, L., Leiserowitz, L. and Lahav, M. (1987) Design of polymeric inhibitors for the control of crystal polymorphism - induced enantiomeric resolution of racemic histidine by crystallization. *J. Am. Chem. Soc.* **109**, 1869-1871

- 15 Carter, P. W. and Ward, M. D. (1994) Directing polymorph selectivity during nucleation of anthranilic acid on molecular substrates. *J. Am. Chem. Soc* **116**, 769-770
- 16 Weissbuch, I., Leisorowitz, L. and Lahav, M. (1994) Tailor-made and charge-transfer auxiliaries for the control of the crystal polymorphism of glycine. *Adv. Mat.* **6**, 952-956
- 17 Bonafede, S. J. and Ward, M. D. (1995) Selective nucleation and growth of an organic polymorph by ledge-directed epitaxy on a molecular-crystal substrate. *J. Am. Chem. Soc.* **117**, 7853-7861
- 18 Davey, R. J., Blagden, N., Potts, G. D. and Docherty, R. (1997) Polymorphism in molecular crystals: Stabilization of a metastable form by conformational mimicry. *J. Am. Chem. Soc.* **119**, 1767-1772
- 19 Chow, A. H.-L., Chow, P. K. K., Zhongshan, W. and Grant, D. J. W. (1985) Modification of acetaminophen crystals: influence of growth in aqueous solutions containing *p*-acetoxyacetanilide on crystal properties. *Int. J. Pharm.* **24**, 239-258
- 20 Chow, A. H.-L. and Grant, D. J. W. (1988) Modification of acetaminophen crystals. II. Influence of stirring rate during solution-phase growth on crystal properties in the presence and absence of *p*-acetoxyacetanilide. *Int. J. Pharm.* **41**, 29-39
- 21 Chow, A. H.-L. and Grant, D. J. W. (1988) Modification of acetaminophen crystals. III. Influence of initial supersaturation during solution-phase growth on crystal properties in the presence and absence of *p*-acetoxyacetanilide. *Int. J. Pharm.* **42**, 123-133
- 22 Hendriksen, B. A. and Grant, D. J. W. (1995) The effect of structurally related substances on the nucleation kinetics of paracetamol (acetaminophen). *J. Cryst. Growth* **156**, 252-260
- 23 Hendriksen, B. A., Grant, D. J. W., Meenan, P. and Green, D. A. (1998) Crystallisation of paracetamol (acetaminophen) in the presence of structurally related substances. *J. Cryst. Growth* **183**, 629-640
- 24 Finnie, S. D., Ristic, R. I., Sherwood, J. N. and Zikic, A. M. (1999) Morphological and growth rate distributions of small self-nucleated paracetamol crystals grown from pure aqueous solutions. *J. Cryst. Growth* **207**, 308-318

- 25 Raghavan, S. L., Trividic, A., Davis, A. F. and Hadgraft, J. (2001) Crystallization of hydrocortisone acetate: influence of polymers. *Int. J. Pharm.* **212**, 213-221
- 26 Valder, C. and Merrifield, D. (1996) Pharmaceutical Technology. *SmithKline Beecham R&D News* **32**, 1
- 27 Shekunov, B. Y. and Grant, D. J. W. (1997) *In situ* optical interferometric studies of the growth and dissolution behaviour of paracetamol (acetaminophen). 1. Growth kinetics. *J. Phys. Chem. B.* **101**, 3973-3979
- 28 Shekunov, B. Y. and York, P. (2000) Crystallization processes in pharmaceutical technology and drug delivery design. *J. Cryst. Growth* **211**, 122-136
- 29 Ristic, R. I. (2002) The role of structural defects and interfacial instabilities in the growth behaviour of paracetamol. *Int. J. Mod. Phys. B* **16**, 329-337
- 30 Haleblan, J. K. (1975) Characterization of habits and crystalline modification of solids and their pharmaceutical applications. *J. Pharm. Sci.* **64**, 1269-1287
- 31 York, P. (1983) Solid-state properties of powders in the formulation and processing of solid dosage forms. *Int. J. Pharm.* **14**, 1-28
- 32 Grant, D. J. W. and York, P. (1986) A disruption index for quantifying the solid-state disorder induced by additives or impurities. 2. Evaluation from heat of solution. *Int. J. Pharm.* **28**, 103-112
- 33 York, P. (1992) Crystal engineering and particle design for the powder compaction process. *Drug Dev. Ind. Pharm.* **18**, 677-721
- 34 Chow, K. Y., Go, J., Mehdizadeh, M. and Grant, D. J. W. (1984) Modification of adipic acid crystals: influence of growth in the presence of fatty acid additives on crystal properties. *Int. J. Pharm.* **20**, 3-34
- 35 Byrn, S. R. (1976) Mechanisms of solid-state reactions of drugs. *J. Pharm. Sci.* **65**, 1-22
- 36 Karpova, E. A. and Tarahovsky, Y. S. (2001) Altering the morphology of crystals of a macromolecule without changing the unit cell (A case study of ribosome crystals). *J. Cryst. Growth* **232**, 610-617
- 37 Ristic, R. I., Finnie, S., Sheen, D. B. and Sherwood, J. N. (2001) Macro- and micromorphology of monoclinic paracetamol grown from pure aqueous solution. *J. Phys. Chem. B.* **105**, 9057-9066

- 38 Yoshizaki, I., Sato, T., Igarashi, N., Natsuisaka, M., Tanaka, N., Komatsu, H. and Yoda, S. (2001) Systematic analysis of supersaturation and lysozyme crystal quality. *Acta Cryst.* **D57**, 1621-1629
- 39 Garnier, S., Petit, S. and Coquerel, G. (2002) Influence of supersaturation and structurally related additives on the crystal growth of alpha-lactose monohydrate. *J. Cryst. Growth* **234**, 201-219
- 40 Boistelle, R. and Astier, J. P. (1988) Crystallization mechanisms in solution. *J. Cryst. Growth* **90**, 14-30
- 41 Hao, Z. M. and Iqbal, A. (1997) Some aspects of organic pigments. *Chem. Soc. Rev.* **26**, 203-213
- 42 Altieri, R. J. and Thompson, D. C. (1996) in Inhalation aerosols series, lung biology in health and disease, vol. 94 (Hickey, A. J., ed.), pp. 5, Marcel Dekker, New York
- 43 Couvreur, P., Dubernet, C. and Puisieux, F. (1995) Controlled drug delivery with nanoparticles - current possibilities and future trends. *Eur. J. Pharm. Biopharm.* **41**, 2-13
- 44 Watanabe, A., Yamaoka, Y. and Takada, K. (1982) Crystal habits and dissolution behaviour of aspirin. *Chem. Pharm. Bull.* **30**, 2958-2963
- 45 Cano, H., Gabas, N. and Canselier, J. P. (2001) Experimental study on the ibuprofen crystal growth morphology in solution. *J. Cryst. Growth* **224**, 335-341
- 46 Granberg, R. A., Ducreux, C., Gracin, S. and Rasmuson, Å. C. (2001) Primary nucleation of paracetamol in acetone-water mixtures. *Chem. Eng. Sci.* **56**, 2305-2313
- 47 Marshall, P. V. and York, P. (1989) Crystallization solvent induced solid state and particulate modifications of nitrofurantoin. *Int. J. Pharm.* **55**, 257-263
- 48 Marshall, P. V. and York, P. (1991) The compaction properties of nitrofurantoin samples crystallized from different solvents. *Int. J. Pharm.* **67**, 59-65
- 49 Klug, D. L. (1993) in Handbook of industrial crystallization (Myerson, A., ed.), pp. 65-87, Butterworth-Heinemann, Boston

- 50 Weissbuch, I., Leiserowitz, L. and Lahav, M. (1995) in Crystallization technology handbook (Mersmann, A., ed.), pp. 401-457, Marcel Dekker, New York
- 51 Fairbrother, J. E. and Grant, D. J. W. (1978) The crystal habit modification of a tablet lubricant, adipic acid. *J. Pharm. Pharmacol.* **30**, S19
- 52 Black, S. N., Davey, R. J. and Halcrow, M. (1986) The kinetics of crystal growth in the presence of tailor-made additives. *J. Cryst. Growth* **79**, 765-774
- 53 Davey, R. J., Black, S. N., Logan, D., Maginn, S. J., Fairbrother, J. E. and Grant, D. J. W. (1992) Structural and kinetic features of the crystal growth inhibition - adipic acid growing in the presence of n-alkanoic acids. *J. Chem. Soc. Faraday. Trans.* **88**, 3461-3466
- 54 Myerson, A. S. and Jang, S. M. (1995) A comparison of binding-energy and metastable zone width for adipic acid with various additives. *J. Cryst. Growth* **156**, 459-466
- 55 Davey, R. J., Black, S. N., Goodwin, A. D., Mackerron, D., Maginn, S. J. and Miller, E. J. (1997) Crystallization in polymer films: Control of morphology and kinetics of an organic dye in a polysilicone matrix. *J. Mater. Chem.* **7**, 237-241
- 56 Kato, T., Suzuki, T., Amamiya, T., Irie, T., Komiyama, M. and Yui, H. (1998) Effects of macromolecules on the crystallization of CaCO₃ the formation of organic/inorganic composites. *Supramol. Sci.* **5**, 411-415
- 57 Williams-Seton, L., Davey, R. J., Lieberman, H. F. and Pritchard, R. G. (2000) Disorder and twinning in molecular crystals: impurity-induced effects in adipic acid. *J. Pharm. Sci.* **89**, 346-354
- 58 Al-Jibbouri, S. and Ulrich, J. (2001) The influence of impurities on crystallization kinetics of sodium chloride. *Cryst. Res. Technol.* **36**, 1365-1375
- 59 Prasad, K. V. R., Ristic, R. I., Sheen, D. B. and Sherwood, J. N. (2001) Crystallization of paracetamol from solution in the presence and absence of impurity. *Int. J. Pharm.* **215**, 29-44
- 60 Wilkins, S. J., Coles, B. A., Compton, R. G. and Cowley, A. (2002) Mechanism and kinetics of salicylic acid dissolution in aqueous solution under defined hydrodynamic conditions via atomic force microscopy: the

- effects of the ionic additives NaCl, LiCl and MgCl₂, the organic additives 1-propanol, 2-propanol, and the surfactant sodium dodecyl sulphate. *J. Phys. Chem. B.* **106**, 4763-4774
- 61 Garti, N. and Zour, H. (1997) The effect of surfactants on the crystallization and polymorphic transformation of glutamic acid. *J. Cryst. Growth* **172**, 486-498
- 62 Simonelli, A. P., Mehta, S. C. and Higuchi, W. I. (1970) Inhibition of sulfathiazole crystal growth by polyvinylpyrrolidone. *J. Pharm. Sci.* **59**, 633-638
- 63 Borka, L. and Haleblan, J. K. (1990) Crystal polymorphism of pharmaceuticals. *Acta Pharm. Jugosl.* **40**, 71-94
- 64 Borka, L. (1991) Review of crystal polymorphism of substances in the European Pharmacopoeia. *Pharm. Acta Helv.* **66**, 16-22
- 65 Sato, K. (1993) Polymorphic transformations in crystal growth. *J. Phys. D: Appl. Phys.* **26**, B77-B84
- 66 Gavezzotti, A. and Filippini, G. (1995) Polymorphic forms of organic crystals at room conditions - thermodynamic and structural implications. *J. Am. Chem. Soc.* **117**, 12299-12305
- 67 Khoshkhoo, S. and Anwar, J. (1993) Crystallization of polymorphs - the effect of solvent. *J. Phys. D: Appl. Phys.* **26**, B90-B93
- 68 Kaneniwa, N., Otsuka, M. and Hayashi, T. (1985) Physicochemical characterization of indomethacin polymorphs and the transformation kinetics in ethanol. *Chem. Pharm. Bull.* **33**, 3447-3455
- 69 Kaneniwa, N., Ichikawa, J. and Matsumoto, T. (1988) Preparation of phenylbutazone polymorphs and their transformation in solution. *Chem. Pharm. Bull.* **36**, 1063-1073
- 70 (July 1998) Abbott Laboratories, Letter to healthcare providers. <http://www.fda.gov/medwatch/safety/1998/norvir.htm>
- 71 Dunitz, J. D. and Bernstein, J. (1995) Disappearing polymorphs. *Acc. Chem. Res.* **28**, 193-200
- 72 Byrn, S., Pfeiffer, R., Ganey, M., Hoiberg, C. and Poochikian, G. (1995) Pharmaceutical solids: A strategic approach to regulatory considerations. *Pharm. Res.* **12**, 945-954

- 73 Hancock, B. C., Shamblin, S. L. and Zografi, G. (1995) Molecular mobility of amorphous pharmaceutical solids below their glass-transition temperatures. *Pharm. Res.* **12**, 799-806
- 74 Haleblian, J. and McCrone, W. J. (1969) Pharmaceutical applications of polymorphism. *Pharm. Sci.* **58**, 911-929
- 75 Stinson, S. C. (1993) Chiral Drugs. *Chem. Eng. News* **71**, 38
- 76 Li, Z. J. and Grant, D. J. W. (1997) Relationship between physical properties and crystal structures of chiral drugs. *J. Pharm. Sci.* **86**, 1073-1078
- 77 (1987) Food and drug administration guideline for submitting supporting documentation in drug applications for the manufacture of drug substances. FDA Centre for Drug Evaluation and Research: Office of Drug Evaluation, Rockville, MD
- 78 Byrn, S. R., Pfeiffer, R. R., Stephenson, G., Grant, D. J. W. and Gleason, W. B. (1994) Solid-state pharmaceutical chemistry. *Chem. Mater.* **6**, 1148-1158
- 79 SSCI Analytical and Custom Research Service. <http://www.ssci-inc.com>
- 80 (1992) Code of Federal Regulations, Title 21. *Food and drugs* **Parts 210-211**
- 81 Desiraju, G. R. (1997) Crystal gazing: Structure prediction and polymorphism. *Science* **278**, 404-405
- 82 Desiraju, G. R. (1997) Designer crystals: Intermolecular interactions, network structures and supramolecular synthons. *Chem. Commun.*, 1475-1482
- 83 Gavezzotti, A. (1994) Are crystal structures predictable. *Acc. Chem. Res.* **27**, 309-314
- 84 Gavezzotti, A. (1997) Computer simulations of organic solids and their liquid-state precursors. *Faraday Discuss.* **106**, 63-77
- 85 Gavezzotti, A. and Filippini, G. (1996) Computer prediction of organic crystal structures using partial X-ray diffraction data. *J. Am. Chem. Soc.* **118**, 7153-7157
- 86 Gavezzotti, A. and Filippini, G. (1998) Self-organization of small organic molecules in liquids, solutions and crystals: Static and dynamic calculations. *Chem. Commun.*, 287-294
- 87 Kuznetsov, Y. G., Konnert, J., Malkin, A. J. and McPherson, A. (1999) The advancement and structure of growth steps on thaumatin crystals visualized by atomic force microscopy at molecular resolution. *Surf. Sci.* **440**, 69-80

- 88 Li, T., Morris, K. R. and Park, K. (2000) Influence of solvent and crystalline supramolecular structure on the formation of etching patterns on acetaminophen single crystals: a study with atomic force microscopy and computer simulation. *J. Phys. Chem. B.* **104**, 2019-2032
- 89 Beyer, T., Day, G. M. and Price, S. L. (2001) The prediction, morphology, and mechanical properties of the polymorphs of paracetamol. *J. Am. Chem. Soc.* **123**, 5086-5094
- 90 Mehta, S. C., Bernardo, P. D., Higuchi, W. I. and Simonelli, A. P. (1970) Rate of crystal growth of sulfathiazole and methylprednisolone. *J. Pharm. Sci.* **59**, 638-644
- 91 Zipp, G. L. and Rodríguez-Hornedo, N. (1993) Growth mechanism and morphology of phenytoin and their relationship with crystallographic structure. *J. Phys. D: Appl. Phys.* **26**, B48-B55
- 92 Zipp, G. L. and Rodríguez-Hornedo, N. (1993) The mechanism of phenytoin crystal growth. *Int. J. Pharm.* **98**, 189-201
- 93 Durbin, S. D. and Feher, G. (1990) Studies of crystal growth of proteins by electron microscopy. *J. Mol. Biol.* **212**, 763-774
- 94 Michinomae, M., Mochizuki, M. and Ataka, M. (1999) Electron microscopic studies on the initial process of lysozyme crystal growth. *J. Cryst. Growth* **197**, 257-262
- 95 Braun, N., Tack, J., Fischer, M., Bacher, A., Bachmann, L. and Weinkauf, S. (2000) Electron microscopic observations on protein crystallization: adsorption layers, aggregates and crystal defects. *J. Cryst. Growth* **212**, 270-282
- 96 Shekunov, B. Y., Grant, D. J. W., Latham, R. J. and Sherwood, J. N. (1997) *In situ* optical interferometric studies of the growth and dissolution behaviour of paracetamol (acetaminophen) crystals. 3. Influence of growth in the presence of *p*-acetoxyacetanilide. *J. Phys. Chem. B.* **101**, 9107-9112
- 97 Zikic, A. M., Ristic, R. I. and Sherwood, J. N. (1998) An instrument for *in situ* growth rate characterization of mechanically strained crystals. *Rev. Sci. Instrum.* **69**, 2713-2719
- 98 Burton, W. K., Cabrera, N. and Frank, F. C. (1951) The growth of crystals and the equilibrium structure of their surfaces. *Phil. Trans. R. Soc., Lond.* **A243**, 299-358

- 99 Bennema, P. (1967) Analysis of crystal growth models for slightly supersaturated solutions. *J. Cryst. Growth* **1**, 225-232
- 100 Bennema, P. (1967) Interpretation of the relation of the rate of crystal growth and low supersaturation. *J. Cryst. Growth* **1**, 278-287
- 101 Bennema, P. (1984) Spiral growth and surface roughening: development since Burton, Cabrera and Frank. *J. Cryst. Growth* **69**, 182-197
- 102 Gilmer, G. H., Ghez, R. and Cabrera, N. (1971) An analysis of combined surface and volume diffusion processes in crystal growth. *J. Cryst. Growth* **8**, 79-93
- 103 Chernov, A. A. (1989) Formation of crystals in solutions. *Contemp. Phys.* **30**, 251-276
- 104 Needham, G. (1958) The practical use of the microscope, C. C. Thomas, Springfield, Il
- 105 Danesh, A. (2000) Thesis in School of Pharmaceutical Sciences, University of Nottingham
- 106 Li, L. and Rodríguez-Hornedo, N. (1992) Growth kinetics and mechanisms of glycine crystals. *J. Cryst. Growth* **121**, 33-38
- 107 Lechuga-Ballesteros, D. and Rodríguez-Hornedo, N. (1995) Effects of molecular structure and growth kinetics on the morphology of L-alanine crystals. *Int. J. Pharm.* **115**, 151-160
- 108 Lechuga-Ballesteros, D. and Rodríguez-Hornedo, N. (1995) The influence of additives on the growth kinetics and mechanisms of L-alanine crystals. *Int. J. Pharm.* **115**, 139-149
- 109 Agar, A. W., Alderson, R. H. and Chescoe, D. (1974) Principles and practice of electron microscopy, North Holland, Amsterdam
- 110 Hunter, E. E. (1984) Practical electron microscopy, Praeger Scientific, New York
- 111 Reimer, L. (1985) Scanning electron microscopy, physics of image formation and microanalysis, vol. 45, Springer, Berlin
- 112 Oebbeke, I. (1998) New possibilities of material analysis and evaluation by ESEM - environmental scanning electron microscope. *Prakt. Metallogr. - Pract. Metallogr.* **35**, 61-70
- 113 Bondioli, F., Corradi, A. B., Ferrari, A. M., Manfredini, T. and Baldi, G. T. I. (2000) Environmental scanning electron microscopy (ESEM) investigation of

- the reaction mechanism in praseodymium-doped zircon. *J. Am. Ceram. Soc.* **83**, 1518-1520
- 114 Grassmann, O. and Lobmann, P. (2003) Morphogenetic control of calcite crystal growth in sulphonic acid based hydrogels. *Chem.-Eur. J.* **9**, 1310-1316
- 115 Dailey, L. A., Schmehl, T., Gessler, T., Wittmar, M., Grimminger, F., Seeger, W. and Kissel, T. (2003) Nebulization of biodegradable nanoparticles: impact of nebulizer technology and nanoparticle characteristics on aerosol features. *J. Control. Release* **86**, 131-144
- 116 Li, Z. G., Harlow, R. L., Foris, C. M., Li, H., Ma, P., Vickery, R. D., Maurin, M. B. and Toby, B. H. (2002) New applications of electron diffraction in the pharmaceutical industry: polymorph determination by using a combination of electron diffraction and synchrotron X-ray powder diffraction techniques. *Microsc. Microanal.* **8**, 134-138
- 117 Patterson, J., Bary, A. and Rades, T. (2002) Physical stability and solubility of the thermotropic mesophase of fenoprofen calcium as pure drug and in a tablet formulation. *Int. J. Pharm.* **247**, 147-157
- 118 Binnig, G., Quate, C. F. and Gerber, C. (1986) Atomic force microscope. *Phys. Rev. Lett.* **56**, 930-933
- 119 Lal, R. and John, S. A. (1994) Biological applications of atomic force microscopy. *Am. J. Physiol.* **266**, C1-C21
- 120 Roberts, C. J., Williams, P. M., Davies, M. C., Jackson, D. E. and Tendler, S. J. B. (1994) Atomic force microscopy and scanning tunnelling microscopy: refining techniques for studying biomolecules. *Trends Biotechnol.* **12**, 127-132
- 121 Ikai, A. (1996) STM and AFM of bio/organic molecules and structures. *Surf. Sci. Rep.* **26**, 261-332
- 122 Shao, Z., Mou, J., Czajkowsky, D. M., Yang, J. and Yuan, J.-Y. (1996) Biological atomic force microscopy: what is achieved and what is needed. *Adv. Phys.* **45**, 1-86
- 123 Allen, S., Davies, M. C., Roberts, C. J., Tendler, S. J. B. and Williams, P. M. (1997) Atomic force microscopy in analytical biotechnology. *Trends Biotechnol.* **15**, 101-105
- 124 Amato, I. (1997) Candid cameras for the nanoworld. *Science* **276**, 1982-1985

- 125 Magonov, S. N. and Reneker, D. H. (1997) Characterization of polymer surfaces with atomic force microscopy. *Annu. Rev. Mater. Sci.* **27**, 175-222
- 126 Vansteenkiste, S. O., Davies, M. C., Roberts, C. J., Tendler, S. J. B. and Williams, P. M. (1998) Scanning probe microscopy of biomedical interfaces. *Prog. Surf. Sci.* **57**, 95-136
- 127 McPherson, A., Malkin, A. J., Kuznetsov, Y. G. and Plomp, M. (2001) Atomic force microscopy applications in macromolecular crystallography. *Acta Cryst.* **D57**, 1053-1060
- 128 Reproduced with the kind permission of C. J. Roberts, School of Pharmaceutical Sciences, University of Nottingham.
- 129 Fritz, M., Radmacher, M., Cleveland, J. P., Allersma, M. R., Stewart, R. J., Gieselmann, R., Janmey, P., Schmidt, C. F. and Hansma, P. K. (1995) Imaging globular and filamentous proteins in physiological buffer solutions with tapping mode atomic force microscopy. *Langmuir* **11**, 3529-3535
- 130 Yip, C. M. and Ward, M. D. (1996) Atomic force microscopy of insulin single crystals: direct visualization of molecules and crystal growth. *Biophys. J.* **71**, 1071-1078
- 131 Hansma, H. G., Kim, K. J., Laney, D. E., Garcia, R. A., Argaman, M., Allen, M. J. and Parsons, S. M. (1997) Properties of biomolecules measured from atomic force microscope images: a review. *J. Struct. Biol.* **119**, 99-108
- 132 Yau, S.-T., Thomas, B. R. and Vekilov, P. G. (2000) Molecular mechanisms of crystallization and defect formation. *Phys. Rev. Lett.* **85**, 353-356
- 133 Basnar, B., Friedbacher, G., Brunner, H., Vallant, T., Mayer, U. and Hoffmann, H. (2001) Analytical evaluation of tapping mode atomic force microscopy for chemical imaging of surfaces. *Appl. Surf. Sci.* **171**, 213-225
- 134 Danesh, A., Connell, S. D., Davies, M. C., Roberts, C. J., Tendler, S. J. B., Williams, P. M. and Wilkins, M. J. (2001) An *in situ* dissolution study of aspirin crystal planes (100) and (001) by atomic force microscopy. *Pharm. Res.* **18**, 299-303
- 135 Durbin, S. D. and Carlson, W. E. (1992) Lysozyme crystal growth studied by atomic force microscopy. *J. Cryst. Growth* **122**, 71-79
- 136 Palocz, G. T., Smith, B. L., Hansma, P. K., Walters, D. A. and Wendman, M. A. (1998) Rapid imaging of calcite crystal growth using atomic force microscopy with small cantilevers. *Appl. Phys. Lett.* **73**, 1658-1660

- 137 Campbell, P. A., Mayer, M. A., Kerherve, G. and Roux, D. L. (2000) Dynamic processes at surfaces: Crystal growth and dissolution studied by atomic force microscopy. *Microsc. Anal.* **75**, 17-19
- 138 Mauri, A. and Moret, M. (2000) Growth of potassium sulphate crystals in the presence of organic dyes: in situ characterization by atomic force microscopy. *J. Cryst. Growth* **208**, 599-614
- 139 Moret, M. (2000) Influence of organic dyes on potassium sulphate crystal growth: a joint morphological and atomic force microscopy analysis. *Mater. Chem. Phys.* **66**, 177-188
- 140 Ester, G. R., Price, R. and Halfpenny, P. J. (1999) The relationship between crystal growth and defect structure: a study of potassium hydrogen phthalate using X-ray topography and atomic force microscopy. *J. Phys. D.: Appl. Phys.* **32**, A128-A132
- 141 Malkin, A. J., Kuznetsov, Y. G. and McPherson, A. (1999) In situ atomic force microscopy studies of surface morphology, growth kinetics, defect structure and dissolution in macromolecular crystallization. *J. Cryst. Growth* **196**, 471-488
- 142 Rong, L., Yamane, T. and Niimura, N. (2000) Measurement and control of the crystal growth rate of tetragonal hen egg-white lysozyme imaged with an atomic force microscope. *J. Cryst. Growth* **217**, 161-169
- 143 Land, T. A., Yoreo, J. J. D. and Lee, J. D. (1997) An *in situ* investigation of canavalin crystallization kinetics. *Surf. Sci.* **384**, 136-155
- 144 Kuznetsov, Y. G., Malkin, A. J. and McPherson, A. (1999) AFM studies of the nucleation and growth mechanisms of macromolecular crystals. *J. Cryst. Growth* **196**, 489-502
- 145 Land, T. A. and Yoreo, J. J. D. (2000) The evolution of growth modes and activity of growth sources on canavalin investigated by in situ atomic force microscopy. *J. Cryst. Growth* **208**, 623-637
- 146 Onuma, K., Ito, A., Tateishi, T. and Kameyama, T. (1995) Growth kinetics of hydroxyapatite crystal revealed by atomic force microscopy. *J. Cryst. Growth* **154**, 118-125
- 147 Onuma, K., Ito, A., Tateisha, T. and Kameyama, T. (1995) Surface observations of synthetic hydroxyapatite single crystal by atomic force microscopy. *J. Cryst. Growth* **148**, 201-206

- 148 Onuma, K., Ito, A. and Tateishi, T. (1996) Investigation of a growth unit of hydroxyapatite crystal from the measurements of step kinetics. *J. Cryst. Growth* **167**, 773-776
- 149 Astier, J. P., Bokern, D., Lapena, L. and Veessler, S. (2001) α -amylase crystal growth investigated by *in situ* atomic force microscopy. *J. Cryst. Growth* **226**, 294-302
- 150 Malkin, A. J., Kuznetsov, Y. G. and McPherson, A. (1996) Defect structure of macromolecular crystals. *J. Struct. Biol.* **117**, 124-137
- 151 Malkin, A. J., Kuznetsov, Y. G., Land, T. A., Yoreo, J. J. D. and McPherson, A. (1995) Mechanisms of growth for protein and virus crystals. *Nature Struct. Biol.* **2**, 956-959
- 152 Ng, J. D., Kuznetsov, Y. G., Malkin, A. J., Keith, G., Giegé, R. and McPherson, A. (1997) Visualization of RNA crystal growth by atomic force microscopy. *Nucleic Acids Res.* **25**, 2582-2588
- 153 Chernov, A. A. (1984) Crystal Growth, vol. 36, Springer-Verlag, Berlin
- 154 Land, T. A., Malkin, A. J., Kuznetsov, Y. G., McPherson, A. and Yoreo, J. J. D. (1995) Mechanisms of protein crystal growth: an atomic force microscopy study of canavalin crystallization. *Phys. Rev. Lett.* **75**, 2774-2777
- 155 Land, T. A., Malkin, A. J., Kuznetsov, Y. G., McPherson, A. and Yoreo, J. J. D. (1996) Mechanisms of protein and virus crystal growth: an atomic force microscopy study of canavalin and STMV. *J. Cryst. Growth* **166**, 893-899
- 156 Kuznetsov, Y. G., Smol'sky, I. L., Chernov, A. A. and Rozhansky, V. N. (1981) Realization of the dislocation-free growth of ADP crystals under x-ray topographic monitoring *in situ*. *Dokl. Akad. Nauk. SSSR* **260**, 864-867
- 157 Kuznetsov, Y. G., Malkin, A. J., Glantz, W. and McPherson, A. (1996) *In situ* atomic force microscopy studies of protein and virus crystal growth mechanisms. *J. Cryst. Growth* **168**, 63-73
- 158 Malkin, A. J., Land, T. A., Kuznetsov, Y. G., McPherson, A. and Yoreo, J. J. D. (1995) Investigation of virus crystal growth mechanisms by *in situ* atomic force microscopy. *Phys. Rev. Lett.* **75**, 2778-2781
- 159 Malkin, A. J., Kuznetsov, Y. G. and McPherson, A. (1996) Incorporation of microcrystals by growing protein and virus crystals. *Proteins* **24**, 247-252

- 160 Malkin, A. J., Kuznetsov, Y. G., Glantz, W. and McPherson, A. (1996) Atomic force microscopy studies of surface morphology and growth kinetics in thaumatin crystallization. *J. Phys. Chem.* **100**, 11736-11743
- 161 Malkin, A. J., Kuznetsov, Y. G. and McPherson, A. (1997) An *in situ* AFM investigation of catalase crystallization. *Surf. Sci.* **393**, 95-107
- 162 Derksen, A. J., Enkevort, W. J. P. v. and Couto, M. S. (1994) Behaviour of steps on the (001) face of K₂Cr₂O₇ crystals. *J. Phys. D.: Appl. Phys.* **27**, 2580-2591
- 163 Jiang, X. N., Xu, D., Sun, D. L., Yuan, D. R., Lu, M. K., Guo, S. Y. and Zhang, G. H. (2002) Ex situ atomic force microscopy studies of growth mechanisms of cadmium mercury thiocyanate crystals. *J. Cryst. Growth* **234**, 480-486
- 164 Masaki, N., Machida, K., Kado, H., Yokoyama, K. and Yohda, T. (1991) Atomic force microscope images of the surfaces of aspirin at submolecular resolution. *Chem. Pharm. Bull.* **39**, 1899-1901
- 165 Masaki, N., Machida, K., Kado, H., Yokoyama, K. and Tohda, T. (1992) Molecular-resolution images of aspirin crystals with atomic force microscopy. *Ultramicroscopy* **42-44**, 1148-1154
- 166 Danesh, A., Davies, M. C., Hinder, S. J., Roberts, C. J., Tendler, S. J. B., Williams, P. M. and Wilkins, M. J. (2000) Surface characterization of aspirin crystal planes by dynamic chemical force microscopy. *Anal. Chem.* **72**, 3419-3422
- 167 Flieger, K. (1994) Aspirin: A new look at an old drug. www.fda.gov/opacom/catalog/aspirin/history.html
- 168 <http://users.erols.com/bioplantin/reference/aspirin/history.html>.
- 169 Glaser, R. (2001) Aspirin. An ab initio quantum-mechanical study of conformational preferences and of neighbouring group interactions. *J. Org. Chem* **66**, 771-779
- 170 Vane, J. R. (1971) Inhibition of prostaglandin synthesis as a mechanism of action for aspirin-like drugs. *Nature-New Biol.* **231**, 232-235
- 171 Jamali, F. and Mitchell, A. G. (1973) The recrystallization and dissolution of acetylsalicylic acid. *Acta. Pharm. Suec.* **10**, 343-352

- 172 Kim, Y., Machida, K., Taga, T. and Osaki, K. (1985) Structure redetermination and packing analysis of aspirin crystal. *Chem. Pharm. Bull.* **33**, 2641-2647
- 173 Kim, Y., Matsumoto, M. and Machida, K. (1985) Specific surface energies and dissolution behaviour of aspirin. *Chem. Pharm. Bull.* **33**, 4125-4131
- 174 Kim, Y. and Machida, K. (1986) Vibrational spectra, normal coordinates and infrared intensities of aspirin crystal. *Chem. Pharm. Bull.* **34**, 3087-3096
- 175 Khan, Z. F. and Anwar, M. (1987) Crystal growth studies of acetylsalicylic acid: studies of effect of various physical parameters. X-ray crystallography by powder method. *J. Pure Appl. Sci.* **6**, 35-41
- 176 Meenan, P. (1997) Crystal morphology predictive techniques to characterize crystal habit: application to aspirin (C₉H₈O₄). *ACS Symp. Ser.* **667**, 2-17
- 177 Tawashi, R. (1968) Aspirin: dissolution rates of the two polymorphic forms. *Science* **160**, 76
- 178 Apelblat, A. and Manzurola, E. (1999) Solubilities of *o*-acetylsalicylic, 4-aminosalicylic, 3,5-dinitrosalicylic, and *p*-toluic acid, and magnesium-DL-aspartate in water from T = (278 to 348)K. *J. Chem. Thermodynamics* **31**, 85-91
- 179 Florence, A. T. and Attwood, D. (1988) Physicochemical principles of pharmacy, Macmillan Press, London
- 180 Edwards, L. J. (1950) The hydrolysis of aspirin. A determination of the thermodynamic dissociation constant and a study of the reaction kinetics by ultra-violet spectrophotometry. *Trans. Faraday Soc.* **46**, 723-735
- 181 Kuznetsov, Y. G., Malkin, A. J. and McPherson, A. (2001) The influence of precipitant concentration on macromolecular crystal growth mechanisms. *J. Cryst. Growth* **232**, 114-118
- 182 Kandel, D. and Weeks, J. D. (1992) Step bunching as a chaotic pattern formation process. *Phys. Rev. Lett.* **69**, 3758-3761
- 183 Kandel, D. and Weeks, J. D. (1994) Step motion, patterns, and kinetic instabilities on crystal surfaces. *Phys. Rev. Lett.* **72**, 1678-1681
- 184 Kandel, D. and Weeks, J. D. (1995) Simultaneous bunching and debunching of surface steps: theory and relation to experiments. *Phys. Rev. Lett.* **74**, 3632-3635

- 185 Liu, D.-J., Weeks, J. D. and Kandel, D. (1997) Velocity function models of step dynamics: theory of current induced step bunching on Si (111) surfaces. *Surf. Rev. Lett.* **4**, 107-113
- 186 Vekilov, P. G., Lin, H. and Rosenberger, F. (1997) Unsteady crystal growth due to step-bunching cascading. *Phys. Rev. E.* **55**, 3202-3214
- 187 Rosenberger, F. (1999) Proteins as a key to advanced crystal growth studies. *Cryst. Res. Technol.* **34**, 163-165
- 188 Aizenberg, J. (2000) Patterned crystallization of calcite in vivo and in vitro. *J. Cryst. Growth* **211**, 143-148
- 189 Stupp, S. I. and Braun, P. V. (1997) Molecular manipulation of microstructures: biomaterials, ceramics, and semiconductors. *Science* **277**, 1242-1248
- 190 Bunker, B. C., Rieke, P. C., Tarasevich, B. J., Campbell, A. A., Fryxell, G. E., Graff, G. L., Song, L., Lui, J., Virden, J. W. and McVay, G. L. (1994) Ceramic thin-film formation on functionalized interfaces through biomimetic processing. *Science* **264**, 48-55
- 191 Mann, S. (1993) Molecular tectonics in biomineralization and biomimetic materials chemistry. *Nature* **365**, 499-505
- 192 Mann, S. and Ozin, G. A. (1996) Synthesis of inorganic materials with complex form. *Nature* **382**, 313-318
- 193 Landau, E. M., Levanon, M., Leiserowitz, L., Lahav, M. and Sagiv, J. (1985) Transfer of structural information from Langmuir monolayers to three-dimensional growing crystals. *Nature* **318**, 353-356
- 194 Frostman, L. M. and Ward, M. D. (1997) Nucleation of molecular crystals beneath alkanesulphonate monolayers. *Langmuir* **13**, 330-337
- 195 Levi, Y., Albeck, S., Brack, A., Weiner, S. and Addadi, L. (1998) Control over aragonite crystal nucleation and growth: An in vitro study of biomineralization. *Chem. Eur. J.* **4**, 389-396
- 196 Albeck, S., Addadi, L. and Weiner, S. (1996) Regulation of calcite crystal morphology by intracrystalline acidic proteins and glycoproteins. *Connect. Tissue Res.* **35**, 419-424
- 197 Albeck, S., Weiner, S. and Addadi, L. (1996) Polysaccharides of intracrystalline glycoproteins modulate calcite crystal growth in vitro. *Chem. Eur. J.* **2**, 278-284

- 198 Addadi, L. and Weiner, S. (1985) Interactions between acidic proteins and crystals: stereochemical requirements in biomineralization. *Proc. Natl. Acad. Sci. USA* **82**, 4110-4114
- 199 Addadi, L., Moradian, J., Shay, E., Maroudas, N. G. and Weiner, S. (1987) A chemical model for the cooperation of sulphates and carboxylates in calcite crystal nucleation: relevance to biomineralization. *Proc. Natl. Acad. Sci. USA* **84**, 2732-2736
- 200 Askay, I. A., Trau, M., Manne, S., Honma, I., Yao, N., Zhou, L., Fenter, P., Eisenberger, P. M. and Gruner, S. M. (1996) Biomimetic pathways for assembling inorganic thin films. *Science* **273**, 892-898
- 201 Berman, A., Ahn, D. J., Lio, A., Salmeron, M., Reichert, A. and Charych, D. (1995) Total alignment of calcite at acidic polydiacetylene films: cooperativity at the organic-inorganic interface. *Science* **269**, 515-518
- 202 Feng, S. and Bein, T. (1994) Vertical aluminophosphate molecular sieve crystals grown at inorganic-organic interfaces. *Science* **265**, 1839-1841
- 203 Firouzi, A., Kumar, D., Bull, L. M., Besier, T., Sieger, P., Huo, Q., Walker, S. A., Zasadzinski, J. A., Glinka, C., Nicol, J., Margolese, D., Stucky, G. D. and Chmelka, B. F. (1995) Cooperative organization of inorganic-surfactant and biomimetic assemblies. *Science* **267**, 1138-1143
- 204 Archibald, D. D., Qadri, S. B. and Gaber, B. P. (1996) Modified calcite deposition due to ultrathin organic films on silicon substrates. *Langmuir* **12**, 538-546
- 205 Aizenberg, J., Black, A. J. and Whitesides, G. M. (1999) Oriented growth of calcite controlled by self-assembled monolayers of functionalized alkanethiols supported on gold and silver. *J. Am. Chem. Soc.* **121**, 4500-4509
- 206 Ostuni, E., Yan, L. and Whitesides, G. M. (1999) The interaction of proteins and cells with self-assembled monolayers of alkanethiolates on gold and silver. *Colloids Surf., B: Biointerfaces* **15**, 3-30
- 207 DeRose, J. A., Thundat, T., Nagahara, L. A. and Lindsay, S. M. (1991) Gold grown epitaxially on mica: conditions for large area flat surfaces. *Surf. Sci.* **256**, 102-108
- 208 Strong, L. and Whitesides, G. M. (1988) Structures of self-assembled monolayer films of organosulphur compounds adsorbed on gold single crystals: Electron diffraction studies. *Langmuir* **4**, 546-558

- 209 Whitesides, G. M. and Laibinis, P. E. (1990) Wet chemical approaches to the characterization of organic surfaces: self-assembled monolayers, wetting and the physical-organic chemistry of the solid-liquid interface. *Langmuir* **6**, 87-96
- 210 Troughton, E. B., Bain, C. D., Whitesides, G. M., Nuzzo, R. G., Allara, D. L. and Porter, M. D. (1988) Monolayer films prepared by the spontaneous self-assembly of symmetrical and unsymmetrical dialkyl sulphides from solution onto gold substrates: structure, properties, and reactivity of constituent functional groups. *Langmuir* **4**, 365-385
- 211 Bain, C. D. and Whitesides, G. M. (1989) Modelling organic surfaces with self-assembled monolayers. *Angew. Chem. Int. Ed. Engl.* **28**, 506-516
- 212 Whitesides, G. M., Ostuni, E., Takayama, S., Jiang, X. and Ingber, D. (2001) Soft lithography in biology and biochemistry. *Annu. Rev. Biomed. Eng.* **3**, 335-373
- 213 Kane, R. S., Takayama, S., Ostuni, E., Ingber, D. E. and Whitesides, G. M. (1999) Patterning proteins and cells using soft lithography. *Biomaterials* **20**, 2363-2376
- 214 Wilbur, J. L., Kim, E., Xia, Y. and Whitesides, G. M. (1995) Lithographic moulding: a convenient route to structures with sub-micrometre dimensions. *Adv. Mat.* **7**, 649-652
- 215 Jackman, R. J., Wilbur, J. L. and Whitesides, G. M. (1995) Fabrication of submicrometre features on curved substrates by microcontact printing. *Science* **269**, 664-666
- 216 Pfohl, T., Kim, J. H., Yasa, M., Miller, H. P., Wong, G. C. L., Bringezu, F., Wen, Z., Wilson, L., Kim, M. W., Li, Y. and Safinya, C. R. (2001) Controlled modification of microstructured silicon surfaces for confinement of biological macromolecules and liquid crystals. *Langmuir* **17**, 5343-5351
- 217 Higashi, N., Takahashi, M. and Niwa, M. (1999) Immobilization of DNA through intercalation at self-assembled monolayers on gold. *Langmuir* **15**, 111-115
- 218 Sun, X., He, P., Lui, S., Ye, J. and Fang, Y. (1998) Immobilization of single-stranded deoxyribonucleic acid on gold electrode with self-assembled aminoethanethiol monolayer for DNA electrochemical sensor applications. *Talanta* **47**, 487-495

- 219 Huang, E., Zhou, F. and Deng, L. (2000) Studies of surface coverage and orientation of DNA molecules immobilized onto preformed alkanethiol self-assembled monolayers. *Langmuir* **16**, 3272-3280
- 220 Chen, C. S. (2000) Using self-assembled monolayers to pattern ECM proteins and cells on substrates. *Methods Mol. Biol.* **139**, 209-219
- 221 Patel, N., Davies, M. C., Hartshorne, M., Heaton, R. J., Roberts, C. J., Tendler, S. J. B. and Williams, P. M. (1997) Immobilization of protein molecules onto homogeneous and mixed carboxylate-terminated self-assembled monolayers. *Langmuir* **13**, 6485-6490
- 222 Patel, N., Davies, M. C., Heaton, R. J., Roberts, C. J., Tendler, S. J. B. and Williams, P. M. (1998) A scanning probe microscopy study of the physisorption and chemisorption of protein molecules onto carboxylate terminated self-assembled monolayers. *Appl. Phys. A - Mat. Sci. Process.* **66**, S569-S574
- 223 Harder, P., Grunze, M., Dahint, R., Whitesides, G. M. and Laibinis, P. E. (1998) Molecular conformation in oligo(ethylene glycol)-terminated self-assembled monolayers on gold and silver surfaces determines their ability to resist protein adsorption. *J. Phys. Chem. B.* **102**, 426-436
- 224 Zhang, S., Yan, L., Altman, M., Lässle, M., Nugent, H., Frankel, F., Lauffenburger, D. A., Whitesides, G. M. and Rich, A. (1999) Biological surface engineering: a simple system for cell pattern formation. *Biomaterials* **20**, 1213-1220
- 225 Chen, C. S., Mrksich, M., Huang, S., Whitesides, G. M. and Ingber, D. E. (1998) Micropatterned surfaces for control of cell shape, position, and function. *Biotechnol. Prog.* **14**, 356-363
- 226 Mrksich, M., Dike, L. E., Tien, J., Ingber, D. E. and Whitesides, G. M. (1997) Using microcontact printing to pattern the attachment of mammalian cells to self-assembled monolayers of alkanethiolates on transparent films of gold and silver. *Exp. Cell Res.* **235**, 305-313
- 227 Chee, M., Yang, R., Hubbell, E., Berno, A., Huang, X. C., Stern, D., Winkler, J., Lockhart, D. J., Morris, M. S. and Fodor, S. P. A. (1996) Accessing genetic information with high-density DNA arrays. *Science* **274**, 610-614

- 228 Karlsson, R., Roos, H., Fagerstam, L. and Persson, B. (1994) Kinetic and concentration analysis using BIA technology. *Methods Compan. Methods Enzymol.* **6**, 99-110
- 229 Szabo, A., Stolz, L. and Granow, R. (1995) Surface plasmon resonance and its use in biomolecular interaction analysis. *Curr. Opin. Struct. Biol.* **5**, 699-705
- 230 Nealy, P. F., Black, A. J., Wilbur, J. L. and Whitesides, G. M. (1997) Micro- and nanofabrication techniques based on self-assembled monolayers. *Mol. Electronics*, 343-367
- 231 Kang, J. F., Zaccaro, J., Ulman, A. and Myerson, A. (2000) Nucleation and growth of glycine crystals on self-assembled monolayers on gold. *Langmuir* **16**, 3791-3796
- 232 Tarasevich, B. J., Rieke, P. C. and Liu, J. (1996) Nucleation and growth of oriented ceramic films onto organic interfaces. *Chem. Mater.* **8**, 292-300
- 233 Frostman, L. M., Bader, M. M. and Ward, M. D. (1994) Nucleation and growth of molecular crystals on self-assembled monolayers. *Langmuir* **10**, 576-582
- 234 Aizenberg, J., Black, A. J. and Whitesides, G. M. (1999) Control of crystal nucleation by patterned self-assembled monolayers. *Nature* **398**, 495-498
- 235 Küther, J. and Tremel, W. (1997) Stabilization of aragonite on thiol-modified gold surfaces: effect of temperature. *Chem. Commun.*, 2029-2030
- 236 Heywood, B. R. and Mann, S. (1994) Molecular construction of oriented inorganic materials - Controlled nucleation of calcite and aragonite under compressed Langmuir monolayers. *Chem. Mater.* **6**, 311-318
- 237 Heywood, B. R. and Mann, S. (1994) Template-directed nucleation and growth of inorganic materials. *Adv. Mater.* **6**, 9-20
- 238 Mann, S., Heywood, B. R., Rajam, S. and Walker, J. B. A. (1991) Structural and stereochemical relationships between Langmuir monolayers and calcium carbonate. *J. Phys. D. - Appl. Phys.* **24**, 154-164
- 239 Delamarche, E. and Michel, B. (1996) Structure and stability of self-assembled monolayers. *Thin Solid Films* **273**, 54-60
- 240 Larsen, N. B., Biebuyck, H., Delamarche, E. and Michel, B. (1997) Order in microcontact printed self-assembled monolayers. *J. Am. Chem. Soc.* **119**, 3017-3026

- 241 www.utah.edu/umed/courses/year2/pharm/study/rx04.pdf.
- 242 www.daylight.com/meetings/emu00/Sayle/pkapredict.html.
- 243 Pishko, M. V., Revzin, A. and Simonian, A. L. (2002) Mass transfer in amperometric biosensors based on nanocomposite thin films of redox polymers and oxidoreductases. *Sensors* **2**, 79-90
- 244 Jensen, P., Barabási, A.-L., Larralde, H., Havlin, S. and Stanley, H. E. (1994) Deposition, diffusion and aggregation of atoms on surfaces: A model for nanostructure growth. *Phys. Rev. B* **50**, 15316-15329
- 245 Jensen, P., Barabási, A.-L., Larralde, H., Havlin, S. and Stanley, H. E. (1994) Model incorporating deposition, diffusion, and aggregation in submonolayer nanostructures. *Phys. Rev. E* **50**, 618-621
- 246 Lee, C. and Barabási, A.-L. (1998) Spatial ordering of islands grown on patterned surfaces. *App. Phys. Letts.* **73**, 2651-2653
- 247 Tan, Z.-J., Zou, X.-W. and Jin, Z.-Z. (2001) Extended DDA model: deposition, diffusion and aggregation with power-law adsorption. *Phys. Letts. A* **282**, 121-124
- 248 Frisbie, C. D., Rozsnyai, L. F., Noy, A., Wrighton, M. S. and Lieber, C. M. (1994) Functional group imaging by chemical force microscopy. *Science* **265**, 2071-2074
- 249 Okabe, Y., Akiba, U. and Fujihira, M. (2000) Chemical force microscopy of -CH₃ and -COOH terminal groups in mixed self-assembled monolayers by pulsed-force-mode atomic force microscopy. *Appl. Surf. Sci.* **157**, 398-404
- 250 Okabe, Y., Furugori, M., Tani, Y., Akiba, U. and Fujihira, M. (2000) Chemical force microscopy of microcontact-printed self-assembled monolayers by pulsed-force-mode atomic force microscopy. *Ultramicroscopy* **82**, 203-212
- 251 Fujihira, M., Furugori, M., Akiba, U. and Tani, Y. (2001) Study of microcontact printed patterns by chemical force microscopy. *Ultramicroscopy* **86**, 75-83
- 252 Cabrera, N. and Vermilyea, D. A. (1958) in Growth and perfection of crystals (Doremus, R. H. and Turnbull, D., eds.), pp. 393-410, Wiley, New York
- 253 Megrab, N. A., Williams, A. C. and Barry, B. W. (1995) Oestradiol permeation through human skin and silastic membrane - effects of propylene-glycol and supersaturation. *J. Control. Release* **36**, 277-294

- 254 Usui, F., Maeda, K., Kusai, A., Nishimura, K. and Yamamoto, K. (1997) Inhibitory effects of water-soluble polymers on precipitation of RS-8359. *Int. J. Pharm.* **154**, 59-66
- 255 Iervolino, M., Raghavan, S. L. and Hadgraft, J. (2000) Membrane penetration enhancement of ibuprofen using supersaturation. *Int. J. Pharm.* **198**, 229-238
- 256 Raghavan, S. L., Trividic, A., Davis, A. F. and Hadgraft, J. (2000) Effect of cellulose polymers on supersaturation and in vitro membrane transport of hydrocortisone acetate. *Int. J. Pharm.* **193**, 231-237
- 257 Pellett, M. A., Davis, A. F. and Hadgraft, J. (1994) Effect of supersaturation on membrane-transport. 2. Piroxicam. *Int. J. Pharm.* **111**, 1-6
- 258 Duddu, S. P., Fung, F. K. Y. and Grant, D. J. W. (1993) Effect of the opposite enantiomer on the physicochemical properties of (-)-ephedrinium 2-naphthalenesulphonate crystals. *Int. J. Pharm.* **94**, 171-179
- 259 Duddu, S. P., Fung, F. K. Y. and Grant, D. J. W. (1996) Effects of crystallization in the presence of the opposite enantiomer on the crystal properties of (SS)-(+)-pseudoephedrinium. *Int. J. Pharm.* **127**, 53-63
- 260 Gu, C.-H. and Grant, D. J. W. (2002) Relationship between particle size and impurity incorporation during crystallization of (+)-pseudoephedrine hydrochloride, acetaminophen, and adipic acid from aqueous solution. *Pharm. Res.* **19**, 1068-1070
- 261 (1996) 40 Years of Paracetamol. Advertisement feature. *Pharm. J.*, 256
- 262 Martino, P. D., Conflant, P., Drache, M., Huvenne, J.-P. and Guyot-Hermann, A.-M. (1997) Preparation and physical characterization of forms II and III of paracetamol. *J. Therm. Anal.* **48**, 447-458
- 263 Singh, T. P., Bhat, T. N. and Vijayan, M. (1973) Crystallization and crystal data of acetaminophen and metamizol. *Curr. Sci.* **42**, 384
- 264 Bhattacharya, G. C., Naqvi, S. A. A. and Guha, S. (1975) A preliminary report on the crystal structure of phenacetin, paracetamol, solasodine monohydrate and 4-phenyl 5,7-dihydroxy 6-isovaleryl 8-isopentnyl coumarin. *Indian J. Phys.* **49**, 65-68
- 265 Haisa, M., Kashino, S., Kawai, R. and Maeda, H. (1976) The monoclinic form of *p*-hydroxyacetanilide. *Acta Cryst.* **B32**, 1283-1285
- 266 Welton, J. M. and McCarthy, G. J. (1988) X-ray powder data for acetaminophen (C₈H₉NO₂). *Powder Diff.* **3**, 102-103

- 267 Nichols, G. (1998) Optical properties of polymorphic forms I and II of paracetamol. *Microscope* **46**, 117-122
- 268 Naumov, D. Y., Vasilchenko, M. A. and Howard, J. A. K. (1998) The monoclinic form of acetaminophen at 150K. *Acta Cryst.* **C54**, 653-655
- 269 Wilson, C. C. (2000) Variable temperature study of the crystal structure of paracetamol (*p*-hydroxyacetanilide), by single crystal neutron diffraction. *Z.Kristallogr.* **215**, 693-701
- 270 Moynihan, H. A. and O'Hare, I. P. (2002) Spectroscopic characterisation of the monoclinic and orthorhombic forms of paracetamol. *Int. J. Pharm.* **247**, 179-185
- 271 Haisa, M., Kashino, S. and Haeda, H. (1974) The orthorhombic form of *p*-hydroxyacetanilide. *Acta Cryst.* **B30**, 2510-2512
- 272 Martino, P. D., Guyot-Hermann, A. M., Conflant, P., Drache, M. and Guyot, J. C. (1996) A new pure paracetamol for direct compression: the orthorhombic form. *Int. J. Pharm.* **128**, 1-8
- 273 Nichols, G. and Frampton, C. S. (1998) Physicochemical characterization of the orthorhombic polymorph of paracetamol crystallized from solution. *J. Pharm. Sci.* **87**, 684-693
- 274 Femi-Oyewo, M. N. and Spring, M. S. (1994) Studies on paracetamol crystals produced by growth in aqueous solutions. *Int. J. Pharm.* **112**, 17-28
- 275 Garekani, H. A., Ford, J. L., Rubinstein, M. H. and Rajabi-Siahboomi, A. R. (2000) Highly compressible paracetamol: I: crystallization and characterization. *Int. J. Pharm.* **208**, 87-99
- 276 Garekani, H. A., Ford, J. L., Rubinstein, M. H. and Rajabi-Siahboomi, A. R. (2000) Highly compressible paracetamol - II. Compression properties. *Int. J. Pharm.* **208**, 101-110
- 277 Fachaux, J. M., Guyot-Hermann, A. M. and Guyot, J. C. (1993) Compression ability improvement by solvation/desolvation process: application to paracetamol for direct compression. *Int. J. Pharm.* **99**, 99-107
- 278 Fachaux, J. M., Guyot-Hermann, A. M., Guyot, J. C., Conflant, P., Drache, M., Veessler, S. and Boistelle, R. (1995) Pure paracetamol for direct compression. Part I. Development of sintered-like crystals of paracetamol. *Powder Technol.* **82**, 123-128

- 279 Fachaux, J. M., Guyot-Hermann, A. M., Guyot, J. C., Conflant, P., Drache, M., Veessler, S. and Boistelle, R. (1995) Pure paracetamol for direct compression. Part II. Study of the physicochemical and mechanical properties of sintered-like crystals of paracetamol. *Powder Technol.* **82**, 129-133
- 280 McGregor, P. A., Allan, D. R., Parsons, S. and Pulham, C. R. (2002) Preparation and crystal structure of a trihydrate of paracetamol. *J. Pharm. Sci.* **91**, 1308-1311
- 281 Finnie, S., Prasad, K. V. R., Sheen, D. B. and Sherwood, J. N. (2001) Microhardness and dislocation identification studies on paracetamol single crystals. *Pharm. Res.* **18**, 674-681
- 282 Dittert, L. W., Caldwell, H. C., Adams, H. J., Irwin, G. M. and Swintowsky, J. V. (1968) Acetaminophen prodrugs. 1. Synthesis, physiochemical properties and analgesic activity. *J. Pharm. Sci.* **57**, 774-783
- 283 Baugess, C. T., Sadik, F., Fincher, J. H. and Hartman, C. W. (1975) Hydrolysis of fatty acid esters of acetaminophen in buffered pancreatic lipase systems.1. *J. Pharm. Sci.* **64**, 117-120
- 284 Granberg, R. A. and Rasmuson, Å. C. (1999) Solubility of paracetamol in pure solvents. *J. Chem. Eng. Data* **44**, 1391-1395
- 285 Grant, D. J. W., Mehdizadeh, M., Chow, A. H.-L. and Fairbrother, J. E. (1984) Non-linear van't Hoff solubility-temperature plots and their pharmaceutical interpretation. *Int. J. Pharm.* **18**, 25-38
- 286 Romero, S., Reillo, A., Escalero, B. and Bustamanate, P. (1996) The behaviour of paracetamol in mixtures of amphiprotic-aprotic solvents. Relationship of solubility curves to specific and nonspecific interactions. *Chem. Pharm. Bull.* **44**, 1061-1064
- 287 Li, T., Morris, K. R. and Park, K. (2001) Influence of tailor-made additives on etching patterns of acetaminophen single crystals. *Pharm. Res.* **18**, 398-402
- 288 Land, T. A., Martin, T. L., Potapenko, S., Palmore, G. T. and Yoreo, J. J. D. (1999) Recovery of surfaces from impurity poisoning during crystal growth. *Nature* **399**, 442-445
- 289 Nakada, T., Sazaki, G., Miyashita, S., Durbin, S. D. and Komatsu, H. (1999) Direct AFM observations of impurity effects on a lysozyme crystal. *J. Cryst. Growth* **196**, 503-510

- 290 Khlobystov, A. N., Champness, N. R., Roberts, C. J., Tendler, S. J. B., Thompson, C. and Schröder, M. (2002) Anion exchange in co-ordination polymers: a solid-state or a solvent-mediated process? *CrystEngComm* **4**, 426-431
- 291 Thompson, C., Allen, S., Champness, N. R., Davies, M. C., Khlobystov, A. N., Roberts, C. J., Schröder, M., Tendler, S. J. B., Wilkinson, M. J. and Williams, P. M. Using microscopic techniques to reveal the anion exchange mechanisms of crystalline co-ordination polymers. Manuscript in preparation. *J. Microsc.*
- 292 Lehn, J. M. (1999) Dynamic combinatorial chemistry and virtual combinatorial libraries. *Chem. Eur. J.* **5**, 2455-2463
- 293 Yaghi, O. M., Li, H., Davis, C., Richardson, D. and Groy, T. L. (1998) Synthetic strategies, structure patterns, and emerging properties in the chemistry of modular porous solids. *Acc. Chem. Res.* **31**, 474-484
- 294 Munakata, M., Wu, L. P., Yamamoto, M., Kuroda-Sowa, T. and Maekawa, M. (1996) Construction of three-dimensional supramolecular coordination copper(I) compounds with channel structures hosting a variety of anions by changing the hydrogen-bonding mode and distances. *J. Am. Chem. Soc.* **118**, 3117-3124
- 295 Munakata, M., Wu, L. P., Ning, G. L., Kuroda-Sowa, T., Maekawa, M., Suenaga, Y. and Maeno, N. (1999) Construction of metal sandwich systems derived from assembly of silver(I) complexes with polycyclic aromatic compounds. *J. Am. Chem. Soc.* **121**, 4968-4976
- 296 Prior, T. J. and Rosseinsky, M. J. (2001) Crystal engineering of a 3-D coordination polymer from 2-D building blocks. *Chem. Comm.*, 495-496
- 297 Olenyuk, B., Whiteford, J. A., Fechtenkotter, A. and Stang, P. J. (1999) Self-assembly of nanoscale cuboctahedra by coordination chemistry. *Nature* **398**, 796-799
- 298 Jung, O.-S., Kim, Y. J., Lee, Y.-A., Park, J. K. and Chae, H. K. (2000) Smart molecular helical springs as tunable receptors. *J. Am. Chem. Soc.* **122**, 9921-9925
- 299 Blake, A. J., Baum, G., Champness, N. R., Chung, S. S. M., Cooke, P. A., Fenske, D., Khlobystov, A. N., Lemenovskii, D. A., Li, W. S. and Schröder, M. (2000) Long-range chain orientation in 1-D co-ordination polymers as a

- function of anions and intermolecular aromatic interactions. *J. Chem. Soc., Dalton Trans.*, 4285-4291
- 300 Blake, A. J., Champness, N. R., Cooke, P. A., Nicolson, J. E. B. and Wilson, C. (2000) Multi-modal bridging ligands; effects of ligand functionality, anion and crystallization solvent in silver (I) co-ordination polymers. *J. Chem. Soc., Dalton Trans.*, 3811-3819
- 301 Min, K. S. and Suh, M. P. (2000) Silver(I)-polynitrile network solids for anion exchange: anion-induced transformation of supramolecular structure in the crystalline state. *J. Am. Chem. Soc.* **122**, 6834-6840
- 302 Jung, O.-S., Kim, Y. J., Lee, Y. A., Chae, H. K., Jang, H. G. and Hong, J. (2001) Structures and related properties of AgX bearing 3,3'-thiobispyridine ($X^- = \text{NO}_3^-$, BF_4^- , ClO_4^- , and PF_6^-). *Inorg. Chem.* **40**, 2105-2110
- 303 Lee, E., Kim, J., Heo, J., Whang, D. and Kim, K. (2001) A two-dimensional polyrotaxane with large cavities and channels: a novel approach to metal-organic open-frameworks by using supramolecular building blocks. *Angew. Chem., Int. Ed.* **40**, 399-402
- 304 Pan, L., Woodlock, E. B., Wang, X., Lam, K. C. and Rheingold, A. L. (2001) Novel silver(I)-organic coordination polymers: conversion of extended structures in the solid state as driven by argentophilic interactions. *Chem. Commun.* **18**, 1762-1763
- 305 Biradha, K., Hongo, Y. and Fujita, M. (2000) Open square-grid coordination polymers of the dimensions 20 x 20 Å: remarkably stable and crystalline solids even after guest removal. *Angew. Chem., Int. Ed.* **39**, 3843-3845
- 306 Tschinkl, M., Schier, A., Riede, J. and Gabbai, F. P. (1999) Micropore decoration with bidentate Lewis acids: spontaneous assembly of 1,2-bis(chloromercurio)tetrafluorobenzene. *Angew. Chem. Int. Ed.* **38**, 3547-3549
- 307 Li, H., Eddaoudi, M., Richardson, D. A. and Yaghi, O. M. (1998) Porous germanates: synthesis, structure, and inclusion properties of $\text{Ge}_7\text{O}_{14.5}\text{F}_2 \cdot [(\text{CH}_3)_2\text{NH}_2]_3(\text{H}_2\text{O})_{0.86}$. *J. Am. Chem. Soc.* **120**, 8567-8568
- 308 Li, H., Davis, C. E., Groy, T. L., Kelley, D. G. and Yaghi, O. M. (1998) Coordinatively unsaturated metal centres in the extended porous framework of $\text{Zn}_3(\text{BDC})_3 \cdot 6\text{CH}_3\text{OH}$ (BDC = 1,4-benzenedicarboxylate). *J. Am. Chem. Soc.* **120**, 2186-2187

- 309 Goodgame, D. M. L., Grachvogel, D. A. and Williams, D. J. (1999) A new type of metal-organic large-pore zeotype. *Angew. Chem. Int. Ed.* **38**, 153-156
- 310 Abrahams, B. F., Jackson, P. A. and Robson, R. (1998) A robust (10,3)-a network containing chiral micropores in the Ag^I coordination polymer of a bridging ligand that provides three bidentate metal-binding sites. *Angew. Chem. Int. Ed.* **37**, 2656-2659
- 311 Blake, A. J., Champness, N. R., Khlobystov, A. N., Parsons, S. and Schröder, M. (2000) Controlled assembly of dinuclear metallacycles into a three-dimensional helical array. *Angew. Chem. Int. Ed.* **39**, 2317-2320
- 312 Sawaki, T., Dewa, T. and Aoyama, Y. (1998) Immobilization of soluble metal complexes with a hydrogen-bonded organic network as a supporter. A simple route to microporous solid Lewis acid catalysis. *J. Am. Chem. Soc.* **120**, 8539-8540
- 313 Noro, S., Kitazawa, S., Kondo, M. and Seki, K. (2000) A new, methane adsorbent, porous co-ordination polymer [$\{\text{CuSiF}_6(4,4'\text{-bipyridine})_2\}_n$]. *Angew. Chem., Int. Ed.* **39**, 2082-2084
- 314 Yaghi, O. M. and Li, H. (1996) T-shaped molecular building units in the porous structure of Ag(4,4'-byp).NO₃. *J. Am. Chem. Soc.* **118**, 295-296
- 315 Robinson, F. and Zaworotko, M. J. (1995) Triple interpenetration in [Ag(4,4'-bipyridine)][NO₃], a cationic polymer with a 3-dimensional motif generated by self-assembly of T-shaped building blocks. *J. Chem. Soc., Chem. Commun.*, 2413-2414
- 316 Yaghi, O. M. and Li, H. (1995) Hydrothermal synthesis of a metal-organic framework containing large rectangular channels. *J. Am. Chem. Soc.* **117**, 10401-10402
- 317 Vittal, J. J. and Yang, X. (2002) Interconvertible supramolecular transformations. *Cryst. Growth Des.* **2**, 259-262
- 318 Fujita, M., Kwon, Y. J., Washuzi, S. and Ogura, K. (1994) Preparation, clathration ability, and catalysis of a 2-dimensional square network material composed of cadmium (II) and 4,4'-bipyridine. *J. Am. Chem. Soc.* **116**, 1151-1152
- 319 Yaghi, O. M., Li, G. and Li, H. (1995) Selective binding and removal of guests in a microporous metal-organic framework. *Nature* **378**, 703-706

- 320 Yaghi, O. M., Li, H. and Groy, T. L. (1996) Construction of porous solids from hydrogen-bonded metal complexes of 1,3,5-benzenetricarboxylic acid. *J. Am. Chem. Soc.* **118**, 9096-9101
- 321 Min, K. S. and Suh, M. P. (2001) Self-assembly and selective guest binding of three-dimensional open-framework solids from a macrocyclic complex as a trifunctional metal building block. *Chem. Eur. J.* **7**, 303-313
- 322 Gardner, G. B., Venkataraman, D., Moore, J. S. and Lee, S. (1995) Spontaneous assembly of a hinged co-ordination network. *Nature* **374**, 792-795
- 323 Kiang, Y. H., Gardner, G. B., Lee, S., Xu, Z. and Lobkovsky, E. B. (1999) Variable pore size, variable chemical functionality, and an example of reactivity with porous phenylacetylene silver salts. *J. Am. Chem. Soc.* **121**, 8204-8215
- 324 Seo, J. S., Whang, D., Lee, H., Jun, S. I., Oh, J., Jeon, Y. J. and Kim, K. (2000) A homochiral metal-organic porous material for enantioselective separation and catalysis. *Nature* **404**, 982-985
- 325 Dewa, T., Endo, K. and Aoyama, Y. (1998) Dynamic aspects of lattice inclusion complexation involving a phase change. Equilibrium, kinetics, and energetics of guest-binding to a hydrogen-bonded flexible organic network. *J. Am. Chem. Soc.* **120**, 8933-8940
- 326 Endo, K., Koike, T., Sawaki, T., Hayashida, O., Masuda, H. and Aoyama, Y. (1997) Catalysis by organic solids. Stereoselective Diels-Alder reactions promoted by microporous molecular crystals having an extensive hydrogen-bonded network. *J. Am. Chem. Soc.* **119**, 4117-4122
- 327 Kang, J. and Jr, J. R. (1997) Acceleration of a Diels-Alder reaction by a self-assembled molecular capsule. *Nature* **385**, 50-52
- 328 Lin, W., Wang, Z. and Ma, L. (1999) A novel octupolar metal-organic NLO material based on a chiral 2D coordination network. *J. Am. Chem. Soc.* **121**, 11249-11250
- 329 Evans, O. R., Xiong, R., Wang, Z., Wong, G. K. and Lin, W. (1999) Crystal engineering of acentric diamondoid metal-organic co-ordination networks. *Angew. Chem., Int. Ed.* **38**, 536-538
- 330 Kahn, O. (2000) Chemistry and physics of supramolecular magnetic materials. *Acc. Chem. Res.* **33**, 647-657

- 331 Pan, L., Woodlock, E. B., Wang X. T. and Zheng C. (2000) A new porous three-dimensional lanthanide co-ordination polymer. *Inorg. Chem.* **39**, 4174
- 332 Cardew, P. T. and Davey, R. J. (1985) The kinetics of solvent-mediated phase transformations. *Proc. R. Soc., Lond. A.* **398**, 415-428
- 333 Pina, C. M., Fernández-Díaz, L., Prieto, M. and Putnis, A. (2000) In situ atomic force microscope observations of a dissolution-crystallisation reaction: the phosgenite-cerussite transformation. *Geochim. Cosmochim. Acta* **64**, 215-221
- 334 Pina, C. M., Fernández-Díaz, L. and Prieto, M. (1996) Topotaxy relationships in the transformation phosgenite-cerussite. *J. Cryst. Growth* **158**, 340-345
- 335 Booth, J., Hong, Q., Compton, R. G., Prout, K. and Payne, R. M. (1997) Gypsum overgrowths passivate calcite to acid attack. *J. Colloid Interface Sci.* **192**, 207-214
- 336 Booth, J., Compton, R. G. and Atherton, J. H. (1998) Mechanism of solid/liquid interfacial reactions. Atomic force microscopy studies of the self-passivating reaction between solid *p*-Chloranil and aqueous phase N,N-Dimethylphenylenediamine. *J. Phys. Chem. B.* **102**, 3980-3985
- 337 Fujita, M., Aoyagi, M., Ibukuro, F., Ogura, K. and Yamaguchi, K. (1998) Made-to-order assembling of [2]catenanes from palladium(II)-linked rectangular molecular boxes. *J. Am. Chem. Soc.* **120**, 611-612
- 338 Gudbjartson, H., Biradha, K., Poirer, K. M. and Zaworotko, M. J. (1999) Novel nanoporous coordination polymer sustained by self-assembly of T-shaped moieties. *J. Am. Chem. Soc.* **121**, 2599-2600
- 339 Tei, L., Lippolis, V., Blake, A. J., Cooke, P. A. and Schröder, M. (1998) Nitrile functionalised pendant-arm derivatives of [9]aneN₃ as new multidentate ligands for inorganic crystal engineering ([9]aneN₃ = 1,4,7-triazacyclononane). *Chem. Commun.*, 2633-2634
- 340 Carlucci, L., Ciani, G. and D. M. Proserpio, C. C., Milan, Italy. Personal communication.
- 341 Reproduced with the kind permission of N. R. Champness, School of Chemistry, University of Nottingham.

- 342 Xiong, R. G., Lewandowski, B. J. and Huang, S. D. (1999) Crystal structure of diaqua-4,4'-bipyridinezinc nitrate $Zn(4,4'-bipy)(H_2O)_2(NO_3)_2$: a one-dimensional coordination polymer. *Z. Kristallogr.* **214**, 461-462
- 343 Anderson, J. G., Doraiswamy, L. K. and Larson, M. A. (1998) Microphase-assisted "autocatalysis" in a solid-liquid reaction with a precipitating product - I. Theory. *Chem. Eng. Sci.* **53**, 2451-2458
- 344 Anderson, J. G., Larson, M. A. and Doraiswamy, L. K. (1998) Microphase-assisted "autocatalysis" in a solid-liquid reaction with a precipitating product - II. Experimental. *Chem. Eng. Sci.* **53**, 2459-2468
- 345 Davey, R. J., Cardew, P. T., McEwan, D. and Sadler, D. E. (1986) Rate controlling processes in solvent-mediated phase-transformations. *J. Cryst. Growth* **79**, 648-653
- 346 Rodríguez-Hornedo, N., Lechuga-Ballestros, D. and Wu, H. J. (1992) Phase-transition and heterogeneous epitaxial nucleation of hydrated and anhydrous theophylline crystals. *Int. J. Pharm.* **85**, 149-162
- 347 Smith, A. L. (1973) Particle Growth in Suspensions, Academic Press, London
- 348 Zaworotko, M. J. (1998) From disymmetric molecules to chiral polymers: a new twist for supramolecular synthesis? *Angew. Chem. Int. Ed.* **37**, 1211-1213
- 349 Zaworotko, M. J. (2001) Superstructural diversity in two dimensions: crystal engineering of laminated solids. *Chem. Comm.*, 1-9
- 350 Moulton, B. and Zaworotko, M. J. (2001) From molecules to crystal engineering: Supramolecular isomerism and polymorphism in network solids. *Chem. Rev.* **101**, 1629-1658

Acknowledgements

First of all, I wish to thank my academic and industrial supervisors, Dr. Clive Roberts, Prof. Saul Tendler, Dr. Mike Wilkinson, Dr. Stephanie Allen, Prof. Martyn Davies, and Dr. Phil Williams, all of whom have provided me with expert guidance. Special thanks to Clive for tirelessly reading my chapters and papers, and never holding back when I had written a load of rubbish. Thank you also to the EPSRC and GlaxoSmithKline for funding this project.

To my hilarious colleagues Lisa, Nicola, and Shellie, who provided me with endless hours of amusement in and out of the lab, thank you for letting me become one of the freaks that you all seem to know.

Thanks to Mum, Alan, and Stacey for all the love and support they have given me throughout the last few years, and for hardly ever asking the dreaded “How is your writing up going?” question.

Lastly, but most importantly, I want to thank my little rock Vicki. Thank you for the unlimited love, patience and strength you have showed me. You truly are my angel. I love you, and I’m forever in your debt! WYMM?

Publications

Anion exchange in co-ordination polymers: a solid-state or a solvent-mediated process? A. N. Khlobystov, N. R. Champness, C. J. Roberts, S. J. B. Tendler, C. Thompson, M. Schröder. (2002) *CrystEngComm*. **4**, 426-431.